The Spatial Political Economy of Discontent

Vanschoonbeek, Jakob

KU Leuven

26 June 2024

THE SPATIAL POLITICAL ECONOMY OF DISCONTENT

Jakob Vanschoonbeek*, †

Abstract

The recent rise and distinct geography of populism highlights the need for high resolution data on the economic and political landscapes and improved spatial political economy models that explain their interrelation. This paper shows that divergent development generates political externalities in lagging regions. To do so, it develops a dynamic spatial political economy model that integrates redistributive taxation and agglomerated economic growth in a standard economic geography framework. It finds that divergent development induces skill-biased labor mobility towards faster growing locations, simultaneously reducing their willingness to pay redistributive taxes and increasing their electoral influence on redistributive policy. To empirically validate and calibrate the model, the Spatial Political Economy in Europe Database (SPEED) is introduced, containing newly georeferenced electoral maps, political party classifications and gridded (per capita) GDP estimates for most European countries in the 17^{th} release of the Constituency-Level Electoral Archive (CLEA). Instrumental variable regressions exploiting geographically-determined differences in economic growth potential confirm a strong constituency-level causal relation between underdevelopment and radical vote shares in the past two centuries. Counterfactual simulations suggests that policies that enhance labor mobility or income redistribution may both increase radical vote shares at least in the short run, as they risk fueling backlash in lagging and leading regions respectively.

Keywords: Economic geography, political economy, political discontent, long-term effects of divergent development, quantitative model

JEL Classification: C51, C61, C63, D72, E01, H23, R12, R13

*KU Leuven - University of Leuven, Research Centre for Regional Economics (VIVES)
†Postdoctoral Fellow of the Research Foundation - Flanders (FWO)

1 Introduction

Interregional economic divergence is on the rise in many parts of the developed world (Storper, 2018; Rodríguez-pose, 2018; Rosés & Wolf, 2021a). Both in the United States and Europe, interregional inequality has increased sharply in the past 40 years after a period of regional convergence, see figure 1a. Simultaneously, the past half-century is also characterized as an era of political fragmentation (Inglehart & Norris, 2016; Rodrik, 2018b; Inglehart & Norris, 2019; Vanschoonbeek, 2020). On both sides of the Atlantic, countries recently experience a geographical polarization of votes, with gains in populism, extremism and separatism in some regions and pluralism and cosmopolitanism in others, see figure 1b. Both processes also seem interconnected, as intensifying geographical political divisions may lead to political gridlock, inefficient convergence policies and less economic stability (Voorheis, McCarty, Shor, & Rogers, 2015; Funke, Schularick, & Trebesch, 2016). The World Economic Forum (2017, p.13) therefore identified the combination of economic inequality and political polarization as the biggest threat of this century, as it risks *"fraying the social solidarity on which the legitimacy of our economic and political systems rests"*.

Figure 1: **Spatial economic and political divergence in Europe**

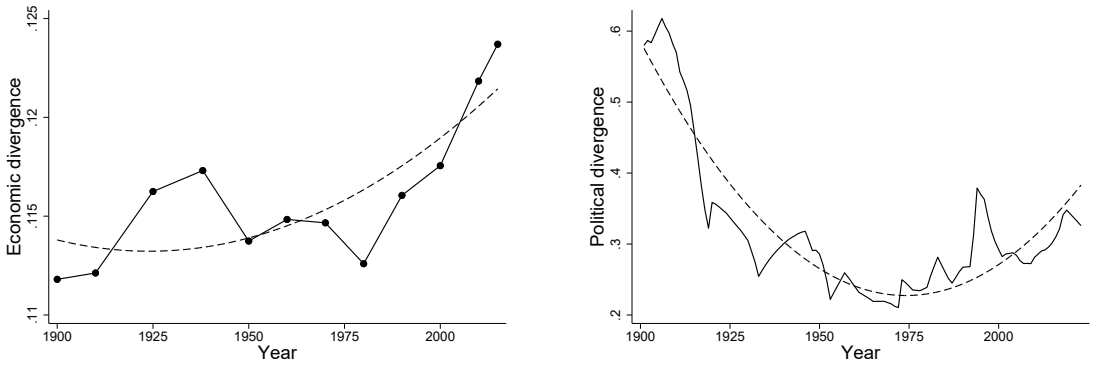

(a) Herfindahl index of regional GDP (b) Regional political distinctiveness

Sources: Figure 1a shows the population-weighted Herfindahl index of subnational GDP for the countries in Rosés and Wolf (2021a); figure 1b shows their vote-weighted electoral distinctiveness as defined in Vanschoonbeek (2020), using constituency-level electoral results from Kollman et al. (2023). Distinctiveness in future non-election years is approximated by linear extra- and interpolation at the country level.

While the notion that economic development is unequal across space is hardly new, our understanding of the relations between the economic and political landscapes remains elusive for at least three reasons. First, economic geography models typically omit a political layer that describes how unequal development influences collective choice processes on the optimal design of public policies, tax schemes and income redistribution. In fact, their 'excessive' focus on agglomeration externalities such as congestion has recently been blamed for their inability to anticipate the rapid ascent and distinct geography of populism in the past few years (Rodríguez-pose, 2018). Second, as pointed out by Storper (2018), the standard assumption that labor mobility equalizes utility across space sharply contrasts with the notion of a geography of discontent. Finally, the empirical literature on the

determinants of political discontent remains inconclusive on the relative importance and precise role of economic and non-economic considerations. As a result, the effectiveness of putative economic policies that aim to alleviate political tensions by enhancing labor mobility and redistributing incomes also remains unclear (Eichengreen, 2018).

This paper wants to bridge the gap between economic geography and political economy. Its primary objective is to develop and empirically validate a dynamic spatial political economy model that incorporates redistributive taxation in a standard economic geography framework, to explore how divergent development influences equilibrium tax burdens, welfare and political discontent. This also provides a useful framework to anticipate how future development paths may affect the prevalence of discontent and to evaluate the effectiveness of policies that aim to better spread political satisfaction.

A first aim of this paper is to build an empirical foundation for spatial political economy by overcoming several existing data limitations. First, electoral data is typically not georeferenced and, if it is, lacks historical coverage. This complicates analysis at a high spatial resolution and prevents their linkage to other subnational data. Second, economic and electoral data are often reported for different administrative boundaries, constraining empirical analysis to aggregated spatial units that e.g. encompass rural and urban areas. Third, there is no consensus on how to categorize parties on the political spectrum while existing classifications typically only consider recent periods and/or large political parties. This complicates a comprehensive historical analysis of cross-country electoral trends.

To overcome these limitations, I develop the Spatial Political Economy in Europe Database (SPEED) containing *(i)* georeferenced electoral maps, *(ii)* (per capita) GDP estimates and *(iii)* harmonized political party names linked to several party classification systems for all the constituencies of 28 European countries in the 17^{th} release of the Constituency-Level Electoral Archive (CLEA), a worldwide repository of constituency-level electoral results. All data and code are made available through a dedicated webpage (Vanschoonbeek, 2024). SPEED combines the information of three ancillary datasets:

- **Geo-Referenced European Electoral Districts (GREED):** constructed from a variety of primary and secondary sources and covering 44993 constituencies in 28 countries across 689 general elections between 1847 and 2023.
- **Gridded European Economic Data (GEED):** combines spatial disaggregation methods and gridded proxy variables on nighttime lights and market access to provide gridded estimates of population and GDP at a high spatial resolution of 5-arcminutes for the period 1800-2023. Estimates are harmonized with several authoritative (sub)national sources and are sufficiently finegrained to be aggregated to arbitrary administrative boundaries using standard spatial weighting methods.
- **European Political Taxonomy (EPT):** harmonizes 6198 European political party names; links them to party classifications of Inglehart and Norris (2019) and Rooduijn et al.'s (2019) PopuList; and adds Wikipedia-scraped party ideology tags and po-

litical positions with more complete time and party coverage. Linkages to other classification schemes could easily be implemented using the Party Facts database.

These data allow to establish several empirical regularities related to the economic and political landscapes of Europe at a fine spatial resolution and over a long time period. With respect to the economic landscape, tracing their historical evolution at a 5' $\times$ 5' resolution (roughly 50 km^2), gridded estimates of population and GDP grew more spatially concentrated over the past two centuries. Where the 20% most populous locations represented 67% of the population in 1800, their share grew to 84% in 2000. Spatial concentration grew even more pronounced in the available gridded GDP estimates: the top 20 percentile grid cells represented around 69% of GDP in 1800 and around 94% in 2000. Country-specific Herfindahl indices of gridded GDP moreover confirm that these trends were prevalent throughout Europe, as most countries experienced growing spatial inequality. Finally, the spatial distribution of per capita GDP exhibits a growing right tail. All of these findings are consistent with the notion of divergent economic development.

With respect to the political landscape, this paper takes a pragmatic approach in using a binary definition to measure political discontent as the electoral performance of 'radical' parties that operate on the fringes of the political spectrum and aim to attract particular segments of the electorate that are disillusioned with the status quo and are distinguished from 'mainstream' parties advocating moderate policy changes within the existing system to maximize overall political satisfaction. Using each party's combined typological information in the EPT, radical parties include both extremist parties that are (majority) classified as 'far left', 'far right' or 'separatist'; and populist parties that claim to defend the interests of a common people against a corrupt elite.[1] While inherently reductive, this definition does allow to shed some light on recent worries related to the electoral disappearance of mainstream parties in many Western countries.[2]

Using this perspective to take a look at the available electoral data reveals that Europe was hit by two historical waves of discontent: while mainstream political parties remained dominant until the interbellum, they first lost electoral ground during a wave of extremism which reduced their voter base to 60% of valid votes, after which they gradually recovered until the emergence of a second populist wave of similar magnitude, starting in the 1990s and continuing today. Though European populism turns out to have some minor historical precursors that date back all the way to the end of the 19^{th} century, these results confirm the sudden increase in political salience of populism from the 1990s onwards. Notably, both waves of discontent arose after a period of accelerating economic divergence, see figure 1a. Herfindahl indices of extremist and populist vote shares suggest that they are

[1] The literature tends to use 'populism', 'far right' and 'far left' interchangeably. This is because populism is described as 'thin-centered', lacking an ideology, while its distinctive anti-elitism is often compatible with political extremism. The proposed definition here therefore remains close to the existing literature.

[2] Guriev and Papaioannou (2022, p. 765) find that a *"continuous measure of populism is highly correlated with binary classifications"*, suggesting that a binary definition is less reductive than at first seems.

more spatially concentrated than mainstream vote shares, suggesting that the shift from mainstream to radicalist parties contributed to the recent surge in geographical political polarization in figure 1b. They are also more prevalent in unequal countries with high P80/P20 per capita GDP ratio's. Finally, a closer look at the three countries experiencing the highest radical vote shares in their most recent election, Hungary, Italy and the Czech Republic, reveals a strong correlation between the constituency-level population share in the bottom quintile of gridded per capita GDP and radical voting. All of these findings point to the existence of links between the economic and political landscapes in Europe.

I subsequently incorporate these empirical regularities in a dynamic spatial political economy model to investigate how well divergent economic development can explain the timing and location of political discontent. The model centers on an economy consisting of several locations that may differ in their productive amenities, such that more productive localities offer higher *ceteris paribus* wages, and are each endowed with exogeneous housing stocks, such that more populous locations face higher *ceteris paribus* housing costs. Production in each location is done by a representative firm producing a costlessly tradable final good using effective labor in a skill-neutral manner, such that it only depends on the total amount of effective labor in a location, not on its skill distribution. Locations also have non-productive ('residential') amenities to capture non-economic factors influencing each location's desirability, such as climate or recreational facilities, to ensure the model's amenability to quantitative analysis.[3] Productive amenities evolve over time according to an exogeneous law of motion that is increasing in the amount of human capital: locations with higher effective labor supplies also have a higher probability to obtain an upward shift in their productive amenity in the next period, resulting in divergent development.

Agents are freely mobile *between* but not *within* periods and differ both in their human capital endowments and their preferences over locations. In each period, they first choose their place of residence to maximize their expected utility from housing and final good consumption, implying that all workers of identical type obtain identical utility in equilibrium, though their nominal wages may differ. Productive locations offer higher wages and are better able to attract effective labor which, in turn, increases productivity growth, generating standard agglomeration effects. Finally, within each period and after location choices have been made, mainstream and radical political parties compete in an election to determine a flat distortive income tax to finance lump-sum income redistribution scheme.

To study the emergence of political discontent in this framework, I assume that a representative mainstream party favors the tax rate most preferred by the median tax voter. Defining political discontent as the within-period utility discrepancy between mainstream and individually optimal tax rates, I assume voters become alienated and susceptible to radicalism when a minimal threshold of discontent is reached. This then allows radical parties to challenge mainstream parties by targeting discontented voters that either favor

[3]Residential amenities can be calibrated to rationalize observed location choices unexplained by the model's economic variables, such as coastal population centers combining low wages with elevated housing prices.

more or less redistribution while neglecting the long-run, between-period impact on location choices and future welfare. This captures the common focus on short term protection policies and neglect of longer run implications observed in populist party manifestos by e.g. Guiso, Herrera, Morelli, and Sonno (2017) and Morelli, Nicolò, and Roberti (2021).

Following Desmet and Rossi-hansberg (2014), I make two crucial assumptions to ensure dynamic tractability. First, I assume that labor mobility is costless *between* periods such that location decisions become static problems that do not depend on (expected) spatial growth patterns in productive amenities. Second, I assume that government decisions are bounded by re-election constraints *within* each period, such that fiscal policy decisions also become static and only depend on current-period welfare. Hence, the only dynamic feature of the model is the exogenous and divergent growth in productive amenities.

This setup allows to derive the four main results of the paper. First, in sharp contrast to the benchmark case of *equal* development, which does not affect income distributions, fiscal preferences or political discontent, unequal development has two distinct - potentially offsetting - effects: a direct effect of magnifying income differences between leading and lagging regions, unambiguously fueling redistributive conflict and discontent; and an indirect effect of triggering labor mobility towards leading regions, which may or may not reduce nominal wage differences for agents of identical type.[4] The degree of labor mobility, in turn, crucially depends on human capital and redistributive taxation. Where labor mobility increases in human capital and primarily encourages high-skill agents to relocate towards more productive locations, contributing to wage polarization, redistributive income taxation discourages labor mobility by rendering spendable income less dependent on wage income and, hence, location. Under the mild assumption that labor mobility is sufficiently low relative to the growing wage differentials between regions, for example due to strong location preferences or housing unaffordability, the former effect dominates and divergent development produces the externality of increasing political dissatisfaction.

Second, the model predicts the emergence of a distinct geography of discontent, which is most likely to cluster in lagging regions. The main reason is that labor mobility is exclusively oriented towards leading locations, causing them to attain increasing electoral weight and influence on redistributive policy. The dwindling political clout of lagging regions makes them especially vulnerable to political discontent and makes their voters susceptible to radical parties offering political platforms that aim to increase redistribution.

Third, skill-biased labor mobility increases discontent in lagging regions by reducing their influence on redistributive policy while the positive tax base effect further increases their willingness to pay taxes. It also reduces the number of alienated voters by homogenizing the fiscal preferences of agents relocating towards more productive locations. This suggests that policies that aim to increase labor mobility have ambiguous effects on the electoral attractiveness of radical parties. Calibrated simulations confirm that endoge-

[4] In the extreme case of perfect labor mobility, the most productive location attracts the full labor force and the model becomes isomorphic to one of equal development.

nously increasing the housing supply in leading locations may temporarily increase the overall radical vote share by increasing discontent in lagging locations. Raising redistributive taxation to compensate lagging regions does the opposite, as it discourages labor mobility and risks increasing discontent in leading regions. Calibrated simulations confirm that increasing redistributive taxation to the level most preferred by the 75^{th} percentile instead of the median voter exerts a discouraging effect on (low-skill) labor mobility and may exacerbate rather than mitigate political frictions between lagging and leading regions.

Finally, when political discontent becomes sufficiently prevalent for radical parties to increase (expected) redistributive policies, labor mobility to leading regions reverses, a process which also hurts their productivity growth. Hence, the model is consistent with the often-observed decline in economic performance under populist rule (Dornbusch & Edwards, 1991; Karlson, 2024), as redistributive transfers make spendable income less dependent on location, causing the efficiency costs also described by Albouy (2009).

To validate the central model predictions that divergent development generates political externalities which mainly emerge if regional inequalities exceed a certain threshold and are likely to cluster in poorer constituencies, I leverage constituency-level differences in terrain ruggedness and distances to the historical Roman road network to isolate exogenous variation in their long-run economic development. Several studies suggest that Roman roads (Wahl, 2017; Dalgaard, Kaarsen, Olsson, & Selaya, 2022; De Benedictis, Licio, & Pinna, 2023) and flatter terrains (Nunn & Puga, 2012) persistently promote market access and economic growth, generating geographically uneven, path-dependent effects on economic development that do not depend on contemporary political circumstances. I find clear evidence that radical parties tend to be electorally more successful in poorer constituencies whose development is hindered by their remote location and rugged terrain, while they tend to underperform in richer constituencies with more favorable locations and flatter surfaces. The estimated effects sizes are large relative to those in the existing literature and imply, for instance, that a standard deviation decline in a constituency's relative per capita GDP over the period 1992-2023 was associated with an increase proportional to 1.27 standard deviations in the vote share of radical parties. Interestingly, these effects are primarily driven by populist rather than extremist parties, suggesting that the recent wave of populism also marked a spatial turn in political discontent. I also find suggestive evidence that turnout rates, an alternative proxy for political alienation, have been particularly depressed in poorer constituencies throughout the period 1847-2023.

The fact that estimated effect sizes considerably surpass those of the existing literature may be explained by the latter's focus on heterogeneity in local exposure to adverse economic shocks as a source of exogenous variation in economic circumstances: while the model confirms that adverse shocks which magnify spatial inequalities may produce slight increases in discontent, especially if they disproportionally affect lagging regions, the main source for discontent lies in persistent interregional differences in productivity growth, which are largely preexisting to adverse shocks and typically far exceed them in

magnitude. This paper instead uses exogenous variation in constituencies' overall productivities to suggest that the effect of economic circumstances is larger than previously thought and that they may not only have outcome but also explanatory significance, in the terminology of Margalit (2019). Moreover, while the existing empirical literature offers a consistent explanation for the geography of the current wave of populism, it cannot easily explain its timing, as adverse economic shocks have always been present. This paper advances and validates a specific explanation for this timing, namely that spatial inequalities first had to grow sufficiently large before they generate political externalities.

This analysis contributes the recent but fast-growing literature on the political economy of populism, which is excellently surveyed by Margalit (2019), Noury and Roland (2020) and Guriev and Papaioannou (2022). While these survey articles acknowledge the paucity of theoretical work, this analysis is most closely related to a small body of theoretical work that primarily focuses on the role of information asymmetry and elite capture. Acemoglu, Egorov, and Sonin (2013) focus on left-wing populism and develop a model where an incumbent politician can potentially be bribed by a right wing lobby and this leads honest politicians to pander to left wing populist policies when faced with a reelection constraint, to signal their independence to voters. Morelli et al. (2021) formulate a commitment theory of populism, where voters prefer politicians that precommit to populist platforms that are popular today when political trust is low, the perceived influence of interest groups is large and/or monitoring costs are high. Perhaps most closely related is the work by Pástor and Veronesi (2021), who develop a tractable dynamic heterogeneous-agent model, where globalization contributes to inequality and voter's dislike for inequality endogenously triggers a populist backlash against globalization. None of these papers attempt to analyze the distinct geography of populism and its link to economic geography.

It also contributes to a more extensive empirical literature which has largely advanced two competing explanations for the current wave of populism: economic insecurity and cultural backlash.[5] Economic arguments contend that economic insecurity in one way or another eroded voter's trust in incumbent parties and led them to vote for populist or extremist parties promising to break the status quo in their favor. Several empirical studies rely on a mix of electoral, survey and violent protest data to demonstrate that voters' differential exposure to the local labor market effects of adverse trade (Colantone & Stanig, 2018a, 2018b; Dippel, Gold, & Heblich, 2015; Malgouyres, 2017; Autor, Dorn, Hanson, & Majlesi, 2020), labor-saving technological (Caprettini & Voth, 2020), financial (Funke et al., 2016), migration (Tabellini, 2020) or other shocks causally contributed to a subsequent rise in political discontent. Guiso et al. (2017) and Guiso, Herrera, Morelli, and Sonno (2024) add that economic insecurity also lowers turnout rates if it feeds dis-

[5]This juxtaposition of the economic and cultural drivers of populism is a bit of a misnomer, as the cultural-based explanation also has deep economic roots: indeed, the intergenerational value change that drives the generational culture clash is thought to originate in the postwar rise in economic security in the West, which according to Inglehart (1971) caused a generational shift from materialist to postmaterialist values.

illusionment with traditional parties, further magnifying the pool of prospective voters for populist platforms. These effects may also be mediated by the welfare state, as more comprehensive and generous social protection and eligibility for EU structural funds have been found to dampen the prevalence of populism by bolstering economic security (Swank, 2003; Albanese, Barone, & de Blasio, 2022). Guiso, Helios, Morelli, and Sonno (2019) argue that Eurozone countries therefore are more sensitive to the political externalities of adverse economic shocks, because they are more constrained in their fiscal and monetary policy reactions in the face of such shocks. Cultural explanations do not deny the pertinence of economic explanations, but mostly consider them as triggers for deeper cultural grievances related to the (perceived) erosion of traditional social values of once privileged older generations, white men and the less educated. Inglehart and Norris (2016, 2019) are the most well-known advocates and use survey data to establish that cultural variables, such as authoritarianism and anti-migration sentiments, are better and more consistent predictors of self-reported populist voting than economic variables, such as unemployment and occupational class, which they interpret as evidence that cultural backlash offers the most parsimonious explanation for the recent surge in populism. Others have noted that technological advances in communication technology may also have played a role by allowing radical politicians to circumvent traditional mainstream media gatekeepers and more directly communicate with the electorate (Zhuravskaya, Petrova, & Enikolopov, 2020).

I complement this empirical literature in several ways. First, this is the first study that empirically validates a structural spatial political economy model clarifying how adverse shocks affect key policy variables such as redistributive taxation, labor mobility and political discontent. One major advantage is that calibration of the validated model would allow for improved counterfactual analysis that also accounts for general equilibrium effects. Second, I study the effects of persistent regional growth differences, rather than temporary adverse shocks, to evaluate the deeper economic roots of the prevalence of political discontent over longer time periods. The dominant focus on adverse shocks has recently been criticized by Margalit (2019) to conflate outcome with explanatory significance, as they typically leave a large proportion of the variance in populism unexplained, while the present focus on exogenous variation in longer run growth differentials may be better suited to identify the persistent effects of economics-based explanations and the remaining room for alternative explanations.[6] Third, I rely on a database that is unusually rich in terms of spatial resolution and temporal coverage, allowing me to improve both the power to detect (spatial) relations as well as their precision.

Finally, this paper also extends an existing literature that builds on Nordhaus (2006) and Henderson, Storeygard, and Weil (2012) to use satellite data on nighttime lights to proxy for (subnational) GDP when such data is unavailable or unreliable. First, I argue that their use as proxy for economic activity requires an assumption of constancy on the

[6] In other words, the empirical literature identifies how sudden and exogenous *changes* in ecomomic insecurity affect radicalism, but remains silent on their *level* effects.

GDP elasticity of nighttime light across time and space, without which changes in light emissions cannot be unambiguously related to changes in local economic output. This paper, in contrast, develops a method that first spatializes reported country GDP using nighttime lights yet subsequently harmonizes the estimates with available information on subnational GDP shares to account for first-order regional differences in the GDP elasticity of nighttime light. A validation check approximates the resulting estimation error of gridded GDP estimates by their discrepancy with the coarser alternative estimates in the G-ECON database of Nordhaus and Chen (2016) and finds them to be clustered around zero and lacking a consistent relation with the amount of nighttime light, suggesting that they are truly random and independent of the proxy variable. Second, using crossvalidation, I demonstrate that an alternative population-based proxy variable of market access achieves comparable accuracy and precision in approximating reported subnational GDP in several authoritative sources yet has much greater data availability, allowing to drastically expand the historical coverage of gridded GDP estimates.

As a cautious remark, the main objective of this paper is positive rather than normative. Several studies link the rise of populism to adverse welfare effects of political gridlock, isolationism and slowing economic growth, yet others like Rodrik (2018a) have suggested that some forms of populism may be beneficial if they serve to avoid elite capture of political institutions. This paper does not aim to take a normative stand on the desirability of political radicalism, but rather seeks to understand the extent to which its electoral presence can be traced back to developments in economic geography.

The remainder of this paper is structured as follows. Section 1 describes the data which is used in section 2 to present some stylized facts. These serve as input for the development of the spatial economy in section 3. Section 4 than uses a calibrated version of the model to derive several model implications. Section 5 develops a strategy to empirically validate the model's central political implications. Section 6 concludes.

2 Data: the Spatial Political Economy in Europe Database

To analyze long-run empirical relations between the economic and the political landscapes at a fine-grained spatial resolution, I construct a database covering 28 European countries between 1800 and 2020. This section provides a broad overview of the data construction and relegates the full details to the extensive data appendix A. To capture the economic landscape, I allocate reported population and GDP figures to a 1' × 1' gridded map in a way that is consistent with existing (sub)national data sources, as described in section 2.2. To capture the political landscape, I georeference the electoral constituencies and synthesize information on party categorizations covered in the 17^{th} version of the CLEA, as described in section 2.3. Section 2.4 than clarifies how economic variables can be linked to the political landscape using standard spatial aggregation methods. Before outlining the data construction, section 2.1 first provides a minimal working example.

2.1 Motivating example: the 2017 general election in France

The fact that political and economic variables are often reported for different administrative boundaries complicates an analysis of their empirical relations at the high levels of spatial resolution that are often dictated by theoretical models. The availability of gridded estimates can overcome this issue if they are sufficiently finegrained to be aggregated to arbitrary administrative boundaries using spatial weighting procedures. To illustrate the rationale behind this approach, I first consider the general election of 2017 in France. Figure 2 illustrates the issues by first showing the 96 European NUTS3 regions of France, the most spatially disaggregated level for which economic data is reported in Eurostat (2023a), and juxtaposing these with the 539 French (mainland) electoral constituencies for which voting data is reported in the 2017 general election. Figure 2c clarifies that the economic landscape is much coarser than the political landscape. One solution is to aggregate political data to the administrative level of the economic data, as is often done in the existing literature, but clearly this approach sacrifices a lot of granularity.

Figure 2: **The economic and political landscapes of France (2017)**

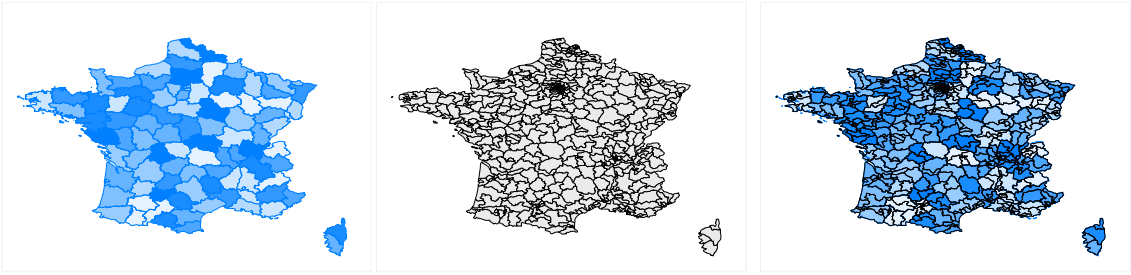

(a) 96 NUTS3 regions (b) 539 electoral constituencies (c) Overlap

Note: Figure 2a shows the French NUTS3 regions (version 2021), the most disaggregated administrative division for which economic data is reported in Eurostat (2023a). Figure 2b shows the geofreferenced electoral constituencies of the French general election in 2017. Figure 2c shows an overlap of the economic and political landscapes.

Therefore, the methodology presented below develops a procedure to spatialize national population and GDP figures to a spatial grid with a resolution of 5 arcminutes using proxy variables, which can subsequently be reaggragated to the level of the French constituencies. Figure 3 visualizes several intermediary steps: figure 3a depicts the subnational GDP shares reported at the NUTS3 level in Eurostat (2023a) used to harmonize the gridded GDP estimates; figure 3b shows gridded values for the Litpop proxy variable capturing population and nighttime light density as described in section 2.2; and figure 3c shows the resulting gridded per capita GDP estimates obtained by allocating reported French country GDP from Bolt and Van Zanden (2020) in proportion to the Litpop proxy of figure 3b and subsequent harmonization with subnational GDP shares in figure 3a.

Figure 3: **Spatializing reported (sub)national GDP for 2017 France**

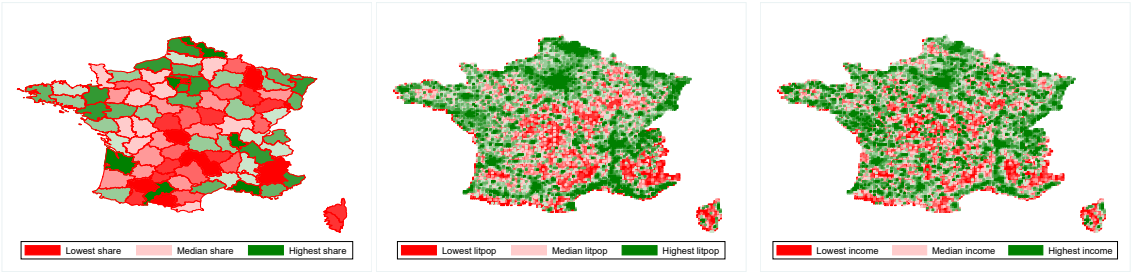

(a) Reported GDP (NUTS3) (b) Litpop (c) Gridded per capita GDP

Note: Figure 3a shows reported 2017 subnational GDP for French NUTS3 regions in Eurostat (2023a); figure 2b shows gridded Litpop for the year 2017; figure 2c shows the spatialized per capita GDP distribution.

Finally, under the assumption of uniform distributions within grid cells, these gridded population and GDP estimates can be reaggregated to the French electoral constituencies in proportion to their surface area using the georeferenced electoral districts discussed in section 2.3. Figure 4 shows the results of this exercise. First, 4a shows the spatial weight matrix of non-zero grid cell weights confirming that a large fraction of around one third of the grid cells in figure 3c are entirely aggregated to the level of electoral consituencies with a weight of 1. Of the 16198 grid cells making up France, 44% have spatial weights larger than .95 or smaller than .05, suggesting that the assumption of uniform population and GDP distributions within grid cells only matters for roughly half of the grid cells to produce accurate results. Moreover, section 2.2 and appendix A.1.3 suggest that spatial aggregation in proportion to surface area produces unbiased estimates of the true GDP in the other half of the grid cells. Finally, figure 4b visualizes the resulting per capita GDP estimates for the electoral constituencies, which now allow to analyze the relation between per capita GDP and electoral behavior in 539 rather than 96 spatial units.

Figure 4: **Per capita GDP estimates for the 2017 French constituencies**

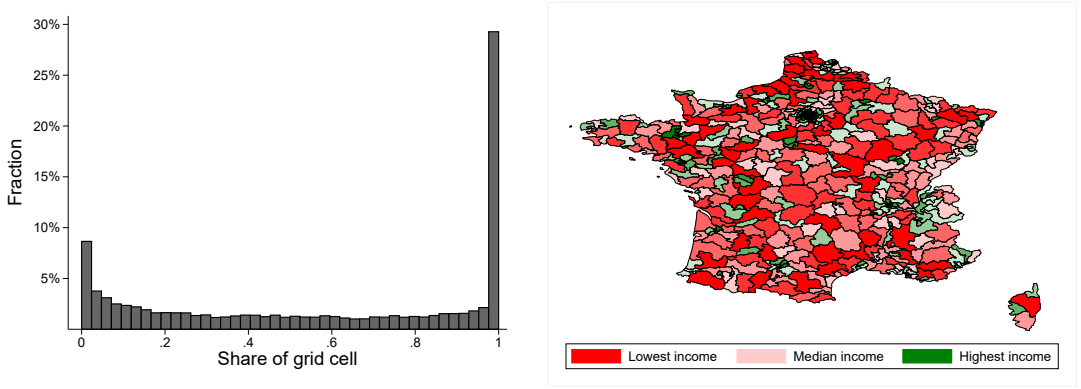

(a) Spatial grid weights, λ^Z

(b) Per capita GDP, $\hat{y}$

Note: Figure 4a shows the distribution of spatial weights to aggregate gridded estimates to the electoral constituencies for the 2017 general election in France. Figure 4b shows the corresponding per capita GDP estimates.

2.2 Data on the economic landscape

2.2.1 Gridded population

Gridded population estimates are derived from climate change research and are harmonized with authoritative (sub)national data sources, which also functions as a useful check on their accuracy. Denote the raw gridded population estimate for grid cell g in year t by $\hat{n}^{raw}_{g,t}$ and assume that the spatial grid is defined over a set of administrative borders that partitions grid cells into countries, indexed by $c \in \{1, \ldots, C\}$, each of which is potentially further subdivided into subnational regions, indexed by $r \in \{1, \ldots, R\}$. The administrative partitioning of each grid cell into countries is described by a cell-specific and time invariant $(1 \times C)$ national spatial weight vector, λ^c_g, with the c^{th} element describing the share of surface area of the grid cell that pertains to country c, $0 \leq \lambda_{g,c} \leq 1$. Similarly, the $(1 \times R)$ subnational spatial weight vector, λ^r_g, contains as r^{th} element the share of grid cell g's surface area in subnational region r, $0 \leq \lambda_{g,r} \leq 1$.

Harmonization of raw gridded population estimates with existing sources is then obtained by applying two multiplicative calibration weights, $\upsilon^c_{g,t}$ and $\upsilon^r_{g,t}$ as follows

$$\hat{n}_{g,t} = \underbrace{\upsilon^c_{g,t}\upsilon^r_{g,t}}_{\upsilon_{g,t}} \hat{n}^{raw}_{g,t} \left(\lambda^c_g, \lambda^r_g\right) \tag{1}$$

where the subnational calibration weight, $\upsilon^r_{g,t}$, is first calibrated to ensure that subnational population shares match reported subnational population shares in a target subnational source and the national calibration weight, $\upsilon^c_{g,t}$, is subsequently calibrated to ensure that total gridded country populations equal those reported in a target national source.

Four notes are in order before describing the data sources. First, to accommodate that subnational data sources usually have incomplete time and country coverage, $\upsilon^r_{g,t}$ is set to 1 in country-years without subnational but with national data, such that the corresponding

estimates are at least harmonized with available national data. Second, country-years without reported country population cannot be harmonized; their gridded population estimates are hindcasted from the last harmonized data point using the evolution in raw gridded population by setting $\upsilon^c_{g,t} = \upsilon^c_{g,\bar{t}}$ with $\bar{t}$ the earliest available year in the national target source. Third, grid coarsity requires spatial aggregation of calibration weights for grid cells belonging to more than one (sub)national unit, see equations (2A) and (4A). This induces small discrepancies between estimated and reported population shares, especially for small (sub)national regions covering few grid cells. Nevertheless, table 1 shows that calibration weights considerably reduce these discrepancies to become negligible. Fourth, national calibration weights harmonize gridded population estimates with total country population even though the gridded estimates exclude some overseas territories. Although excluded territories usually represent only a small fraction of country population, e.g. the population of the overseas territories represented 3.3% of the French population in 2022, this may explain some discrepancies between gridded and reported country populations.

To implement this methodology, gridded population estimates for the period 1800-2023 are taken from the HYDE database version 3.3 at a resolution of 5 arc minutes. The estimates are available at a yearly frequency from 1950 onwards and at a decennial frequency before that. Assuming population evolves gradually over time, as in the other sources, missing population observations before 1950 are linearly interpolated at the grid cell level. The Maddison database (Bolt & Van Zanden, 2020, MDB) serves as the national target source and is extended to 2020 using country population figures in ARDECO (2022). The subnational target sources include the available NUTS3 population figures from Eurostat (2023b, ES) and ARDECO (2022, AR) and the historical estimates in Rosés and Wolf (2019, 2021a, 2021b, RW). Data availability by (sub)national data source is summarized in appendix table A1 while appendix table A2 illustrates the accuracy of the uncalibrated gridded population estimates and the gain in accuracy from the application of calibration weights for each of the (sub)national population sources.

To obtain the final calibrated gridded population estimates, I use the most fine-grained calibration weights available and define $\upsilon^r_{g,t}$ in equation (1) as follows:

$$\upsilon^r_{g,t} = \begin{cases} \upsilon^{r,AR}_{g,t} & \text{if } t \in \mathbf{T}^{AR}_g \\ \upsilon^{r,ES}_{g,t} & \text{if } t \notin \mathbf{T}^{AR}_g \;\&\; t \in \mathbf{T}^{ES}_g \\ \upsilon^{r,RW}_{g,t} & \text{if } t \notin \mathbf{T}^{AR}_g \;\&\; t \notin \mathbf{T}^{ES}_g \;\&\; t \in \mathbf{T}^{RW}_g \\ 1 & \text{if } t \notin \mathbf{T}^{AR}_g \;\&\; t \notin \mathbf{T}^{ES}_g \;\&\; t \notin \mathbf{T}^{RW}_g \end{cases} \tag{2}$$

with $\mathbf{T}^{SS}_g$ a vector containing the years for which population in subnational source SS is reported for each country covering grid cell g in year t, such that $\int_{r=1}^{R} \upsilon^{r,SS}_{g,t} = 1$.

Table 1 assesses the reliability of this procedure by reporting the correlation and normalized Root Mean Squared Prediction Error (NRMSPE) of the (un)calibrated gridded population estimates and the population figures in various (sub)national sources. In addi-

tion to their quasi-perfect correlation coefficients, even uncalibrated gridded population is fairly consistent with the reported population figures in the (sub)national target sources with NRMSPE's amounting to just 5.5% to 24.2% of the standard deviation of population in the target source. Nevertheless, calibration further improves the consistency by considerably reducing the normalized RMSPE further. Appendix A.1.2 provides further validation checks which confirm the reliability of this approach.

Table 1: **Calibrated gridded population: estimation accuracy**

Target	*Spatial unit*	*Coverage*	*# C (# R)*	*N*	**Uncalibrated**		**Calibrated**	
					ρ	$NRMSPE$	ρ	$NRMSPE$
Bolt and Van Zanden (2020)	Countries	1800-2023		5072	1	.055	1	.001
Rosés and Wolf (2021b)	Regions ($\approx$ NUTS2)	1900-2015	16 (172)	19902	.97	.242	1	.035
Eurostat (2023b)	NUTS3 regions	1990-2023	28 (1356)	33059	.99	.153	1	.077
ARDECO (2022)	NUTS3 regions	1960-2023	28 (1346)	86144	.98	.196	1	.078

Note: This table summarizes the correlation (ρ) and normalized Root Mean Squared Prediction Error ($NRMSPE$) of (un)calibrated gridded population estimates and reported population figures in several (sub)national target sources, using the standard deviation of population in the target source as normalizing factor. It also details the number of countries, C, subnational regions, R, and observations, N. Calibrated population is computed from equation (1) with the calibration weights from equation (2).

2.2.2 Gridded GDP

Gridded GDP estimates are obtained by extending existing methodologies to spatially disaggregate reported country GDP using proxy variables and subsequently harmonizing them with several authoritative (sub)national sources, which is also shown to serve as a useful way to account for spatial differences in the GDP elasticity of the proxy variable. I start from the assumption that every populated grid cell produces output, $y_{g,t}$. While country and subnational output, $Y_{c,t} = \sum_{g=1}^{G} \lambda_{g,c} y_{g,t}$ and $Y_{r,t} = \sum_{g=1}^{G} \lambda_{g,r} y_{g,t}$, are reported in (sub)national sources for a set of C countries and R regions, gridded GDP is unobserved and needs to be estimated. I assume, moreover, that there exists a grid-level proxy variable, $z_{g,t}$, that is correlated with output according to the following accounting identity[7]

$$y_{g,t} = \beta_{g,t} z_{g,t} \tag{3}$$

where $\beta_{g,t}$ denotes the time-varying grid-level output elasticity of the proxy variable.

In the empirical application, I rely on two proxy variables that are often used and that are available at the desired spatial resolution. For the more recent period, I use satellite-based measurements of nighttime lights (NTL) and adjust them for the potential issues of top- and bottom-coding as well as spatio-temporal variations in the output elasticity of NTL. As satellite data is unavailable before 1992, for the preceding period, I rely on a population-based measure of market access (PMA). Population density is regularly used as a proxy for local economic performance in historical studies, when information on actual output levels is unavailable, under the assumption that population size reflects the capacity of local economies to produce economic surplus for their residents (Bosker, Buringh, & van Zanden, 2013; Acemoglu, Johnson, & Robinson, 2002). They have also been used in

[7] Henderson et al. (2012) found a linear functional form appropriate for the nighttime light proxy.

more recent periods in cases when the available economic data is restricted, see e.g. Baum-Snow, Brandt, Henderson, Turner, and Zhang (2015). Table 3 below further bolsters the proxy reliability of PMA and shows that it has comparable and often stronger predictive accuracy for reported (sub)national GDP in several sources in comparison to NTL.

I nevertheless assume that $z_{g,t}$ may be subject to measurement error, for example due to the cleaning of satellite images of NTL to remove lights from flares or volcanoes. As a result, we have to rely on a set of $M \in [\,1, 2, \dots\,)$ measurements of $\hat{z}^m_{g,t}$, indexed by $m \in M$, with each measurement subject to additive measurement error as follows

$$\hat{z}^m_{g,t} = z_{g,t} + \epsilon^{z^m}_{g,t} \tag{4}$$

with $\epsilon^{z^m}_{g,t}$ the mean-zero error due to mismeasurement in the proxy variable.

Finally, the grid-level elasticities $\beta_{g,t}$ are also unknown and have to be estimated too. The output elasticity of NTL, for instance, likely differs across time and space due to differences in the sectoral composition, e.g. because electricity-intensive production processes emit more light.[8] Assume that the available estimate for $\beta_{g,t}$ is of the form

$$\hat{\beta}_{g,t} = \beta_{g,t} + \epsilon^{\beta}_{g,t} \tag{5}$$

with $\epsilon^{\beta}_{g,t}$ the mean-zero grid-level deviation from the estimated output elasticity, $\hat{\beta}_{g,t}$.

Subsituting these expressions for $\hat{z}_{g,t}$ and $\hat{\beta}_{g,t}$ in equation (3) yields

$$\hat{y}_{g,t} = \left(\beta_{g,t} + \epsilon^{\beta}_{g,t}\right) \underbrace{\sum_{m=1}^{M} \omega_{m,g,t} \left(z^m_{g,t} + \epsilon^{z^m}_{g,t}\right)}_{\text{weighted average value for proxy } z} \tag{6}$$

with $0 \leq \omega_{m,g,t} \leq 1$ the linear weights aggregating information from M measurements of proxy z in grid cell g at time t, where $\sum_{m=1}^{M} \omega_{m,g,t} = 1$. Denoting the weighted average value for the proxy variable with $\bar{z}_{g,t} = \sum_{m=1}^{M} \omega_{m,g,t} \hat{z}^m_{g,t}$ and slightly rewriting yields that

$$\hat{y}_{g,t} = \beta_{g,t}\bar{z}_{g,t} \underbrace{+\beta_{g,t}\bar{\epsilon}^{\bar{z}}_{g,t} + \bar{z}_{g,t}\epsilon^{\beta}_{g,t} + \epsilon^{\beta}_{g,t}\bar{\epsilon}^{\bar{z}}_{g,t}}_{\text{Estimation error, } \epsilon^{y}_{g,t}} \tag{7}$$

Based on the assumptions of the error structure, the bias in gridded GDP estimates thus converges to 0 as the number of grid cells in the analysis gets large, $G \to \infty$, if the measurement error in the proxy variable, $\bar{\epsilon}^{\bar{z}}_{g,t}$, is independent of the output elasticity of the proxy variable, $\beta_{g,t}$; the estimation errors in the output elasticities of the proxy variable, $\epsilon^{\beta}_{g,t}$, are unrelated to the values of the proxy variable, $\bar{z}_{g,t}$; and the measurement errors are independent of each other. In what follows, I assume that the mismeasurement in the proxy variables is truly random and hence unrelated to any other factors such that $E\left(\bar{\epsilon}^{\bar{z}}_{g,t} \mid \beta_{g,t}\right) = E\left(\bar{\epsilon}^{\bar{z}}_{g,t} \mid \epsilon^{\beta}_{g,t}\right) = E\left(\bar{\epsilon}^{\bar{z}}_{g,t}\right) = 0$. This assumption is in line with much of the

[8] In this light, Henderson et al. (2012) state that *"the increased production of steel and software both represent additions to GDP, but the former results in a larger increase in visible light"*.

existing literature on using satellite-based measurements of NTL as a proxy for economic activities, where the measurement error in NTL is usually modelled as mean-zero noise. Under this assumption, the main source of bias stems from the potential correlation of the measurement error in the output elasticity and the proxy variable, $E\left(\bar{z}_{g,t}\epsilon^{\beta}_{g,t}\right)$. Appendix figure A16 performs an indirect test of the bias by approximating the estimation error, $\epsilon^{\beta}_{g,t}$, by the discrepancy between the gridded GDP estimates and the coarser alternative estimates in Nordhaus and Chen's (2016) G-ECON database, finding no evidence of their correlation with the NTL proxy variable. This suggests that $\hat{y}_{g,t}$ is an unbiased predictor of local economic output and that it is reasonable to also assume that $E\left(\bar{z}_{g,t}\epsilon^{\beta}_{g,t}\right) = 0$.

To minimize the (variance of the) estimation error in the output elasticity of the proxy, I exploit (sub)national information to calibrate $\beta_{g,t}$ such that gridded GDP is maximally consistent with (sub)national data in authoritative sources. Following equation (3), gridded GDP estimates can be obtained by disaggregating reported national GDP to grid cells in proportion to the sum of their effective proxy values, adjusted for their grid-specific output elasticities. To harmonize the gridded output estimates with the available (sub)national information, two multiplicative calibration weights, $\kappa^{c}_{g,t}$ and $\kappa^{r}_{g,t}$, are applied

$$\hat{z}_{g,t} = \underbrace{\kappa^{c}_{g,t}\kappa^{r}_{g,t}}_{\kappa_{g,t}\approx\hat{\beta}_{g,t}} \underbrace{\sum_{m=1}^{M}\left(\omega^{*}_{m,g,t}\hat{z}^{m}_{g,t}\right)}_{\hat{\bar{z}}_{g,t}} \tag{8}$$

Note that $\kappa_{g,t}$ accounts for observed differences in the relation between the aggregated proxy and (sub)national GDP to account for first-order spatio-temporal differences in the (sub)national output elasticity of the proxy variable, $\hat{\beta}_{g,t}$, based on the available data.

In practice, I start by determining the weights for different measurements of the proxy variable if $M > 1$. Starting from the simplifying assumption that the proxy variable is sufficiently strongly correlated with the outcome variable that $\beta_{g_1,t} \approx \beta_{g_2,t}$ for any $\{g_1, g_2\} \in c$, relative importance weights for each measurement m, $\omega^{*}_{m,g,t}$, are determined to minimize the Mean Absolute Error (MAE) between disaggregated and reported subnational GDP shares in each country-year when $\kappa^{c}_{g,t} = \kappa^{r}_{g,t} = 1$. This assumption is in line with most of the existing literature using NTL as economic proxy, which typically abstracts from spatio-temporal differences in the output elasticity of NTL and demonstrates that even unadjusted measurements of NTL are good predictors of local economic activities, and is further supported by the validation checks in appendix A.1.3. Subsequently, the subnational calibration weight, $\kappa^{r}_{g,t}$, is first calibrated such that subnational gridded GDP shares in total gridded country GDP match those reported in a target subnational source and the national calibration weight, $\kappa^{c}_{g,t}$, is subsequently calibrated to equalize gridded country GDP with reported country GDP in a national target source. This serves to account for any remaining discrepancies between gridded and reported subnational output shares that may emerge from spatial differences in the output elasticity of the proxy variable, $\beta_{g,t}$.

Five notes are in order before describing the data. First, to accommodate that subnational data sources usually have incomplete time and country coverage, $\kappa^r_{g,t}$ is set to 1 in country-years without subnational but with national data, such that the corresponding estimates are at least harmonized with available national data. Second, as the estimation procedure essentially disaggregates reported economic output, gridded estimates cannot be obtained for country-years lacking GDP figures in Bolt and Van Zanden (2020). Note, however, that empirical analysis could still be done on the values of these proxy variables directly, under the common assumption of constant outcome elasticity. Third, grid coarsity requires spatial aggregation of calibration weights for grid cells belonging to more than one (sub)national unit, see equations (9A) and (11A). This induces small discrepancies between estimated and reported GDP, especially for small (sub)national regions covering few grid cells. Nevertheless, table 2 shows that calibration weights considerably reduce these discrepancies to become negligible. Fourth, national calibration weights harmonize gridded GDP estimates with reported country GDP even though the grid excludes some overseas territories. Although excluded territories usually represent only a small fraction of country GDP, e.g. the GDP of the overseas territories represented 1.8% of French GDP in 2021, this may explain some discrepancies between gridded and reported country GDP. Fifth, harmonization with country GDP in the Maddison database also ensures their cross-country comparability, as GDP is expressed in real terms there (2011 US dollars).

To implement this methodology, for the recent period, I obtain stable NTL from the DMSP from the National Oceanic and Atmospheric Administration (2013) for the maximal available period of 1992-2013 and the extended VIIRS-like NTL data constructed from a cross-sensor calibration of DMSP data for the period 2000–2012 and a composition of monthly VIIRS NTL data for the period 2013–2023 from Chen et al. (2021a).[9] I first deal with the known issue of bottom-coding by imputing missing NTL values in populated grid cells by multiplying gridded population with the nearest available measurement of per capita NTL and otherwise with the minimal contemporaneous per capita values of NTL in the NUTS3-region or the country. I subsequently deal with top-coding by computing Litpop estimates, $Litpop^s_{g,t} = \hat{n}_{g,t} NTL^{s,i}_{g,t}$, which have been shown to improve the accuracy of GDP disaggregation (Wang & Sun, 2022). Finally, I account for grid-level differences in the output elasticities of NTL between both sources by extending Litpop trajectories in each source based on their predicted growth rates from their simple bivariate correlation.

These satellite-based proxies for local economic performance are complemented with a population-based measure of market access, PMA, that is available for much longer time spans and is computed from the gridded population estimates as follows:

$$PMA_{g,t} = \hat{n}_{\tilde{g},t}\Big(\sum_{\tilde{g}=1}^{G} \frac{\hat{n}_{\tilde{g},t}}{d_{g,\tilde{g}}}\Big) \quad , \; d_{g,g} = 1 \tag{9}$$

[9] As explained in Kim, Gibson, and Boe-Gibson (2023, p. 4-5), in the DMSP, 'stable' *"means that ephemeral lights, from sources such as fires and gas flaring, are removed before the annual composite is built up"*.

with $d_{g,\tilde{g}}$ the distance in km between grid cell g and grid cell $\tilde{g}$. Mirroring the computation of Litpop, inverse spatial weighted population is multiplied by the grid cell's own population estimate to ensure that if two grid cells have access to an equally large spatially weighted population, the most populous grid cell attains a higher measured PMA. Appendix figure A41 shows the resulting gridded PMA estimates for selected years.

Bolt and Van Zanden (2020, MDB) serves as the main national target source for real country GDP and is extended to 2023 using the country GDP figures in ARDECO (2023). The main subnational target sources are NUTS3 GDP in ARDECO (2023, AR) and regional GDP in in Rosés and Wolf (2019, 2021a, 2021b, RW). Data availability by (sub)national data source is summarized in appendix table A3.

Before discussing the construction of the final gridded GDP estimates, table 2 illustrates the accuracy of the (un)calibrated gridded GDP estimates obtained from disaggregating reported country GDP using the proxy variables in the third column, and the gain in accuracy from the application of calibration weights to harmonize them to each of the (sub)national target sources in accordance with equation (8). Harmonization with the national target is quasi complete, with perfect correlation coefficients for all proxy variables and normalized Root Mean Squared Errors (NRMSPE) close to 0. Even when proxy variables are only calibrated to sum to country GDP, their predictive accuracy for the distribution of GDP across subnational units is fairly accurate with correlation coefficients ranging from .97 to .99 and RMSPE's ranging from .137 to .254 standard deviations of subnational GDP in the target source. Adding calibration weights for subnational target sources drastically improves the accuracy to quasi-perfect correlations and considerable reductions in NRMSPE. The most important takeway from table 2, however, is visible in the grey lines, which indicate that the PMA proxy has equal or improved accuracy over the NTL proxy, when accuracy is measured by the common NRMSPE with reported (sub)national GDP. Hence if NTL is considered an appropriate proxy for local economic output, by this metric, PMA should be too, drastically increasing their historical coverage.

Table 2: **Calibration of gridded GDP: estimation accuracy**

National target	*Subnational target*	*Proxy*	*Coverage*	*# C (# R)*	**National target**					**Subnational target**				
						Uncalibrated		**Calibrated**			**Uncalibrated**		**Calibrated**	
					N	ρ	*NRMSPE*	ρ	*NRMSPE*	*N*	ρ	*NRMSPE*	ρ	*NRMSPE*
Bolt and Van Zanden (2020)	Eurostat (2023b)	Litpop	2000-2022	26 (1165)	640	.96	.633	1	.002	25340	.98	.229	1	.05
		PMA	2000-2022	26 (1165)	640	.98	.267	1	.002	25340	.97	.238	1	.051
Bolt and Van Zanden (2020)	ARDECO (2022)	Litpop	1993-2023	*27 (1344)*	863	.95	.686	1	.002	41664	.98	.254	1	.055
		PMA	1993-2023	27 (1344)	863	.96	.267	1	.002	41664	.97	.235	1	.055
		PMA	1980-2023	27 (1344)	1222	.96	.293	1	.002	57376	.97	.23	1	.059
Bolt and Van Zanden (2020)	Rosés and Wolf (2021b)	Litpop	1993-2015	*16 (172)*	644	.97	1.033	1	.002	3956	.99	.185	1	.008
		PMA	1993-2015	16 (172)	644	.87	.465	1	.001	3956	.99	.137	1	.005
		PMA	1900-2015	16 (172)	2745	.87	.736	1	.001	19952	.99	.171	1	.006
Bolt and Van Zanden (2020)		Litpop	1993-2023	*28*	863	.97	.456	1	.001					
		PMA	1993-2023	28	863	.87	.315	1	.002					
		PMA	1800-2023	28	4682	.87	.571	1	.001					

Note: This table summarizes the correlation (ρ) and normalized Root Mean Squared Prediction Error ($NRMSPE$) of (un)calibrated gridded GDP estimates and reported GDP in several (sub)national target sources and for two proxy variables, using the standard deviation of GDP in the target source as normalizing factor. Uncalibrated estimates are standardized prior to computing the NRMSPE for the national target, to bring them to the same scale. The number of countries, C, subnational regions, R, and observations, N, are also reported. Statistics for the PMA-proxy in grey rows are restricted to the subsample for which the $Litpop$-proxy is also available, to allow clean comparisons of predictive accuracy. Gridded GDP is computed from equation (8) with the calibration weights from equation (10).

Motivated by this, the final estimates are obtained using the most fine-grained combinations of calibration weights and proxies and defining $v^r_{g,t}$ in equation (8) as:

$$\{\kappa^r_{g,t}, \hat{\tilde{z}}_{g,t}\} = \begin{cases} \left\{\kappa^{r,AR}_{g,t}, \hat{Litpop}_{g,t}\right\} & \text{if } t \in \mathbf{T}^{AR,LP}_g \\ \left\{\kappa^{r,AR}_{g,t}, \hat{PMA}_{g,t}\right\} & \text{if } t \notin \mathbf{T}^{AR,LP}_g \ \& \ t \in \mathbf{T}^{AR,PMA}_g \\ \left\{\kappa^{r,RW}_{g,t}, \hat{PMA}_{g,t}\right\} & \text{if } t \notin \mathbf{T}^{AR,LP}_g \ \& \ t \notin \mathbf{T}^{AR,PMA}_g \ \& \ t \in \mathbf{T}^{RW,PMA}_g \\ \left\{\kappa^{r,MDB}_{g,t}, \hat{PMA}_{g,t}\right\} & \text{if } t \notin \mathbf{T}^{AR,LP}_g \ \& \ t \notin \mathbf{T}^{AR,PMA}_g \ \& \ t \notin \mathbf{T}^{RW,PMA}_g \ t \in \mathbf{T}^{MDB,PMA}_g \\ \{1, \varnothing\} & \text{if } t \notin \mathbf{T}^{pma,MDB}_g \end{cases} \tag{10}$$

with $\mathbf{T}^{SS,P}_g$ a vector containing years with data on GDP in subnational source SS ánd proxy P for each country covering grid cell g in year t, such that $\int_{r=1}^{R} \kappa^{r,SS,P}_{g,t} = 1$.

Table 2 evaluates the accuracy of the gridded GDP estimates by reporting their correlation and NRMSPE with the (sub)national GDP figures reported in the target sources listed in the first column. Gridded GDP estimates correlate perfectly with reported (sub)national GDP figures in all sources and attain NRMSPE's that are similar to those of the gridded population estimates reported in table 1. Appendix A.1.3 reports additional cross-validation checks confirming that both proxy variables are unbiased predictors of (sub)national economic performance in several authoritative data sources. Notably, appendix figure A16 shows that the discrepancy between these gridded GDP estimates and the coarser estimates contained in Nordhaus and Chen's (2016) G-ECON database cluster around zero and that there is no consistent relation between these estimation errors and the value of the proxy variable, further suggesting that estimation errors are truly random.

Table 3: **Calibrated gridded GDP: estimation accuracy**

Target	*Spatial unit*	*Coverage*	*# C (# R)*	*N*	ρ	*NRMSPE*
Eurostat (2023b)	NUTS3 regions	2000-2022	26 (1165)	25340	1	.053
ARDECO (2022)	NUTS3 regions	1980-2023	27 (1344)	57376	1	.071
Rosés and Wolf (2021b)	Regions ($\approx$ NUTS2)	1900-2015	16 (172)	19952	1	.047
Bolt and Van Zanden (2020)	Countries	1800-2023		4682	1	.002

Note: This table summarizes the correlation and normalized Root Mean Squared Prediction Error ($NRMSPE$) of the gridded GDP estimates and (sub)national GDP reported in the target sources mentioned in the first column. Gridded GDP is computed from equation (8) with the calibration weights as determined in equations (9A) and (11A).

2.3 Data on the political landscape

2.3.1 Cleaning and correcting electoral data in the CLEA

To construct country- and election-specific time series of constituency-level party vote shares for national elections to the lower house, I mainly rely on the 17^{th} release of the CLEA. As spatial analysis can only be conducted on territorial constituencies, I first eliminate non-territorial constituencies such as constituencies of 'postal' or 'foreign' voters. Moreover, as the analysis focuses on the European mainland, I also eliminate non-European constituencies such as *Greenland* in Denmark or the *départements d'outre-mer* in France, even if georeferenced constituencies are available in the database. In terms of political parties, I only collect information on specific, known parties ignoring votes for

'unknown', 'other' or 'miscellaneous' parties as well as invalid votes. In case of plural voting, where possible, I aggregate votes according to the 'one man, one vote'-principle while only taking into account the first-ballot results during multiple-ballot elections. Additionally, in uncontested elections, I assume that the winning party received all valid votes expressed in the constituency and otherwise approximate this by multiplying the average fraction of valid votes in total eligible votes in the other available constituencies in the country with the number of eligible votes in the constituency. Appendix table A6 lists a number of corrections and extensions to CLEA to ensure data quality and completeness.

2.3.2 Georeferencing electoral constituencies in the CLEA

I rely on a wide range of sources to construct georeferenced maps with a preference for official sources, though their scarcity implies that the majority of maps are derived from Wikipedia. One complication is that some secondary sources do not report constituency names on the map: in such cases, names were added by first geocoding all constituency names in CLEA, which typically refer to cities or regions, to allocate unique matches to the respective georeferenced constituencies and subsequently conducting a desk search to allocate missing and conflicting constituency names. As electoral boundaries typically span several elections, with few exceptions, the same georeferenced map covers multiple elections in the CLEA. The current database provides a total of 689 georeferenced maps between 1848 and 2023, see table 4 for a broad summary. Appendix A.2.1 gives a more detailed breakdown of the sources and construction and provides the minimal working example of georeferencing the electoral constituencies of the 1907 general German election.

Table 4: **Historical coverage of georeferenced electoral constituencies**

Country	#	*CLEA elections*	*Missings*	*Country*	#	*CLEA elections*	*Missings*
Austria	26	1919-2013	0	Latvia	8	1995-2018	0
Belgium	67	1847-2019	0	Lithuania	8	1992-2020	0
Bulgaria	14	1991-2023	0	Luxembourg	23	1919-2018	0
Czech Republic	10	1990-2021	0	Netherlands	39	1886-2021	1 (2021)
Denmark	70	1849-2019	0	Norway	37	1882-2021	11 (1882-1915)
Estonia	8	1992-2019	0	Poland	9	1991-2019	0
Finland	39	1907-2023	0	Portugal	17	1975-2022	0
France	12	1910-2017	0	Romania	7	1990-2016	1 (2012)
Germany	41	1871-2017	0	Slovakia	10	1990-2020	0
Greece	30	1926-2019	0	Slovenia	7	1996-2018	0
Hungary	9	1990-2022	0	Spain	15	1977-2019	0
Iceland	48	1874-2017	0	Sweden	49	1872-2022	13 (1872-1905)
Ireland	31	1922-2020	0	Switzerland	50	1848-2019	0
Italy	21	1919-2018	0	UK	48	1832-2019	38 (1832-1979)

Note: this table reports the number (#) of elections and their time coverage for each European country in the 17^{th} release of the Constituency-Level Electoral Archive (Kollman et al., 2023). The last column highlights the elections for which no georeferenced constituencies could be constructed. Further information is given in appendix A.2.

2.3.3 Classifying political parties in the CLEA

Political parties in the CLEA are classified by linking their names to existing classification systems and their ideological positions on Wikipedia. As political parties are not consistently named, e.g. due to language differences, their names are first harmonized by identifying their associated Wikipedia pages using keyword search. They are subsequently linked to ideology tags and political positions scraped from Wikipedia and two existing party classification systems of Inglehart and Norris (2019) and Rooduijn et al.'s (2019) PopuList. While the latter two already classify parties on the populist and far left/right dimensions, in Wikipedia, left populist parties are identified with the ideological tag of *'left wing populism'* or the combined ideological and positional tags of *'populist'* and *'(far) left'*. A similar procedure defines centre and right populist parties. Far left parties are identified with the ideological tags of *'(euro)communism'*, *'marxism'*, *'trotskyism'*, *'stalinism'* and *'collectivism'* or with the positional tag *'far left'*. Far right parties are identified with the ideological tags of *'far right'*, *'neo-nazism'*, *'antisemitism'* and *'nazism'* or with the positional tag *'far right'*. Separatist parties are solely identified from Wikipedia with the ideological tag of *'separatism'*, as it is the only source classifying parties on this dimension. The umbrella category of 'populist' parties contains the sets of 'left', 'centre' and 'right' populist parties while 'extremist' parties are either 'far left', 'far right' or 'separatist'. Radical parties are defined as either populist, extremist or a combination of both.

In practice, the baseline analysis relies on a majority definition which considers a political party as (left/right/centre) populist, separatist, far left or far right if classified as such in at least two sources. As Inglehart and Norris (2019) and Rooduijn et al.'s (2019) classification systems lack historical coverage before 1989 and party coverage among smaller parties, an alternative definition classifies parties from the union of all three classifications, requiring them to be classified by at least one source. A full overview of the synthesized classification by country and party is provided in appendix table A8, while table 5 summarizes the number of populist, extremist and hybrid (populist and extremist) political parties in the CLEA by country. In most countries, extremist parties outnumber populist ones, consistent with the notion that the rise of populism is a recent phenomenon. These dimensions also seem far from being mutually exclusive, as several parties are classified both as extremist and populist. In raw numbers, radical parties have been most prevalent in Italy and Spain while they are least frequent in Sweden, Norway and Luxembourg.

2.4 Linking the economic and the political landscapes

The georeferenced maps allow to determine the election-specific $(1 \times Z)$ spatial weight matrix for each country c and each election year t, $\lambda^{Z}_{g,c,t}$, with the g^{th} element describing the share of surface area of grid cell g belonging to constituency ζ. Assuming uniform population and GDP distributions within grid cells, constituency-level estimates for population and GDP can than simply be computed as $\hat{N}_{\zeta,t} = \sum_{g=1}^{G} \lambda^{Z}_{g,c,t} \hat{n}_{g,t}$ and $\hat{Y}_{\zeta,t} = \sum_{g=1}^{G} \lambda^{Z}_{g,c,t} \hat{z}_{g,t}$,

Table 5: **Extremist and populist parties by country in CLEA**

Country	*P*	*E*	*P+E*	*R*	*Country*	*P*	*E*	*P+E*	*R*
Austria	8	8	2	14	Latvia	11	4	2	13
Belgium	9	13	8	14	Lithuania	11	9	3	17
Bulgaria	23	19	12	30	Luxembourg	2	2	1	3
Czech Republic	13	11	4	20	Netherlands	3	5	1	7
Denmark	3	13	3	13	Norway	1	2	0	3
Estonia	5	4	2	7	Poland	9	15	7	17
Finland	8	14	4	18	Portugal	9	10	6	13
France	5	11	4	12	Romania	9	8	5	12
Germany	10	22	5	27	Slovakia	15	9	7	17
Greece	13	27	10	30	Slovenia	10	4	2	12
Hungary	18	21	14	25	Spain	26	81	21	86
Iceland	2	4	1	5	Sweden	4	5	3	6
Ireland	0	7	0	7	Switzerland	8	15	6	17
Italy	17	33	7	43	UK	10	27	6	31

Note: The number of populist, P, extremist, E, hybrid, $P + E$, and radical , R, parties in the CLEA by country.

with $\hat{n}_{g,t}$ and $\hat{z}_{g,t}$ as defined in equations (1) and (8).[10]

3 Stylized facts

This section utilizes the Spatial Political Economy in Europe Database to analyze historical trends in the economic and political landscapes in Europe at an unusually fine spatial resolution and over an unusually long time frame. It first provides evidence that there were marked geographical differences in economic growth over the past two centuries, consistent with the notion of divergent economic development. It then provides electoral evidence that Europe experienced two waves of political discontent which roughly coincided with periods of accelerated economic divergence. Finally, it presents empirical evidence that discontent mainly surfaced in the most unequal countries. These stylized facts form the basis for the development of the dynamic spatial political economy model in section 3.

3.1 The economic landscape

Figure 5 shows the spatial cumulative distribution of gridded population and GDP for every available half-century between 1800 and 2020, depicting more recent data points in darker shades of grey. Both figures suggest that economic activities grew more spatially concentrated over time. While the top population quintile represented 67% of the population in 1800, it covered 84% in 2000. The trend is even more pronounced for GDP, where the top quintile covered 69% of total GDP in 1800 yet around 94% in 2000. This is consistent notion of persistent regional growth differentials in Europe.

[10]Note that the assumptions of uniform population and GDP distributions within grid cells are warranted by the validation checks in section A.1.2 and A.1.3, as similar assumptions do not lead to systematic discrepancies between aggregated and reported subnational data from several authoritative sources.

Figure 5: **Spatial cumulative distribution functions in selected years**

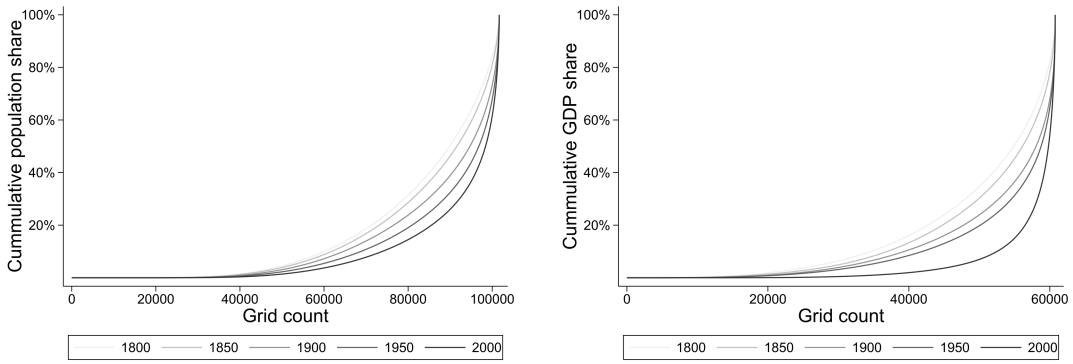

(a) Population (b) GDP

Note: Figure 5a shows the cumulative distribution of population across the spatial grid of Europe in selected years; figure 5b shows the spatial cumulative distribution of GDP, for the subset of grid cells for which GDP estimates are available in 1800 to ensure intertemporal comparability. More details on the spatial grids and the spatial distributions of population and GDP can be found in appendix figures A38 and A39.

Figure 6 also accounts for population to verify whether the increasing spatial concentration of economic output magnified or reduced income differences. The latter would be expected in case of sufficient labor mobility to the faster-growing locations in Europe. To do so, it shows the Lorenz curve of gridded per capita GDP in selected years, depicting the share of income for each gridded per capita GDP percentile. The figure suggests that incomes also grew more unequal over time, consistent with the notion of growing income differences between leading and lagging regions in terms of economic growth.

Figure 6: **Lorenz curves in selected years**

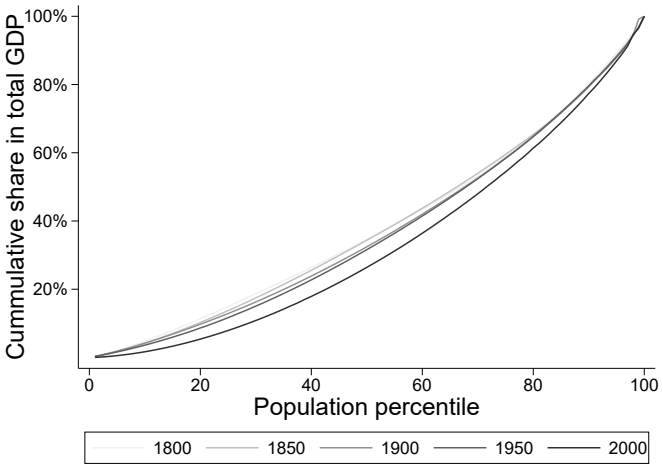

Note: This figure shows the Lorenz curve of per capita GDP in selected years. The curve is computed from gridded population and per capita GDP estimates for the subset of grid cells for which GDP estimates are available in 1800. More details on the spatial grid and the spatial distributions of per capita GDP is shown in appendix figure A40.

Figure 7 provides more historical context by plotting different versions of the population-weighted Herfindahl index of gridded GDP between 1900 and 2015, all indexed to the base

year of 1900. For reference, the dashed line shows the index computed from the subnational GDP data in Rosés and Wolf (2019), the most comprehensive alternative historical source for such computations. The figure shows a continued increase in the spatial concentration of subnational GDP to its peak in 2015, with interruptions after WWII and the 1980s, for the subsample of 16 countries with data availability. However, recomputing the index for the same set of countries using the gridded GDP estimates, the full black line shows that accounting for within-country variation in spatial concentration markedly alters this conclusion: while the evolution is similar prior to WWII, the gridded Herfindahl index suggests a more pronounced decline in spatial concentration after the world wars and a slighter increase since the 1990s, settling below the historical peak in the first half-century. Finally, computing the gridded Herfindahl index for all 28 countries, including the 12 countries lacking data in Rosés and Wolf (2019), offers a more representative picture for Europe with an initial rise in spatial concentration, followed by a subsequent fall in the immediate postwar period and a subsequent rise from the 1990 onwards to its current peak in 2015. The most comprehensive index of spatial concentration thus suggests two waves of concentration: an early wave which started in the interbellum and peaked just after WWI and a recent wave starting in the 1990s and continuing up until today.

Figure 7: **Herfindahl indices of gridded GDP, 1900-2015**

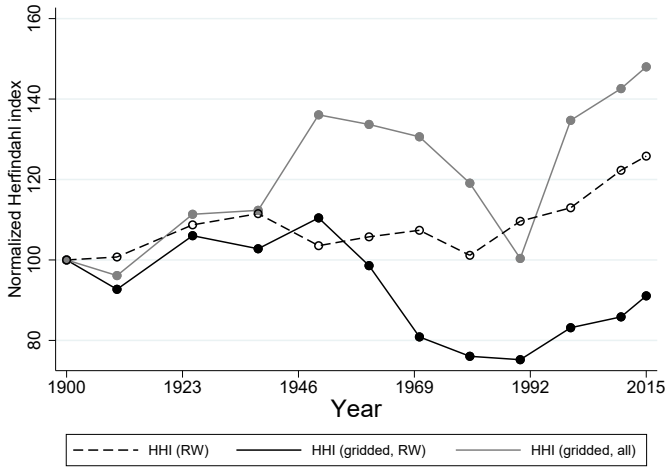

Note: This figure compares the population-weighted Herfindahl index of regional GDP computed for the available years and regional GDP data in Rosés and Wolf (2019) (dashed line, hollow dots) with the population-weighted Herfindahl indices of gridded GDP, computed for the subset of countries available in RW (black) and for the full set of countries in the sample (grey). The Herfindahl indices are all indexed to the baseline year of 1900 for comparability.

Finally, figure 8 investigates the extent to which the increase in the spatial concentration of economic output was prevalent across countries, by comparing country-specific gridded Herfindahl indices of GDP in 1900 and 2000 (left panel) and 1992 and 2023 (right panel). Note that gridded GDP estimates in the right panel are fully based on satellite information of NTL and do not rely on the newly introduced PMA-proxy. Both figures confirm that both the long- and short-run increase in spatial economic concentration was

common across Europe, with most countries (below the 45°-line) experiencing an increase in their Herfindahl index. This is consistent with the notion that the phenomenon of divergent economic development was a shared experience for nearly all European countries.

Figure 8: **Country-specific evolutions in spatial concentration**

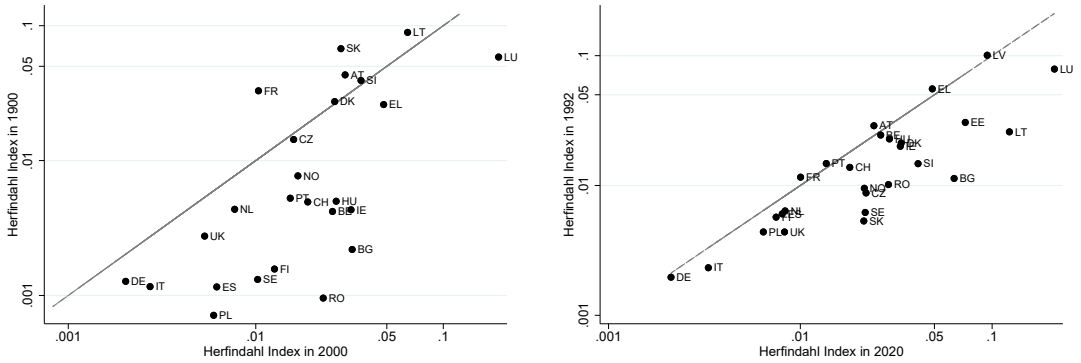

(a) Between 1900 and 2000

(b) Between 1992 en 2023

Note: Figure 8a shows the country-specific evolution in the Herfindahl index of gridded GDP between 1900 and 2000; 8b shows the evolution between 1992 and 2020, when satellite data is available to estimate gridded GDP.

3.2 The political landscape

Figure 9 shows the historical evolution in the combined vote share of mainstream, extremist and populist parties in Europe over the past two centuries. Parties are classified as extremist or populist if they are classified as such in at least one of the sources of section 2.3.3, to accommodate that two of the three classification schemes lack historical coverage before 1980. The left panel shows the raw electoral results, which depend on the countries holding elections. The right panel linearly inter- and extrapolates vote shares by party type at the country-level to eliminate the impact of the country sample and offer a more representative picture of the historical prevalence of political discontent in Europe.

Though extremist parties covered some electoral ground in some countries throughout the 19^{th} century, figure 8b shows that they remain largely irrelevant until a first wave of discontent, mainly driven by extremist parties, emerges after WWI and peaks in the interbellum at around 40% of valid votes before slowly petering out until WWII. Subsequently, radical party vote shares stabilize at around 20% of valid votes before they rise again from the 1990s onwards, this time driven by populist parties, stabilizing at their current peak of around 40% of valid votes. Strikingly, both waves of discontent arose during a period of accelerating economic divergence, see figure 7. Appendix figure A20 offers a more detailed picture by party taxonomy; appendix figure A49 shows country-specific results.

Figure 10 considers the importance of the spatial dimension by analyzing whether there are differences in the geographic distribution of the vote shares of each party type across electoral constituencies. To do so, it plots the historical evolution in the normalized

Figure 9: **Radical party vote shares in Europe: 1800-2023**

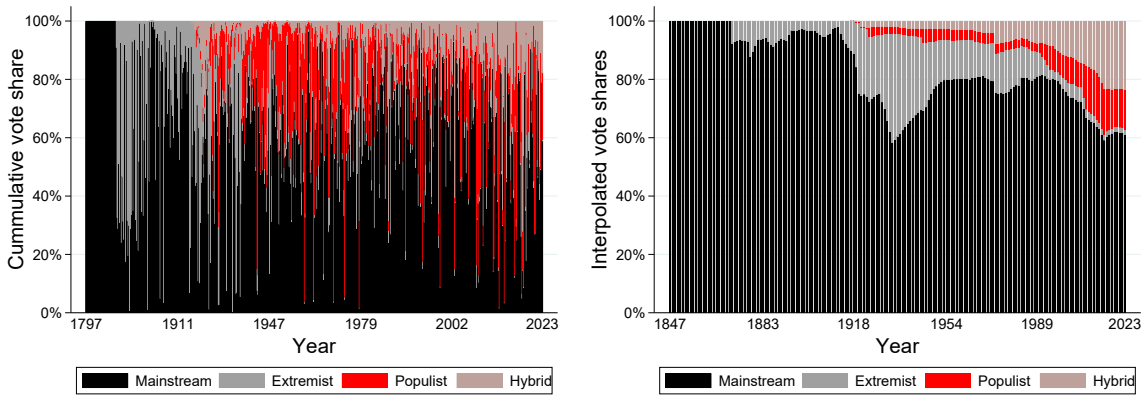

(a) Consecutive national elections (b) Interpolated national elections

Sources: Figure 9 shows vote shares of radical parties in all available elections, using the union of the classifications in table A8. Vote shares are averaged if multiple elections took place in a single year. Figure 9a shows the raw results, while 9b linearly inter- and extrapolates future non-election years at the country-level to account for selection.

Herfindahl indices of constituency-level party vote shares for each party type. The left panel shows the indices between 1871, when the first radical party enters the electoral scene (see figure 9a), and 2023 using a minimal definition to classify parties as populist or extremist based on any of the three classification schemes of section 2.3.3; the right panel shows the results between 1980 and 2023, using a majority definition to classify parties. Interestingly, both figures suggest that extremist and populist vote shares tend to be more spatially concentrated in particular constituencies than those of mainstream parties. This is consistent with the notion that political discontent has a distinct geography, which becomes more clearly visible in periods when radical parties are on the electoral rise.

Figure 10: **Herfindahl indexes of mainstream, extremist and populist votes**

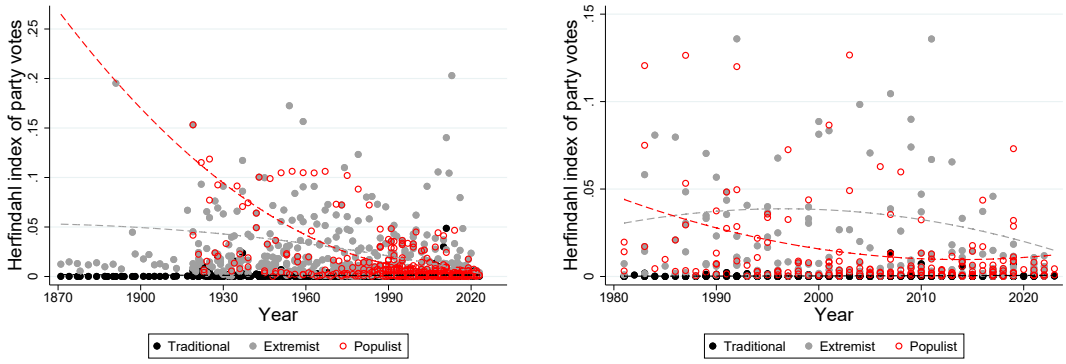

(a) Between 1871 and 2023 (b) Between 1980 en 2023

Note: Figure 10a shows the normalized Herfindahl indexes of mainstream, extremist and populist vote shares for each election in the sample, where parties are classified as extremist or populist if they are categorized as such by at least one of the three classifications in table A8. Figure 10b shows the corresponding normalized Herfindahl indexes for the post-1980 period and uses a majority-definition to classify parties, which are categorized as extremist or populist if they are considered as such by at least two of the three classifications in table A8.

3.3 Links between the economic and political landscapes

Figure 11 visualizes the distribution of constituency-level party vote shares for radical parties separately for countries in each quartile of the P80/P20 per capita GDP income ratio. The left panel restricts itself to the 1992-2023 period, for which gridded GDP estimates are based on satellite information on NTL, using a majority definition to classify parties as radical; the right panel considers the whole 1847-2023 period and uses a minimal definition to classify parties. Both figures clearly show that the distribution of radical party vote shares becomes more right tailed in more unequal countries that belong to higher quartiles of the P80/P20 per capita GDP income ratio. This is consistent with the notion that more economically unequal countries are more sensitive to political discontent.

Figure 11: **Radicalism by P80/P20 per capita GDP inequality quartile**

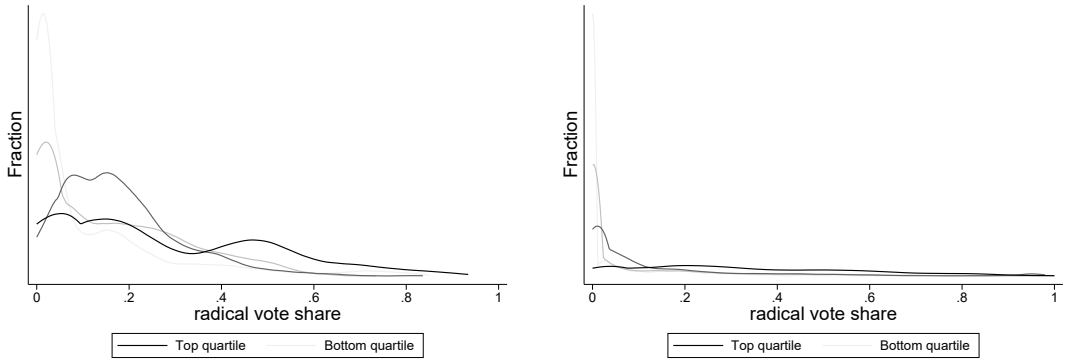

(a) Between 1992 and 2023

(b) Between 1847 en 2023

Note: This figure shows the distribution of radical vote shares for constituencies of countries in each quartile of P80/P20 per capita GDP income inequality: constituencies in the most egalitarian bottom quartile are shown in the lightest shade of grey while inegalitarian countries are shown in the darker shade. Figure 11a uses a majority definition while 11b uses minimalist definition requiring only one source to categorize a party as radical in table A8.

Table 6 further fleshes this out for the most recent wave of discontent in the period 1992-2023, by investigating how radical party vote shares - which were previously shown to be relatively spatially concentrated - correlate with local economic circumstances and whether this correlation is more pronounced in more economically unequal countries. To do so, I estimate the constituency-level relation between radical party vote shares and three indicators of a constituency's economic performance: its relative per capita GDP and its population share in the bottom and top quintiles of gridded per capita GDP, and their interaction with a country's P80/P20 income inequality ratio. While per capita GDP is perhaps the most standard indicator of economic performance, the latter two variables also capture the distribution of per capita GDP within constituencies by accounting for pockets of high and low income populations. Formally, I estimate the following regression

$$D_{\zeta,c,e,t} = \beta + \beta_1 y_{\zeta,t} + \sum_{q=2}^{3} \mathbf{Q}_{c,t}^{q} + \sum_{q=2}^{3} y_{\zeta,t} \times \mathbf{Q}_{c,t}^{q} + \epsilon_{\zeta,e,t} \tag{11}$$

where the dependent variable, $D_{c,e,t}$, is the vote share of radical parties in constituency ζ of country c in general election e in year t. $y_{\zeta,t}$ is either a constituency's relative per capita GDP, $\bar{\bar{y}} = \frac{y_{\zeta,t}}{y_{c,t}}$, its population share in the bottom quintile of per capita GDP, $\dot{y}_{\zeta,t}$, or its population share in the top quintile of per capita GDP, $\dot{y}_{\zeta,t}$. $\mathbf{Q}^q_{\zeta,t}$ is a dummy variable indicating whether a country's P80/P20 income inequality ratio is in the q^{th} quartile.

Table 6: **Divergent development and discontent, 1992-2023: OLS estimates**

	$\bar{\bar{y}}$	$\dot{y}$	$\dot{y}$	$\bar{\bar{y}}$	$\dot{y}$	$\dot{y}$
y	-.03***	.04	-.04***	-.03***	.07***	-.03**
	(.01)	*(.03)*	*(.01)*	*(0)*	*(.01)*	*(.01)*
$Q^2_{P80/P20}$				.06	.05	.05
				(.07)	*(.06)*	*(.06)*
$Q^3_{P80/P20}$				.04	.1**	.07
				(.04)	*(.04)*	*(.04)*
$Q^4_{P80/P20}$				.17	.15*	.17*
				(.1)	*(.09)*	*(.1)*
$y \times Q^2_{P80/P20}$				-.01	-.02	-.03
				(.02)	*(.05)*	*(.02)*
$y \times Q^3_{P80/P20}$				.03***	-.16***	0
				(.01)	*(.01)*	*(.01)*
$y \times Q^4_{P80/P20}$				-.01	.03	-.05*
				(.01)	*(.04)*	*(.03)*
N	18442	18442	18442	18442	18442	18442
Adjusted R ^{2}	.006	.003	.005	.093	.093	.091

Note: This table reports OLS results from equation (11). Dependent variables: the combined constituency-level party vote shares obtained by radical parties during general elections in the CLEA. Political parties are majority classified as radical if they are categorized as such by at least two of the three classifications in table A8. Independent variables: relative per capita GDP, $y = \bar{\bar{y}}$, or the ratio of constituency to country per capita GDP; the population share in the bottom or top quintile of gridded per capita GDP within each country, $y = \dot{y}$ and $y = \dot{y}$; and $Q^2_{P80/P20}$ through $Q^4_{P80/P20}$ dummy variables indicating countries that are in the second, third and fourth quartiles of the P80/P20 per capita GDP ratio. Constituency-level GDP is approximated by spatializing reported country GDP using satellite data on nighttime lights, see section 2.2. Total observations, N, and adjusted R^2 are reported in the bottom. Standard errors are robust to heteroskedasticity and clustered at the country-level.

The first three columns of table 12 indicate that economic backwardness is correlated with radical party vote shares in the specifications without dummies for each quartile of economic inequality: higher per capita GDP is associated with lower radical vote shares; a larger population share in the bottom per capita GDP quintile correlates with more electoral radicalism, though this effect cannot be precisely estimated; and more inhabitants in a country's top quintile of per capita GDP reduce the electoral success of radical parties. Adding dummies for P80/P20 per capita GDP ratio quartiles strengthens these results considerably: more unequal countries situated in higher quartiles of the P80/P20 per capita GDP ratio in themselves experience elevated radical vote shares in comparison to countries in the bottom quartile, but the correlation with the economic indicators now becomes consistently statistically significant and in most cases more pronounced in higher quartiles. The addition of information on economic inequality also increases the explana-

tory power of the model, as measured by the adjusted R^2. In terms of interpretation, the fifth column implies that a country in the top quartile of the P80/P20 per capita GDP ratio can expect to experience a 15 percentage point (p.p.) increase in the electoral success of radical parties in comparison to a country in the bottom quartile, while every percentage point increase in its population share in the bottom quintile of per capita GDP is associated with a further increase in radical vote shares with .1 percentage point.

Figure 12 provides a final piece of empirical evidence by zooming in on the three countries which attained the highest radical vote shares in their most recent election covered in the CLEA: Hungary in 2018, Italy in 2018 and the Czech Republic in 2017. For each case study, the figure ranks constituencies by their population share in the bottom quintile of per capita GDP from left (no poor population) to right (highest poor population share) and plots each constituency's radical party vote share. Each figure shows that constituencies with larger poor population shares had a clear tendency to vote for radical parties. For reference, the figures also plots each constituencies population share in the top per capita GDP quintile (dashed line) to show the opposite also seems true: constituencies with larger rich population shares also were the least likely to vote for radical parties. These results corroborate those in table 6 and suggest that political discontent is more prevalent in lagging regions, consistent with most of the existing literature on this topic.

Figure 12: **Three recent case studies**

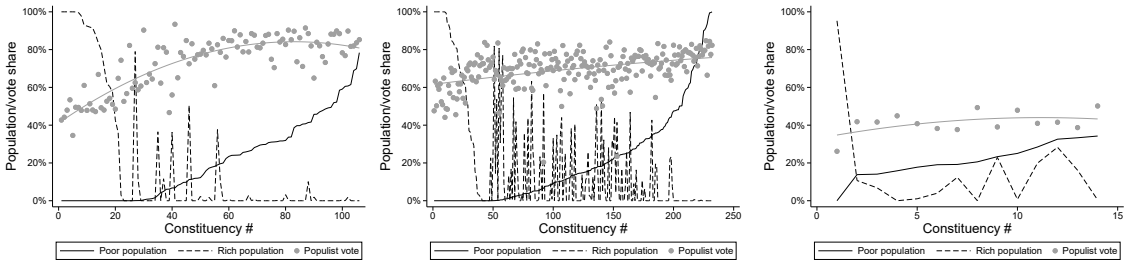

(a) Hungary (2018)) (b) Italy (2018) (c) Czech Republic (2017)

Note: This figure shows the distribution of radical party vote shares (grey) across all the constituencies in the top three countries with the largest overall vote share in their most recent general election. Constituencies are ordered according to their population share in the bottom quintile of per capita GDP (full black line) and subsequently on their population share in the top quintile of per capita GDP (dashed line). Political parties are majority-classified as radical if they are categorized as such by at least two of the three classifications in table A8.

4 A dynamic spatial political economy model

The model extends the standard, static Rosen-Roback model of location choice (Rosen, 1979; Roback, 1982) along two dimensions. First, it makes it dynamic by introducing path-dependent economic growth differentials favoring agglomerated locations. This reproduces the empirical stylized fact of divergent development in section 3. Second, it incorporates a political layer by introducing a redistributive government which decides on a lump-sum transfer scheme. The main novelty of the model is that it allows to analyze the emergence

of political discontent in the spatial equilibrium, which is here defined as the discrepancy between government-decided and individually preferred amounts of income redistribution. This, in turn, allows for model predictions on the location and timing of the electoral rise of radical parties, which capitalize on the presence of alienated voters with a minimal amount of political discontent, that can be validated against observed data.[11]

4.1 Environment and endowments

The economy consists of L locations, indexed by $l \in \{1, \ldots, L\}$, and N agents, indexed by $n \in \{1, \ldots, N\}$. Locations are endowed with an exogenous and inelastic housing stock of $\bar{H}$ units of housing and differ in their productive and non-productive ('residential') amenities, a_l and ϵ_l. The housing stock is owned by absentee landlords who spend their rental income on final consumption. Freely mobile agents differ in their human capital levels, s, drawn from a Pareto distribution with shape parameter $\alpha > 1$ and lower bound 1, $s_n \sim P(\alpha)$. Following Rosen (1979) and Roback (1982), agents have idiosyncratic preferences for each location, $\xi_{l,n}$, drawn from a Fréchet distribution with shape parameter ϵ.

4.2 Production and wage income

There is a representative firm in each location, l, which produces a final good using only labor. The final good can be costlessly traded across locations.[12] Production technology is location specific as it depends on local productive amenities, a_l. Following Parkhomenko (2021), human capital is used in a perfectly interchangeable manner in production

$$Y_l = a_l \int_{s=1}^{S} s N_l(s)\, ds = a_l \underbrace{S_l}_{\substack{\text{Total human} \\ \text{capital at } l}} \tag{12}$$

with $N_l(s)$ the mass of workers with skill level s in location l.

Under perfect competition, workers earn their marginal product as income such that a worker n with human capital endowment s_n earns the following gross wage in location l

$$w_{l,n}(s_n) = \frac{\partial Y_l}{\partial N_l(s_n)} = a_l s_n \tag{13}$$

4.3 Government and taxation

The government levies an income tax to finance a lump-sum redistribution scheme. Following Bolton and Roland (1997), taxation is assumed to lead to a tax distortion, $\psi \geq 1$, such that an income tax of τ generates $\left(\tau - \frac{\tau^{\psi}}{\psi}\right)$ in revenues and the cost of taxation equals $\frac{\tau^{\psi}}{\psi}$. The magnitude of ψ allows to indirectly account for the labor supply response

[11] In what follows, I omit the time subscript t to simplify notation unless needed for clarity.

[12] The assumption of costless trade implies that consumption prices are identical across locations and, hence, that the model abstracts from consumption-cost-of-living differences.

to income taxation in a parsimonious manner. Taxes are decided by the political party that wins the election, which is held within each period after location choices are made.

While gross wage income is given by equation (13), conditional on the amount of redistributive income taxation, τ, an agent locating in l attains the following net income:

$$y_{l,n}(s_n) = (1-\tau)\, a_l s_n + \left(\tau - \frac{\tau^\psi}{\psi}\right)\frac{Y}{N} \tag{14}$$

with Y total output in the economy, $\sum_{l=1}^{L} Y_l$, and $\left(\tau - \frac{\tau^\psi}{\psi}\right)\frac{Y}{N}$ the lump-sum transfer.

4.4 Preferences and consumption

Agents derive utility from the consumption of the final good, c, and housing, h, in Cobb-Douglas fashion.[13] Worker n with skill s_n locating in location l attains the following utility

$$U_{l,n}(s_n) = \underbrace{\xi_{l,n}}_{\substack{\text{idiosyncratic} \\ \text{part of } U}} \underbrace{\epsilon_l \big(c(s_n)\big)^{\mu} \big(h(s_n)\big)^{1-\mu}}_{\substack{\text{common part} \\ \text{of } U,\ \tilde{U}_{l,n}(s)}} \tag{15}$$

Conditional on the human capital endowment and equilibrium income taxation, optimal consumption and housing decisions yield the following expenditure functions

$$\begin{aligned} c^*_{l,n}(s_n,\tau) &= \mu\left[(1-\tau)\, a_l s_n + \left(\tau - \frac{\tau^\psi}{\psi}\right)\frac{Y}{N}\right] \\ h^*_{l,n}(s_n,\tau) &= \bar{H}\frac{(1-\tau)\, a_l s_n + \left(\tau - \frac{\tau^\psi}{\psi}\right)\frac{Y}{N}}{(1-\tau)\, a_l S_l + \left(\tau - \frac{\tau^\psi}{\psi}\right)\frac{Y}{N} N_l} \end{aligned} \tag{16}$$

4.5 Location choices

Freely mobile workers make location choices to maximize their utility. The first order conditions determining optimal consumption imply that the indirect utility of agent n with human capital endowment s_n if he decides to live in location l can be written as

$$v_{l,n}(s_n,\tau) = \xi_{l,n}\epsilon_l \left(c^*_{l,n}(s_n)\right)^{\mu}\left(h^*_{l,n}(s_n)\right)^{1-\mu} = \xi_{l,n}\delta_l(s_n,\tau) \tag{17}$$

The *ex ante* probability that an agent with human capital endowment s will choose locate at l when the equilibrium tax rate equals τ^* is given by the following ratio

$$\pi_l(s,\tau^*) = \frac{\delta_l(s,\tau^*)^{\epsilon}}{\int_{k=1}^{L}\delta_k(s,\tau^*)^{\epsilon}\, dk} \tag{18}$$

[13] Empirical evidence supports the standard Cobb-Douglas implication of fixed expenditure shares on housing, see e.g. Redding and Turner (2015).

4.6 Political choices

After location choices are made, political parties compete in elections to determine the amount of income taxation, τ^*. Agents are myopic and only care about current-period pay-offs when deciding on their vote. A representative mainstream parties proposes the tax rate that is most preferred by the median tax voter, taking into account the tax distortion, ψ. That is, the mainstream party competes in elections proposing the tax rate

$$\tau^*\big(L, N, \alpha, \epsilon, \mathbf{a}, \psi, \eta\big) = \max\left(\min\left(\arg\max_{\tau} E\big(U\left(\tilde{s}\right) \mid L, N, \alpha, \epsilon, \mathbf{a}, \psi, \eta\big), 1\right), 0\right) \tag{19}$$

with $U\left(\tilde{s}, \tau\right)$ the expected utility of the median skill agent with human capital endowment $\tilde{s} = \sqrt[\alpha]{2}$, where the expectation is taken with respect to all the location choice probabilities.

Note that, like governments, agents also have ideal points with respect to the redistributive tax, $\tau^*_{n,l_n}\left(s_n\right)$, which for an agent, n, with skill s_n locating at l^*_n equals

$$\tau^*_n = \tau^*_{n,l^*_n}\left(s_n\right) = \max\left(\min\left(\arg\max_{\tau} E\big(U\left(s_n, \tau^*\right) \mid L, N, \alpha, \epsilon, \mathbf{a}, \psi, \eta, \tau^*\big), 1\right), 0\right) \tag{20}$$

I follow Callander and Carbajal (2021) in modelling voter alienation using these ideal points and assume agents become alienated from the mainstream party when its redistributive policy is too far removed from their preferred tax rate. Formally, an agent n with human capital endowment s_n located at l^*_n and with ideal point τ^*_n votes for the mainstream party if its discontent, $D_{l^*_n,n}\left(s_n, \tau^*, \tau^*_n\right)$ does not exceed the threshold λ

$$D_{l^*_n,n}\left(s_n, \tau^*, \tau^*_n\right) = \frac{\left|U_{l^*_n,n}\left(s_n, \tau^*\right) - U_{l^*_n,n}\left(s_n, \tau^*_n\right)\right|}{U_{l^*_n,n}\left(s_n, \tau^*\right)} < \lambda \tag{21}$$

and otherwise abstains and becomes susceptible for political radicalism. λ captures the region of tolerance, beyond which an agent withdraws mainstream support.

Radical parties compete with mainstream parties by targeting alienated voters which prefer more or less redistribution. I distinguish between 'right' and 'left' radical parties, which compete in elections by respectively proposing the tax rates most preferred by the median alienated voters favoring lower or higher redistributive taxes, $\underline{\tau}$ and $\bar{\tau}$. Alienated voters will respectively vote for left and right radicalist parties if they are sufficiently alienated, such that their discontent exceeds $\lambda + \lambda_a$ and otherwise abstain from voting:

$$\begin{aligned}
D_{l^*_n,n}\left(s_n, \tau^*, \tau^*_n\right) > \lambda + \lambda_a \;\&\; \tau^*_n > \tau^* \quad &\Rightarrow \text{Vote for left radical party} \\
D_{l^*_n,n}\left(s_n, \tau^*, \tau^*_n\right) > \lambda + \lambda_a \;\&\; \tau^*_{n,l^*_n} < \tau^* \quad &\Rightarrow \text{Vote for right radical party} \\
\lambda < D_{l,n}\left(s_n, \tau^*, \tau^*_n\right) < \lambda + \lambda_a \quad &\Rightarrow \text{Abstain}
\end{aligned} \tag{22}$$

where λ_a accounts for differences in the turnout rate in electoral data and formalizes Guiso et al.'s (2024) recent finding that voter alienation initially reduces voter participation and eventually increases the willingness to vote for populist parties.

Hence, the equilibrium tax rate equals

$$\tau\big(L, N, \alpha, \epsilon, \mathbf{a}, \psi, \eta, \lambda, \lambda_a\big) = \begin{cases} \tau^* & \text{if } \mathbf{V}^* \geq \bar{\mathbf{V}} \;\&\; \mathbf{V}^* \geq \underline{\mathrm{V}} \\ \bar{\tau} & \text{if } \bar{\mathbf{V}} > \mathbf{V}^* \;\&\; \bar{\mathbf{V}} > \underline{\mathrm{V}} \\ \underline{\tau} & \text{if } \underline{\mathrm{V}} > \mathbf{V}^* \;\&\; \underline{\mathrm{V}} > \bar{\mathbf{V}} \end{cases} \tag{23}$$

with $\mathbf{V}^*$, $\bar{\mathbf{V}}$ and $\underline{\mathrm{V}}$ the votes received by the mainstream, left and right radical parties as described in equations (21) and (22) and $\underline{\tau}$ and $\bar{\tau}$ respectively capturing the tax rates most preferred by the median voter of the right and left radical parties.

4.7 Technological innovation

Technological innovation of local productive amenities, a_l, occurs between periods. Innovation has a common component that is shared across locations and an idiosyncratic component that depends on locations' human capital stocks. First, each location faces a multiplicative technology shock, o_l, drawn from a common uniform distribution with mean μ_a and standard deviation σ_a, $o_l \sim \mathcal{U}\left(\mu_a - \sigma_a, \mu_a + \sigma_a\right)$. Second, each location has a probability ϕ of obtaining an idiosyncratic technological innovation, ι_a, that is proportional to their effective labor share, $\phi_l = S_l / \sum_{k=1}^{L} S_k$, which is draw from a Pareto distribution with shape parameter $\upsilon > 1$ and lower bound 1, $\iota_a \sim P\left(\upsilon\right)$. Hence, the expected growth of the production technology $a_{l,t}$ in location l with effective labor $S_{l,t}$ at time t equals

$$E\left(a_{l,t+1} \mid a_{l,t}, S_{l,t}, S_t, \mu_a, \iota_a\right) = \underbrace{\left(\frac{\iota_a + \phi_{l,t} - 1}{\iota_a - 1}\right)}_{\substack{\text{Idiosyncratic} \\ \text{component}}} \mu_a a_{l,t} \tag{24}$$

Note that the idiosyncratic component implies that innovation will be greater in agglomerated locations with higher effective labor shares, as these have a higher probability of successful idiosyncratic innovations. Moreover, this agglomeration benefit is self-reinforcing as more productive locations are better capable of attracting additional workers, see equation (18), which further accelerates their idiosyncratic productivity growth.

4.8 Timing in the model

Figure 13 further illustrates the timing in the model. First, agents make location choices conditional on the current-period spatial distribution of productive amenities and the expected redistributive income tax rate as detailed in equation (17). After location choices have been made, agents vote in a general election to determine the redistributive tax rate as detailed in equations (21) and (22); the winning party implements its proposed tax rate. After this, production occurs from equation (12) and consumption occurs from equation (16). Finally, technological innovation occurs between periods t and $t+1$ as described in equation (24) and determines the next-period spatial distribution of productive amenities.

Figure 13: **Timing in theoretical model**

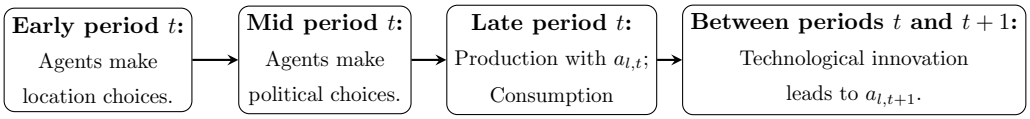

4.9 Definition and computation of the spatial equilibrium

4.9.1 Definition

Conditional on the number of locations, L, and agents, N, the initial spatial distribution of productive and non-productive amentities, $\mathbf{a} = (a_1, \ldots, a_L)$ and $\epsilon = (\epsilon_1, \ldots, \epsilon_L)$, the realized skill distribution, $\mathbf{s} = (s_1, \ldots, s_N)$, the realized location preference distribution, $\xi = (\xi_{n,1}, \ldots, \xi_{l,n})$, the housing expenditure share, $1 - \mu$, the tax distortion, ψ, and the common and idiosyncratic innovation parameters, μ_a and ι, an *ex post* spatial equilibrium is given by a set of real functions, $\left(w\left(s_n\right), R_l, N_l, c_n\left(s_n\right), h_n\left(s\right), Y_l, P, \tau\right)$, such that

- Agents locate optimally such that wages satisfy (13), total income satisfies (14), rents satisfy (20A) and location choices satisfy (18).
- The general election determines the redistributive income tax rate, τ, satisfying (23).
- Representative firms produce final consumption goods satisfying equation (12).
- Agents and absentee landlords make optimal consumption decisions that satisfy equation (16).
- Goods markets clear such that P is given by (21A).
- Labor markets clear such that $\int_{l=1}^{L} N_l = N$.
- Housing markets clear such that $\int_{n \in l} h_n^*\left(s_n\right) dn = \bar{H}$ for all l.

4.9.2 Computation

I employ a nested fixed point algorithm that determines the equilibrium by repeatedly solving for the fixed points of the spatial distribution of (effective) labor at candidate values of the equilibrium tax rate until the solutions converge. As equation (23) does not allow to solve for the equilibrium tax rate analytically, the inner loop proceeds by conducting a grid search over potential values of τ between 0 (no taxation) and 1 (full taxation), to determine the tax rate that is most preferred by the median tax voter, conditional on the candidate solution for the spatial equilibrium in the outer loop. Specifically, let the initial guesses for the (effective) local labor supplies, aggregate production and the tax rate respectively equal $N_{l,1} = N/L$, $S_{l,1} = \frac{\alpha}{\alpha - 1} N_{l,1}$, $Y_1 = S \frac{\int_l a_l}{L}$ and $\tau_1 = 0$. The equilibrium can be determined from the following recursive process:

$$
\begin{cases}
\text{Outer loop} \begin{cases}
l^*_{n,i}\left(s_n, \tau_i\right) & = \arg\max_{l \in L} v_{n,l,i}\Big(\tau_i, s_n, \mathbf{N}_i\left(\tau_i\right), \mathbf{S}_i\left(\tau_i\right), Y_i\left(\tau_i\right)\Big) \quad \forall n \in N \\
N_{l,i+1}\left(\tau_i\right) & = \int_n^N \mathbf{I}_{l=l^*_{n,i}(\tau_i)} dn \quad \forall l \in L \\
S_{l,i+1}\left(\tau_i\right) & = \int_n^N \mathbf{I}_{l=l^*_{n,i}(\tau_i)} s_n dn \quad \forall l \in L \\
Y_{i+1}\left(\tau_i\right) & = \int_l^L a_l S_{li+1}\left(\tau_i\right) dl
\end{cases} \\
\text{Inner loop} \begin{cases}
\tau^*_{n,i+1} & = \arg\max_{\tau} U_{n,l^*_{n,i}}\left(s_n, N_{l,i+1}\left(\tau_i\right), S_{l,i+1}\left(\tau_i\right), Y_{i+1}\left(\tau_i\right)\right) \quad \forall n \in N \\
\tau_{i+1} & = \tilde{\tau}\Big(\mathbf{N}_{i+1}\left(\tau_i\right), \mathbf{S}_{i+1}\left(\tau_i\right), Y_{i+1}\left(\tau_i\right)\Big)
\end{cases}
\end{cases}
\tag{25}
$$

with $\mathbf{I}_{l=l^*_{n,i}(\tau^s)}$ an indicator equal to 1 if agent n decides to locate in location l in iteration i; $\tau^*_{n,i+1}$ the preferred tax rate for each agent, determined by a grid search with step size $\Delta t = .01$, and $\tilde{\tau}$ the median value of τ^*_n. Equation (25) is iterated until it converges to a fixed point for $i \to i^* : \int_{l=1}^L \left|N_{l,i} - N_{l,i+1}\right| / N < C$, with C the convergence criterion. The tax proposed by the mainstream party, $\tau^* = \tau_i$, determines discontent in equation (21), the vote shares for radical parties in (22) and the equilibrium tax rate in equation (23).

5 Model implications

One seemingly trivial implication of the model, and one that is perhaps sometimes overlooked in the existing literature, is that redistributive income taxation transfers income from leading to lagging regions, reducing the level of interregional economic inequality. To see this, note that the indirect utility in equation (17) implies that redistributive taxation gradually equalizes welfare across agent types by lump-sum redistributing from high to low earners, allowing low-skill agents to benefit from spatially concentrated productivity benefits at the cost of tax and (as discussed below) location choice distortions. This implies that existing spatial development models that lack a political layer, such as Desmet and Rossi-hansberg (2014) and Desmet, Nagy, and Rossi-Hansberg (2018), risk overstating the spatial income and welfare inequalities resulting from spatially concentrated growth, as part of the proceeds are redistributed from productive to less productive regions through the tax system. Appendix B.1.2 follows this logic to establish the following proposition

Proposition 1 *Denote the Gini coefficient computed on gross income, $w_{l,n}(s_n)$, by G^w, and the net income Gini coefficient (after taxes and transfers), $y_{l,n}(s_n)$, as G^y. In equilibrium, $G^w \geq G^y$, and G^w overstates the true level of interregional economic inequality.*

The dependence of location choices on redistributive taxation in equation (18) has two further implications. First, tax increases primarily discourage low-skill agents to move to locations with high productive amenities. Intuitively, redistributive taxation lowers labor mobility for low-skilled agents by shifting their main source of income from wage income to the lump-sum transfer, while high-skilled agents are net contributors to the tax system and therefore become more dependent on productive amenities to maintain real consumption levels when taxes rise. Interestingly, skill-neutral production is thus consistent with skill sorting and redistributive income taxation contributes to wage polarization in this model, fully consistent with von Ehrlich and Overman's (2020) empirical findings for Europe. This also implies that even an increase in the housing supply may leave some spatial inequalities intact and may be less effective in increasing labor mobility as hitherto thought, see e.g. Hsieh and Moretti (2019). The recent decline in labor mobility in the US and other countries may consequently be partially explained by the gradual expansion of the welfare state. Proposition 2, proven and illustrated in appendix B.1.3, formalizes this result

Proposition 2 *Redistributive taxation lowers labor mobility. Furthermore, incomplete redistributive taxation primarily discourages labor mobility for low-skill agents:* $0 < \tau < 1 : s_1 > s_2 \;\&\; a_1 > a_2 \;\Rightarrow \pi_l(s_1, \tau) > \pi_1(s_2, \tau)$.

A second implication of equation (18) is that, in addition to the tax distortion, there is also a spatial cost of taxation. As previously highlighted by Albouy (2009), income taxation not only reduces total output by the tax distortion capturing adverse labor supply reactions parameterized by ψ, but also by discouraging labor mobility to productive locations as determined by $\pi_l(\tau, s)$. Existing spatial development models lacking a political layer may overstate the efficiency gains of agglomeration, as part of these are compensated by heightened redistributive pressures which increase the amount of output lost to tax and location choice distortions. The following proposition, proven in appendix B.1.4, decomposes the total cost of taxation in the tax distortion cost and the spatial cost and determines when spatial costs of taxation dominate the non-spatial distortion costs.

Proposition 3 *The total cost of public funding for a tax increase from τ_1 to $\tau_2 > \tau_1$, $C(\tau_1, \tau_2)$, can be decomposed as*

$$C(\tau_1, \tau_2) = \underbrace{Y(\tau_1)\left[\frac{\tau_2^{\psi}}{\psi} - \frac{\tau_1^{\psi}}{\psi}\right]}_{\substack{\text{increase in tax distortion} \\ \text{at initial tax base}}} + \underbrace{Y(\tau_1) - Y(\tau_2)}_{\substack{\text{reduction in tax base} \\ \text{through spatial cost}}} + \underbrace{\frac{\tau_2^{\psi}}{\psi}\left[Y(\tau_2) - Y(\tau_1)\right]}_{\substack{\text{reduction in tax distortion} \\ \text{through spatial cost of taxation}}} \tag{26}$$

The indirect spatial cost of taxation exceeds the direct distortion cost if $\frac{Y(\tau_2)}{Y(\tau_1)} < \frac{\psi - 2\tau_2^{\psi} - \tau_1^{\psi}}{1 - \tau_2^{\psi}}$.

While proposition 3 quantifies the cost of taxation, equation (17) implies a declining marginal utility from housing, such that housing transfers from rich to poor are welfare increasing. From a welfare perspective, then, the main benefit of redistributive taxation in this model is to reduce the housing purchasing power of the highest earners to equalize housing consumption. Absent tax distortion costs, aggregate within-period utility would be maximized by full taxation and equal housing consumption.

Proposition 4 captures the first central result linking economic development to political frictions. It states that while tax preferences remain similar and stable over time with *equal* development, they grow at least more spatially diverse with *unequal* development, and also more individually diverse if labor mobility is sufficiently low. The main intuition is that labor mobility is absent with equal development, as there are no wage gains associated with relocation, while wages grow at an identical rate, such that redistributive preferences don't change either. Unequal development, in contrast, affects redistributive preferences along two margins: first, it magnifies wage differentials between leading and lagging regions, reducing the demand for redistribution in the former but increasing them in the latter; second, it induces labor mobility towards leading regions, especially for high-skill agents, granting them larger electoral weight. While the former effect unambiguously magnifies discrepancies in tax preferences between *locations*, the latter effect determines whether divergent development also increases disagreements on the most preferred tax rate between *agents*, since labor mobility acts as a centripetal force that equalizes wages and fiscal preferences by agglomerating agents in locations with similar productive amenities. Proposition 4, proven in appendix B.1.5, formalizes this insight.

Proposition 4 *Denote the variance of individually preferred tax rates within period t by $\sigma_t^{\bar{\tau}^N}(s,\tau_t)$. Let $\int_{s=1}^{\infty}\pi_l(s,\tau_t)\,\tau_l(s,\tau_t)\,\phi(s)\,dl$ denote the tax rate most preferred by location l within period t and denote the corresponding variance by $\sigma^{\bar{\tau}^L}(s,\tau_t)$. Then*

- ⇒ *Under equal development, $\sigma_a = \phi_{l,t} = 0$, the overall and spatial variation in fiscal preferences, $\sigma_t^{\bar{\tau}^N}(s,\tau_t)$ and $\sigma^{\bar{\tau}^L}(s,\tau_t)$, remains constant over time. Moreover, if there are no initial productivity differentials, $a_{l,1} = a$, the variances are minimized.*

- ⇒ *Under divergent development, $\sigma_a > 0$ & $\phi_{l,t} = S_{l,t}/S$, spatial variation in fiscal preferences, $\sigma^{\bar{\tau}^L}(s,\tau_t)$, unambiguously increases over time. There exists a threshold value for the Fréchet parameter of location choice in each period, $\underline{\epsilon}_t$, below which the overall variation in preferred tax rates, $\sigma_t^{\bar{\tau}^N}(s,\tau_t)$, also increases over time.*

One direct corollary of proposition 4 is that unequal development makes it harder for the mainstream party to propose a redistributive tax that satisfies all local electorates to avoid political alienation as defined in equation (21). Proposition 5, proven in appendix B.1.6, traces the consequence of this and highlights that political discontent only depends on the discrepancy between the tax rate proposed by the mainstream party and the one

that is most preferred by individual voters, such that political discontent remains stable with equal development yet grows over time with unequal development.

Proposition 5 *The political discontent of any agent n, $D_{l^*_{n,t},n,t}\left(s_n, \tau^*_t, \tau^*_{n,t}\right)$, only depends on the discrepancy between individually preferred taxes and the tax rate proposed by the mainstream party, $\left|\tau^*_{n,t} - \tau^*_t\right|$, within each period t. Political discontent remains stable over time with equal development and increases in at least one location with divergent development. If labor mobility is sufficiently low, $\epsilon \leq \underline{\epsilon}_t$, aggregate political discontent, $\int_{s=1}^{S}\int_{l=1}^{L} \pi_{l,t}\left(s, \tau^*\right) D_{n,t}\left(s, \tau^*_t\right) \phi\left(s\right) ds$, also increases with divergent development.*

Proposition 6 derives the spatial predictions of the model, by inferring where political discontent is most likely to emerge under divergent development. The model predicts a clear geography of discontent primarily affecting lagging regions. The intuition is fairly straightforward: as labor mobility is exclusively orientated towards leading regions, divergent development gradually increases their electoral weight during elections. As voters in productive locations share a preference for low redistributive taxation, see proposition 4, their growing numbers lead the mainstream party to propose a tax rate that increasingly falls short of the preferred tax rates in lagging locations. Hence, as per proposition 5, the political externalities of divergent development primarily affect lagging locations.

Proposition 6 *With divergent development, the tax proposed by the mainstream party, τ^*, is increasingly determined by leading regions due to their increasing electoral weight. Political externalities primarily affect lagging regions.*

Proposition 6 has three corollaries. First, the political externalities of divergent development crucially depend on mobility. Labor mobility attracts the labor supply to productive locations, increasing the average wage and hence the marginal utility of taxation. This increases the willingness to pay taxes, especially in lagging locations, rendering their tax preferences even more distinct. Mobility also reduces the number of voters in lagging regions, which are most susceptible to discontent, see proposition 6. As labor mobility favors high-skill agents, it risks increasing radical vote shares by contributing to the geographical polarization of wages and fiscal preferences until reaching lower-skilled agents. Policies that target labor mobility by increasing the housing supply, $\bar{H}$, in leading regions or reducing the weight of location preferences, ϵ, may therefore backlash at least in the short run. This is confirmed in proposition 7 and further detailed in appendix B.1.8.

Proposition 7 *Increasing mobility may increase radical vote shares in the short run.*

Second, while redistributive taxation reduces political discontent in lagging regions, it also risks backlash in more populous leading regions, as it does not address its root cause of fiscal preference heterogeneity. Though redistributive policies have often been suggested as an adequate answer to political radicalism, see e.g. Eichengreen (2018) and Albanese et al. (2022), in this model, increasing redistributive taxation has the opposite effects of

lowering labor mobility and increasing political discontent, see proposition 8.

Proposition 8 *Increasing redistributive taxation increases radical vote shares.*

Finally, while adverse productivity shocks in lagging regions are predicted to increase radicalism, by locally increasing redistributive preferences, when they are small relative to the magnitude of productive amenities, their effects on radical vote shares remain small. This may explain why existing studies which rely on exogenous adverse shocks fail to find explanatory significance of economic insecurity, in the words of Margalit (2019). The following proposition, further discussed in appendix B.1.10 summarizes this logic.

Proposition 9 *An adverse productivity shock of size Δ_s in a subset of lagging regions increases political discontent. If the size of the shock is small relative to productive amenities, a_l, the effect on radical vote shares is also small.*

6 Model calibration

To solve the model numerically, I calibrate it to match some key moments in the observed data. While the objective is not to achieve consistent calibration to a particular case study, the main aim is to ensure that the model broadly resembles observed historical data on agglomeration, growth and inequality for the European countries in my sample. Since these moments depend on all the parameters, they cannot be directly calibrated. Therefore, the parameter values are calibrated to minimize the sum of differences between unweighted average country data and selected model moments, standardized by the standard deviation in the observed data.[14] Several counterfactual scenarios adapt this baseline calibration to analyze how focal outcomes would change with equal development, increasing labor mobility and increasing redistributive transfers. Table 7 provides an overview of the calibrated variables and exogenous parameters in the model, the sources for the functional form assumptions made and the specification of the counterfactual scenarios.

With respect to the externally calibrated parameters, the dynamic spatial model consists of 30 locations and 10000 agents and is simulated for 200 time periods, where the initial time period corresponds to the year 1800 and each time period covers one year. This allows to analyze model implications for the long-run consequences of unequal development of section 2 in sufficient spatial detail. The μ parameter captures the fixed expenditure share on the consumption good, which is calibrated to .76 based on Davis and Ortalo-Magné's (2011) finding of stable housing expenditure shares of 24% from several micro datasets for the US. The shape parameter of the Fréchet distribution of location preferences crucially determines labor mobility in the model, and was previously estimated

[14] More specifically, index M target variables by $m = \{1, \ldots, M\}$ and denote the average observed value and its standard deviation in year t by $\phi_{m,t}$ and $\phi^{sd}_{m,t}$. Denote the corresponding simulated value by $\hat{\phi}_{m,t}$. Calibration minimizes $\sum_{m=1}^{M} \sum_{t=1}^{T} \frac{|\phi_{m,t} - \hat{\phi}_{m,t}|}{\phi^{sd}_{m,t}}$. The set of target variables is listed in table 8.

Table 7: **Functional forms and parameter values of the calibrated model**

Variable	*Functional form*	*Interpretation*	*Source*
u	$u_{l,n} = \xi_{l,n}\epsilon_l \left(c\left(s_n\right)\right)^{\mu}\left(h\left(s_n\right)\right)^{1-\mu}$	Individual utility	Redding and Turner (2015)
a	$a_{l,t+1} = \left(\frac{\iota_a + \phi_{l,t}^{\psi} - 1}{\iota_a - 1}\right)\mu_a a_{l,t}$	Local productive amenities	Desmet and Rossi-hansberg (2014)
ϵ	ϵ_l	Local residential amenities	Ahlfeldt, Redding, Sturm, and Wolf (2015)
H	$\bar{H}$	Fixed housing supply in each location	.
s	$s \sim P\left(\alpha\right)$	Human capital distribution	Gennaioli, La Porta, Lopez-De-Silanes, and Schleifer (2013)
ξ	$\xi \sim F\left(\epsilon\right)$	Location preference distribution	Rosen (1979) & Roback (1982)
ψ	$\frac{t^{\psi}}{\psi}$	Tax distortion, cost of taxation	Bolton and Roland (1997)
Parameter	*Value*	*Interpretation*	*External source / Target moment*
L	30	# locations	.
N	10000	# agents	.
T	200	# time periods (t=1 corresponding to the year 1800)	.
$\bar{H}$	1	# Fixed housing supply in each location	.
μ	.76	Fixed expenditure share on the consumption good	Davis and Ortalo-Magné (2011)
α	1.8	Shape parameter of the Pareto distribution of human capital	Gross household income Gini coefficient (CLIO Infra, 2014)
ϵ_l	1	Local residential amenities	Monte, Redding, and Rossi-hansberg (2018)
ξ	3.3	Shape parameter of the Fréchet distribution of location preferences	Monte et al. (2018)
ψ	1.7	Tax distortion parameter	Social expenditure shares in GDP (OECD.Stat, 2024)
μ_a	1.002+.0001177t	Mean of common technological innovation multiplier	Country-level per capita GDP growth (Vanschoonbeek, 2024)
σ_a	.03	Variance of common technological innovation multiplier	
ι	30	Idiosyncratic technological innovation multiplier	
λ	.0531	Region of tolerance for political alienation	Recent radical vote share in figure 9b
Counterfactual scenarios			
Scenario	*Description*		
Equal development	$\sigma_a = 0$, $\phi_t = 0$, μ_a calibrated to match economy-wide growth in baseline model.		
Increasing mobility	$H_l = \frac{a_l^{\bar{y}_l}}{\sum_k^L a_k^{\bar{y}_l}} L$		
Increasing redistribution	Mainstream party proposes tax most preferred by the upper quartile tax voter.		

to equal 3.3 in US counties (Monte et al., 2018). At this value, the simulated evolution in the top quintile population ratio closely resembles the growth rate in the share of the population living in the 20% most populuous European NUTS3 regions, see table 8.

Turning to the internally calibrated parameters, the shape parameter of the human capital distribution, α, is an important source of income inequality in the model, hence it is mainly calibrated such that the resulting Gini coefficient of gross household incomes, y, resemble those reported in CLIO Infra (2014). The distortion cost of taxation is modeled á la Bolton and Roland (1997) and mainly affects the equilibrium redistributive tax rate, which is calibrated such that simulated tax rates match the share of social expenditures in GDP as reported by OECD.Stat (2024). Finally, the technological innovation parameters, σ_a, μ_a and ι, mainly determine the overall growth rate of economic output, Y, and hence are respectively calibrated to 1.002+.0001177t, .03 and 30 such that simulated economic growth resembles observed country-level per capita GDP growth in the SPEED.

Table 8: **Targeted moments in selected years: model versus data**

Target	*Value*	$t \in \{1, 50\}$	$t \in \{50, 100\}$	$t \in \{100, 150\}$	$t \in \{150, 200\}$	*Figure*
P20/P80 population ratio growth	Data	-.001 - .001	0 - .002	-.002 - .003	-.003 - .009	A50a
	Model	.004	.002	.001	.002	
Per capita GDP growth	Data	-.01 - .02	-.01 - .03	-.03 - .05	.01 - .04	A50b
	Model	.01	.01	.02	.02	
Social expenditures	Data	. - .	. - .	. - .	.17 - .22	A50c
	Model	.21	.21	.2	.21	
Gross household income gini	Data	.42 - .51	.4 - .46	.37 - .44	.32 - .38	A50d
	Model	.37	.38	.39	.41	

Note: This table reports observed and simulated values for the growth rate in the top population quintile ratio and real per capita GDP, social expenditure shares and income Ginis in different time periods. Observed data is reported as the 95% confidence interval of the unweighted average value in the available country sample. $t = 1$ corresponds to the year 1800 in the observed data. The last column refers to more detailed appendix figures.

Table 8 shows that the simulated model is fairly consistent with observed data. The population share of the 20% most populated locations in the simulation model tracks the

growth rate of the top quintile gridded population estimates for the European countries in the SPEED quite well. The model also closely replicates per capita GDP growth and the available information on social expenditures. Finally, the nominal wage distributions are consistent with observed Gini coefficients even though the model does not account for e.g. the large shocks of both world wars. Simulated income inequality is comparatively low in initial periods and turns comparatively high in later periods.

The determination of radical vote shares in equation (22) merits some additional discussion as it depends on the region of tolerance, λ, which is unobserved. To deal with this, I depart from the stylized fact that radical parties obtained an average vote share of around 40% in the most recent elections in Europe, see figure 9b, and calibrate λ to the 60^{th} percentile value of political discontent, D, in period $t = 200$ in the baseline model, to replicate this stylized fact. In this way, exactly 40% of the electorate votes for a radical party in the terminal period in the baseline model. This threshold value for λ is then also used to assess the evolution of radical vote shares in counterfactual scenarios.

Turning to these counterfactual scenarios, to understand the role of unequal development, I first contrast the baseline results with those obtained under equal development, by enforcing common technological innovation, setting $\sigma_a = \phi_t = 0$ and calibrating μ_a such that total output growth under equal development matches that of the baseline scenario. Eichengreen (2018) proposes two policies to relieve the political tensions of divergent development: increasing labor mobility and income redistribution. To explore the effectiveness of both in the model, a second counterfactual increases labor mobility by endogenizing the local housing supply through a law of motion that is non-decreasing in local productive amenities, $H_l = f(a_l)$ with $f'(a_l) > 0$. More specifically, at the end of each period, each location's housing supply is updated as $H_{l,t+1} = a_{l,t+1}^{\sqrt[5]{t}} \left(\sum_k^L a_{k,t+1}^{\sqrt[5]{t}} \right)^{-1} L$.[15] This shifts the simulated P80/P20 population ratio to 1 in the terminal period, $t = 200$, resembling the typical observed quintile population ratio's for the year 2000 in the European sample. A third counterfactual scenario investigates the effect of increasing redistributive transfers by assuming that the mainstream party proposes the tax rate preferred by the 75^{th} percentile tax voter instead of the median (50^{th} percentile) tax voter.

While the more standard findings of the baseline model are relegated to appendix B.3, figure 14 starts by highlighting two central baseline results. First, figure 14a shows that divergent development is associated with an increase in the average amount of political discontent and confirms that the spatial inequalities magnify the aggregate utility losses of centrally determined redistributive transfers. Second, figure 14b shows that political discontent - in relative terms - is primarily located in the least productive locations in the terminal period. This suggests that agglomeration economies may trigger negative political spillovers, as the excessive concentration of economic activity could fuel interregional re-

[15] Note that location choices in equation (32A) depend on housing supplies, but not political discontent in equation (21). Hence, this specification of the endogeneous housing supply allocates a larger share of the fixed total housing supply of L units to productive locations without this directly affecting discontent.

Figure 14: **Political externalities of divergent development**

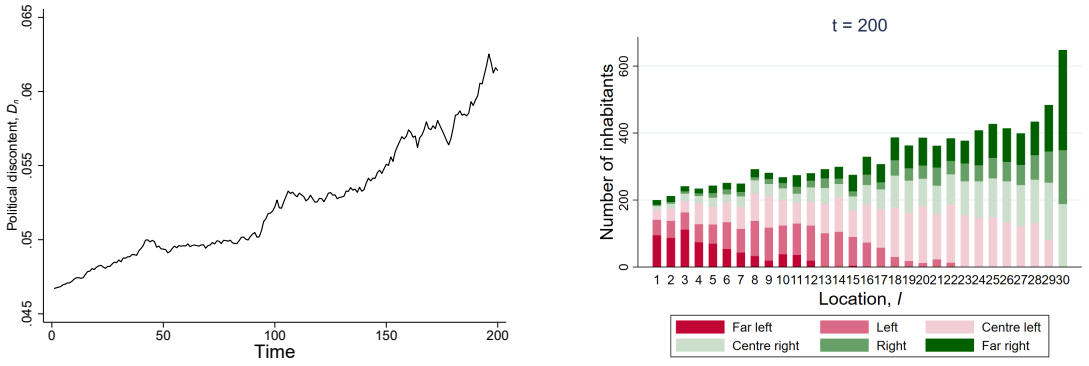

(a) Political discontent

(b) Political alienation by location

Note: Figure 14a shows the evolution of average political discontent, defined in equation (21), in the baseline calibration, see table 7. Figure 14b shows the prevalence of alienated voters across locations by quartiles of political discontent. 'Right' ('left') agents prefer redistributive tax rates to drop (rise), see equation (22): 'far right', 'right' and 'centre right' respectively comprises the top, second and bottom two quartiles of political discontent, with a similar categorization used for 'left' agents. Locations are sorted from least (l=1) to most (l=30) productive.

distributive conflicts that can be exploited by radical parties. If political radicalism comes with its own costs, for instance stemming from government instability and more difficult policy formulation, the political cost of agglomeration may well outweigh its benefits.

More generally, the calibrated model allows to analyze how (un)equal development affects several untargetted economic and political outcomes: population density and human capital endowments in the 20% most productive locations, N^{P20} and $\bar{s}^{P20}$; equilibrium tax rates, τ^*, from equation (19); within-period fiscal preference heterogeneity, $\sigma^{\tau^*_N}$, as measured by the variance in individual tax preferences in equation (20); average political discontent, $\bar{D}$, from equation (21); radical vote shares in the country, the 20% most productive locations and the 80% least productive locations from equation (22), RVS, RVS^{P20} and RVS^{P80}; and the ratio of population-weighted productive amenities in the 20% most and 80% least productive locations, $a^{P20/P80}$, as a measure of regional inequality.

Table 9 provides an overview of the main results by showing the average values of these focal outcomes for each consecutive 50-period time window in the model, with standard deviations between brackets; more details can be found in appendix figure A51. The first grey row confirms that population does not agglomerate under equal development, while the population share of the 20% most productive locations does increase in each other scenario. Increasing mobility strengthens agglomeration while redistributive transfers, by making spendable income less dependent on wages, weakens it. Second, only under divergent development is economic growth associated with skill-biased labor mobility to leading locations, which becomes more pronounced with redistributive taxes and progressively increasing labor mobility. Equilibrium tax rates remain fairly stable and are higher in the redistributive scenario, as intended. Interestingly, equilibrium tax rates also rise with labor mobility in the long run, as nominal wage compression increases the willingness to pay taxes. Within-period fiscal preference heterogeneity, $\sigma^{\tau^{*N}}$, remains stable with equal

Table 9: **Simulated results across scenarios**

Outcome	*Scenario*	$t \in 1 \rightarrow 50$	$t \in 51 \rightarrow 100$	$t \in 101 \rightarrow 150$	$t \in 151 \rightarrow 200$	*Figure*
N^{P20}	baseline	.257 (.012)	.273 (.007)	.297 (.003)	.311 (.005)	A51a
	ED	.231 (.001)	.231 (.001)	.231 (.001)	.231 (.001)	
	LM	.285 (.03)	.359 (.015)	.405 (.015)	.475 (.023)	
	MV	.253 (.012)	.274 (.003)	.282 (.005)	.294 (.005)	
$\bar{s}^{P20}$	baseline	2.29 (.016)	2.305 (.006)	2.308 (.007)	2.338 (.013)	A51b
	ED	2.241 (.007)	2.241 (.008)	2.241 (.008)	2.241 (.008)	
	LM	2.267 (.01)	2.281 (.01)	2.3 (.007)	2.307 (.011)	
	MV	2.309 (.026)	2.352 (.009)	2.379 (.016)	2.409 (.019)	
τ^*	baseline	.268 (.001)	.268 (.001)	.267 (.001)	.273 (.004)	A51c
	ED	.265 (0)	.265 (0)	.265 (0)	.265 (0)	
	LM	.266 (.001)	.266 (.001)	.27 (.001)	.273 (.003)	
	MV	.43 (.003)	.444 (.004)	.455 (.004)	.467 (.004)	
$\sigma^{\bar{\tau}^{*N}}$	baseline	.197 (.003)	.202 (.002)	.213 (.002)	.225 (.004)	A51d
	ED	.192 (0)	.192 (0)	.192 (0)	.192 (0)	
	LM	.197 (.004)	.209 (.003)	.218 (.003)	.235 (.007)	
	MV	.197 (.004)	.207 (.002)	.212 (.002)	.223 (.003)	
$\bar{D}$	baseline	.048 (.001)	.05 (.001)	.053 (.001)	.058 (.002)	A51e
	ED	.047 (0)	.047 (0)	.047 (0)	.047 (0)	
	LM	.048 (.001)	.052 (.001)	.055 (.001)	.062 (.003)	
	MV	.085 (.001)	.09 (.002)	.095 (.001)	.1 (.002)	
RVS	baseline	.267 (.018)	.293 (.012)	.338 (.007)	.379 (.015)	A51f
	ED	.235 (0)	.235 (0)	.235 (0)	.235 (0)	
	LM	.27 (.024)	.328 (.009)	.359 (.011)	.408 (.02)	
	MV	.353 (.002)	.364 (.004)	.375 (.003)	.386 (.004)	
RVS^{P20}	baseline	.29 (.024)	.321 (.014)	.36 (.005)	.39 (.011)	A51g
	ED	.234 (.002)	.234 (.002)	.234 (.002)	.234 (.002)	
	LM	.283 (.021)	.33 (.01)	.354 (.006)	.365 (.01)	
	MV	.433 (.037)	.523 (.017)	.575 (.015)	.621 (.017)	
RVS^{P80}	baseline	.278 (.037)	.334 (.018)	.418 (.018)	.499 (.029)	A51g
	ED	.223 (.001)	.224 (0)	.224 (0)	.224 (0)	
	LM	.289 (.054)	.4 (.012)	.462 (.034)	.599 (.033)	
	MV	.286 (.028)	.251 (.004)	.238 (.013)	.207 (.008)	
$a^{P20/P80}$	baseline	1.154 (.069)	1.254 (.051)	1.418 (.02)	1.522 (.038)	A51h
	ED	1 (0)	1 (0)	1 (0)	1 (0)	
	LM	1.154 (.079)	1.366 (.044)	1.484 (.037)	1.68 (.091)	
	MV	1.159 (.084)	1.349 (.026)	1.425 (.028)	1.54 (.038)	

development but grows in all other scenarios, especially under increasing labor mobility. Finally, the last grey row indicates that regional inequality remains stable with equal development but rises in each other scenario, especially in when labor is mobile.

Turning to the political landscape, political discontent, $\bar{D}$, rises with unequal but not with equal development, see also proposition 5. Consistent with propositions 7 and 8, average political discontent rises both with labor mobility and especially with enhanced redistributive taxes. Radical vote shares remain stable under equal development but grow over time with unequal development, though never exceeding 50%. Compared to the baseline scenario, radical vote shares are consistently higher under increasing labor mobility and redistributive transfers. Interestingly, the geography of discontent is clearly located in the least productive locations in the baseline and labor mobility scenarios but switches to leading locations with increased redistributive transfers. This suggests that increasing redistribution to compensate lagging regions may produce backlash in leading locations but that increasing mobility to improve access to better paying jobs may generate the opposite externality of fuelling discontent with those left behind in lagging regions.

7 Model validation

Both the comparative statics of the dynamic spatial political economy model in section 5 and the baseline simulations in section 6 indicate that the political externalities of divergent development primarily fall on underdeveloped regions. This section develops an instrumental variables approach to validate this model prediction by leveraging plausibly exogenous variation in long-run growth determinants. Complementing the existing literature's focus on exogenous trade shocks, the main aim of this exercise is thus to uncover the political externalities of exogenous variation in longer run growth fundamentals, which presumably have more economic significance due to their compounding effect.

I focus on three measurements of economic performance: relative per capita GDP, $\bar{y}$, computed as the ratio of constituency to country-wide per capita GDP; the population share in grid cells belonging to the bottom quintile of country-level per capita GDP, $\dot{y}$; and the population share in grid cells belonging to the top quintile of country-level per capita GDP, $\dot{y}$. While the former captures persistent level differences in per capita GDP across constituencies, the latter capture differences in the prevalence of rich and poor population strata *within* constituencies. All variables are computed from the gridded data and constituency maps for each available election covered in the SPEED, see section 2.

To deal with endogeneity, I follow several studies that argue that differences in proximity to the historical Roman road network (Wahl, 2017; Dalgaard et al., 2022; De Benedictis et al., 2023) and terrain flatness (Nunn & Puga, 2012) provide exogenous variation in long-run growth potential by persistently affecting market access. I exploit constituency-level variation in terrain ruggedness, measured as the standard deviation of grid-level elevation within each constituency, and their distance to the nearest Roman road to measure exogenous differences in their long term growth potential. Constituency-level terrain ruggedness is computed from the elevation dataset of U.S. Geological Survey (2010) while each constituency's centroid distance to the historical Roman road network is computed from the map of McCormick, Huang, Zambotti, and Lavash (2013). Roman road distances are demeaned by subtracting the average distance to the nearest road within each country to account for cross-country differences in location relative to the Roman road network.

I use this information to estimate the following 2SLS-equation

$$\begin{aligned} y_{\zeta,t} &= \alpha + \alpha_1 dist_{\zeta} + \alpha_2 ruggedness_{\zeta} + \epsilon_{\zeta,t} \\ D_{\eta,c,e,t} &= \beta + \beta_1 y_{\zeta,t} + \epsilon_{\zeta,t} \end{aligned} \tag{27}$$

where y is either relative per capita GDP of constituency ζ in election t or its poor or rich population share as previously discussed; *dist* and *ruggedness* are the instruments capturing the demeaned distance to the nearest Roman road and terrain ruggedness; and D is either the combined vote share for radical, extremist or populist parties as discussed in section 2.3.3. The baseline results focus on the 1992-2023 period, when constituency-level per capita GDP can be estimated from satellite-based information on nighttime lights,

and relies on a majority definition which classifies parties as radical, extremist or populist if they are classified as such in at least two of the three classification sources in appendix table A8. Appendix tables A11 to A13 highlight that the results are robust to expanding the time coverage to 1847-2023 or the use of a minority definition to classify parties. Since I want to determine the extent to which divergent development can explain the timing and location of radicalism, I refrain from including country or year fixed effects.[16]

The baseline results reported in table 10 shows that the first stage coefficients consistently have the expected signs and are always statistically significant, resulting in high first-stage F-statistics in most cases. The Hansen J test for the null hypothesis of the validity of the overidentifying restrictions fails to reject the null hypothesis in all cases except, even though using poor population shares as an indicator of relative underdevelopment yields a somewhat weaker first stage correlation with the instruments.

Table 10: **Divergent development and discontent, 1992-2023: 2SLS-estimates**

	Radicalism			Extremism			Populism		
	$\bar{\bar{y}}$	$\underline{y}$	$\dot{y}$	$\bar{\bar{y}}$	$\underline{y}$	$\dot{y}$	$\bar{\bar{y}}$	$\underline{y}$	$\dot{y}$
y	-.43**	.71***	-.86*	-.14	.23	-.29	-.35**	.58***	-.69*
	(.19)	*(.21)*	*(.44)*	*(.13)*	*(.17)*	*(.29)*	*(.16)*	*(.2)*	*(.36)*
Method	2SLS	2SLS	2SLS	2SLS	2SLS	2SLS	2SLS	2SLS	2SLS
N	18442	18442	18442	18442	18442	18442	18442	18442	18442
Hansen J p-value	.23	.12	.49	.51	.45	.57	.47	.27	.74
First stage results:									
Roman road distance	-.54**	.37**	-.23**	-.54**	.37**	-.23**	-.54**	.37**	-.23**
	(.22)	*(.13)*	*(.1)*	*(.22)*	*(.13)*	*(.1)*	*(.22)*	*(.13)*	*(.1)*
Ruggedness	-.02***	.01**	-.01***	-.02***	.01**	-.01***	-.02***	.01**	-.01***
	(0)	*(0)*	*(0)*	*(0)*	*(0)*	*(0)*	*(0)*	*(0)*	*(0)*
F-statistic	14.4	5.2	35.6	14.4	5.2	35.6	14.4	5.2	35.6

Note: This table reports 2SLS from equation (27). Dependent variables: the combined constituency-level party vote shares of radical, extremist or populist parties in the CLEA. Political parties are classified as radical, extremist or populist if they are categorized as such by at least two of the three classifications in table A8. The mean (and standard deviation) of radical, extremist and populist vote shares in the panel are .159 (.172), .111 (.139) and .124 (.16). Independent variables, y: relative per capita GDP, $\bar{\bar{y}}$, or the ratio of constituency to country per capita GDP; and the population share in the bottom or top quintile of gridded per capita GDP, $\underline{y}$ and $\dot{y}$. Constituency-level GDP is approximated by spatializing reported country GDP using satellite data on nighttime lights, see section 2.2. Independent variables are instrumented by centered distances to Roman roads and ruggedness; the first stage results are reported in the bottom panel. The overlapping mean (and standard deviation) of $\bar{\bar{y}}$, $\underline{y}$ and $\dot{y}$ are .982 (.51), .212 (.228) and .194 (.304). Total observations, N, and the Hansen J test of overidentifying restrictions are reported in the middle panel. Standard errors are robust to heteroskedasticity and clustered at the country-level.

More interestingly, the effect of divergent development is fully consistent with model predictions, where radicalism decreases with relative per capita GDP as well as rich population shares yet rises with poor population shares. The estimated effect sizes for radicalism are also quite substantive: a standard deviation increase in relative per capita GDP (.51) and the rich population share (.304) respectively reduce radical vote shares by 21.4 p.p. and 26.1 p.p. while a standard deviation increase in poor population shares (.23) increase radical vote shares with 16.3 p.p., roughly accounting for half of the recent vote shares of 40% in figure 9b. Subsequent columns indicate these results to be primarily driven by

[16] Appendix table A13 presents results for a model that includes country and year fixed effects.

populist vote shares, which seem most sensitive to divergent development. These results imply that constituencies whose economic development is hampered by their remote location or uneven terrain are much more likely to lead the recent electoral rise in radicalism. Moreover, the effect sizes are also much larger than those in the existing literature, which typically finds standard deviation elasticities between 2 p.p. and 10 p.p., see Margalit (2019).

Finally, table 11 relies on an alternative indicator of political alienation, namely the turnout rate. Note that equation (22) of the spatial political economy model implies that turnout differences are also informative for the presence of alienation, as prospective voters will only decide not to vote if they reach a minimum amount of political discontent. The results are in line with those of table 11 and indicate that turnout rates are primarily depressed in constituencies which, due to their location and geography, tend to have large population shares in the bottom quintile of per capita GDP while turnout rates rise with relative per capita GDP and population shares in the top quintile of per capita GDP.

Table 11: **Divergent development and turnout, 1847-2023: 2SLS-estimates**

	Turnout		
	$\bar{\bar{y}}$	$\underset{\cdot}{y}$	$\dot{y}$
y	.21*	-.11**	.42*
	(.12)	*(.05)*	*(.26)*
Method	2SLS	2SLS	2SLS
N	41945	41945	41945
Hansen J p-value	.4	.31	.48
First stage results:			
Roman road distance	-.53***	.83***	-.27***
	(.17)	*(.23)*	*(.08)*
Ruggedness	-.01***	.01**	-.01***
	(0)	*(0)*	*(0)*
F-statistic	7.3	9.7	8.8

Note: This table reports 2SLS from equation (27). Dependent variable: constituency-level turnout rates computed from the CLEA. The mean (and standard deviation) of turnout equals .759 (1.647). Independent variables, y: relative per capita GDP, $\bar{\bar{y}}$, or the ratio of constituency to country per capita GDP; and the population share in the bottom or top quintile of gridded per capita GDP, $\underset{\cdot}{y}$ and $\dot{y}$. Constituency-level GDP is approximated by spatializing reported country GDP using satellite data on nighttime lights or, if that is unavailable, an indicator of market access, see section 2.2. Independent variables are instrumented by centered distances to Roman roads and ruggedness; the first stage results are reported in the bottom panel. The mean (and standard deviation) of $\bar{\bar{y}}$, $\underset{\cdot}{y}$ and $\dot{y}$ are .969 (.387), .228 (.328) and .173 (.313). Total observations, N, and the Hansen J test of overidentifying restrictions are reported in the middle panel. Standard errors are robust to heteroskedasticity and clustered at the country-level.

8 Conclusion

While it has long been known that political cleavages tend to have a spatial pattern, the recent rise and distinct geography of populism has puzzled the social sciences and highlighted the need for high resolution data on the economic and political landscapes as well as updated theoretical models that allow to make sense of their empirical relations. This paper develops a dynamic spatial political economy model that incorporates redistributive taxation and agglomerated growth in a standard economic geography framework and finds that divergent development is simultaneously able to account for the timing and location

of vote shares for radical political parties. Divergent development induces labor mobility towards faster growing locations, reducing their willingness to pay redistributive taxes while simultaneously increasing their electoral influence on redistributive policy, such that the redistributive frictions of divergent development primarily affect lagging locations. Subsequent counterfactual analysis suggests that policies that enhance labor mobility and income redistribution respectively risk fueling electoral backlash in lagging and leading locations, such that there may be no panacea for the rise of radicalism in the short run.

To validate and calibrate the model, the paper introduces the Spatial Political Economy in Europe Database (SPEED), which contains high-resolution and long-run data on the political and economic landscapes. The main novelty for the economic landscape is the introduction of a population-based measure of market access as a proxy for local economic performance, which is demonstrated to attain comparable accuracy yet has much wider historical coverage than the often-used nighttime light proxy. The main novelty for the political landscape lies in the development of a comprehensive database of georeferenced electoral districts for nearly all European elections covered in the CLEA. The data offer broad evidence for synchronized movements in the economic and political landscapes, where periods of rising regional inequality coincide with two historical waves of political radicalism in the past two centuries. Instrumental variable regressions exploiting geographical differences in economic growth potential confirm a strong constituency-level causal relation between economic underdevelopment and vote shares for radical parties.

Although these results should not be interpreted to imply that divergent development is the sole determinant of political radicalism, which may also be driven by factors not included in the present model, they do imply a reappraisal of the economic explanations for populism and extremism. In addition, the model also implies that as long as economic development differs across space, as it has tended to be during the past two centuries in Europe, economic growth may generate adverse political externalities that allow radical parties to cement their electoral attractiveness in affected regions.

While this paper takes the novel step of integrating politics into a standard model of economic geography, the focus on simplicity and tractability explains the omission of several other factors that may mediate the relation between economic and political landscapes. For instance, the model abstracts from the cultural explanations that are highlighted in the existing literature. The current focus on redistributive policy also abstracts from the political discontent generated by non-redistributive policies such as the provision of public goods and place-based investments in local productive amenities. The absence of history implies that the model can not speak to the possible relevance of more idiosyncratic features such as historical experience or institutions, e.g. electoral thresholds or multi-round elections. The model is merely intended as a starting point for improved understanding of the linkages between the economic and political landscapes.

On the empirical front, the SPEED could be complemented with spatially disaggregated survey data on economic characteristics and political preferences to further validate

the model's microfoundations. Such data would allow to verify whether the least-educated and the lowest earners *within* lagging constituencies effectively have the largest tendency to vote for radical parties, as predicted by the model. Gethin, Martínez-Toledano, and Piketty's (2022) pioneering data efforts may offer a fruitful avenue. In addition, SPEED could also be complemented with quantitative information on the policy positions of different political parties. This could shed some light on the spillovers of the electoral success of radical parties on the policy platforms of mainstream parties. More broadly, while the focus of the current paper is on the geography of discontent, the data could also shed new light on some longstanding empirical debates in political economic geography, such as the historical urban-rural electoral divide (Lipset & Rokkan, 1967; Rodden, 2019, 2023) or the impact of low density and remoteness on voting (Bazzi, Fiszbein, & Gebresilasse, 2020).

References

Acemoglu, D., Egorov, G., & Sonin, K. (2013). A Political Theory of Populism. *The Quarterly Journal of Economics*, *128*(2), 771–805.

Acemoglu, D., Johnson, S., & Robinson, J. A. (2002). Reverals of Fortune: Geography and Institutions in the Making of the Modern WOrld Income Distribution. *Quarterly Journal of Economics*, *117*(4), 1231–1294.

Ahlfeldt, G. M., Redding, S. J., Sturm, D. M., & Wolf, N. (2015). The Economics of Density: Evidence From the Berlin Wall. *Econometrica*, *83*(6), 2127–2189.

Albanese, G., Barone, G., & de Blasio, G. (2022). Populist Voting and Losers' Discontent: Does Redistribution Matter? *European Economic Review*, *141*(2021), 1–21.

Albouy, D. (2009). The Unequal Geographic Burden of Federal Taxation. *Journal of Political Economy*, *117*(4), 635–667.

ARDECO. (2022). *Total Population on 1 January (Demographic Statistics).* Retrieved from https://urban.jrc.ec.europa.eu/ardeco/manager?lng=en

ARDECO. (2023). *GDP at current prices.* Retrieved from https://urban.jrc.ec.europa.eu/ardeco/explorer/view/20019?depth=step&territoryArea=eu

Autor, D., Dorn, D., Hanson, G., & Majlesi, K. (2020). Importing Political Polarization? The Electoral Consequences of Rising Trade Exposure. *American Economic Review*, *110*(10), 3139–3183.

Baum-Snow, N., Brandt, L., Henderson, V., Turner, M., & Zhang, Q. (2015). Transport Infrastructure, Urban Growth and Market Access in China. In *55th congress of the european regional science association: "world renaissance: Changing roles for people and places"* (pp. 1–50).

Bazzi, S., Fiszbein, M., & Gebresilasse, M. (2020). Frontier Culture: the Roots and Persistence of "Rugged Individualism" in the United States. *Econometrica*, *88*(6), 2329–2368.

Bolt, J., & Van Zanden, J. L. (2020). Maddison Style Estimates of the Evolution of the World Economy. A New 2020 Update. *Maddison-Project Working Paper 15*, 1–43. Retrieved from https://www.rug.nl/ggdc/historicaldevelopment/maddison/releases/maddison-project-database-2020?lang=en

Bolton, P., & Roland, G. (1997). The Breakup of Nations: a Political Economy Analysis. *The Quarterly Journal of Economics*, *112*(4), 1057–1090.

Bosker, M., Buringh, E., & van Zanden, J. L. (2013). From Baghdad to London: Unraveling Urban Development in Europe, the Middle East, and North Africa, 800-1800. *Review of Economics and Statistics*, *95*(4), 1418–1437.

Callander, S., & Carbajal, J. C. (2021). Cause and Effect in Political Polarization: A Dynamic Analysis. *Journal of Political Economy*, *forthcomin*, 1–61.

Caprettini, B., & Voth, H.-J. (2020). Rage against the Machines : Labor-Saving Technology and. *American Economic Review: Insights*, *2*(3), 305–320.

Chen, Z., Yu, B., Yang, C., Zhou, Y., Yao, S., Qian, X., ... Wu, J. (2021a). An Extended Time Series (2000-2018) of Global NPP-VIIRS-like Nighttime Light Data from a Cross-Sensor Calibration. *Earth System Science Data*, *13*(3), 889–906.

Chen, Z., Yu, B., Yang, C., Zhou, Y., Yao, S., Qian, X., ... Wu, J. (2021b). *An Extended Time-Series (2000-2018) of Global NPP-VIIRS-like Nighttime Light Data Version 4.* Retrieved from https://dataverse.harvard.edu/dataset.xhtml?persistentId=doi:10.7910/DVN/YGIVCD

CLIO Infra. (2014). *Gross Household Income Gini per Country.* Retrieved from https://clio-infra.eu/Indicators/IncomeInequality.html

Colantone, I., & Stanig, P. (2018a). Global Competition and Brexit. *American Political Science Review*, *112*(2), 201–218.

Colantone, I., & Stanig, P. (2018b). The Trade Origins of Economic Nationalism: Import Competition and Voting Behavior in Western Europe. *American Journal of Political Science*, *62*(4), 936–953.

Dalgaard, C. J., Kaarsen, N., Olsson, O., & Selaya, P. (2022). Roman roads to prosperity: Persistence and non-persistence of public infrastructure. *Journal of Comparative Economics*, *50*(4), 896–916.

Davis, M. A., & Ortalo-Magné, F. (2011). Household Expenditures, Wages, Rents. *Review of Economic Dynamics*, *14*(2), 248–261.

De Benedictis, L., Licio, V., & Pinna, A. (2023). From the historical Roman road network to modern infrastructure in Italy. *Journal of Regional Science*, 1–30.

Desmet, K., Nagy, D. K., & Rossi-Hansberg, E. (2018). The Geography of Development. *Journal of Political Economy*, *126*(3), 903–983.

Desmet, K., & Rossi-hansberg, E. (2014). Spatial Development. *American Economic Review*, *104*(4), 1211–1243.

Dippel, C., Gold, R., & Heblich, S. (2015). Globalization and its (Dis-)Content: Trade Shocks and Voting Behavior. *NBER Working Paper 21812*, 1–54.

Dornbusch, R., & Edwards, S. (1991). The Macroeconomics of Populism. In *The macroeconomics of populism in latin america volume* (pp. 7–13). University of Chicago Press. Retrieved from http://www.nber.org/books/dorn91-1

Eichengreen, B. (2018). *The Populist Temptation.* Oxford: Oxford University Press.

Eurostat. (2023a). *Gross domestic product (GDP) at current market prices by NUTS 3 regions.* Retrieved from https://ec.europa.eu/eurostat/databrowser/product/page/NAMA_10R_3GDP__custom_7573457

Eurostat. (2023b). *Population on 1 January by Broad Age Group, Sex and NUTS 3 Region.* Retrieved from https://ec.europa.eu/eurostat/databrowser/view/DEMO_R_PJANAGGR3__custom_7573500/default/table

Funke, M., Schularick, M., & Trebesch, C. (2016). Going to Extremes: Politics After Financial Crises, 1870–2014. *European Economic Review*, *88*, 227–260.

Gay, V. (2021). Mapping the Third Republic: A Geographic Information System of France (1870–1940). *Historical Methods*, *54*(4), 189–207.

Gennaioli, N., La Porta, R., Lopez-De-Silanes, F., & Schleifer, A. (2013). Human Capital and Regional Development. *The Quarterly Journal of Economics*, *128*(1), 105–164.

Gethin, A., Martínez-Toledano, C., & Piketty, T. (2022). Brahmin Left Versus Merchant Right: Changing Political Cleavages in 21 Western Democracies, 1948-2020. *Quarterly Journal of Economics*, *137*(1), 1–48.

Gibson, J., Olivia, S., & Boe-Gibson, G. (2020). Night Lights in Economics: Sources and Uses. *Journal of Economic Surveys*, *34*(5), 955–980.

Gibson, J., Olivia, S., Boe-Gibson, G., & Li, C. (2021). Which Night Lights Data Should We Use In Economics, and Where? *Journal of Development Economics*, *149*, 1–12. doi: 10.1016/j.jdeveco.2020.102602

GISCO. (2023). *The Geographic Information System of the Commission - NUTS Statistical Administrative Units Shapefile.* Retrieved from https://ec.europa.eu/eurostat/web/gisco/geodata/reference-data/administrative-units-statistical-units/nuts

Goldewijk, K. K., Beusen, A., Doelman, J., & Stehfest, E. (2017). Anthropogenic Land Use Estimates for the Holocene - HYDE 3.2. *Earth System Science Data*, *9*(2), 927–953.

Goldewijk, K. K., Beusen, A., & Janssen, P. (2010). Long-Term Dynamic Modeling of Global Population and Built-Up Area in a Spatially Explicit Way: HYDE 3 . 1. *The Holocene*, *20*(4), 565–573.

Guiso, L., Helios, H., Morelli, M., & Sonno, T. (2019). Global Crises and Populism: The Role of Eurozone Institutions. *Economic Policy*, *34*(97), 95–139.

Guiso, L., Herrera, H., Morelli, M., & Sonno, T. (2017). Demand and Supply of Populism. *EIEF Working Paper Series 1703*, 1–66.

Guiso, L., Herrera, H., Morelli, M., & Sonno, T. (2024). Economic Insecurity and the Demand of Populism in Europe. *Economica*, *forthcomin*.

Guriev, S., & Papaioannou, E. (2022). The Political Economy of Populism. *Journal of Economic Literature*, *60*(2), 753–832.

Henderson, J. V., Storeygard, A., & Weil, D. N. (2012). Measuring Economic Growth from Outer Space. *American Economic Review*, *102*(2), 994–1028. doi: 10.1257/aer.102.2.994

Herrmann, M., & Döring, H. (2023). Party Positions from Wikipedia Classifications of Party Ideology. *Political Analysis*, *31*(1), 22–41.

Hsieh, C. T., & Moretti, E. (2019). Housing Constraints and Spatial Misallocation. *American Economic Journal: Macroeconomics*, *11*(2), 1–39. doi: 10.1257/MAC.20170388

Inglehart, R. F. (1971). The Silent Revolution in Europe: Intergenerational Change in Post-Industrial Societies. *The American Political Science Review*, *65*(4), 991–1017.

Inglehart, R. F., & Norris, P. (2016). Trump, Brexit, and the Rise of Populism: Economic Have-Nots and Cultural Backlash. *HKS Faculty Research Working Paper Series*, *26*, 1–52.

Inglehart, R. F., & Norris, P. (2019). *Cultural Backlash Trump, Brexit, and Authoritarian Populism*. Cambridge: Cambridge University Press.

Karlson, N. (2024). *Reviving Classical Liberalism Against Populism*. Palgrave Macmillan Cham.

Kim, B., Gibson, J., & Boe-Gibson, G. (2023). Measurement Errors in Popular Night Lights Data May Bias Estimated Impacts of Economic Sanctions: Evidence from Closing the Kaesong Industrial Zone. *Economic Inquiry*(September), 1–15.

Kollman, K., Caramani, D., Backer, D., & Lublin, D. (2023). *Constituency-level Elections Archive Lower Chamber Elections Archive, Release 17 [data file and codebook]*. Retrieved from http://www.electiondataarchive.org

Lipset, S. M., & Rokkan, S. (1967). *Party Systems and Voter Alignments: Cross-National Perspectives*. New York: Free Press.

Malgouyres, C. (2017). Trade Shocks and Far-Right Voting : Evidence from French Presidential Elections. *EUI Working Paper RSCAS 2017/21*, 1–25.

Margalit, Y. (2019). Economic insecurity and the causes of populism, reconsidered. *Journal of Economic Perspectives*, *33*(4), 152–170.

McCormick, M., Huang, G., Zambotti, G., & Lavash, J. (2013). *DARMC Roman Road Network (version 2008)*. Retrieved from https://dataverse.harvard.edu/dataset.xhtml?persistentId=doi:10.7910/DVN/TI0KAU

Monte, B. F., Redding, S. J., & Rossi-hansberg, E. (2018). Commuting , Migration, and Local Employment Elasticities. *American Economic Review*, *108*(12), 3855–3890.

Morelli, M., Nicolò, A., & Roberti, P. (2021). A Commitment Theory of Populism. *CESifo Working Paper No. 9473*, 1–49.

Nagy, D. K. (2022). Quantitative Economic Geography Meets History: Questions, Answers and Challenges. *Regional Science and Urban Economics*, *94*, 1–14. doi: 10.1016/j.regsciurbeco.2021.103675

National Oceanic and Atmospheric Administration. (2013). *Version 4 DMSP-OLS Nighttime Lights Time Series*. Retrieved from https://ngdc.noaa.gov/eog/dmsp/downloadV4composites.html

Nordhaus, W. D. (2006). Geography and Macroeconomics: New Data and New Findings. *Proceedings of the National Academy of Sciences of the United States of America*, *103*(10), 3510–3517.

Nordhaus, W. D., & Chen, X. (2016). *Global Gridded Geographically Based Economic Data (G-Econ), v4*. Retrieved from https://sedac.ciesin.columbia.edu/data/set/spatialecon-gecon-v4

Noury, A., & Roland, G. (2020). Identity Politics and Populism in Europe. *Annual Review of Political Science*, *23*, 421–439.

Nunn, N., & Puga, D. (2012). Ruggedness: The blessing of bad geography in Africa. *Review of Economics and Statistics*, *94*(1), 20–36.

OECD.Stat. (2024). *Social Expenditure in Percentage of Gross Domestic Product.* Retrieved from https://data-explorer.oecd.org/?lc=en&fs[0]=Topic%2C1%7CSociety%23SOC%23%7CSocialprotection%23SOC_PRO%23&pg=0&fc=Topic&bp=true&snb=12

Parkhomenko, A. (2021). Homeownership, Polarization, and Inequality. *Working Paper*, 1–74.

Pástor, L., & Veronesi, P. (2021). Inequality Aversion, Populism, and the Backlash against Globalization. *Journal of Finance*, *76*(6), 2857–2906.

Redding, J., & Turner, M. A. (2015). Transportation Costs and the Spatial Organization of Economic Activity. In G. Duranton, J. V. Henderson, & W. Strange (Eds.), *Handbook of regional and urban economics* (5th ed., Vol. 5, pp. 1339–1398). Elsevier B.V.

Roback, J. (1982). Wages , Rents , and the Quality of Life. *Journal of Political Economy*, *90*(6), 1257–1278.

Rodden, J. A. (2019). *Why Cities Lose: The Deep Roots of the Urban-Rural Political Divide.* New York: Basic Books.

Rodden, J. A. (2023). The Urban-Rural Divide in Historical Political Economy. In *The oxford handbook of historical political economy* (p. C41P1-C41N4). Oxford: Oxford University Press.

Rodríguez-pose, A. (2018). The Revenge of the Places That Don't Matter (and What To Do About It). *Cambridge Journal of Regions, Economy and Society*, *11*, 189–209.

Rodrik, D. (2018a). Is Populism Necessarily Bad Economics? *AEA Papers and Proceedings*, *108*(108), 196–199.

Rodrik, D. (2018b). Populism and the economics of globalization. *Journal of International Business Policy*, *1*(1-2), 12–33. Retrieved from https://doi.org/10.1057/s42214-018-0001-4 doi: 10.1057/s42214-018-0001-4

Rooduijn, M., Van Kessel, S., Froio, C., Pirro, A., De Lange, S., Halikiopoulou, D., ... Taggart, P. (2019). *The PopuList: An Overview of Populist, Far Right, Far Left and Eurosceptic Parties in Europe.* Retrieved from www.popu-list.org

Rosen, S. (1979). Wage-Based Indexes of Urban Quality of Life. In P. Mieszkowski & M. Strassheim (Eds.), *Current issues in urban economics* (2nd ed., pp. 74–104). Baltimore, Maryland.

Rosés, J. R., & Wolf, N. (2019). *The Economic Development of Europe's Regions - A Quantitative History since 1900.* New York: Routledge.

Rosés, J. R., & Wolf, N. (2021a). *Regional growth and inequality in the long-run: Europe, 1900-2015* (Vol. 37) (No. 1). Oxford University Press. doi: 10.1093/oxrep/graa062

Rosés, J. R., & Wolf, N. (2021b). *Rosés-Wolf database, version 6.* Retrieved from https://www.wiwi.hu-berlin.de/de/professuren/vwl/wg/roses

-wolf-database-on-regional-gdp

Storper, M. (2018). Separate Worlds ? Explaining the Current Wave of Regional Economic Polarization. *Journal of Economic Geography*, *18*, 247–270.

Swank, D. (2003). Globalization, the welfare state and right-wing populism in Western Europe. *Socio-Economic Review*, *1*(2), 215–245. doi: 10.1093/soceco/1.2.215

Tabellini, M. (2020). Gifts of the Immigrants, Woes of the Natives: Lessons from the Age of Mass Migration. *The Review of Economic Studies*, *87*(1), 454–486.

U.S. Geological Survey. (2010). *Global Multi-resolution Terrain Elevation Data 2010.* Retrieved from https://topotools.cr.usgs.gov/gmted_viewer/viewer.htm

Vanschoonbeek, J. (2020). Regional (in)stability in Europe a Quantitative Model of State Fragmentation. *Journal of Comparative Economics*, *48*(3), 605–641.

Vanschoonbeek, J. (2024). *Spatial Political Economy in Europe Database (SPEED).* Retrieved from https://sites.google.com/site/jakobvanschoonbeek/data/spatial-political-economy-data

von Ehrlich, M., & Overman, H. G. (2020). Place-Based Policies and Spatial Disparities across European Cities. *The Journal of Economic Perspectives*, *34*(3), 128–149.

Voorheis, J., McCarty, N., Shor, B., & Rogers, S. (2015). *Unequal Incomes, Ideology and Gridlock: How Rising Inequality Increases Political Polarization.* Retrieved from http://ssrn.com/abstract=2649215https://ssrn.com/abstract=2649215Electroniccopyavailableat:http://ssrn.com/abstract=2649215

Wahl, F. (2017). Does European development have Roman roots? Evidence from the German Limes. *Journal of Economic Growth*, *22*(3), 313–349.

Wang, T., & Sun, F. (2022). Global Gridded GDP Data Set Consistent with the Shared Socioeconomic Pathways. *Scientific Data*, *9*(221), 1–10.

World Economic Forum. (2017). *The Global Risks Report 2017* (Tech. Rep.). Geneva: World Economic Forum. Retrieved from http://www3.weforum.org/docs/GRR/WEF_GRR16.pdf

Zhuravskaya, E., Petrova, M., & Enikolopov, R. (2020). Political Effects of the Internet and Social Media. *Annual Review of Economics*, *12*, 415–438.

A Data construction and sources

Political cleavages often have a distinct geography while politico-economic theories often have implications that can most adequately be validated at the high spatial resolution of cities or electoral constituencies. Yet applied work in the field of spatial political economy is complicated by the lack of sufficiently granular geocoded electoral and socio-economic data, which are often reported for differing administrative boundaries, and suitable cross-country operationalizations of political party classifications. This appendix describes the construction of a spatial political economy database for Europe, which aims to provide an empirical foundation for applied work on the relations between the geographical, political and economic landscapes in Europe. All of the data and code are made available here.

A.1 Economic landscape

Empirical research in economic geography has long been hampered by a lack of high-resolution spatial data, which becomes even more sparse as one goes back in time (Nordhaus, 2006; Nagy, 2022). The main reason is that most socio-economic data is collected on the basis of administrative boundaries, which are not always compatible across variables or time, such that data from different sources cannot always be easily linked. This section improves existing methodologies to provide yearly gridded estimates of population and GDP for a large sample of European countries and a large timeframe, at a high spatial resolution of 5-arcminutes, which is sufficiently finegrained to be aggregated to arbitrary administrative boundaries using standard spatial weighting methods. Section A.1.1 provides further details on the construction of the spatial grid. Section A.1.2 explains the methodology and sources to estimate gridded population and reports some validation checks. Section A.1.3 similarly describes the data sources and methodology to estimate gridded GDP and harmonize them with existing sources, ending with a battery of validation checks.

A.1.1 Construction of the 5-arcminute grid map of Europe

I first generate a rectangular spatial grid that overlays the map of Europe with a northwest corner at (24° 34' 60"W 71° 19' 60"N) and a southeast corner at (31° 59' 60"E 34° 44' 60"N). Note that territories outside of these borders, such as Greenland in Denmark or the *Départements d'outre-mer* in France, are therefore not considered. I populate this grid with 298081 grid cells with a resolution of 5' latitude by 5' longitude, which have an average surface area of 51 km^2.[17] This resolution is mainly chosen because it is the highest spatial resolution for which long-term time series of gridded population are available, see section A.1.2. Appendix figure A37 shows the full spatial grid used in subsequent computations and overlays it with current borders of European NUTS3 regions.[18]

[17] A large fraction of grid cells are located in the sea and are ignored in subsequent estimations. The European landmass of the 28 countries in the sample cover 101408 grid cells (NUTS version 2021).

[18] In what follows, shapefiles for different versions of the NUTS-classification are taken from GISCO (2023).

Figure A1 provides some detailed snap shots of the grid to clarify the level of spatial detail. Figure A1a shows the grid cells located on the land mass in central Europe, as determined by their intersection with current NUTS 2021 borders, clearly visualizing Belgium, Luxembourg and parts of France, Germany, the Netherlands and the UK. It also shows the borders of all the NUTS3 regions within the NUTS1 region of London (code *"UKI"*) in red. Figure A1b zooms in on London and shows that its surface area is covered by around 60 individual grid cells. Finally, figure A1c highlights a single grid cell in the north west of central London, showing how its surface area is allocated to five separate NUTS3 regions: *"UKI31"*, *"UKI32"*, *"UKI33"*, *"UKI71"* and *"UKI72"*. The share of the surface area allocated to each NUTS3 region is indicated between brackets. As discussed later, under the assumption of uniform distribution within grid cells, grid cell data can be allocated to aggregate administrative borders using these shares as spatial weights.

Figure A1: **Spatial grid: details**

(a) Grid cells in the center of Europe

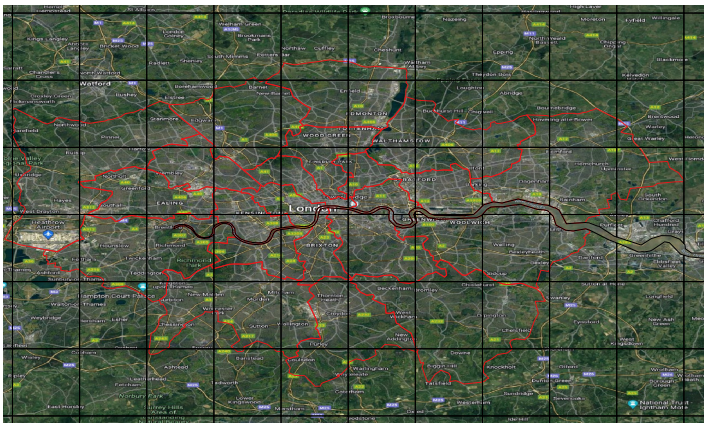

(b) Grid cells around London

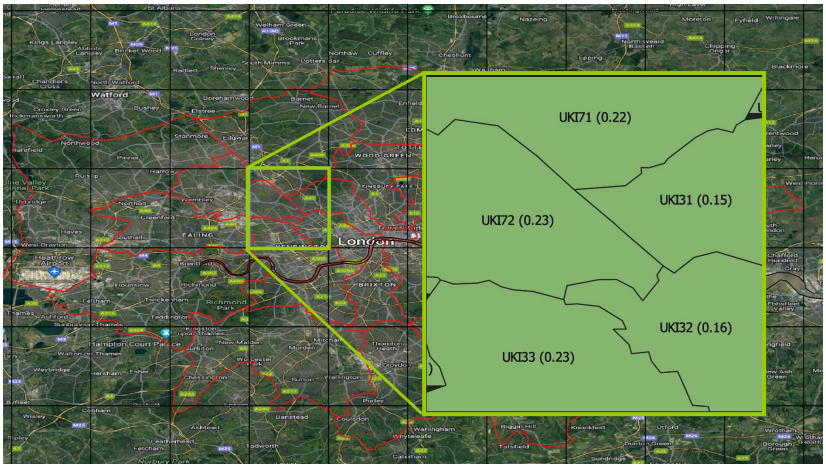

(c) Administrative borders in London grid cell

Note: This figure shows several details of the 5-arcminute spatial grid. Figure A1a shows mainland grid cells in the center of Europe and highlights the current NUTS3 regions of London (UKI) in red. Figure A1b overlays a satelite image of London with the spatial grid and its current NUTS3 regions in red. Figure A1c highlights the administrative NUTS3 borders of one particular grid cell and the share of grid cell surface area they represent.

Figure A2: **Grid cell count and surface area of current NUTS3 regions**

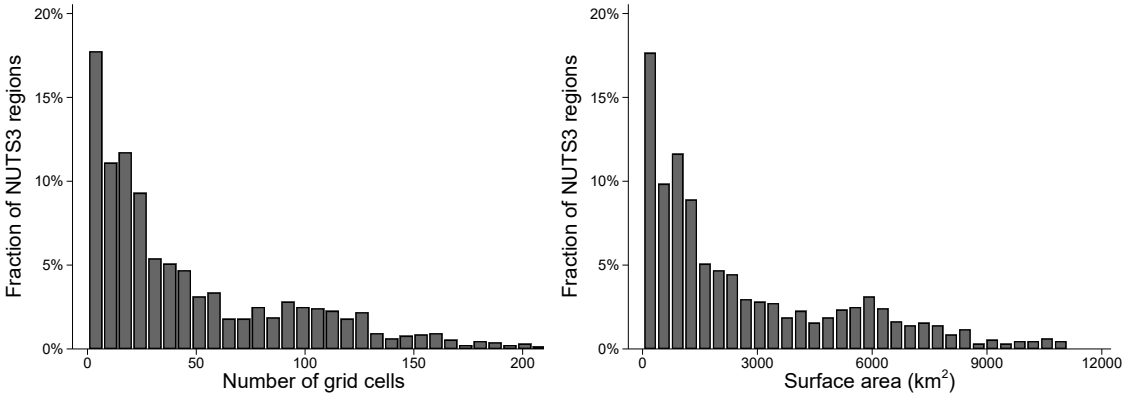

(a) Grid cell count

(b) Surface area (km^2)

Note: Figures A2a and A2b show the distributions of grid cells and surface area for each of the current 1347 NUTS3 regions (version 2021) in the sample. Each distribution is truncated at the 95^{th} percentile to increase legibility.

Figure A2 provides an additional measure of the degree of spatial detail by showing the distribution of grid cell counts and surface area across current NUTS3 regions. Figure A2a shows that NUTS3 regions are typically composed of several dozens of grid cells, with the average region comprising 75 grid cells. Similarly, the distribution of the surface areas of current NUTS3 regions shown in figure A2b confirms that they typically amount to several multiples of the average grid cell area of 51 km^2, with an average surface area of 3819 km^2. As the NUTS3 level is currently the most disaggregated spatial level for which socio-economic variables in Europe are reported, these figures illustrate the considerable gain in spatial resolution attained in the database. For instance, while questions related to the urban-rural divide are difficult to analyze as several NUTS3 regions encompass both, this level of spatial detail would allow for a more appropriate empirical investigation.

A.1.2 Estimating gridded population

Section 2 explains how climate change research forms the basis for the gridded population estimates, since it has recently provided such estimates for extremely long time horizons in order to study anthropogenic climate change. The main refinement is to harmonize these estimates to make them consistent with reported population figures in authoritative (sub)national data sources. To do so, each gridded population estimate is scaled with a calibration weight to ensure that *i)* the gridded population *counts* within country borders sum to total country population in a target national source and *ii)* the subnational gridded population *shares* equal those reported in a target subnational source. In the empirical application, I use total country population in the Maddison database (Bolt & Van Zanden, 2020) as the target national source and NUTS3 population shares in Eurostat (2023b) and ARDECO (2022) for recent years as well as regional populations in Rosés and Wolf (2019) for more distant time periods as the subnational targets, see equation (2).

Methodology

Harmonization of raw gridded population estimates with existing sources can be obtained by determining the two multiplicative calibration weights, $\upsilon^c_{g,t}$ and $\upsilon^r_{g,t}$ in equation (1), where the subnational calibration weight, $\upsilon^r_{g,t}$, is first calibrated to ensure that subnational population shares of each region r within the borders of a particular country c, $\frac{\hat{N}^{raw}_{r,t}}{\sum_{r\in c}\hat{N}^{raw}_{r,t}}$, match reported subnational population shares in a target subnational source, $\frac{N_{r,t}}{\sum_{r\in c}N_{r,t}}$. This boils down to first computing the scaling factor that equalizes estimated and reported subnational population shares for each subnational region, r

$$\upsilon_{r,t} = \frac{N_{r,t}/\sum_{r\in c}N_{r,t}}{\hat{N}^{raw}_{r,t}/\sum_{r\in c}\hat{N}^{raw}_{r,t}} \qquad \forall r \in R \tag{1A}$$

and subsequently accounting for the population allocation across subnational units in each grid cell by applying subnational spatial weights to obtain the final calibration weight as

$$\upsilon^r_{g,t} = \sum_{r\in g}\lambda_{g,r}\upsilon_{r,t} \tag{2A}$$

The national calibration weight, $\upsilon^c_{g,c}$, is similarly calibrated to ensure that total gridded country population counts of each country c, $\sum_{g=1}^{G}\lambda_{g,c}\upsilon^r_{g,t}\hat{n}^{raw}_{g,t}$, equal those reported in a target national source, $N_{c,t}$. Again, this first requires the computation of the scaling factor necessary to equalize total gridded and reported country populations for each country, c

$$\upsilon_{c,t} = \frac{N_{c,t}}{\sum_{g=1}^{G}\lambda_{g,c}\upsilon^r_{g,t}\hat{n}^{raw}_{g,t}} \qquad \forall c \in C \tag{3A}$$

and proportionally allocating them to grid cells based on their relative surface area

$$\upsilon^c_{g,t} = \sum_{r\in g}\lambda_{g,r}\upsilon_{c,t} \tag{4A}$$

Final grid-specific calibration weights for each combination of a national and subnational targets can be obtained by multiplying subnational and national calibration weights

$$\upsilon_{g,t} = \begin{cases} \upsilon^c_{g,t}\upsilon^r_{g,t} & \text{if } \upsilon^c_{g,t} \notin \varnothing \;\&\; \upsilon^r_{g,t} \notin \varnothing \\ \upsilon^c_{g,t} & \text{if } \upsilon^c_{g,t} \notin \varnothing \;\&\; \upsilon^r_{g,t} \in \varnothing \\ \upsilon^c_{g,\bar{t}} & \text{if } \upsilon^c_{g,t} \in \varnothing \;\&\; \upsilon^r_{g,t} \in \varnothing \end{cases} \tag{5A}$$

Data sources

To implement this methodology, gridded population estimates for the period 1800-2023 are taken from the HYDE database version 3.3, which provides gridded population estimates at a spatial resolution of 5 arc minutes for the whole world from 10000 BC to the present day. The database combines historical population estimates from statistical

agencies, censuses and historical atlases with ancillary information on soil quality, land cover, roads, terrain slopes, distance to water, village locations and archaeological case studies to allocate total country population to the grid (Goldewijk, Beusen, Doelman, & Stehfest, 2017; Goldewijk, Beusen, & Janssen, 2010). Gridded population estimates are available at a yearly frequency from 1950 onwards and at a decennial frequency before that. Assuming population evolves gradually over time, as in the other sources, missing population observations before 1950 are linearly interpolated at the grid cell level.

These estimates are subsequently harmonized with the available country population figures in the Maddison database (Bolt & Van Zanden, 2020), which functions as the main national target source. The Maddison database is one of the most comprehensive and widely used sources for national historical population data that aggregates existing information on total population for constant country borders from a range of sources, including censuses, statistical agencies and academic case studies. As the most recent 2020 version of the database only covers the years until 2017, country populations are extended to 2021 using their evolution in ARDECO (2022).

To also ensure that gridded population estimates reflect reported subnational population shares, I rely on the available NUTS3 population figures from Eurostat (2023b) for the period 1990-2023 and from ARDECO (2022) for the period 1960-2023.[19] For the period of 1800-2015, I rely on the subset of countries included in Rosés and Wolf (2019, 2021a, 2021b), who use national historical statistics to provide estimates of subnational population counts that usually coincide with the NUTS2-level at roughly decennial frequency. When information on subnational population shares is unavailable, gridded population estimates are only harmonized with the national target source, see equation (2). Relevant shapefiles of the NUTS-classification are obtained from GISCO (2023) for the first two subnational target sources, while a shapefile for the last is provided by Rosés and Wolf (2021b). Data availability by (sub)national data source is summarized in table A1.

Table A1: Availability of (sub)national population data

Country	**National**	**Subnational**			*Country*	**National**	**Subnational**		
	Maddison	*Roses&Wolf*	*ARDECO*	*Eurostat*		*Maddison*	*Roses&Wolf*	*ARDECO*	*Eurostat*
AT	1800-2023	1900-2015	1960-2023	2001-2023	IS	1950-2023	.	1960-2023	2003-2023
BE	1800-2023	1900-2015	1960-2023	2000-2023	IT	1800-2023	1900-2015	1960-2023	1990-2023
BG	1800-2023	.	1960-2023	1990-2023	LT	1950-2023	.	1960-2023	2001-2023
CH	1800-2023	1900-2015	1960-2023	1990-2023	LU	1950-2023	1950-2015	1960-2023	1990-2023
CZ	1950-2023	.	1960-2023	1992-2023	LV	1950-2023	.	1960-2023	2001-2023
DE	1800-2023	1900-2015	1960-2023	2000-2023	NL	1800-2023	1900-2015	1960-2023	2003-2023
DK	1800-2023	1900-2015	1960-2023	2007-2023	NO	1800-2023	1900-2015	1960-2023	2005-2020
EE	1950-2023	.	1960-2023	2000-2023	PL	1800-2023	.	1960-2023	2014-2023
EL	1800-2023	.	1960-2023	1991-2023	PT	1800-2023	1900-2015	1960-2023	1992-2023
ES	1800-2023	1900-2015	1960-2023	1990-2023	RO	1800-2023	.	1960-2023	1995-2023
FI	1800-2023	1900-2015	1960-2023	1990-2023	SE	1800-2023	1900-2015	1960-2023	2000-2023
FR	1800-2023	1900-2015	1960-2023	1990-2023	SI	1950-2023	.	1960-2023	2003-2023
HU	1800-2023	.	1960-2023	2001-2023	SK	1950-2023	.	1960-2023	2002-2023
IE	1800-2023	1900-2015	1960-2023	2012-2023	UK	1800-2023	1900-2015	1960-2023	2002-2019

Note: This table summarizes the availability of (sub)national population data for the four (sub)national population data sources.

[19] Relevant maps at different NUTS versions are obtained from GISCO (2023).

Validation checks

Before discussing the construction of the final calibrated gridded population estimates, I first illustrate the accuracy of the uncalibrated gridded population estimates and the gain in accuracy from the application of calibration weights for each of the (sub)national population sources. To obtain a gridded population dataset that is maximally consistent with existing (sub)national data sources, I compute calibration weights from equation (4A) for four combinations of national and subnational targets listed in table A2. To get as wide a time coverage as possible, I first restrict the harmonization to total country population in (Bolt & Van Zanden, 2020, MDB), which is available for the 1800-2023 period for most countries, and do not harmonize with other subnational sources. The last row of the table indicates that even uncalibrated gridded country population is strongly correlated with reported country population, with a perfect correlation and a RMSP that amounts to only .035 standard deviations of gridded country population. This observation, in combination with the distribution of gridded calibration weights strongly centered around one in figure A3a, underscores the accuracy of the raw gridded population estimates in the HYDE database. Nevertheless, the normalized RMSPE shrinks to zero after calibrating gridded population estimates, leading to complete consistency between gridded and reported country populations, as also visible in the black dots in figures A3b and the absolute percentage discrepancies of calibrated gridded population estimates with the MDB data in figure A3c.

Table A2: **Correlation of gridded population with (sub)national sources**

				National target					Subnational target				
				Uncalibrated			Calibrated		Uncalibrated			Calibrated	
National target	*Subnational target*	*Coverage*	*# C (# R)*	*N*	*ρ*	*NRMSPE*	*ρ*	*NRMSPE*	*N*	*ρ*	*NRMSPE*	*ρ*	*NRMSPE*
Bolt and Van Zanden (2020)	Eurostat (2023b)	1990-2023	28 (1356)	691	1	.035	1	0	33059	.99	.153	1	.075
Bolt and Van Zanden (2020)	ARDECO (2022)	1960-2023	28 (1346)	1792	1	.028	1	0	86144	.98	.196	1	.078
Bolt and Van Zanden (2020)	Rosés and Wolf (2021b)	1900-2015	16 (172)	1806	1	.033	1	0	19902	.97	.242	1	.024
Bolt and Van Zanden (2020)		1800-2023	28	5072	1	.055	1	0					

Note: This table summarizes the time and country coverage for each combination of national and subnational targets in the first two columns. It also lists the number of countries (C), subnational regions (R) and gridded estimates (N) as well as their correlation with reported country population in the national target source (ρ) and the Normalized Root Mean Squared Prediction Error ($NRMSPE$), scaled by the standard deviation of gridded country population. Where relevant, it also reports diagnostics for subnational populations.

Figure A3: **Calibration weights and estimation accuracy (NT: MDB, SNT: none)**

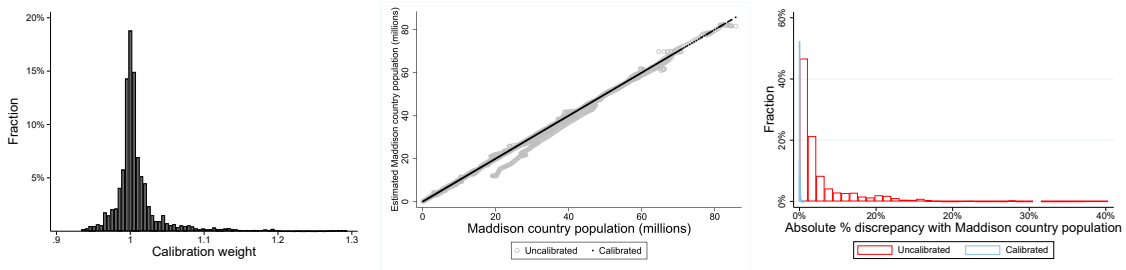

(a) Calibration weight distribution, $v_{g,t}$ (b) National population correlation (c) National percentage discrepancy

Note: Figure A3a shows the distribution of calibration weights that harmonize gridded population with total country population in MDB. The distribution is truncated at the 1^{st} and 99^{th} percentiles. Figure A3b plots reported against uncalibrated (grey) and calibrated (black) gridded country population. Figure A3c shows the distribution of their absolute percentage discrepancy.

To also account for subnational population information, I subsequently harmonize

gridded population estimates both to country population in MDB and subnational population in Rosés and Wolf (2021b, RW) which has the widest temporal coverage but lacks full country coverage (see table A1) and only contains data for fairly large subnational regions. Table A2 shows that though uncalibrated gridded population estimates are strongly correlated with reported subnational population in RW, the normalized RMSPE for subnational population is markedly worse than for national populations and amounts to .242 standard errors of gridded subnational population. The imperfect fit is also visible in the grey dots in figures A4b and A4d. Nevertheless, calibration weights remain centered around 1 in figure A4a, confirming that there appears to be no systematic bias in the raw data. Applying these calibration weights considerably improves the correspondence between gridded and reported subnational population in RW, resulting in a perfect correlation and vanishing percentage discrepancies with reported population, reducing the normalized RMSPE to .024. This is also apparent in the reduction in the percentage discrepancy of calibrated gridded and reported subnational population in figure A4e.

Figure A4: **Calibration weights and estimation accuracy (NT: MDB, SNT: RW)**

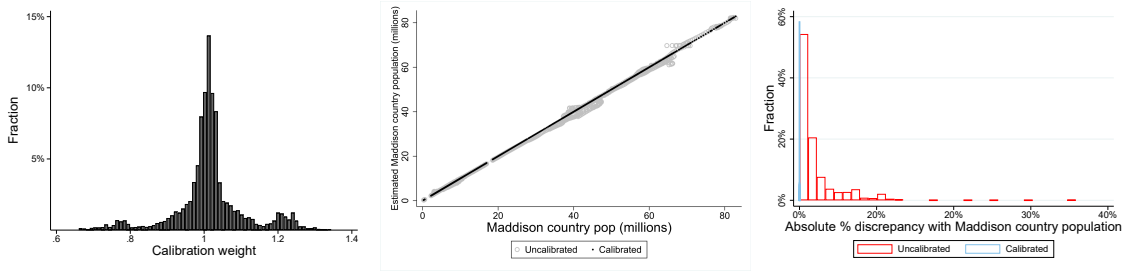

(a) Calibration weight distribution, $v_{g,t}$ (b) National population correlation (c) National population discrepancy

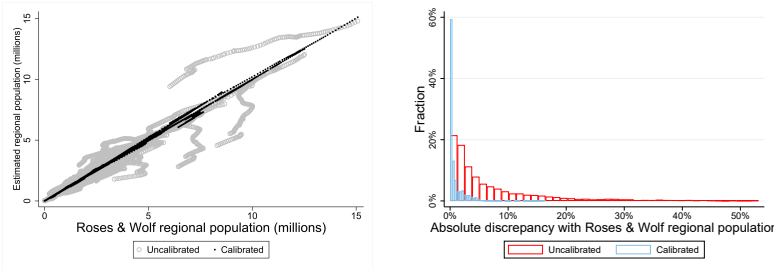

(d) Subnational population correlation (e) Subnational population discrepancy

Note: Figure A4a shows the distribution of calibration weights that harmonize gridded population with MDB country and RW regional population, truncated at the 1^{st} and 99^{th} percentiles. Figures A4b and A4d plot reported against uncalibrated (grey) and calibrated (black) gridded estimates. Figure A4c and A4e shows the distributions of their percentage discrepancies.

I also account for more recent and spatially disaggregated population data by harmonizing gridded population with total country population in the Maddison database and national population shares in ARDECO (2022, AR), which has full country coverage at the NUTS3-level, mostly from the 1980s onwards, see table A1. Interestingly, table A2 implies that uncalibrated gridded population estimates correlate more strongly with the more finegrained regional population data in ARDECO (2022) and that the normalized RMSPE also is comparatively low. This strong consistency between gridded and reported

subnational population is also confirmed by calibration weights that are strongly centered around 1 in figure A5a. Applying these weights drastically improves the correspondence between gridded and reported NUTS3-populations, moving from the grey to the black dots in figures A5b and A5d. Nevertheless, due to grid coarsity, as some NUTS3-regions have very small surface areas, the normalized RMSPE of calibrated estimates is not driven to 0 but rather to .078, implying that small discrepancies between gridded and reported population remains for a small number of NUTS3-regions, see figures A5c and A5e.

Figure A5: **Calibration weights and estimation accuracy (NT:MDB, SNT:AR)**

(a) Calibration weight distribution, $v_{g,t}$ (b) National population correlation (c) National population discrepancy

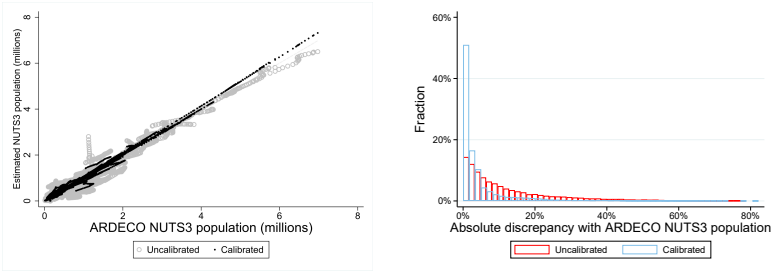

(d) Subnational population correlation (e) Subnational population discrepancy

Note: Figure A5a shows the distribution of calibration weights that harmonize gridded population with MDB country and AR NUTS3 population, truncated at the 1^{st} and 99^{th} percentiles. Figures A5b and A5d plot reported against uncalibrated (grey) and calibrated (black) gridded estimates. Figure A5c and A5e shows the distributions of their percentage discrepancies.

Finally, I also harmonize gridded population estimates jointly to the country population in MDB and the NUTS3 population in Eurostat (2023b, ES). As summarized in table A1, ES has the most restricted time coverage but covers all countries in the sample. Figure A6 confirms the results to be similar to those of AR, which is no surprise given their perfect correlation for the 2615627 overlapping observations between 1990 and 2023.

Calibrated gridded population

The main message from these validation checks is that the raw gridded population estimates in HYDE 3.3 are fairly consistent with more aggregated population data in several authoritative (sub)national data sources, but that rescaling them with fairly moderate calibration weights allows to achieve (almost) full consistency. Therefore, the final calibrated gridded population estimates are obtained by using the most fine-grained calibration weights available as defined in equations (5A) and (2). Table 1 confirmed that uncalibrated gridded population is fairly consistent with reported population but that

Figure A6: **Calibration weights and estimation accuracy (NT:MDB, SNT:ES)**

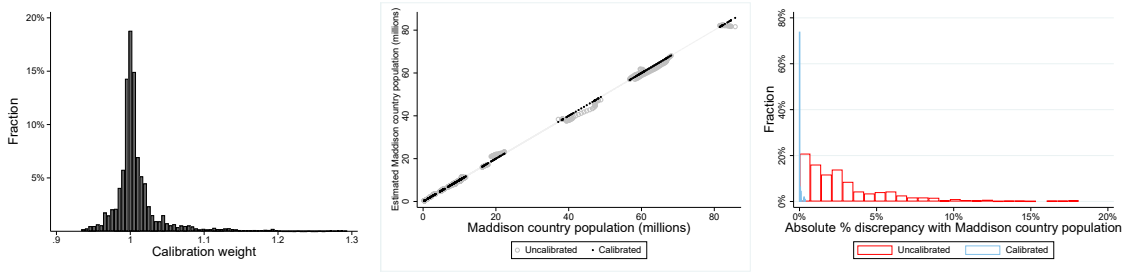

(a) Calibration weight distribution, $v_{g,t}$ (b) National population correlation (c) National population discrepancy

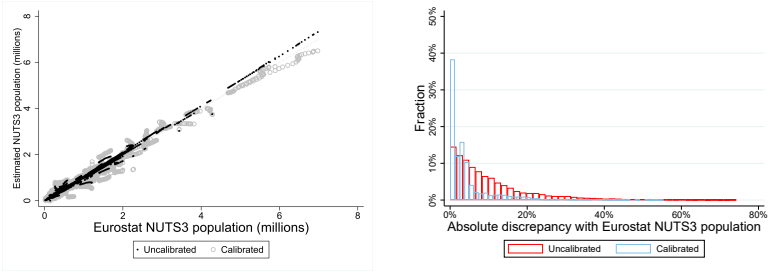

(d) Subnational population correlation (e) Subnational population discrepancy

Note: Figure A6a shows the distribution of calibration weights that harmonize gridded population with MDB country and ES NUTS3 population, truncated at the 1^{st} and 99^{th} percentiles. Figures A6b and A6d plot reported against uncalibrated (grey) and calibrated (black) gridded estimates. Figure A6c and A6e shows the distributions of their percentage discrepancies.

calibration further improves the consistency. This improvement of fit is also visible when comparing the correlation between uncalibrated (grey) and calibrated (black) gridded population estimates and reported (sub)national population in the various sources in the left panel as well as their percentage discrepancies in the right panels of figure A7.

Appendix figure A38 depicts the resulting estimated spatial distribution of population for every half-century between 1800 and 2000. What is especially striking is the stability in population density, which has not visibly changed much in Europe over the past two centuries, underscoring the notion of spatially clustered economic growth. Appendix figure A42 illustrates the estimated population trajectory for the grid cell with the highest estimated population in 1800, which saw its population rise until the 20^{th} century but experienced a population decline after World War II.

A.1.3 Estimating gridded GDP

While existing databases such as the G-ECON database developed by Nordhaus and Chen (2016) provide gridded estimates of GDP, they usually do so at a coarser spatial resolution with limited temporal coverage.[20] Therefore, I extend existing methodologies to disaggregate country-level GDP estimates to grid cells of 5 arcminutes using suitable proxy variables. In analogy to the gridded population estimates, gridded GDP estimates are harmonized with reported GDP (shares) in several authoritative (sub)national sources, which is also shown to serve as a useful procedure to account for spatial differences in the

[20] G-ECON, for instance, only provides estimates at the 1°-resolution for 1990, 1995, 2000 and 2005.

Figure A7: **Estimation accuracy: calibrated gridded population**

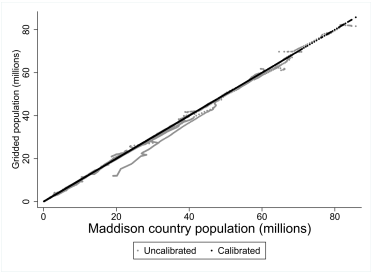

(a) National population correlation

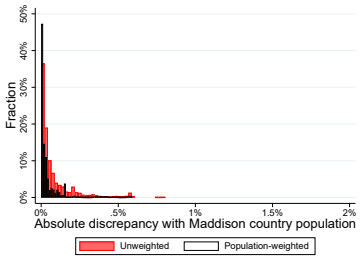

(b) National population discrepancy

MDB

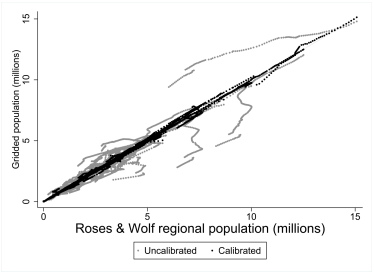

(c) Subnational population discrepancy

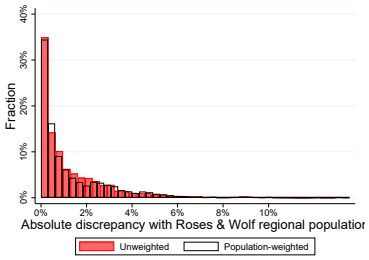

(d) Subnational population discrepancy

RW

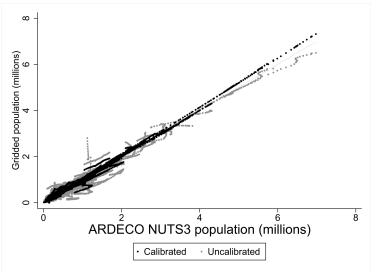

(e) Subnational population discrepancy

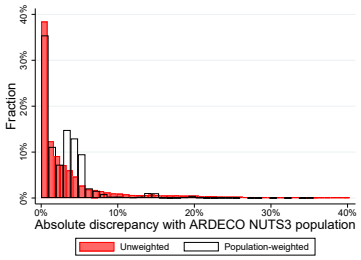

(f) Subnational population discrepancy

AR

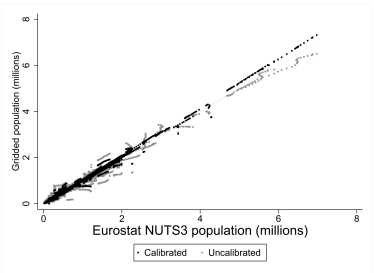

(g) Subnational population discrepancy

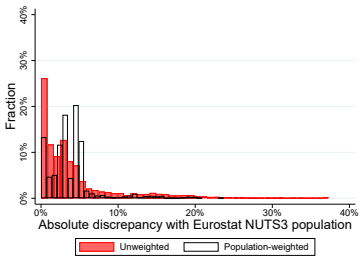

(h) Subnational population discrepancy

ES

Note: This figure plots calibrated gridded population estimates defined in equations (1) and (2) against reported country population in Bolt and Van Zanden (2020, MDB), regional population in Rosés and Wolf (2021b, RW) and NUTS3-population in ARDECO (2022, AR) and Eurostat (2023b, ES) (left panels);and the distribution of their percentage discrepancies (right panels).

GDP elasticity of the proxy variable. Hence, each gridded proxy variable is scaled with a calibration weight designed to ensure that *i)* gridded GDP within country borders sums

to total country GDP in a target national source and *ii)* subnational gridded GDP shares in country GDP equal those reported in a target subnational source. In the empirical application, I will combine satellite-based information on night-time lights (NTL) as proxy for economic activities in recent years and a population-based measure of market access (PMA) for more distant years, when the availability of gridded proxy variables becomes severely restricted. Night-time light data are first adjusted to account for known issues of top- and bottom-coding. Mirroring the previous section, I use total country GDP in the Maddison database (Bolt & Van Zanden, 2020) as the target national source and NUTS3 GDP shares in Eurostat (2023a) and ARDECO (2023) for recent years as well as regional GDP in Rosés and Wolf (2019) for more distant time periods as the subnational targets.

Methodology

Estimation of equation (8) first requires the optimal weights of different measurements of the proxy variable in cases where $M > 1$. Intuitively, uncalibrated measurements of the proxy variable are linearly aggregated to maximize predictive accuracy with respect to subnational GDP in each country-year, giving more weight to measurements that are better predictors. Note that if all measurements, M, can be assumed to be unbiased, this weighting scheme mainly serves to minimize the variance in gridded GDP estimates. More formally, denoting the $(1 \times M)$ vector of importance weights for the M measurements of the proxy variable incountry c in year t by $\omega^*_{c,t}$, with the m^{th} element equal to $\omega^*_{m,c,t}$, optimal weights for the different measurements of the proxy variable in are defined as

$$\omega^*_{c,t} = \arg\min_{\omega_{c,t}} \sum_{r \in c} \underbrace{\left| \frac{\sum_{g=1}^{G} \lambda_{g,r} \left(\sum_{m=1}^{M} \omega_{m,c,t} \hat{z}^m_{g,t} \right)}{\sum_{g=1}^{G} \sum_{\tilde{r} \in c} \lambda_{g,\tilde{r}} \left(\sum_{m=1}^{M} \omega_{m,c,t} \hat{z}^m_{g,t} \right)} - \frac{Y_{r,t}}{Y_{c,t}} \right|}_{\text{absolute disaggregation error in region } r \text{ of country } c \text{ in year } t} \tag{6A}$$

and are minimized through a grid search with a step size of $\Delta\omega = .01$.

Grid-level importance weights can subsequently be obtained by spatially weighting these optimal country-year weights proportional to the surface area of each country

$$\omega^*_{g,t} = \sum_{c=1}^{C} \lambda_{g,c} \omega^*_{c,t} \tag{7A}$$

Subsequently, any remaining discrepancies between disaggregated (sub)national GDP estimates and reported (sub)national GDP in target data sources that may emerge from spatial differences in the output elasticity of the proxy variable, $\beta_{g,t}$, are maximally eliminated by calibrating the (sub)national calibration weights, $\kappa^r_{g,t}$ and $\kappa^c_{g,t}$. The subnational calibration weight, $\kappa^r_{g,t}$, is first calibrated to ensure that disaggregated subnational GDP shares of each region r in country c, $\frac{\sum_{g \in r} \lambda_{g,r} \sum_{m=1}^{M} \left(\omega^*_{m,g,t} \hat{z}_{g,t} \right)}{\sum_{\tilde{r} \in c} \sum_{g \in \tilde{r}} \lambda_{g,\tilde{r}} \left(\sum_{m=1}^{M} \omega^*_{m,g,t} \hat{z}_{g,t} \right)}$, match reported subnational GDP shares in a target subnational source, $\frac{Y_{r,t}}{Y_{c,t}}$. This first requires the computation of the scaling factor that equalizes estimated and reported subnational GDP shares

$$\kappa_{r,t} = \frac{Y_{r,t} / \sum_{r \in c} Y_{r,t}}{\sum_{\tilde{r} \in c} \sum_{g \in \tilde{r}} \lambda_{g,\tilde{r}} \left(\sum_{m=1}^{M} \omega^*_{m,g,t} \hat{z}_{g,t} \right) / \sum_{g \in r} \lambda_{g,r} \left(\sum_{m=1}^{M} \omega^*_{m,g,t} \hat{z}_{g,t} \right)} \tag{8A}$$

and subsequently accounting for the GDP allocation across subnational units in each grid cell by applying subnational spatial weights to obtain the final calibration weight as

$$\kappa^r_{g,t} = \sum_{r \in g} \lambda_{g,r} \kappa_{r,t} \tag{9A}$$

The national calibration weight, $\kappa^c_{g,c}$, is similarly calibrated to ensure that total gridded country GDP in each country c, $\sum_{g=1}^{G} \lambda_{g,c} \kappa^r_{g,t} \left(\sum_{m=1}^{M} \omega^*_{m,g,t} \hat{z}_{g,t} \right)$, equals that of its reported GDP in a target national source, $Y_{c,t}$. This first requires the computation of the scaling factor necessary to equalize total gridded and reported GDP for each country, c

$$\kappa_{c,t} = \frac{Y_{c,t}}{\sum_{r \in c} \sum_{g \in r} \lambda_{g,r} \kappa^r_{g,t} \left(\sum_{m=1}^{M} \omega^*_{m,g,t} \hat{z}_{g,t} \right)} \tag{10A}$$

and proportionally allocating them to grid cells based on their relative surface area

$$\kappa^c_{g,t} = \sum_{r \in g} \lambda_{g,r} \kappa_{c,t} \tag{11A}$$

Final grid-specific calibration weights for each combination of a national and subnational targets can be obtained by multiplying subnational and national calibration weights

$$\kappa_{g,t} = \begin{cases} \kappa^c_{g,t} \kappa^r_{g,t} & \text{if } \kappa^c_{g,t} \notin \varnothing \ \& \ \kappa^r_{g,t} \notin \varnothing \\ \kappa^c_{g,t} & \text{if } \kappa^c_{g,t} \notin \varnothing \ \& \ \kappa^r_{g,t} \in \varnothing \end{cases} \tag{12A}$$

Data sources

There are two main sources for measurements of NTL: the Defense Meteorological Satellite Program Operational Linescan System (DMSP) that started in 1970 and the Visible Infrared Imaging Radiometer Suite (VIIRS) from a satellite launched in 2011. The DMSP reports the intensity of NTL in 6-bit digital numbers (DN) ranging from 0 (no light) to 63 (saturation) that have no interpretation as radiance values, at a spatial resolution of 30 arc-seconds. Inconsistent satellite calibration precludes temporal consistency as *"the same DN value in different years could correspond to different radiance values"* (Kim et al., 2023, p. 5). VIIRS data are measured with sensors that have better light detection capacity and are reported in nano Watts per square centimeter per steradian and range from 0 to 41543 in the data, at a 15 arc-second resolution. While VIIRS data are widely considered superior to DMSP data, whose original purpose was military rather than scientific and mainly served to detect moon-lit clouds to improve air force weather forecasts, the latter's wider temporal availability from 1992 explains its wider use in economic studies (Gibson, Olivia, & Boe-Gibson, 2020). I obtain stable NTL from the DMSP from the

National Oceanic and Atmospheric Administration (2013) for the maximal available period of 1992-2013 and the extended VIIRS-like NTL data constructed from a cross-sensor calibration of DMSP data for the period 2000–2012 and a composition of monthly VIIRS NTL data for the period 2013–2023 from Chen et al. (2021a).[21]

Despite their widespread use in economic studies to proxy for local economic activities, especially in developing countries where data quality is low, satellite-based measurements of NTL suffer from several issues that may affect their reliability (Gibson, Olivia, Boe-Gibson, & Li, 2021). The most important drawbacks for present purposes include top-coding (censor saturation preventing the detection of NTL beyond a ceiling), bottom-coding (censor incapacity to measure NTL in dimly lit areas, causing false zeroes) and blurring (the bleeding of NTL to neighbouring grid cells). While the issue of blurring is most prevalent at fine spatial resolutions of 30 arc seconds, it becomes progressively less relevant at coarser resolutions and hence is unlikely to materially affect my estimates (Gibson et al., 2020). Wang and Sun (2022) explain how the issues of bottom and top censoring can respectively be alleviated by combining NTL data with gridded population estimates and assigning a value of 1 to the NTL in nonilluminated but populated grid cells and multiplying NTL data with gridded population to compute so-called Litpop, ensuring that of two grid cells with the maximal NTL value, the most populated gets a higher score.

Rather than assigning an arbitrary value of 1, I first deal with bottom-coding by imputing missing NTL values in populated grid cells by multiplying gridded population with the nearest available measurement of per capita NTL and otherwise with the minimal contemporaneous per capita values of NTL in the NUTS3-region or the country. Hence, the imputed measurement of NTL in data source $s \in \{DSMP, VIIRS\}$ for grid cell g belonging to NUTS3-region r of country c at time t is computed as

$$NTL^{s,i}_{g,t} = \begin{cases} NTL^{s}_{g,t} & \text{if } \hat{n}_{g,t} > 0 \;\&\; NTL^{s}_{g,t} \notin \varnothing \\ \frac{NTL_{g,\tilde{t}}}{\hat{n}_{g,\tilde{t}}}\hat{n}_{g,t} & \text{if } \hat{n}_{g,t} > 0 \;\&\; NTL_{g,t} \in \varnothing \;\&\; \exists \tilde{t} : NTL_{g,\tilde{t}} \neq \varnothing \\ \min_t^{r,s}\left(\frac{NTL}{\hat{n}}\right)\hat{n}_{g,t} & \text{if } \hat{n}_{g,t} > 0 \;\&\; NTL_{g,t} \in \varnothing \;\forall t \;\&\; \min_t^{r,s}\left(\frac{NTL}{\hat{n}}\right) \notin \varnothing \\ \min_t^{c,s}\left(\frac{NTL}{\hat{n}}\right)\hat{n}_{g,t} & \text{if } \hat{n}_{g,t} > 0 \;\&\; NTL_{g,t} \in \varnothing \;\forall t \;\&\; \min_t^{r,s}\left(\frac{NTL}{\hat{n}}\right) \in \varnothing \\ 0 & \text{if } \hat{n}_{g,t} = 0 \end{cases} \tag{13A}$$

where $\varnothing$ denotes the empty set, $\tilde{t}$ denotes the closest year to t for which NTL is measured for grid cell g in source s, $\tilde{t} = argmin_{\tilde{t}} \left|t - \tilde{t}\right| : NTL^{s}_{g,\tilde{t}} \notin \varnothing$, and $\min_t^{r,s}\left(\frac{NTL}{\hat{n}}\right)$ denotes minimum per capita NTL in source s for NUTS3-region r covering most of grid cell g.

Bottom coding appears to be an issue in both data sources: of the 1779599 populated grid cells covered by the DMSP, 1523739 (86%) are illuminated while only 919002 (51%) of the 1784863 populated grid cells in the VIIRS-like data are illuminated. Appendix figure A43 confirms that bottom-coding is primarily problematic in grid cells with low population

[21] As explained in Kim et al. (2023, p. 4-5), in the DMSP, 'stable' *"means that ephemeral lights, from sources such as fires and gas flaring, are removed before the annual composite is built up"*.

density, as unilluminated cells are typically clustered in grid cells with comparatively low gridded population estimates. This is also confirmed by the raw numbers: average gridded population in the DMSP data amounts to 5912 but this reduces to just 236 in the subset of unilluminated grid cells; for the VIIRS-like data, average gridded population amounts to 6017 when computed across the full grid but just 968 when computed for dark cells. Hence imputing NTL serves to avoid underestimating economic performance in sparsely populated areas. Figure A8 shows the results of the imputation procedure by comparing the raw (black) and imputed (red) NTL measurements, separately for NTLs from the DMSP and the VIIRS. As expected, the distributions become more left tailed by imputing values for dimly lit grid cells while leaving the right tail largely intact.

Figure A8: **Raw versus imputed NTL**

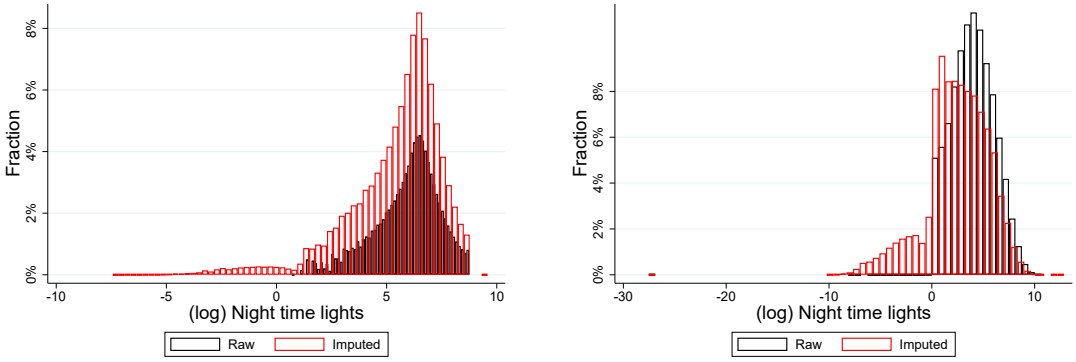

(a) DMSP (b) VIIRS

Note: This figure shows the distribution of raw and imputed log NTL for DMSP and VIIRS.

I subsequently deal with top-coding by computing grid-level estimates of Litpop in each source, $Litpop^{s}_{g,t} = \hat{n}_{g,t} NTL^{s,i}_{g,t}$, which have been shown to improve the accuracy of GDP disaggregation (Wang & Sun, 2022). Finally, I account for differences in the local elasticities of NTL between both sources by extending Litpop trajectories in each source s_1 relying on its predicted growth rates from the following simple bivariate model

$$Litpop^{s_1}_{g,t} = \beta_g Litpop^{s_2}_{g,t} + \epsilon_{g,t} \tag{14A}$$

with $Litpop^{s_2}_{g,t}$ the measurement in the alternative source, s_2. After expressing alternative luminosity measurements in the units of the baseline source, I use $\hat{Litpop}^{s_1}_{g,t} = \hat{\beta}_g Litpop^{s_2}_{g,t}$ to maximally extend the baseline series forward and backward in time

$$Litpop^{s_1}_{g,t} = \begin{cases} \frac{\hat{Litpop}^{s_1}_{g,t}}{\hat{Litpop}^{s_1}_{g,t-1}} Litpop^{s_1}_{g,t-1} & \text{if } Litpop^{s_1}_{g,t} \text{ is missing but } Litpop^{s_1}_{g,t-1} \text{ is observed} \\ \frac{\hat{Litpop}^{s_1}_{g,t}}{\hat{Litpop}^{s_1}_{g,t+1}} Litpop^{s_1}_{g,t+1} & \text{if } Litpop^{s_1}_{g,t} \text{ is missing but } Litpop^{s_1}_{g,t+1} \text{ is observed} \end{cases} \tag{15A}$$

Figure A9 compares the original (black) with the extended Litpop distribution (red) and shows that the extension leaves the original distribution entirely intact.

Gridded GDP estimates are subsequently harmonized with the available country GDP figures in the Maddison database (Bolt & Van Zanden, 2020), which functions as the main

Figure A9: **Imputed versus extended Litpop**

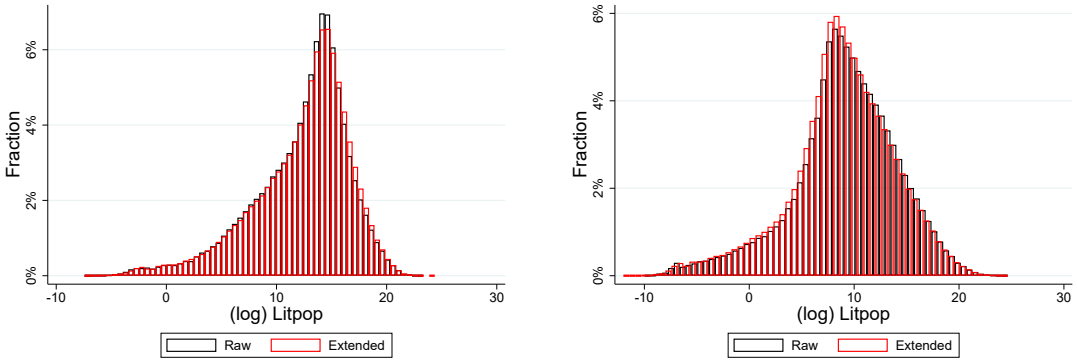

(a) DMSP (b) VIIRS

Note: This figure shows the distribution of raw and extended log litpop, separately for DMSP and VIIRS.

national target source. As the most recent 2020 version of the database only covers the years until 2018, country GDPs are extended to 2023 using their evolution inARDECO (2023). To also ensure that gridded GDP estimates reflect observed subnational GDP shares, I rely on the available NUTS3 GDP figures from Eurostat (2023a) for the period 1990-2022 and from ARDECO (2023) for the period 1980-2023. For the period of 1800-2015, I rely on the subset of countries included in Rosés and Wolf (2019, 2021a, 2021b), who rely on national historical statistics to provide estimates of subnational GDP that usually coincide with the NUTS2-level at roughly decennial frequency. When information on subnational GDP shares is unavailable, gridded GDP estimates are only harmonized with the national target source. Relevant shapefiles of the NUTS-classification are obtained from GISCO (2023) for the first two subnational target sources, while a shapefile for the last is provided by Rosés and Wolf (2021b). Iceland is the only country lacking subnational data availability; its gridded GDP estimates are only harmonized with reported country GDP. Data availability by (sub)national data source is summarized in table A1.

Table A3: Availability of (sub)national GDP data

Country	**National**	**Subnational**			*Country*	**National**	**Subnational**		
	Maddison	*Roses&Wolf*	*ARDECO*	*Eurostat*		*Maddison*	*Roses&Wolf*	*ARDECO*	*Eurostat*
AT	1820-2023	1900-2015	1980-2023	2000-2021	IS	1950-2018	.	.	.
BE	1800-2023	1900-2015	1980-2023	2003-2022	IT	1800-2023	1900-2015	1980-2023	2000-2021
BG	1870-2023	.	1990-2023	2000-2021	LT	1973-2023	.	1992-2023	2000-2021
CH	1800-2023	1900-2015	1980-2023	2008-2021	LU	1950-2023	1900-2015	1980-2023	2000-2022
CZ	1970-2023	.	1990-2023	2000-2022	LV	1973-2023	.	1992-2023	2000-2021
DE	1800-2023	1900-2015	1980-2023	2000-2021	NL	1800-2023	1900-2015	1980-2023	2000-2021
DK	1820-2023	1900-2015	1980-2023	2000-2022	NO	1820-2023	1900-2015	1980-2023	2008-2021
EE	1950-2023	.	1993-2023	2000-2022	PL	1800-2023	.	1980-2023	2000-2021
EL	1800-2023	.	1980-2023	2000-2021	PT	1800-2023	1900-2015	1980-2023	2000-2022
ES	1800-2023	1900-2015	1980-2023	2000-2021	RO	1862-2023	.	1980-2023	2000-2021
FI	1800-2023	1900-2015	1980-2023	2000-2021	SE	1800-2023	1900-2015	1980-2023	2000-2021
FR	1800-2023	1900-2015	1980-2023	2000-2021	SI	1952-2023	.	1991-2023	2000-2022
HU	1870-2023	.	1980-2023	2000-2022	SK	1985-2023	.	1993-2023	2000-2022
IE	1820-2023	1900-2015	1980-2023	2000-2021	UK	1800-2023	1900-2015	1980-2023	.

Note: This table summarizes the availability of (sub)national GDP data in the four (sub)national GDP data sources.

Finally, for validation purposes, I also collect data from the G-ECON database (Nordhaus & Chen, 2016), which provides worldwide gridded GDP estimates in USD at a spatial res-

olution of 1 arc degrees at a five-yearly frequency between 1990 and 2005. The estimates are based on economic data collected at the smallest available administrative unit for each country that are further disaggregated using spatial overlays of administrative boundaries and high resolution gridded population estimates.

Validation checks

Table A4 first reports the correlation of the various proxy variables with (sub)national GDP in various sources, where each proxy variable is first aggregated to the administrative division in the (sub)national data source in proportion to their surface area. Gridded population, $\hat{N}$, is included as a reference category to assess the additional explanatory power these proxy variables can offer, beyond what can be inferred from gridded (sub)national population. More detailed scatter plots are offered in appendix figures A44 through A47.

Table A4: Correlations between proxy variables and (sub)national GDP

GDP source	$\hat{N}$	NTL^D	$NTL^{D,i}$	LP^D	$LP^{D,e}$	NTL^V	$NTL^{V,i}$	LP^V	$LP^{V,e}$	PMA
MDB country GDP	.75	.91	.91	.97	.97	.87	.85	.9	.92	.87
RW subnational GDP	.8	.65	.64	.96	.96	.77	.74	.88	.89	.87
AR NUTS3 GDP	.64	.48	.47	.81	.82	.72	.71	.78	.77	.72
ES NUTS3 GDP	.74	.53	.53	.83	.84	.73	.72	.77	.78	.81

Note: This table summarizes the correlations of the proxy variables in each column with (sub)national GDP in each row. Data sources for GDP are Bolt and Van Zanden (2020) (MDB), Rosés and Wolf (2021b) (RW), ARDECO (2023) (AR) and Eurostat (2023a) (ES). The proxy variables are gridded population ($\hat{N}$), nighttime lights (NTL), Litpop (LP) and the population-based measure of market access (PMA). NTL are obtained from the DMSP (^{D}) or VIIRS (^{V}) and are imputed in accordance with equation (13A) to deal with bottom-coding (^{i}). The extended LITPOP data as defined in equation (15A) is identified by the superscript ^{e}.

Six main findings emerge. First, raw NTL data from either source (DMSP or VIIRS) are considerably less correlated with reported subnational output than population and, in this sense, they are worse predictors. Second, imputing NTL in accordance with equation (13A) to deal with bottom-coding has no measurable impact on predictive accuracy, as this does not strengthen the correlation with reported economic output. This may be due to the fact that imputation mainly improves accuracy in low-output grid cells which therefore do not significantly contribute to reported (sub)national output. Third, the use of Litpop rather than NTL to deal with top-coding strongly improves predictive accuracy: in sharp contrast to NTL, Litpop is always considerably *more* positively correlated with reported (sub)national output across all sources. Fourth, extending Litpop using equation (15A) slightly strengthens the correlation with (sub)national output. Fifth, and perhaps somewhat surprisingly, the population-based measure of market access attains similar correlations with reported (sub)national output and hence does not seem to be less accurate according to this metric. This serves to further motivate their use in time periods where satellite-based data remains unavailable. Sixth, all three proxy variables used to estimate gridded GDP, $Litpop^{DMSP}$, $Litpop^{VIIRS}$ and PMA, offer considerable added value in assessing (sub)national economic performance when compared to population. Moreover, note that they already attain strong correlations with (sub)national output even without the calibration weights described in equations (9A) and (11A). This suggests that

spatio-temporal differences in the output elasticity are fairly limited, confirming that the measurement weights in equation (6A) can be adequately calibrated even without accounting for them. Finally, appendix figure A48 shows that the bivariate correlations between these three proxy variables are high as well, consistent with the idea that they all measure the same underlying component, namely local economic performance.

Figure A10 than shows the distribution of these optimal importance weights for the NTL data from the DMSP, computed from equation (7A). As $M = 2$, the corresponding weight for the VIIRS data simply equals $1 - \omega_{g,t,DMSP}$. As can be seen, almost three quarter of grid cells solely rely on NTL data from the DMSP to compute Litpop, while a small minority gives at least some weight to the VIIRS-like NTL from Chen et al. (2021b).

Figure A10: **Optimal measurement weights for DMSP,** $\omega_{g,t,DMSP}$

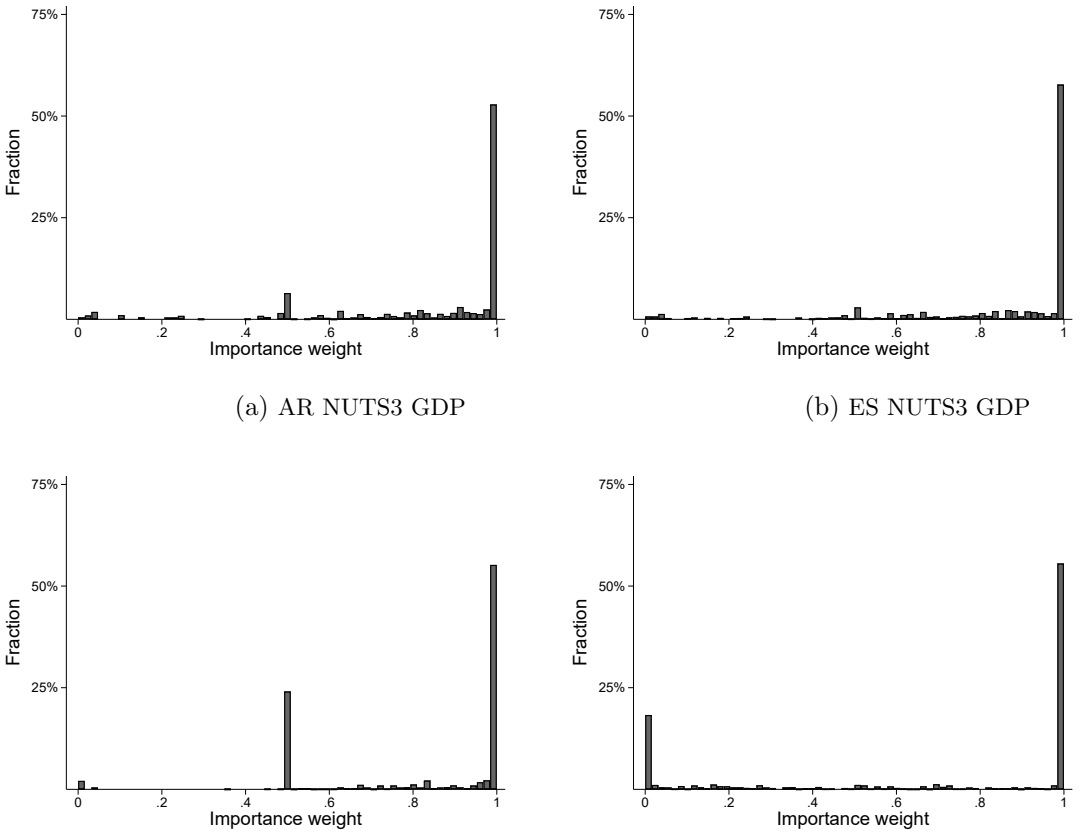

(a) AR NUTS3 GDP

(b) ES NUTS3 GDP

(c) RW regional GDP

(d) MDB national GDP

Note: This figure shows the optimal measurement weight for Litpop from the DMSP, calibrated from equation (7A) in each country-year to minimize the MAE between gross light product shares and reported GDP shares from ARDECO (2023, AR), Eurostat (2023a, ES), Rosés and Wolf (2021b, RW) and Bolt and Van Zanden (2020, MDB).

Figure A11 follows up on this and shows estimates of NUTS3 GDP shares, disaggregated using the gross Litpop products computed from the NTL data in the DMSP, the VIIRS and their optimally weighted combination as defined in equation (8) against reported GDP shares taken from ARDECO (2023). First, the grey dots for both unweighted sources scatter around the 45° ray of equality, confirming the simplifying assumption made

in the methodological section that Litpop is an unbiased predictor of subnational economic activity even when not accounting for spatio-temporal differences in its output elasticity. This is also confirmed by the distribution of prediction errors shown in figure A11b, which clearly clusters around 0 in both sources. Nevertheless, optimally weighted Litpop in black displays less variance around the ray of equality, suggesting that the weighting scheme achieves its goal of providing more precise estimates of regional economic output.

Figure A11: **Predictive accuracy of Litpop-based GDP disaggregation**

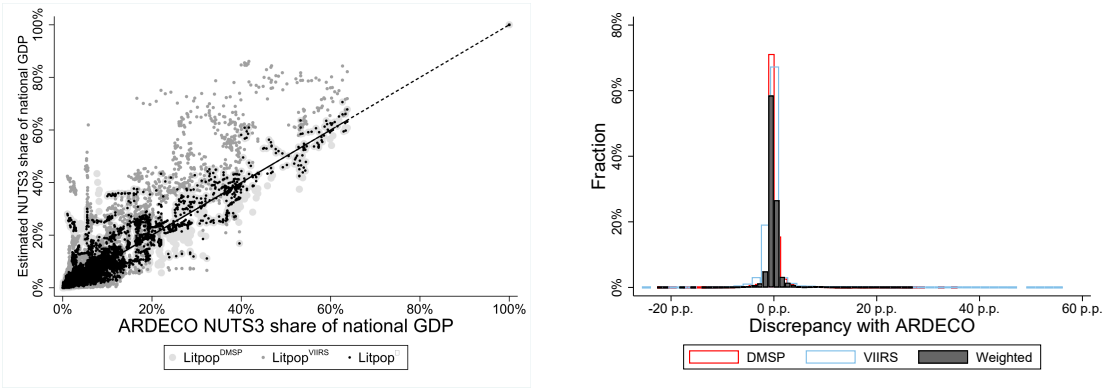

(a) GDP shares

(b) Prediction errors

Note: This figure shows the predictive accuracy of disaggregating GDP using Litpop from DMSP, VIIRS and their weighted combination as defined in equation (7A) against reported NUTS3 GDP shares in ARDECO (2023).

Breaking down the results by (sub)national target and proxy, figure A12 first visualizes the predictive accuracy of disaggregating country GDP with the Litpop proxy and harmonization of the resulting gridded GDP estimates with reported country GDP in Bolt and Van Zanden (2020) and NUTS3 GDP shares in Eurostat (2023a), corresponding to the first row in table 2. As the calibration weights, $\kappa_{g,t}$, partially serve to express Litpop to real GDP in 2011 USD, to see how much Litpop measurements still need to be recalibrated to replicate the regional GDP distribution across NUTS3 units, figure A12a shows the distribution of grid-level calibration weights normalized with the average calibration weight in the country, $\bar{\kappa}_{c,t} = \frac{\sum_{g \in c} \kappa_{g,t}}{\sum_{g \in c} 1}$, where grid cells are uniquely assigned to the country which covers the largest share of their surface. The figure clearly shows that normalized calibration weights tightly cluster around 1, suggesting again that spatio-temporal differences in the output elasticity of Litpop are small and hence can be ignored when determining the measurement weights for the NTL data in equation (7A). Figure A12b confirms the perfect harmonization with the national target source, while figure A12c shows that applying the calibration weights of figure A12a considerably improves the correspondence between gridded and reported NUTS3 GDP shares in Eurostat (2023a), resulting in an almost perfect correlation of 1 and reducing the normalized RMSPE to .05. This is also apparent in the black dots in figure A12c, which cluster on the 45°-line of perfect fit.

A similar picture emerges when looking at the results with ARDECO (2023) as subnational target, which has a wider temporal coverage. Once again, the normalized calibration

Figure A12: **Estimation accuracy (P: Litpop, NT:MDB, SNT:ES)**

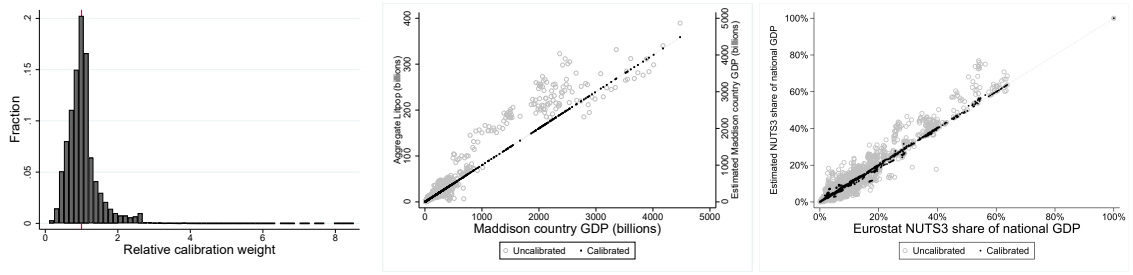

(a) Relative calibration weights, $\frac{\kappa_{g,t}}{\bar{\kappa}_{c,t}}$ (b) National GDP discrepancy (c) Subnational GDP discrepancy

Note: Figure A12a shows the distribution of Litpop calibration weights that harmonize gridded GDP with Maddison country GDP and Eurostat (2023a) NUTS3 GDP shares, scaled by the average calibration weight in the country, $\bar{\kappa}_{c,t}$. Figures A12b shows the discrepancy between reported and estimated country GDP; A12c show the discrepancy of reported and uncalibrated (black) and calibrated (grey) gridded NUTS3 GDP shares.

weights in figure A13 suggest that output elasticities of Litpop typically do not differ much across time and space, though accounting for them considerably improves the correspondance of gridded and reported NUTS3 GDP levels in figure A13c.

Figure A13: **Estimation accuracy (P: Litpop, NT:MDB, SNT:AR)**

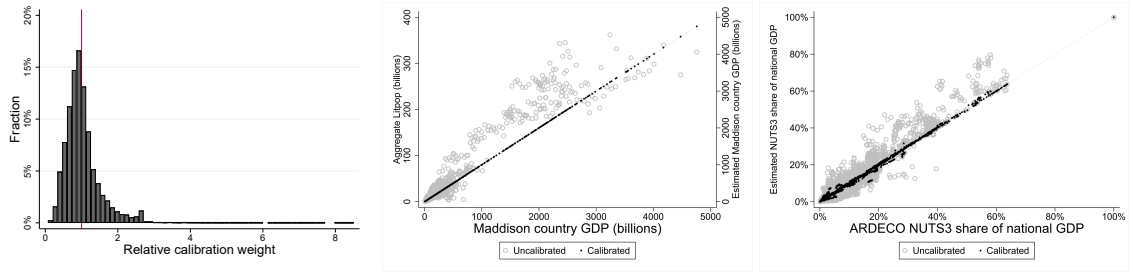

(a) Relative calibration weights, $\frac{\kappa_{g,t}}{\bar{\kappa}_{c,t}}$ (b) National GDP discrepancy (c) Subnational GDP discrepancy

Note: Figure A13a shows the distribution of Litpop calibration weights that harmonize gridded GDP with Maddison country GDP and ARDECO (2023) NUTS3 GDP shares, scaled by the average calibration weight in the country, $\bar{\kappa}_{c,t}$. Figures A13b shows the discrepancy between reported and (un)calibrated estimated country GDP; A13c show the discrepancy of reported and uncalibrated (black) and calibrated (grey) gridded NUTS3 GDP shares.

Figure A14 than looks at the use of the population-based measure of market access, PMA, as a proxy to spatialize country GDP. As this also covers the period before satellite-based images became available, its predictive accuracy can be tested for a larger number of observations. Nevertheless all of the previous findings for satellite-based proxy variables are replicated. The normalized calibration weights in figure A14a cluster even tighter around 1, suggesting that the output elasticity of this proxy variable is even more stable across time and space. Nevertheless, the grey dots in figure A14c suggest that its smoother distribution tends to underestimate GDP in regions with the highest output levels, such that harmonization with subnational data considerably improves accuracy.

Finally, figure A15 visualizes the results for the largest available panel, which combines the PMA proxy with the subnational GDP information in Rosés and Wolf (2021b) for their subset of available countries. Once again, the uncalibrated PMA proxy serves reasonably well and displays no apparent consistent bias. Nevertheless, applying subnational

Figure A14: **Estimation accuracy: (P: PMA, NT:MDB, SNT:AR)**

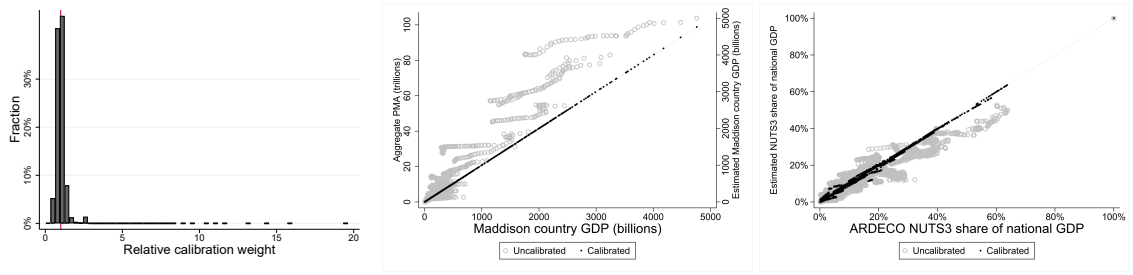

(a) Relative calibration weights, $\frac{\kappa_{g,t}}{\bar{\kappa}_{c,t}}$ (b) National GDP discrepancy (c) Subnational GDP discrepancy

Note: Figure A14a shows the distribution of PMA calibration weights that harmonize gridded GDP with Maddison country GDP and ARDECO (2023) NUTS3 GDP shares, scaled by the average calibration weight in the country, $\bar{\kappa}_{c,t}$. Figures A14b shows the discrepancy between reported and (un)calibrated estimated country GDP; A14c show the discrepancy of reported and uncalibrated (black) and calibrated (grey) gridded NUTS3 GDP shares.

calibration weights almost fully harmonizes gridded and reported NUTS3 GDP levels, moving from the grey to the black dots in figure A15c.

Figure A15: **Estimation accuracy: (P: PMA, NT:MDB, SNT:RW)**

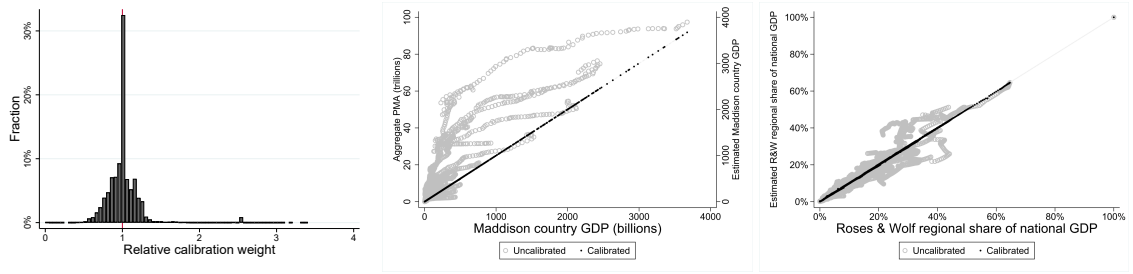

(a) Relative calibration weights, $\frac{\kappa_{g,t}}{\bar{\kappa}_{c,t}}$ (b) National GDP discrepancy (c) Subnational GDP discrepancy

Note: Figure A15a shows the distribution of PMA calibration weights that harmonize gridded GDP with Maddison country GDP and Rosés and Wolf (2021b) regional GDP shares, scaled by the average calibration weight in the country, $\bar{\kappa}_{c,t}$. Figures A15b shows the discrepancy between reported and estimated country GDP; A15c show the discrepancy of reported and uncalibrated (black) and calibrated (grey) gridded NUTS3 GDP shares.

Before moving to a discussion of the construction of the final calibrated gridded GDP estimates, I conclude this section with a final validation check on the assumption of the independence of grid-level measurement errors in the ouput elasticities related to equation (7). Though estimation errors are unobserved and the assumptions on their expected values and independence cannot be directly tested, the results presented here strongly suggest that mismeasurement in the proxy variable is truly random. Additionally assuming that the gridded GDP estimates of Nordhaus and Chen (2016) are accurate allows for an indirect test of the independence of measurement errors in the output elasticities since, under these assumptions, the difference between both GDP estimates can only be due to mismeasurement in the output elasticities. To see this, denote the gridded GDP estimate for grid cel $\tilde{g}$ in year t in the G-ECON database by $y^G_{\tilde{g},t}$. Converting the final gridded GDP estimates later defined in equation (10) to the same spatial resolution based on equation (7), we have that the discrepancy between both, $\Delta_{\tilde{g},t}$, is given by

$$
\begin{aligned}
\Delta_{\tilde{g},t} &= y^G_{\tilde{g},t} - \overbrace{\sum_{g\in\tilde{g}}\left(\beta_{g,t}\bar{z}_{g,t} + \beta_{g,t}\bar{\epsilon}^{\bar{z}}_{g,t} + \bar{z}_{g,t}\epsilon^{\beta}_{g,t} + \epsilon^{\beta}_{g,t}\bar{\epsilon}^{\bar{z}}_{g,t}\right)}^{\text{gridded GDP estimate at spatial resolution of G-ECON}} \\
&= y^G_{\tilde{g},t} - \sum_{g\in\tilde{g}}\left(\beta_{g,t}\bar{z}_{g,t} + \bar{z}_{g,t}\epsilon^{\beta}_{g,t}\right) \\
&= y^G_{\tilde{g},t} - \sum_{g\in\tilde{g}}\bar{z}_{g,t}\left(\beta_{g,t} + \epsilon^{\beta}_{g,t}\right) \\
&= y^G_{\tilde{g},t} - \bar{z}_{\tilde{g},t}\sum_{g\in\tilde{g}}\left(\beta_{g,t} + \epsilon^{\beta}_{g,t}\right) \\
&= y^G_{\tilde{g},t} - \hat{y}_{\tilde{g},t} - \bar{z}_{\tilde{g},t}\epsilon^{\beta}_{\tilde{g},t}
\end{aligned}
\tag{16A}
$$

where the second equality follows from the assumption of truly random measurement errors in the proxy variable, $E\left(\bar{\epsilon}^{\bar{z}}_{g,t} \mid \beta_{g,t}\right) = E\left(\bar{\epsilon}^{\bar{z}}_{g,t} \mid \epsilon^{\beta}_{g,t}\right) = E\left(\bar{\epsilon}^{\bar{z}}_{g,t}\right) = 0$.

Figure A16: **Validation check: comparison with G-ECON**

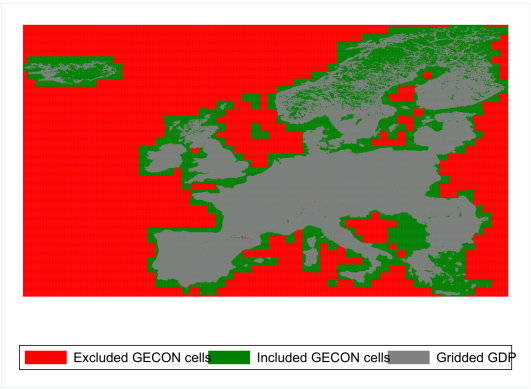

(a) Selected G-ECON grid cells

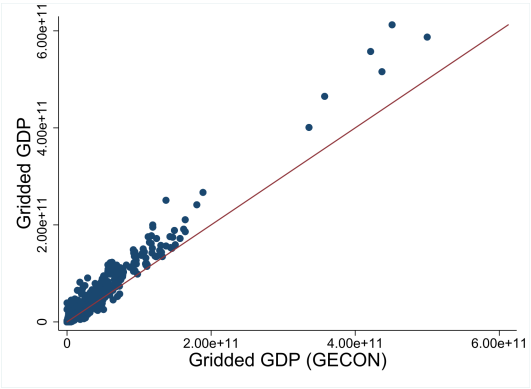

(b) Overlapping grid output discrepancy

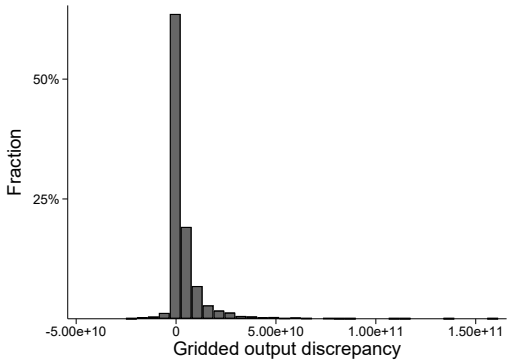

(c) discrepancy distribution

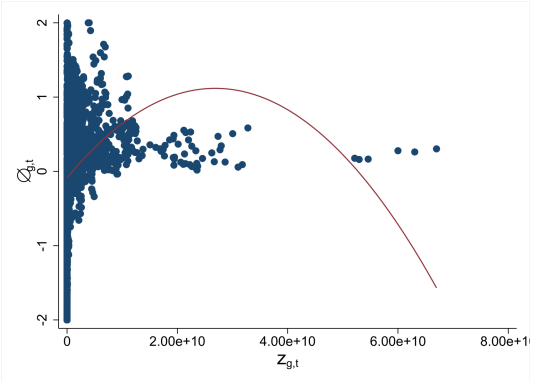

(d) $\bar{\Delta}_{\tilde{g},t}$ versus $\bar{z}_{\tilde{g},t}$

Note: Figure A16a shows the grid cells with GDP estimates in grey and the overlapping grid cells with GDP estimates at the 1-arcdegree resolution in G-ECON in green. Figure A16b shows the discrepancy in estimated and reported gridded GDP in G-ECON, with figure A16c visualizing the distribution of discrepancies. Figure A16d plots the normalized discrepancy, $\bar{\Delta}_{\tilde{g},t} = \left(\hat{y}_{g,t} - y^G_{g,t}\right) / .5\left(\hat{y}_{g,t} + y^G_{g,t}\right)$, against the proxy variable, $\bar{z}_{g,t}$.

To implement this validation check, I first select the subset of gridded GDP estimates in G-ECON that fully overlap with the gridded GDP estimates in the present dataset,

see figure A16a. Figure A16b shows the scatter plot of the gridded GDP estimates in G-ECON, $y^G_{\tilde{g},t}$, and the corresponding aggregated gridded GDP estimates from the present data, $\hat{y}_{\tilde{g},t}$, for all the available years of 1990, 1995, 2000 and 2005. As can be seen, there is an extremely strong correlation of .98 between both sets of estimates, though the present estimates are somewhat higher for larger subnational economies. Figure A16c shows how the distribution of the discrepancies correspondingly clusters around zero, signifying that the present estimates do not appear to be consistently biased by this metric. Finally, I exploit equation (16A) to estimate the (aggregate) measurement error in the output elasticity of the proxy variable as $\hat{\epsilon}^{\beta}_{\tilde{g},t} = \frac{y^G_{\tilde{g},t} - \hat{y}_{\tilde{g},t}}{\bar{z}_{\tilde{g},t}}$, finding no correlation with the proxy variable, $\bar{z}_{\tilde{g},t}$ (ρ= -.02). This is further confirmed in figure A16d, which plots the normalized discrepancy, $\bar{\Delta}_{\tilde{g},t} = \frac{\hat{y}_{\tilde{g},t} - y^G_{\tilde{g},t}}{\frac{1}{2}\left(y^G_{\tilde{g},t} + \hat{y}_{\tilde{g},t}\right)}$, against the proxy variable, Litpop, finding no clear empirical evidence of any consistent relation between discrepancies in estimated and reported gridded GDP and the value of the proxy variable. All of this suggests that the assumption of their independence in equation (7) is valid.

Calibrated gridded GDP

As the validation checks suggest that both proxy variables are unbiased predictors of (sub)national economic performance in several authoritative data sources, gridded GDP estimates are obtained using the most fine-grained combination of proxy variables and calibration weights as defined in equation (10). Mirroring the results in table 3 the close correspondence of gridded and reported subnational GDP is also visible in figure A17, where the estimates consistently cluster on the 45°-line of perfect fit for every source.

Finally, appendix figures A39 and A40 depict the resulting estimates of the spatial distribution of GDP and per capita GDP for every half-century between 1800 and 2000. The gridded GDP estimates correlate heavily with what has been dubbed the 'blue banana' in Europe, which refers to the banana-shaped corridor of heavy urbanization stretching from North West England over the Benelux and German Rhineland to the north of Italy. The estimates imply that this persistent spatially concentrated economic engine of Europe dates back at least to the 19^{th} century. The per capita GDP estimates are formed along similar spatial lines, where the earliest estimates are consistent with traditional accounts of industrialization increased standards of living first in the UK before spreading to mainland Europe starting in the Benelux. The postwar period nevertheless sees a marked rise in per capita GDP in the southern part of the Scandinavian countries. For reference, appendix figure A42 also illustrates the estimated (per capita) GDP trajectory for the grid cell with the highest estimated population in 1800, which saw its estimated GDP rise with two interruptions during the world wars and a period of stagnation in the interwar period.

Figure A17: **Estimation accuracy: calibrated gridded GDP**

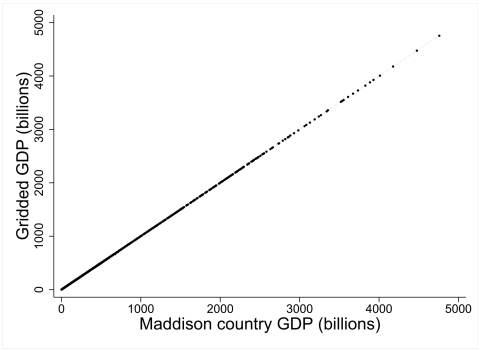

(a) National GDP correlation

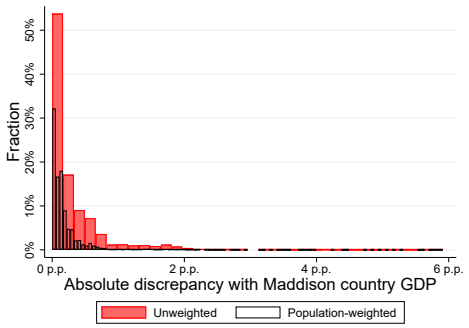

(b) National GDP discrepancy

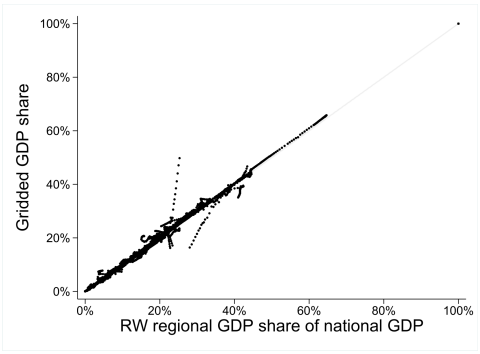

(c) Subnational GDP correlation

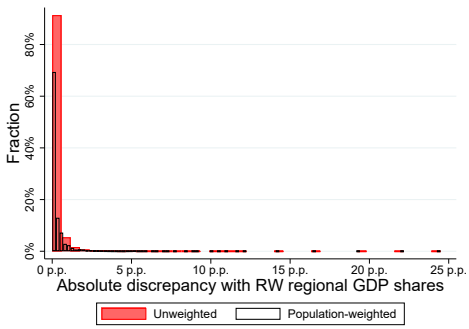

(d) Subnational GDP discrepancy

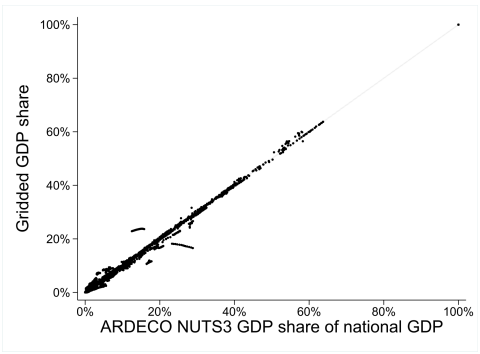

(e) Subnational GDP correlation

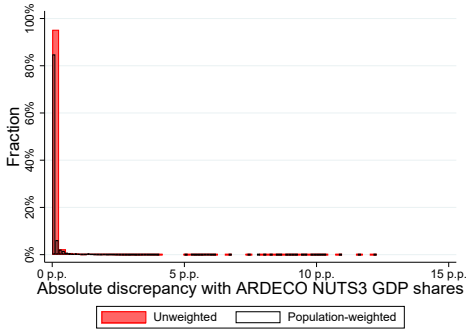

(f) Subnational GDP discrepancy

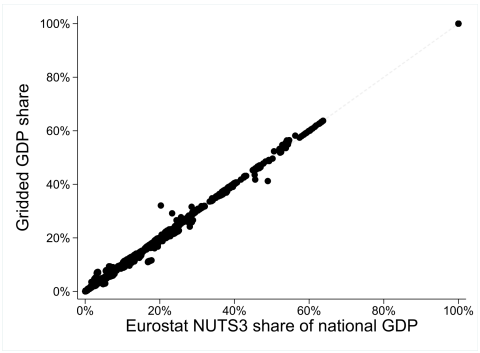

(g) Subnational GDP correlation

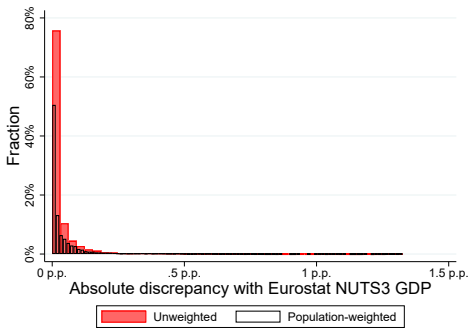

(h) Subnational GDP discrepancy

Note: This figure respectively shows the discrepancy between calibrated gridded GDP estimates as defined in equations (8) and (10) with reported country GDP in Bolt and Van Zanden (2020), regional GDP shares in Rosés and Wolf (2021b) and NUTS3-GDP shares in ARDECO (2023) and Eurostat (2023a).

A.2 Political landscape

To analyze the political landscape, I start from the electoral information on European countries in the 17^{th} release of the CLEA to identify the constituencies that need to be georeferenced and the political parties that need to be classified. Section A.2.1 describes the availability, sources and construction of the maps for each election in the CLEA. Section A.2.2 describes the harmonization and linkage of party names to existing typologies.

A.2.1 Georeferencing electoral constituencies

While some governments have recently started to produce and publicly provide georeferenced maps of electoral constituencies, see e.g. the Office for National Statistics in the UK or the Istituto Nazionale di Statistica in Italy, their historical coverage is typically limited to the most recent election(s), implying that the availability of primary sources for the elections in the CLEA is highly incomplete. I therefore rely on a wide range of secondary sources to maximally georeference the remaining elections, the majority of which are derived from Wikipedia. One additional difficulty is that some secondary sources do not report the names of the constituencies on the map. In these cases, names were added by first geocoding all constituency names in CLEA, which typically refer to cities or regions, to allocate unique matches to the respective georeferenced constituencies and subsequently conducting a desk search to allocate missing or conflicting constituency names.[22] One benefit is that, with few exceptions, electoral boundaries typically span several elections such that the same georeferenced map can serve for multiple elections in the CLEA.

Before giving a country-specific breakdown of the sources and construction of the georeferenced maps, I provide the minimal working example of georeferencing the electoral constituencies of the 1907 general German election. While there exist no primary sources for this election, a contemporary publishing company, Otto Weber Verlag, published a map of the electoral constituencies, as shown in figure A18a. This map was subsequently converted to the more accurate version shown in figure A18b by Wikipedia user Maximilian Dörrbecker (Chumwa). This version is than manually georeferenced using current German borders and other election maps as shown in figure A18c. A desk search identified a related Wikipedia page identifying all constituency names on the map, allowing to uniquely map each constituency to one constituency name in the CLEA. Had this not been the case, all the 397 CLEA-constituency would have had to be geocoded to identify each constituency on the map. Finally, as these constituencies were unaltered for all the Reichstag elections between 1871 and 1918, this georeferenced map can be used for 13 consecutive elections.

A similar procedure was implemented to georeference electoral maps for which no primary sources exists. Table A5 summarizes the data sources for the original maps, the identification of their constituency names in the CLEA and their time coverage, along

[22] The required one-to-one mapping of constituency names in CLEA and the constituencies on the georeferenced map also provided a useful check on the accuracy of the latter.

Figure A18: **Georeferencing the 1907 German election**

(a) Original 1907 map

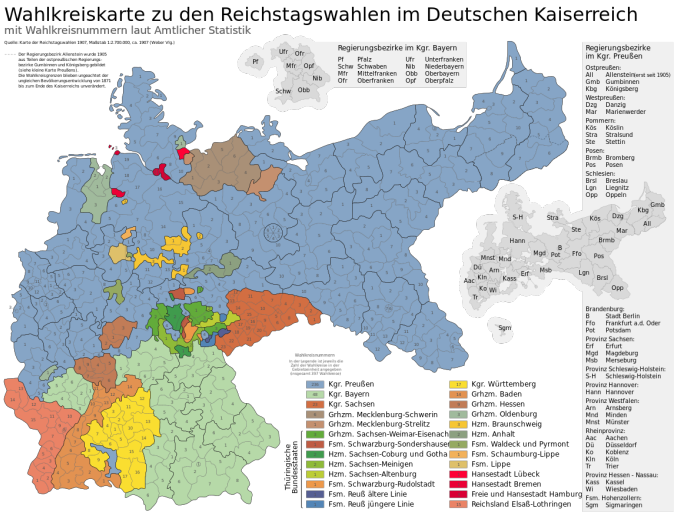

(b) Derived 2008 Wikipedia map

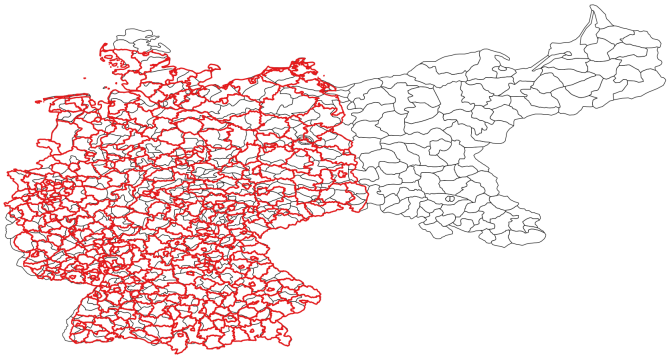

(c) Final georeferenced map

Note: Figure A18a shows the original map of electoral constituencies, A18b shows the derived map published on Wikipedia in 2008, A18c shows an overlay of the final georeferenced map (black) and the 2021 NUTS3 regions (red).

with explanatory notes where relevant. Below I provide more details by country.

Austria: Except for the period 1970-1994, when constituencies coincided with NUTS2 regions, all maps are georeferenced from Wikipedia. As secondary sources do not report constituency names, these were added through a desk search of the constituency names in CLEA. Infrequent boundary changes imply that four maps provide full historical coverage.

Belgium: Decroly, Dessouroux, Rouyet & Vandermotten (2001, figure 1) provide a map of constituencies for the period 1847-1898, when Belgium counted 41 constituencies. In this period, there were frequent partial elections such that the number of constituencies with electoral information in the CLEA ranges from 19 to 41. The subsequent 1900-1991 period is georeferenced from Wikipedia and contains 30 constituencies, though frequent partial elections reduce the number covered in the CLEA sporadically to 15. In 1995, several constituencies were merged, further reducing the total number of constituencies from 30 to 20. The CLEA constituency names identify which former constituencies were merged,

such that the electoral map for 1995 is constructed by merging the relevant constituencies in the 1991 map. Between 1999 and 2019, constituencies coincide with NUTS2 regions.

Bulgaria: As its 31 geographical constituencies remained constant, all electoral maps are georeferenced from Wikipedia.

Czech Republic: The earliest map is georeferenced by searching the CLEA-constituency names on Wikipedia. In later periods, constituencies coincide with NUTS2 regions.

Denmark: The earliest available electoral map is from 1895 on Wikipedia, which is used to georeference the 113 electoral constituencies in the 1895-1915 period. Constituency names were added from a desk search of the CLEA-constituency names, e.g. the different constituencies in Kopenhagen are identified from this 1900 map. While there is no map for the 101 constituencies in 1864-1892, the CLEA constituency names identify which former constituencies were split in 1895, such that the electoral maps for 1864-1892 are reconstructed by merging the relevant constituencies in the 1895 map. For instance, CLEA-constituencies of *'odense i'* and *'odense ii'* in the 1895 election were spatially merged to the *'odense i'* constituency in 1892. In 1864, Denmark lost the duchies of Schleswig, Holstein, and Lauenburg to Germany after the Second Schleswig War, this constituency is manually added in the 1849-1861 period from a map in Olwig & Olwig (2021). Electoral maps for the 1915-2019 period are all georeferenced from Wikipedia, where the election of September 1920, the third general election in that year, became the first election including the northern part of Schleswig, which became part of Denmark after a referendum.

Estonia: All constituencies are georeferenced from Wikipedia. In the general elections of 1995-1999, the *loona-viru* and *ida-viru* constituencies were merged and reconstructed by spatially merging these constituencies from the 2001 electoral map.

Finland: All maps were georeferenced from Wikipedia. Several spatial merges and splits are implemented to the baseline Wikipedia maps of 1930 and 1962 to match constituency border changes identified by constituency name changes in the CLEA between those two years. Between 1939 and 1951, the constituencies of *oulun laanin etelainen* and *oulun laanin pohjoinen* were spatially merged from the 1930 electoral map to the constituency of *oulun laanin*. In 1945, the former Viipurin Province was succeeded by the Kymen Province after territorial losses from WWII. Borders for the successor constituencies of *kymen laanin itainen* and *kymen laanin lantinen* were obtained by redrawing country borders to match current borders and splitting the remainder of the former Viipurin Province in an eastern and a western part, using a Wikipedia map of the historical borders of eastern and western Viipuri. In 1948, *kymen laanin itainen* and *kymen laanin lantinen* are spatially merged to the constituency of *kymen laanin* and the *ahvenmaan laanin* constituency is split from the 1945 constituency of *tutun-porin laanin etelainen* using the electoral map of 1962. In 1954, the constituency of *helsinki laanin* is split from the 1951

uudenmaan laanin constituency using its borders on the electoral map of 1962.

France: The electoral map for the 1910 election is taken from Gay (2021). Some Parisian constituencies are aggregated to the available level of aggregation in Gay (2021), e.g. *Paris 5a* and *Paris 5b* in the CLEA are merged to *Paris 5*, as this is the most disaggregated constituency available in Gay (2021). Electoral maps for the subsequent period are georeferenced from geoelections.free while later maps are georeferenced from Wikipedia. In both cases, constituency names from the CLEA were added by desk searching them on Wikipedia, see e.g. here for the constituency of *Ain 1*. The French government provides a georeferenced map for the 2017 election, the last one covered in the CLEA.

Germany: The earliest electoral maps are georeferenced from the dedicated Wahlen in Deutschland webpage, constituency names are added from the available Wikipedia pages or, lacking these, from crosschecking with earlier and later electoral maps and geocoding remaining CLEA-constituency names not covered in finished maps using Google Maps. From 1998, with one exception, the German government provides georeferenced maps.

Greece: The 99 constituencies of the 1952 election largely coincide with the Greek provinces and are georeferenced from a historical map on Wikipedia. These baseline provinces are spatially merged to the relevant departments in the CLEA-constituency names in the 1926-1956 period, when the number of constituencies ranged from 36 to 99, using the concordance of this Wikipedia page. In this period, the prefectures of *Imathia*, *Pieria* and the *General Administraton of Dodecanese* were only introduced in 1950-1951, see Caramani (2001, p. 479); as the amount of valid votes decreases most drastically in the constituency of *Lesvos* between the successive elections of 1946-1950, all three are spatially merged to *Lesvos* before 1950. The 2015 electoral map from Wikipedia is used for 1958-2015, where the *dept. of gevena* constituency is merged with the *dept. of kozani* constituency before 1974, reflecting the drop in the number of constituencies from 56 to 55. Grevena was created out of parts of the prefectures of Kozani and Larissa and was mostly located in the former. The 2019 election is georeferenced from Wikipedia.

Hungary: All electoral maps georeferenced from Wikipedia. For the 1990-2006 period, CLEA-constituency names are geocoded using Google maps to allocate them to georeferenced constituencies; numbered constituency names are identified from Wikipedia and this map for the Budapest constituencies.

Iceland: In the 1874-1942 period, Icelandic constituencies were based on historical counties (*sýslur*) and free towns (*kaupstadir*) and increased from 19 constituencies in 1874 to 28 in 1942, while the general elections of august 1916, 1922, 1926 and 1930 are only available for a single countrywide constituency. Moreover, some constituency-level electoral results are unavailable due to uncontested elections in the source data for the years 1916, 1919 and 1923, see Caramani (2001). This implies that the number of available con-

stituencies ranges from 1-28 in this period. The baseline electoral map of 1959, containing 28 constituencies, is georeferenced from a Wikipedia map showing Iceland's counties and free towns in 1988, just before they were abolished as administrative units, based on the constituency names in the CLEA. Subsequently, retroactive spatial merges are implemented on this baseline map, mainly based on the information in Caramani (2000, p. 533-534): in july 1942 and previous years, the constituency of *syglufiordu* is merged with *eyjafjaroarsysla*; in 1923 and previous years, the consituencies of *vestur-hunavatnssysla* and *austur-hunavatnssysla* are spatially merged to form the constituency of *hunavatnssyla*; in 1908, 1880 and 1874, the constituency of *vestmannaeyjasýsla* is spatially merged with *rangárvallasýsla*; in 1903 and previous years, the constituencies of *isafjorour*, *akureyri* and *seyoisfjorour* are respectively spatially merged with *vestur-isafjaroarsysla*, *eyjafjaroarsysla* *suour-mulasysla*; in 1902 and previous years, the consituencis of *vestur-isafjaroarsysla* and *norour-isafjaroarsysla* are spatially merged to *isafjardasysla*; in 1874, the constituencies of *vestur-skaptafellssysla* and *austur-skaptafellssysla* are spatially merged to form the constituency of *skaptafellssysla*. The 1959-2017 period is georeferenced from Wikipedia.

Ireland: All electoral maps are georeferenced from Wikipedia and the dedicated Irish Political Maps webpage, which also allows for the identification of all constituency names.

Italy: Most of the electoral maps are georeferenced from Wikipedia, the 1996 is georeferenced from the Centro Italiono Studi Elettorali (CISE). Constituency names can usually be allocated from Wikipedia, in 1994 and 1996 they are allocated by geocoding through Google Maps. The Italian government provides a georeferenced map for the 2018 election.

Latvia: Most maps are georeferenced from Wikipedia, the final 2018 election is georeferenced from the constituency map published by the Latvian National Federation in Canada (LNAK). The five CLEA constituency names are added through a desk search.

Lithuania: All maps are georeferenced from Wikipedia, which also provides constituency names.

Luxembourg: All maps are georeferenced from Wikipedia, the four CLEA constituency names are added through a desk search.

Netherlands: The earliest maps for 1886-1894 are georeferenced from the historical electoral maps published by de Jong, Van Der Kolk & Voerman (2011, p. 39) in collaboration with the Dutch Electoral Council, which also contains constituency names. In this period, the number of constituencies ranged from 37 in 1886 over 41 in 1887 to 84 in 1888-1894. The 1897-1917 period is georeferenced from Wikipedia, constituency names are added through crosschecking with other years and a desk search. Between 1933 and 1948, electoral constituencies coincide with NUTS2 regions. The Dutch government provides a georeferenced map for the more recent elections. Notably, the artificial island of Flevoland, completed in 1968, became an additional, separate Dutch constituency in 1986.

Norway: No electoral maps could be traced for the 1882-1915 period, which is therefore dropped from the analysis. Electoral maps for the 1921-1949 period are georeferenced from the dedicated section on AJRElectionMaps, where a desk search allocated the 29 CLEA-constituency names to their respective georeferenced constituencies. The 1953-2021 period is covered by the georeferenced map in GeoReferenced Electoral Districts Datasets (GRED), published by the CLEA, where the historical constituency of Bergen is added to this map in the 1953-1969 period using its borders on this Wikipedia map.

Poland: Apart from the last 2019 election covered in the CLEA, for which a georeferenced map is available from GeoReferenced Electoral Districts Datasets (GRED), all electoral maps are georeferenced from Wikipedia, which also provides constituency names.

Portugal: All maps are georeferenced from Wikipedia, including constituency names.

Romania: Apart from the 2012 general election, all maps are georeferenced from Wikipedia and the constituency names are allocated through desk search. In 1900, when the number of constituencies drops from 42 to 41, the CLEA-constituency of *ilfov* is spatially merged with *bucuresti*. Though maps of the 315 constituencies of the 2012 election exist, they exclude a legend of the numbered constituencies, which can also not be identified through geocoding. As the CLEA-constituencies can therefore not be allocated to the georeferenced constituencies on a map, this election is dropped from the analysis.

Slovakia: Between 1990 and 1994, electoral constituencies coincided with NUTS3-rgions, after that, general elections are organized in a single nationwide constituency.

Slovenia: All maps are georeferenced from electoral maps published by the Slovenian government, which also provide constituency names.

Spain: All maps are georeferenced from Wikipedia, all 52 constituency names are added through desk search.

Sweden: No electoral maps are available between 1872 and 1905, this period is therefore dropped from the analysis. The earliest available electoral map of the 1908 election is georeferenced from the dedicated section on AJRElectionMaps. Constituency names were subsequently added by geocoding the 201 CLEA-constituency names using Google Maps. The 1911-1920 period is also georeferenced from AJRElectionMaps, where CLEA-constituency names were now added through a desk search. The subsequent 1921-1991 is georeferenced from Wikiepedia, while GeoReferenced Electoral Districts Datasets (GRED) provides a georeferenced map for the last available elections in 2018 and 2022.

Switzerland: Constituencies coincide with the cantonal NUTS3-level. Between 1848 and 1869, national council members were elected by the Landsgemeinde in six cantons, hence electoral results are not available for the constituencies of *Appenzell Innerrhoden*, *Appenzell Ausserrhoden*, *Glarus*, *Nidwalden*, *Obwalden* and *Uri* between these years. The

canton of *Jura* was created in the 1970s and has existed as a separate constituency since the 1979 election, when it split of from the constituency of *Berne*, see also Caramani (2000, p. 919-920). All this implies that the number of constituencies with electoral results ranges from 19 between 1848 and 1869 to 25 between 1872 and 1975 and to 26 after that.

United Kingdom: No maps with legends exist for the 1832-1979 period, though they can potentially be georeferenced from AJRElectionMaps. For now, they are dropped from the analysis. From 1983 onwards, georeferenced maps for the constituent parts of the UK are provided by the UK Government.

Table A5: Detailed data sources

Country	*Election year(s)*	*Constituencies*	*Original map*	*Concordance*	*Note*
Austria	1919-1920	25	Wikipedia (Erinthecute)	Desk search	
	1923-1970	25	Wikipedia (Erinthecute)	Desk search	
	1971-1994	9	NUTS2 (2021)	Desk search	
	1995-2013	43	Wikipedia (Michael Kranewitter)	Legend	
Belgium	1847-1898	19-41	Decroly, Dessouroux, Rouyet & Vandermotten (2001)	Desk search	Frequent partial elections
	1900-1991	15-30	Wikipedia (Wikibelgiaan)	Desk search	Frequent partial elections
	1995	20			Mergers according to CLEA
	1999-2019	11	NUTS2 (2021)	Legend	
Bulgaria	1991-2023	31	Wikipedia (Erinthecute)	Legend	
Czech Republic	1990-1998	8	Wikipedia 1, 2, 3, 4, 5, 6, 7, 8 (TUBS, Norik)	Desk search	
	2002-2021	14	NUTS2 (2021)	Legend	
Denmark	1849-1861	100			Schleswig Holstein added to 1864 map from Olwig & Olwig (2021)
	1864-1892	101	Wikipedia (Gust Justice)	Desk search	Constituencies merged according to CLEA.
	1895-1915	113			Numbered Kopenhagen constituencies allocated using this map
	1920 (may, april)	22	Wikipedia (Gust Justice)	Wikipedia	
	1920 (september)-1968	23			Northern part of Schleswig part of Denmark after referendum
	1971-2005	17	Wikipedia (Gust Justice)	Electoral Geography	
	2007-2019	12	Wikipedia (Gust Justice)	Desk search	
Estonia	1992	12	Wikipedia (Karljohan29)	Des search	
	1995-1999	11	Wikipedia (Ljubinka)	Wikipedia	Merged according to CLEA
	2003-2019	12			
Finland	1907-1919	16	Wikipedia (Joukosi)	Wikipedia	
	1922-1936	16			
	1939	15			Mergers according to CLEA
	1945	15	Wikipedia (unkown)	Legend	Border adjustments from Wikipedia
	1948-1951	15			Mergers and splits according to CLEA
	1954-1958	16			Splits according to CLEA
	1962-2007	15	Wikipedia (Joukosi)	Legend	
	2011-2023	13	Wikipedia (Fenn-O-maniC)	Legend	
France	1910	578	Gay (2021)	Gay (2021)	Some Parision constituecies merged to match the level of aggregation in Gay (2021).
	1973	473	geoelections.free	Desk search	
	1978	474	geoelections.free	Desk search	
	1981	474	geoelections.free	Desk search	
	1986	96	Wikipedia (Impaulrators)	Desk search	
	1988-2007	555	Wikipedia (Goultard59)	Desk search	
	2012-2017	577	French government	French government	
Germany	1871	382	Wahlen in Deutschland	Wikipedia	
	1874	397	Wahlen in Deutschland	Wikipedia	
	1877	397	Wahlen in Deutschland	Wikipedia	
	1878	397	Wahlen in Deutschland	Wikipedia	
	1881	397	Wahlen in Deutschland	Wikipedia	
	1884	397	Wahlen in Deutschland	Wikipedia	
	1887	397	Wahlen in Deutschland	Wikipedia	
	1890	397	Wahlen in Deutschland	Wikipedia	
	1893	397	Wahlen in Deutschland	Wikipedia	
	1898	397	Wahlen in Deutschland	Wikipedia	
	1903	397	Wahlen in Deutschland	Wikipedia	
	1907	397	Wahlen in Deutschland	Wikipedia	
	1912	397	Wahlen in Deutschland	Wikipedia	
	1919	36	Wahlen in Deutschland	Wikipedia	
	1920-1933	35			
	1949	242	Wahlen in Deutschland	Crosschecking & geocoding CLEA constituencies	
	1953	242	Wahlen in Deutschland	Crosschecking & geocoding CLEA constituencies	
	1957	247	Wahlen in Deutschland	Crosschecking & geocoding CLEA constituencies	
	1961	247	Wahlen in Deutschland	Crosschecking & geocoding CLEA constituencies	

continued on next page

continued

Country	*Election year(s)*	*Constituencies*	*Original map*	*Concordance*	*Note*
	1965	248	Wahlen in Deutschland	Crosschecking & geocoding CLEA constituencies	
	1969	248	Wahlen in Deutschland	Crosschecking & geocoding CLEA constituencies	
	1972	248	Wahlen in Deutschland	Crosschecking & geocoding CLEA constituencies	
	1976	248	Wahlen in Deutschland	Crosschecking & geocoding CLEA constituencies	
	1980	248	Wahlen in Deutschland	Crosschecking & geocoding CLEA constituencies	
	1983	248	Wahlen in Deutschland	Crosschecking & geocoding CLEA constituencies	
	1987	248	Wahlen in Deutschland	Wikipedia	
	1990	328	Wahlen in Deutschland	Crosschecking & geocoding CLEA constituencies	
	1994	328	Wahlen in Deutschland	Crosschecking & geocoding CLEA constituencies	
	1998	328	German government	German government	
	2002	299	German government	German government	
	2005	299	German government	German government	
	2009	299	Wahlen in Deutschland	Wikipedia	
	2013	299	German government	German government	
	2017	299	German government	German government	
Greece	1926-1956	38-99	Wikipedia (unknown)	Merged to match CLEA names from Wikipedia	
	1958-1964	55	Wikipedia (Erinthecute)	Desk search	*dept. of gevena* merged with *dept. of kozani*
	1964-2015	56			
	2019	59	Wikipedia (Furfur)		
Hungary	1990-2006	176	Wikipedia (Beroesz)	Geocoding CLEA-constituencies and Wikipedia	Budapest constituency names added from this map
	2014-2022	106	Wikipedia (Mikovari)	Wikipedia	
Iceland	1874-1959 ((june)	1-28	Reconstructed from Wikipedia (Bjarki S)	Wikipedia	Incomplete coverage in 1916, 1919 and 1923; *Jura* split in 1979, see Caramani (2000)
	1959 (october)-1999	8	Wikipedia (Tomi)	Wikipedia	
	2003-2017	6	Wikipedia (Bjarki S)	Wikipedia	
Ireland	1922	26	Wikipedia (Jandk87)	Irish political maps	
	1923	28	Wikipedia (Jandk87)	Irish political maps	
	1927 (june)	28	Wikipedia (Jandk87)	Irish political maps	
	1927 (september)	28	Wikipedia (Jandk87)	Irish political maps	
	1932	28	Wikipedia (Jandk87)	Irish political maps	
	1933	28	Wikipedia (Jandk87)	Irish political maps	
	1937	34	Wikipedia (Jandk87)	Irish political maps	
	1938	34	Wikipedia (Jandk87)	Irish political maps	
	1943	34	Wikipedia (Jandk87)	Irish political maps	
	1944	34	Wikipedia (Jandk87)	Irish political maps	
	1948	40	Wikipedia (Jandk87)	Irish political maps	
	1951	40	Wikipedia (Jandk87)	Irish political maps	
	1954	40	Wikipedia (Jandk87)	Irish political maps	
	1957	40	Wikipedia (Jandk87)	Irish political maps	
	1961	38	Wikipedia (Jandk87)	Irish political maps	
	1965	38	Wikipedia (Jandk87)	Irish political maps	
	1969	42	Wikipedia (Jandk87)	Irish political maps	
	1973	42	Wikipedia (Jandk87)	Irish political maps	
	1977	42	Irish political maps	Irish political maps	
	1981	41	Irish political maps	Irish political maps	
	1982 (february)	41	Irish political maps	Irish political maps	
	1982 (november)	41	Irish political maps	Irish political maps	
	1987	41	Irish political maps	Irish political maps	
	1989	41	Irish political maps	Irish political maps	
	1992	41	Irish political maps	Irish political maps	
	1997	41	Irish political maps	Irish political maps	
	2002	42	Irish political maps	Irish political maps	
	2007	43	Irish political maps	Irish political maps	
	2011	43	Irish political maps	Irish political maps	
	2016	40	Wikipedia (DrRandomFactor)	Wikipedia	
	2022	39	Wikipedia (DrRandomFactor)	Wikipedia	*laois* and *offaly* from the 2016 map merged to the 2022 *laois/offaly* constituency.
Italy	1919	54	Wikipedia (Facquis)	Desk search	

continued on next page

continued

Country	*Election year(s)*	*Constituencies*	*Original map*	*Concordance*	*Note*
	1921	40	Wikipedia (Facquis)	Desk search	
	1946-1953	31	Wikipedia (Romano1979)	Wikipedia	
	1958-1992	32	Wikipedia (Erinthecute)	Wikipedia	
	1994-1996	475	CISE	Geocoded CLEA constituency names	
	2001-2013	27	Wikipedia (Nick84)	Wikibooks	
	2018	232	Italian government	Italian government	
Latvia	1995-2014	5	Wikipedia (JDuggan101)	Desk search	
	2018	5	LNAK	LNAK	
Lithuania	1992-2016	71	Wikipedia (Łukasz Bień)	Wikipedia	
	2020	70	Wikipedia (Łukasz Bień)	Wikipedia	
Luxembourg	1919-2018	4	Wikipedia (JDuggan101)	Desk search	
	1886-1894	37-84	de Jong, Van Der Kolk & Voerman (2011)	de Jong, Van Der Kolk & Voerman (2011)	
	1897-1917	100	Wikipedia (BHJ15)	Crosschecking and desk search	
Netherlands	1922-1929	18	Dutch government	Kiesraad	
	1933-1948	11	NUTS2 (2021)	NUTS2 (2021)	
	1952-2012	18	Dutch government	Kiesraad	Flevoland added in 1986
	1882-1915		Missing, electoral maps unavailable		
Norway	1921-1949	29	AJRElectionMaps	Desk search	
	1953-2021	19-20	GRED	GRED	Bergen added in 1953-1969 from Wikipedia
	1991	37	Wikipedia (Erinthecute)	Wikipedia	
Poland	1993-1997	52	Wikipedia (Erinthecute)	Wikipedia	
	2001-2019-1997	41	GRED	GRED	
Portugal	1975-2022	20	Wikipedia (Erinthecute)	Wikipedia	
	1990-2004	41-42	Wikipedia (Erinthecute)	Desk search	1990: constituency of *ilfov* merged with constituency of *bucuresti*
Romania	2012		Missing, numbered constituency names unavailable		
	2016	42	Wikipedia (Erinthecute)	Desk search	
Slovakia	1990-1994	4	NUTS3 (2021)	NUTS3 (2021)	
	1990-1994	4	NUTS0 (2021)	NUTS0 (2021)	
Slovenia	1996-2014	88	Slovenian Ministry of Public Administration	Slovenian Ministry of Public Administration	
	2018	8	Slovenian Interior Ministry	Slovenian Interior Ministry	
Spain	1977-2019	4	Wikipedia (Erinthecute)	Desk search	
	1872-1905		Missing, electoral maps unavailable		
	1908	201	AJRElectionMaps	Geocoding CLEA constituencies	
Sweden	1911-1920	56	AJRElectionMaps	Desk search	
	1921-1991	28	Wikipedia (Ff152Rr361Af7)	Desk search	
	1994-2022	29	GRED	GRED	
Switzerland	1848-2019	19-26	NUTS3 (2021)	NUTS3 (2021)	1848-1869: no elections in 6 constituencies; constituency of *Jura* absent before 1979
	1832-1979		Missing, electoral maps with legends unavailable		
UK	1983-1992	650	UK Data Service: England, Scotland, Wales, N Ireland	UK Data Service	
	2001-2005	646-650	ONS (Great brittain) / UK Data Service (N Ireland)		
	2010-2019	650	UK Data Service: England, Scotland, Wales, N Ireland	UK Data Service	

Note: This table provides a detailed, country-specific overview of the availability of georeferenced electoral maps and their sources, for each period indicated in the second column. The third column reports the number of constituencies with available electoral data in the CLEA, or its range when they change across elections in this time period. The fourth column reports the source of the baseline map used for georeferencing, with the main contributor between brackets when it is derived from Wikipedia. The fifth column reports the source for the constituency names or the method in which they are allocated: desk searching the CLEA-constituency names to add them to georeferenced constituencies; spatial merges and splits based on constituency name changes in the CLEA; or geocoding the CLEA-constituencies to allocate unique matches and follow up with a desk search to resolve missing or non-unique matches. The last column provides notes where necessary; more detailed information can be found in appendix A.2.1.

A.2.2 Harmonizing and classifying political parties in the CLEA

The political parties in the CLEA are classified as mainstream, populist and extremist by linking their names to existing classification systems and their ideological positions on Wikipedia. As political parties are not consistently named across or even within elections, e.g. due to language differences, they are first harmonized by identifying their associated Wikipedia pages using keyword search. While unmatched party names are retained unaltered, multiple CLEA party names that can be matched to the same Wikipedia page are harmonized to an identical 'harmonized' party name. There are 6198 unique party names in the CLEA, of which 4610 could be matched to Wikipedia pages, reducing the total number of parties to 3018. The full concordance table can be found here.

Political parties are than defined as mainstream, populist or extremist by synthesizing their classification in three sources. I first provide more details on how (many) parties are linked to each source, the information they contain and their primary (dis)advantages.

Inglehart and Norris (2019): Define populist parties as those who employ *"a rhetorical style of communications claiming that (i) the only legitimate democratic authority flows directly from the people, and (ii) established power-holders are deeply corrupt"* (Inglehart & Norris, 2019, p. 66). To operationalize this, they rely on expert assessments of the scores of party positions on anti-elite rethoric and the salience of anti-corruption in the Chapel Hill Expert Survey (CHES) to categorize parties as populist if they score sufficiently high on this populism scale. Similarly, they categorize parties as left-wing and right-wing based on their combined CHES-score on four policy positions related to market deregulation, state management of the economy, redistributive taxes and tax cut preferences, allowing to distinguish left and right populist parties. One advantage is that, with the exception of Iceland, this classification covers all the countries of this analysis. One disadvantage is that the classification only covers the recent 2000-2015 period. Another is that it depends on the political party coverage of the CHES, which is heavily focused on established parties with political representation, such that it contains no information for smaller parties. Finally, it lacks classification for extremist parties on the far left/right or separatist dimensions.

The PopuList: Initiated by *The Guardian*, The PopuList relies on expert assessments of both academics and journalists to classify European political parties that attracted at least 2% of the vote and/or have been represented in the national parliament as 'populist', 'far right' and 'far left'. Populist parties *claim that society is separated into two antagonistic groups, "the pure people" versus "the corrupt elite", and argue that politics should be an expression of the general will of the people*; far right parties *are nativist and authoritarian*; and far left parties *see economic inequality as the basis of existing political and social arrangements and call for a major redistribution of resources from existing political elites* (Rooduijn et al., 2019). It has complete country coverage for the period 1989-2022, more extensive political party coverage and also classifies both extremist and populist parties.

However, it contains no information for the period before 1989 or smaller political parties.

Wikipedia: The largest volunteer-driven database in the world, Wikipedia offers structured information on ideological keywords and left-right positions with potentially unlimited political party-coverage. It has been demonstrated to contain valid and reliable information on the ideological and left-right positions of political parties, which typically correlates well with more conventional scores obtained from expert surveys (Herrmann & Döring, 2023). Information on ideological positions are mainly extracted from Wikipedia infoboxes if they are available, as shown in figure A19a for the example of the Italian *Fratelli d'Italia* party, but if these are unavailable (mainly for small parties), tags are added from the Wikipedia description. To maximize the richness of the ideological classification, tags are both derived from English and national language pages. Party coalitions absorb the ideological positions of their component parts. The full classification of all European political parties in the CLEA can be found here. The ideological classification comprises 219 ideological tags, see appendix table A7, yet most political parties receive at most 5 tags, see figure A19b. Information on political positions is similarly extracted, opting for the most extreme position if political parties receive multiple positions on the left-right scale, resulting in the bimodal distribution shown in figure A19c. The biggest advantage of Wikipedia is that it has complete country and temporal coverage and much more extensive political party coverage. One drawback from the continual updating of information is that the classification depends on the time when the information is extracted.

Figure A19: **Classification derived from Wikipedia**

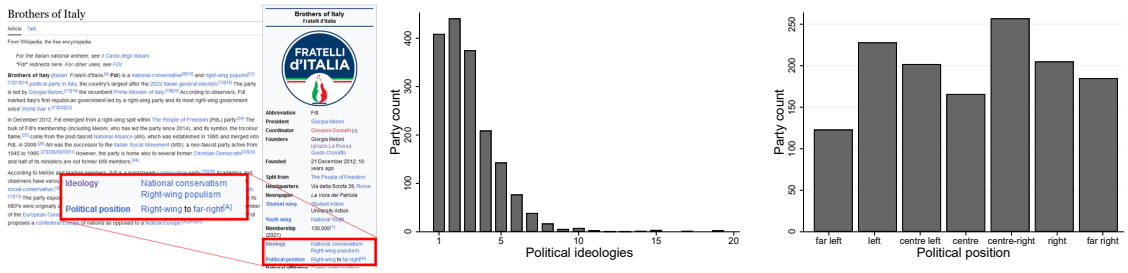

(a) Infobox for *Fratelli d'Italia* (b) Ideological positions per party (c) Political position distribution

Note: Figure A19a shows the infobox in the English Wikipedia article for the *Fratelli d'Italia*; figure A19b shows the frequency distribution of ideology tags across parties; figure A19c shows the distribution of political positions.

For illustrative purposes, I also construct a party taxonomy that uniquely describes each political party by its most salient ideological position. If a political party is classified as populist or extremist, these are assumed to be the most salient ideological positions, otherwise the main ideological category is determined from the Wikipedia description. While the full party taxonomy can be obtained here, appendix table A9 provides a country-specific breakdown of the number of political parties in the CLEA across the most important taxonomic categories. Utilizing this data allows to put European electoral trends in a historical perspective. Figure A20 shows the historical evolution in the aggregate vote

shares of the most salient categories in the party taxonomy over the past two centuries for the available election years. Assuming electoral trends to evolve gradually over time, future non-election years are linearly extra- and interpolated at the country-level. The figure shows that christian, liberal and conservative parties dominated the earliest elections in Europe. From the end of the 19^{th} century onwards, there is a clear electoral rise of socialist parties. The interbellum gave rise to what could be dubbed a first 'extremist' wave of radicalism, when political parties that are considered by observers to be far left and right suddenly gained electoral ground. In the 1980s, the combined electoral force of traditional christian, liberal, conservative and socialist parties erodes again in what could be called second 'populist' wave of radicalism that continues to today. Appendix figure A49 provides a country-specific breakdown of electoral trends.

Figure A20: Aggregate interpolated vote share in Europe by party taxonomy

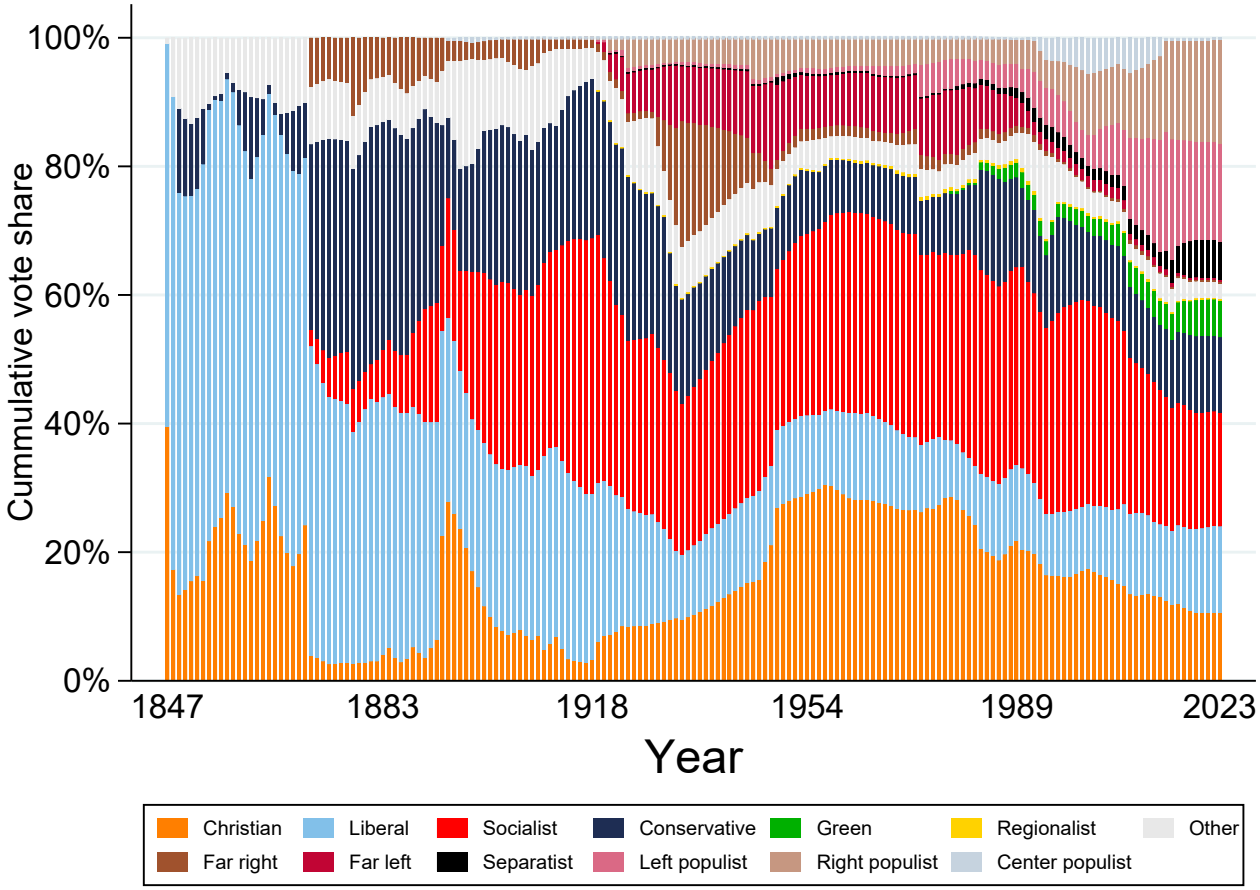

Note: This figure plots historical European trends in the vote shares received by political parties in the the available elections of the CLEA by party taxonomy between 1847 and 2023. Electoral behavior in future non-election years is approximated by linear extra- and interpolation at the country level.

B A Dynamic Spatial Political Economy Model

This appendix provides a more comprehensive description of the spatial political economy model presented in section 2. Section B.1 covers all the intermediary steps in the derivation of the model and provides additional discussion. Section B.2 provides more intuition for the model's primitives, which fully characterize the spatial equilibria. Finally, section B.3 provides more detailed equilibrium results for the baseline calibration in section 6.

B.1 Proofs and further details

B.1.1 Equilibrium consumption in section 4.4

First recall that agents differ in their human capital endowments, s, which are drawn from a Pareto distribution with shape parameter $\alpha > 1$ and lower bound 1, $s_n \sim P(\alpha)$. This implies that the cumulative distribution function (CDF) and probability density function (PDF) of human capital, $\Phi(s)$ and $\phi(s)$, is respectively given by

$$\begin{aligned} \Phi(s) = F_s(x) = Pr(s \leq x) = 1 - \left(\frac{1}{x}\right)^{\alpha} \quad &, \alpha > 1 \\ \phi(s) = f_s(x) = Pr(x < s < x + \delta) = \frac{\alpha}{x^{\alpha+1}} \quad &, \textit{for } \delta \approx 0 \textit{ and } \alpha > 1 \end{aligned} \tag{17A}$$

To recover optimal consumption in equation (16) note that, conditional on the equilibrium income tax rate, τ^*, described in section 4.6, individual utility in equation (15) implies agents optimize their consumption decisions by solving the following Lagrangian

$$\begin{aligned} &\max_{c,h} = \tilde{U}_{l,n}(s_n) \\ &s.t. \qquad pc + r_l h = \underbrace{(1-\tau^*) w_l(s_n)}_{\text{net wage income}} + \underbrace{\left(\tau - \frac{\tau^{\psi}}{\psi}\right)\frac{Y}{N}}_{\text{lump-sum transfer}} \end{aligned} \tag{18A}$$

$$\Rightarrow \mathcal{L}(c,h,\lambda) = \Big(c(s_n)\Big)^{\mu}\Big(h(s_n)\Big)^{1-\mu} - \lambda\left[pc + r_l h - (1-\tau^*) w_l(s_n) - \left(\tau - \frac{\tau^{\psi}}{\psi}\right)\frac{Y}{N}\right]$$

with p the price of the consumption good and r_l the housing rental rate in location l.

Conditional on the human capital endowment and the location choice discussed in sections 4.1 and 4.5 as well as equilibrium income taxation discussed in section 4.6, optimal consumption and housing decisions yield the following individual expenditure functions

$$\left.\begin{array}{l}\frac{\partial \mathcal{L}(c,h,\lambda)}{\partial c}: \mu\left(\frac{c_{l,n}(s_n)}{h_{l,n}(s_n)}\right)^{\mu-1}=\lambda p \\ \frac{\partial \mathcal{L}(c,h,\lambda)}{\partial h}: (1-\mu)\left(\frac{c_{l,n}(s_n)}{h_{l,n}(s_n)}\right)^{\mu}=\lambda r_l\end{array}\right\} \begin{array}{l}\frac{\mu}{p}\left(\frac{c_{l,n}(s_n)}{h_{l,n}(s_n)}\right)^{\mu-1}=\frac{1-\mu}{r_l}\left(\frac{c_{l,n}(s_n)}{h_{l,n}(s_n)}\right)^{\mu} \\ \Rightarrow c^*_{l,n}(s_n)=\frac{\mu}{1-\mu}\frac{r_l}{p}h^*_{l,n}(s_n)\end{array}$$

$$\frac{\partial \mathcal{L}(c,h,\lambda)}{\partial \lambda}: pc^*_{l,n}(s_n)+r_l h^*_{l,n}(s_n)=(1-\tau^*)w_l(s_n)+\left(\tau-\frac{\tau^\psi}{\psi}\right)\frac{Y}{N}$$

Substituting for $c^*_{l,n}(s_n)$

$$\begin{aligned}&\Rightarrow \frac{\mu}{1-\mu}r_l h^*_{l,n}(s_n)+r_l h^*_{l,n}(s_n)=(1-\tau^*)w_l(s_n)+\left(\tau-\frac{\tau^\psi}{\psi}\right)\frac{Y}{N}\\ &\Leftrightarrow \frac{1}{1-\mu}r_l h^*_{l,n}(s_n)=(1-\tau^*)w_l(s_n)+\left(\tau-\frac{\tau^\psi}{\psi}\right)\frac{Y}{N} \qquad (19A)\\ &\Leftrightarrow h^*_{l,n}(s_n)=\frac{1-\mu}{r_l}\left[(1-\tau^*)w_l(s_n)+\left(\tau-\frac{\tau^\psi}{\psi}\right)\frac{Y}{N}\right]\end{aligned}$$

Substituting for $w_l(s_n)$

$$\begin{aligned}&\Leftrightarrow h^*_{l,n}(s_n)=\frac{1-\mu}{r_l}\left[(1-\tau^*)a_l s_n+\left(\tau-\frac{\tau^\psi}{\psi}\right)\frac{Y}{N}\right]\\ &\Leftrightarrow c^*_{l,n}(s_n)=\frac{\mu}{p}\left[(1-\tau^*)a_l s_n+\left(\tau-\frac{\tau^\psi}{\psi}\right)\frac{Y}{N}\right]\end{aligned}$$

such that agents spend a fixed share of μ of their net income on private consumption and the remaining share of $(1-\mu)$ on housing.

With inelastic housing supply, equilibrium rents in each location l, r^*_l, must satisfy

$$\begin{aligned}\bar{H}_l&=\int_{s=1}^{\infty}N\pi_l(s,\tau^*)h^*_{l,n}(s)\phi(s)ds\\ &=\frac{1-\mu}{r_l}\left[\int_{s=1}^{\infty}N\pi_l(s,\tau^*)(1-\tau^*)a_l s\phi(s)ds+\int_{s=1}^{\infty}N\pi_l(s,\tau^*)\left(\tau-\frac{\tau^\psi}{\psi}\right)\frac{Y}{N}\phi(s)ds\right]\\ &=\frac{1-\mu}{r_l}\left[(1-\tau^*)a_l S_l+\left(\tau-\frac{\tau^\psi}{\psi}\right)\frac{Y}{N}N_l\right] \qquad (20A)\end{aligned}$$

$$\Rightarrow r^*_l=\frac{1-\mu}{\bar{H}}\left[(1-\tau^*)a_l S_l+\left(\tau-\frac{\tau^\psi}{\psi}\right)Y\frac{N_l}{N}\right]$$

where the integral in the first line is defined over the full human capital distribution with probability density function $\phi(s)$, see equation (17A), and $\pi_l(s,\tau^*)$ will be later defined in equation (30A) to capture the probability that an agent with human capital endowment s will locate in location l if the equilibrium redistributive tax equals τ^*. Hence $S_l=\int_{n\in l}s_n dn=\int_{s=1}^{\infty}N\pi_l(s,\tau^*)s\phi(s)ds$ captures total skill at location l.

Consistent with standard findings, equilibrium rents thus increase when locations become more productive, a_l, as higher wages induce inhabitants to spend more on housing; increase when locations attract more and/or more-skilled inhabitants, both of which increase the total human capital stock, S_l, and hence total demand for housing in a location; and decrease in the exogenous supply of housing, $\bar{H}$, as the housing supply becomes more

abundant. Agglomeration costs thus temper the attractiveness of highly-productive places by putting an upward pressure on housing prices as local effective labor, S_l, increases. Notably, income redistribution, τ^*, reduces rents in productive locations because they lose their attractiveness when net income depends less on wage income, such that income redistribution undercuts equilibrium rents in productive locations. For similar reasons, the agglomeration costs captured by S_l become less relevant if taxation makes total income less dependent on labor income. In the extreme case of complete taxation, all incomes are independent of location choice and each location becomes equally attractive, yielding identical rents amounting to the Cobb-Douglas fixed share of $(1-\mu)$ of (identical) income.

A similar goods market equilibrium condition yields the price of private consumption:

$$
\begin{aligned}
\overbrace{\left(1-\frac{\tau^{\psi}}{\psi}\right)}^{\text{Tax distortion}}\overbrace{Y}^{\text{Supply}} &= \overbrace{\int_{l=1}^{L}\int_{s=1}^{\infty} N\pi_l\left(s,\tau^*\right)c^*\left(s\right)\phi\left(s\right)dsdl}^{\text{Workers demand}} + \overbrace{\int_{l=1}^{L}\frac{r_l\bar{H}}{p}dl}^{\text{Absentee landlord demand}} \\
\Leftrightarrow \frac{\psi-\tau^{\psi}}{\psi}Y &= \int_{l=1}^{L}\int_{s=1}^{\infty} N\pi_l\left(s,\tau^*\right)\frac{\mu}{p}\left[\left(1-\tau^*\right)a_l s+\left(\tau-\frac{\tau^{\psi}}{\psi}\right)\frac{Y}{N}\right]\phi\left(s\right)dsdl \\
&\quad+\int_{l=1}^{L}\bar{H}\frac{1-\mu}{p\bar{H}}\left[\left(1-\tau^*\right)a_l S_l+\left(\tau^*-\frac{\tau^{*\psi}}{\psi}\right)Y\frac{N_l}{N}\right]dl \\
\Leftrightarrow \frac{\psi-\tau^{\psi}}{\psi}Y &= \int_{l=1}^{L}\frac{\mu}{p}\left[\left(1-\tau^*\right)a_l S_l+\left(\tau^*-\frac{\tau^{*\psi}}{\psi}\right)Y\frac{N_l}{N}\right]dl \\
&\quad+\int_{l=1}^{L}\frac{(1-\mu)}{p}\left[\left(1-\tau^*\right)a_l S_l+\left(\tau^*-\frac{\tau^{*\psi}}{\psi}\right)Y\frac{N_l}{N}\right]dl \\
\Leftrightarrow \frac{\psi-\tau^{\psi}}{\psi}Y &= \frac{\mu}{p}\left(1-\tau^*\right)\int_{l=1}^{L}a_l S_l dl+\frac{\mu}{p}\left(\tau^*-\frac{\tau^{*\psi}}{\psi}\right)\frac{Y}{N}\int_{l=1}^{L}N_l dl \\
&\quad+\frac{(1-\mu)}{p}\left(1-\tau^*\right)\int_{l=1}^{L}a_l S_l dl+\frac{(1-\mu)}{p}\left(\tau^*-\frac{\tau^{*\psi}}{\psi}\right)\frac{Y}{N}\int_{l=1}^{L}N_l dl \quad (21A) \\
\Leftrightarrow \frac{\psi-\tau^{\psi}}{\psi}Y &= \frac{\mu}{p}\left(1-\tau^*\right)Y+\frac{\mu}{p}\left(\tau^*-\frac{\tau^{*\psi}}{\psi}\right)Y \\
&\quad+\frac{(1-\mu)}{p}\left(1-\tau^*\right)Y+\frac{(1-\mu)}{p}\left(\tau^*-\frac{\tau^{*\psi}}{\psi}\right)Y \\
\Leftrightarrow \frac{\psi-\tau^{\psi}}{\psi} &= \frac{\mu}{p}\left(1-\tau^*\right)+\frac{\mu}{p}\left(\tau^*-\frac{\tau^{*\psi}}{\psi}\right)+\frac{(1-\mu)}{p}\left(1-\tau^*\right)+\frac{(1-\mu)}{p}\left(\tau^*-\frac{\tau^{*\psi}}{\psi}\right) \\
\Leftrightarrow \frac{\psi-\tau^{\psi}}{\psi} &= \left(1-\tau^*\right)\left(\frac{\mu+1-\mu}{p}\right)+\left(\tau^*-\frac{\tau^{*\psi}}{\psi}\right)\left(\frac{\mu+1-\mu}{p}\right) \\
\Leftrightarrow \frac{\psi-\tau^{\psi}}{\psi} &= \frac{1-\tau^*}{p}+\frac{\psi\tau^*-\tau^{*\psi}}{\psi p} \\
\Leftrightarrow \frac{\psi-\tau^{\psi}}{\psi} &= \frac{\left(1-\tau^*\right)\psi+\psi\tau^*-\tau^{*\psi}}{\psi p} \\
\Leftrightarrow \psi-\tau^{\psi} &= \frac{\psi-\tau^{*\psi}}{p} \\
\Leftrightarrow p &= \frac{\psi-\tau^{*\psi}}{\psi-\tau^{\psi}}
\end{aligned}
$$

$$\Leftrightarrow p^* = 1$$

with $Y = \int_{l=1}^{L} Y_l dl = \int_{l=1}^{L} a_l S_l dl$ total production of the final good and $N = \int_{l=1}^{L} N_l dl = \int_{n \in l} dn$ total population. Hence the consumption good is a pure numeraire good.

Substituting for p^* and r_l^*, yields the equilibrium consumption choices in equation (16). The equation demonstrates that income redistribution, τ^*, makes equilibrium expenditures, and hence location choices, depend less on wage income, $a_l s_n$, and lets them converge to identical levels determined by the lump-sum transfer, $\left(\tau^* - \frac{\tau^{*\psi}}{\psi}\frac{Y}{N}\right)$.

Equilibrium location choices in section 4.5

Freely mobile workers make location choices to maximize their (indirect) utility as given in equation (17). This utility depends on an agent's idiosyncratic preferences for each location, $\xi_{l,n}$, drawn from a generalized Fréchet distribution, see section 4.1, such that for given shape, location and scale parameters ϵ, ν and ι, they have the following CDF

$$\xi_{l,n} \sim F_\xi(x) = Pr(\xi_{l,n} \leq x) = \mathrm{e}^{-\frac{x-\nu}{\iota}^{-\epsilon}} \tag{22A}$$

and, for suitably small values of δ, the following PDF

$$f_\xi(x) = Pr(x < \xi_{l,n} \leq x + \delta) = \frac{\epsilon}{\iota}\left(\frac{x-\nu}{\iota}\right)^{-1-\epsilon} \mathrm{e}^{-\frac{x-\nu}{\iota}^{-\epsilon}} \tag{23A}$$

Finally, the expected value of each draw equals

$$E(\xi_{l,n}) = \nu + \iota\Gamma\left(1 - \frac{1}{\epsilon}\right) \tag{24A}$$

with Γ denoting the Gamma function.

Letting the location parameter (minimum) $\nu = 1$ and the scale parameter $\iota = 0$, the CDF of the location preference distribution only depends on the scale parameter ϵ

$$\xi_{l,n} \sim F_\xi(x) = Pr(\xi_{l,n} \leq x) = \mathrm{e}^{-x^{-\epsilon}} \tag{25A}$$

while the PDF for small δ reverts to

$$f_\xi(x) = Pr(x < \xi_{l,n} \leq x + \delta) = x^{-1-\epsilon}\mathrm{e}^{-x^{-\epsilon}} \tag{26A}$$

Equation (24A) clarifies how scaling $\xi_{l,n}$ with an arbitrary constant $\delta_{l,s}$ is equivalent to setting the scale parameter $\iota = \delta_{l,s_n}$, such that following equations (22A) and (23A), the unconditional distribution of indirect utility in location l can be described by

$$\begin{aligned} v_{l,n}(s_n) = \xi_{l,n}\delta_l(s_n, \tau^*) \sim & F_{\xi\delta}(x) = \mathrm{e}^{-x^{-\epsilon}\delta_l(s_n,\tau^*)^\epsilon} \\ & f_{\xi\delta}(x) = \epsilon x^{-1-\epsilon}\delta_{l,s}^\epsilon \mathrm{e}^{-x^{-\epsilon}\delta_l(s_n,\tau^*)^\epsilon} \end{aligned} \tag{27A}$$

with $\delta_l(s_n, \tau^*)$ as determined in equation (17).

To characterize the joint distribution of indirect utilities, note that the independence assumption implies that the joint cumulative distribution function has the following form

$$\begin{aligned} F_{v_{l,n}}(x) &= F_{\xi_{n,1}\delta_1(s_n,\tau^*),\ldots,\xi_{l,n}\delta_L(s_n,\tau^*)}(x) \\ &= Pr\left(\xi_{n,1}\delta_1(s_n,\tau^*) \leq x,\ldots,\xi_{l,n}\delta_L(s_n,\tau^*) \leq x\right) \\ &= Pr\left(\xi_{n,1}\delta_1(s_n,\tau^*) \leq x\right) \times \ldots \times Pr\left(\xi_{l,n}\delta_L(s_n,\tau^*) \leq x\right) \\ &= \prod_{l=1}^{L} \mathrm{e}^{-x^{-\epsilon}\delta_l(s_n,\tau^*)^\epsilon} = \mathrm{e}^{-\sum_{l=1}^{L}\left(x^{-\epsilon}\delta_l(s_n,\tau^*)^\epsilon\right)} = \mathrm{e}^{-x^{-\epsilon}\sum_{l=1}^{L}\delta_l(s_n,\tau^*)^\epsilon} \end{aligned} \tag{28A}$$

where the second line follows from the mutual independence assumption.

The *ex ante* probability that the indirect utility of a particular agent n with skill level s_n is highest among all L locations for location l then amounts to[23]

$$\begin{aligned} &Pr\left(\arg\max_k \left\{\xi_{n,k}\delta_k(s_n,\tau^*)\right\} = l\right) \\ &= 1 - Pr\left(\arg\max_k \left\{\xi_{n,k}\delta_k(s_n,\tau^*)\right\} \neq l\right) \\ &= 1 - \int_0^\infty \underbrace{F_{v_{l,n}}(x)}_{\substack{\text{probability that} \\ \xi_{l,n}\delta_l(s_n,t) \leq x}} \underbrace{dF_{v_{n,-l}}(x)}_{\substack{\text{joint probability} \\ \text{density at } x \text{ for } k \neq l}} dx \\ &= 1 - \int_0^\infty \mathrm{e}^{-x^{-\epsilon}\delta_{l,s_n}^\epsilon}\left[\epsilon x^{-1-\epsilon}\int_{k\neq 1}^{L}\delta_k(s_n,\tau^*)^\epsilon \mathrm{e}^{-x^{-\epsilon}\delta_k(s_n,\tau^*)^\epsilon}dk\right]dx \\ &= 1 - \int_0^\infty \epsilon x^{-1-\epsilon}\int_{k\neq 1}^{L}\delta_k(s_n,\tau^*)^\epsilon\, dk\ \mathrm{e}^{-x^{-\epsilon}\delta_{l,s_n}^\epsilon}\mathrm{e}^{-x^{-\epsilon}\int_{k\neq 1}^{L}\delta_k(s_n,\tau^*)^\epsilon dk}dx \\ &= 1 - \int_0^\infty \int_{k\neq 1}^{L}\delta_k(s_n,\tau^*)^\epsilon\, dk\ \epsilon x^{-1-\epsilon}\mathrm{e}^{-x^{-\epsilon}\left(\delta_1^\epsilon + \int_{k\neq 1}^{L}\delta_k(s_n,\tau^*)^\epsilon dk\right)}dx \\ &= 1 - \int_0^\infty \int_{k\neq 1}^{L}\delta_k(s_n,\tau^*)^\epsilon\, dk\ \epsilon x^{-1-\epsilon}\mathrm{e}^{-x^{-\epsilon}\int_{k=1}^{L}\delta_k(s_n,\tau^*)^\epsilon dk}dx \\ &= 1 - \frac{\int_{k\neq 1}^{L}\delta_k(s_n,\tau^*)^\epsilon\, dk}{\int_{k=1}^{L}\delta_k(s_n,\tau^*)^\epsilon\, dk}\int_0^\infty \int_{k=1}^{L}\delta_k(s_n,\tau^*)^\epsilon\, dk\epsilon x^{-1-\epsilon}\mathrm{e}^{-x^{-\epsilon}\int_{k=1}^{L}\delta_k(s_n,\tau^*)^\epsilon dk}dx - 1 \end{aligned} \tag{29A}$$

$$\begin{aligned} &= 1 - \frac{\int_{k\neq 1}^{L}\delta_k(s_n,\tau^*)^\epsilon\, dk}{\int_{k=1}^{L}\delta_k(s_n,\tau^*)^\epsilon\, dk}\left[\mathrm{e}^{-x^{-\epsilon}\int_{k=1}^{L}\delta_k(s_n,\tau^*)^\epsilon dk}\right]_0^\infty \\ &= 1 - \frac{\int_{k\neq 1}^{L}\delta_k(s_n,\tau^*)^\epsilon\, dk}{\int_{k=1}^{L}\delta_k(s_n,\tau^*)^\epsilon\, dk}\left[\mathrm{e}^0 - \mathrm{e}^{-\infty}\right] \\ &= 1 - \frac{\int_{k\neq 1}^{L}\delta_k(s_n,\tau^*)^\epsilon\, dk}{\int_{k=1}^{L}\delta_k(s_n,\tau^*)^\epsilon\, dk}\left[1 - 0\right] \\ &= 1 - \frac{\int_{k\neq 1}^{L}\delta_k(s_n,\tau^*)^\epsilon\, dk}{\int_{k=1}^{L}\delta_k(s_n,\tau^*)^\epsilon\, dk} \end{aligned}$$

[23] Note that the eight line in equation (29A) uses that $\frac{\partial \mathrm{e}^{ax}}{\partial x} = a\mathrm{e}^{ax}$ and that $\frac{\partial \mathrm{e}^{x^a}}{\partial x} = a\mathrm{e}^{x^a}x^{a-1}$, implying that $\frac{\partial \mathrm{e}^{-x^{-\epsilon}\int_{l=1}^{L}\delta_{l,s_n}^\epsilon dl}}{\partial x} = \int_{l=1}^{L}\delta_{l,s_n}^\epsilon dl\,(-\epsilon)\,(-x)^{-\epsilon-1}\,\mathrm{e}^{-x^{-\epsilon}\int_{l=1}^{L}\delta_{l,s_n}^\epsilon dl}$.

$$= \frac{\int_{k=1}^{L} \delta_k \left(s_n, \tau^*\right)^{\epsilon} dk - \int_{k\neq 1}^{L} \delta_k \left(s_n, \tau^*\right)^{\epsilon} dk}{\int_{k=1}^{L} \delta_k \left(s_n, \tau^*\right)^{\epsilon} dk}$$
$$= \frac{\delta_l \left(s_n, \tau^*\right)^{\epsilon}}{\int_{k=1}^{L} \delta_k \left(s_n, \tau^*\right)^{\epsilon} dk}$$

such that the *ex ante* probability that an agent with skill endowment s_n will choose locate at l, $\pi_l(s)$, is given by equation (18). Substituting for $\delta_l(s, \tau^*)$, and abstracting from residential amenities, ϵ_l, $\pi_l(s, \tau^*)$ can be expressed as a ratio of indirect utilities

$$\begin{aligned}
\pi_l\left(s_n, \tau^*\right) &= \frac{\left(\mu^{\mu}\bar{H}^{1-\mu}\frac{(1-\tau^*)a_l s_n + \left(\tau^* - \frac{\tau^{*\psi}}{\psi}\right)\frac{Y}{N}}{\left((1-\tau^*)a_l S_l + \left(\tau^* - \frac{\tau^{*\psi}}{\psi}\right)\frac{Y}{N}N_l\right)^{1-\mu}}\right)^{\epsilon}}{\int_{k=1}^{L}\left(\mu^{\mu}\bar{H}^{1-\mu}\frac{(1-\tau^*)a_k s_n + \left(\tau^* - \frac{\tau^{*\psi}}{\psi}\right)\frac{Y}{N}}{\left((1-\tau^*)a_k S_k + \left(\tau^* - \frac{\tau^{*\psi}}{\psi}\right)\frac{Y}{N}N_k\right)^{1-\mu}}\right)^{\epsilon} dk} \\
&= \frac{\left(\frac{(1-\tau^*)a_l s_n + \left(\tau^* - \frac{\tau^{*\psi}}{\psi}\right)\frac{Y}{N}}{\left((1-\tau^*)a_l S_l + \left(\tau^* - \frac{\tau^{*\psi}}{\psi}\right)\frac{Y}{N}N_l\right)^{1-\mu}}\right)^{\epsilon}}{\int_{k=1}^{L}\left(\frac{(1-\tau^*)a_k s_n + \left(\tau^* - \frac{\tau^{*\psi}}{\psi}\right)\frac{Y}{N}}{\left((1-\tau^*)a_k S_k + \left(\tau^* - \frac{\tau^{*\psi}}{\psi}\right)\frac{Y}{N}N_k\right)^{1-\mu}}\right)^{\epsilon} dk} \\
&= \frac{\left((1-\tau^*)a_l s_n + \left(\tau^* - \frac{\tau^{*\psi}}{\psi}\right)\frac{Y}{N}\right)^{\epsilon}}{\int_{k=1}^{L}\left((1-\tau^*)a_k s_n + \left(\tau^* - \frac{\tau^{*\psi}}{\psi}\right)\frac{Y}{N}\right)^{\epsilon} dk} \\
&\quad \frac{\int_{k=1}^{L}\left((1-\tau^*)a_k S_k + \left(\tau^* - \frac{\tau^{*\psi}}{\psi}\right)\frac{Y}{N}N_k\right)^{\epsilon(1-\mu)} dk}{\left((1-\tau^*)a_l S_l + \left(\tau^* - \frac{\tau^{*\psi}}{\psi}\right)\frac{Y}{N}N_l\right)^{\epsilon(1-\mu)}}
\end{aligned} \tag{30A}$$

This has the standard implications that workers share a *ceteris paribus* preference to live in more productive locations, where $a_l > a_k$, which offer them higher wages, but that they dislike living in dense locations, where $S_l = \int_{s=1}^{\infty} N\pi_l(s, a_l, \tau^*)\, s\phi(s)\, ds > \int_{s=1}^{\infty} N\pi_k(s, a_k, \tau^*)\, \phi(s)\, ds = S_k$, as absent commuting technology the effective labor supply puts an upward pressure on the price of housing consumption. However, what is new is that location choices now also depend on redistributive taxation, τ^*, which serves to lower the attractiveness of productive locations by rendering net income less dependent on wage income and, hence, location. Interestingly, this latter feature also makes the ratio skill-dependent, even though skills are perfect substitutes in production and there are no

differences in returns to skills across cities. By making total income less dependent on wage income, redistributive taxation primarily serves to discourage low-skilled agents to locate in locations with high productive amenities, as they no longer need to relocate to benefit from its productivty. For similar reasons, as high-skilled agents see part of their productivity premium confiscated by the tax system, when taxes rise, they experience an even stronger incentive to locate in productive places to maintain their spending power. To better see this, note that setting $\tau^* = 0$ reverts equation (30A) to

$$\begin{aligned}\pi_l(s_n, 0) &= \frac{a_l^{\epsilon} s_n^{\epsilon}}{\int_{k=1}^{L} a_k^{\epsilon} s_n^{\epsilon} dk} \frac{\int_{k=1}^{L} a_k^{\epsilon(1-\mu)} S_k^{\epsilon(1-\mu)} dk}{a_l^{\epsilon(1-\mu)} S_l^{\epsilon(1-\mu)}} \\ &= \frac{a_l^{\mu\epsilon}}{\int_{k=1}^{L} a_k^{\epsilon} dk} \frac{\int_{k=1}^{L} a_k^{\epsilon(1-\mu)} S_k^{\epsilon(1-\mu)} dk}{S_l^{\epsilon(1-\mu)}} \\ &= \frac{a_l^{\mu\epsilon} S_l^{(\mu-1)\epsilon}}{\int_{k=1}^{L} a_k^{\mu\epsilon} S_k^{(\mu-1)\epsilon} dk} = \pi_l\end{aligned}$$

which no longer depends on skill and only reflects standard wage benefits and congestion costs. Similarly, in the case of full taxation, $\tau^* = 1$, location choices are given by

$$\begin{aligned}\pi_l(s_n, 1) &= \frac{\left(\frac{\psi-1}{\psi}\frac{Y}{N}\right)^{\epsilon}}{\int_{k=1}^{L}\left(\frac{\psi-1}{\psi}\frac{Y}{N}\right)^{\epsilon} dk} \frac{\int_{k=1}^{L}\left(\frac{\psi-1}{\psi}\frac{Y}{N}N_k\right)^{\epsilon(1-\mu)} dk}{\left(\frac{\psi-1}{\psi}\frac{Y}{N}N_l\right)^{\epsilon(1-\mu)}} \\ &= \frac{\left(\frac{\psi-1}{\psi}\frac{Y}{N}\right)^{\epsilon}}{\left(\frac{\psi-1}{\psi}\frac{Y}{N}\right)^{\epsilon}\int_{k=1}^{L} dk} \frac{\left(\frac{\psi-1}{\psi}\frac{Y}{N}\right)^{\epsilon(1-\mu)}\int_{k=1}^{L} N_k^{\epsilon(1-\mu)} dk}{\left(\frac{\psi-1}{\psi}\frac{Y}{N}N_l\right)^{\epsilon(1-\mu)}} \\ &= \frac{1}{L}\frac{\int_{k=1}^{L} N_k^{\epsilon(1-\mu)} dk}{N_l^{\epsilon(1-\mu)}} = \pi\end{aligned}$$

which only depend on agglomeration costs, here captured by the number of inhabitants N_l, such that the probability of choosing location l declines in city population, N_l, yielding a uniform spatial population distribution in equilibrium, $\pi_l(1) = 1/L \,\forall l \in L$.

B.1.2 Proposition 1

The gross income Gini coefficient, $G(w)$, can be computed as

$$\begin{aligned}G(w) &= \frac{\int_{s_1=1}^{\infty}\int_{s_2=1}^{\infty}\phi(s_1)\phi(s_2)\int_{l_1=1}^{L}\int_{l_2}^{L}|w_{l_1}(s_1) - w_{l_2}(s_2)|\, dl_1 dl_2 ds_1 ds_2}{\frac{2}{N}\int_{l=1}^{L}\int_{s=1}^{\infty}\pi_l(s,\tau^*) w_l(s)\phi(s)\, ds dl} \\ &= \frac{N\int_{s_1=1}^{\infty}\int_{s_2=1}^{\infty}\phi(s_1)\phi(s_2)\int_{l_1=1}^{L}\int_{l_2}^{L}|w_{l_1}(s_1) - w_{l_2}(s_2)|\, dl_1 dl_2 ds_1 ds_2}{2Y}\end{aligned} \tag{31A}$$

while, denoting the average wage by $\bar{w} = \frac{Y}{N}$, the net income Gini coefficient, $G(y)$, equals

$$G(y) = \frac{\int_{s_1=1}^{\infty}\int_{s_2=1}^{\infty}\phi(s_1)\phi(s_2)\int_{l_1=1}^{L}\int_{l_2}^{L}|y_{l_1}(s_1) - y_{l_2}(s_2)|\, dl_1 dl_2 ds_1 ds_2}{\frac{2}{N}\int_{l=1}^{L}\int_{s=1}^{\infty}\pi_l(s,\tau^*) y_l(s)\phi(s)\, ds dl}$$

$$
\begin{aligned}
&= \left[N \int_{s_1=1}^{\infty} \int_{s_2=1}^{\infty} \phi(s_1)\,\phi(s_2) \int_{l_1=1}^{L} \int_{l_2}^{L} \left| (1-\tau^*)\, w_{l_1}(s_1) + \left(\tau - \frac{\tau^{\psi}}{\psi}\right) \bar{w} \right. \right. \\
&\left. \left. - (1-\tau^*)\, w_{l_2}(s_2) - \left(\tau - \frac{\tau^{\psi}}{\psi}\right) \bar{w} \right| dl_1 dl_2 ds_1 ds_2 \right] \\
&\left(2 \int_{l=1}^{L} \int_{s=1}^{\infty} \pi_l(s, \tau^*)\,(1-\tau^*)\, w_l(s) + \left(\tau - \frac{\tau^{\psi}}{\psi}\right) \bar{w} \phi(s)\, ds dl \right)^{-1} \\
&= \frac{N \int_{s_1=1}^{\infty} \int_{s_2=1}^{\infty} \phi(s_1)\,\phi(s_2) \int_{l_1=1}^{L} \int_{l_2}^{L} \left| (1-\tau^*)\, w_{l_1}(s_1) - (1-\tau^*)\, w_{l_2}(s_2) \right| dl_1 dl_2 ds_1 ds_2}{2 \int_{l=1}^{L} \int_{s=1}^{\infty} \pi_l(s, \tau^*)\,(1-\tau^*)\, w_l(s)\, ds dl + 2 \left(\tau - \frac{\tau^{\psi}}{\psi}\right) Y} \\
&= \frac{N (1-\tau^*) \int_{s_1=1}^{\infty} \int_{s_2=1}^{\infty} \phi(s_1)\,\phi(s_2) \int_{l_1=1}^{L} \int_{l_2}^{L} \left| w_{l_1}(s_1) - w_{l_2}(s_2) \right| dl_1 dl_2 ds_1 ds_2}{2 (1-\tau^*) Y + 2 \left(\tau - \frac{\tau^{\psi}}{\psi}\right) Y} \\
&= \frac{N (1-\tau^*) \int_{s_1=1}^{\infty} \int_{s_2=1}^{\infty} \phi(s_1)\,\phi(s_2) \int_{l_1=1}^{L} \int_{l_2}^{L} \left| w_{l_1}(s_1) - w_{l_2}(s_2) \right| dl_1 dl_2 ds_1 ds_2}{\left(1 - \frac{\tau^{\psi}}{\psi}\right) 2Y}
\end{aligned}
$$

Consequently, we have that

$$
\begin{aligned}
G(y) &< G(w) \\
\frac{1-\tau^*}{1-\frac{\tau^{\psi}}{\psi}} &< 1 \\
1-\tau^* &< 1 - \frac{\tau^{\psi}}{\psi} \\
\frac{\tau^{\psi}}{\psi} &< t \\
\tau^{\psi-1} &< \psi \\
\tau^* &< \psi^{\frac{1}{\psi-1}}
\end{aligned}
$$

As $0 \leq \tau \leq 1$ and $\psi > 1$ by assumption, this latter inequality is always satisfied.

B.1.3 Proposition 2

Denote the average productive amenity per effective unit of labor by $\bar{a} = \frac{Y}{S}$, and the average human capital endowment by $\bar{s} = \frac{S}{N}$. Further expressing the human capital endowment of agent n as a fraction of the average endowment, $\bar{s} = f_n s_n$ allows to simplify the expression for location choice probabilities in equation (30A) to

$$\pi_l\left(s_n,\tau^*\right)=\overbrace{\underbrace{\frac{\left(\left(1-\tau^*\right)a_l+\left(\tau^*-\frac{\tau^{*\psi}}{\psi}\right)\bar{a}f_n\right)^{\epsilon}}{\int_{k=1}^{L}\left(\left(1-\tau^*\right)a_k+\left(\tau^*-\frac{\tau^{*\psi}}{\psi}\right)\bar{a}f_n\right)^{\epsilon}dk}}_{\text{common across skill types}}\frac{\int_{k=1}^{L}\left(\left(1-\tau^*\right)a_kS_k+\left(\tau^*-\frac{\tau^{*\psi}}{\psi}\right)\frac{Y}{N}N_k\right)^{\epsilon(1-\mu)}dk}{\left(\left(1-\tau^*\right)a_lS_l+\left(\tau^*-\frac{\tau^{*\psi}}{\psi}\right)\frac{Y}{N}N_l\right)^{\epsilon(1-\mu)}}}^{\text{Skill dependent}} \tag{32A}$$

Note that the second fraction does not depend on the human capital endowment, s_n, so the skill-dependency of location choices is restricted to the first fraction. It is easy to see that as long as $\tau \neq 0$ and $\tau \neq 1$, an agent's skill deficit relative to the average skill, f_n, reduces the weight on each location's relative productive amenity when making location choices: for extremely low-skill agents with $f_n \to \infty$, this fraction no longer depends on productivity differentials between locations and location choices are only driven by local differences in housing market pressures captured in the second term. Hence, for any two agents where $s_1 > s_2$, implying $f_1 < f_2$, the former will put more weight on local productive amenities when making location, choices such that if $a_1 > a_2$, $\pi_1\left(s_1,\tau^*\right) > \pi_1\left(s_2,\tau^*\right)$.

The simplified numerical example in figure A21a relies on a particular numerical application to further illustrate that, for any two agents with $s_1 > s_2$ and any two locations with $a_{l_1} > a_{l_2}$, $v_{n,l_1}\left(s_1\right) - v_{n,l_2}\left(s_1\right) > v_{n,l_1}\left(s_2\right) - v_{n,l_2}\left(s_2\right)$. Figure A21b shows how this implies that the location choice probabilities of high-skilled agents decline more slowly with taxation. Hence, denoting the most productive location as L, $s_1 > s_2 \Rightarrow \pi_L\left(s_1\right) > \pi_L\left(s_2\right)$ if $t \neq \{0,1\}$ and, more generally, there exists a threshold location, $\bar{l}$ in any productivity-ordered set of locations such that $\pi_l\left(s_1\right) > \pi_l\left(s_2\right)$ if $l > \bar{l}$ and vice versa.

Figure A21: **Skill heterogeneity in the tax elasticity of location choice**

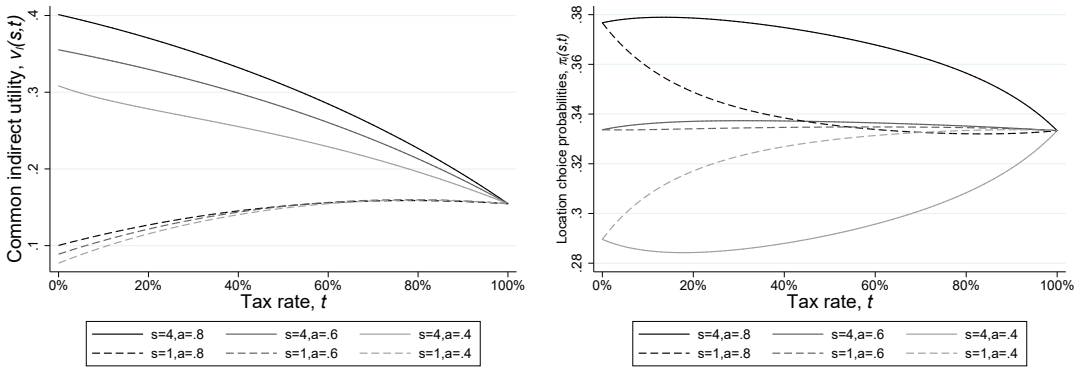

(a) Common indirect utility, $\tilde{v}_l\left(s,\tau\right)$ (b) Location choice probability, $\pi_l\left(s,\tau\right)$

Note: This figure shows how indirect utility computed from (17) and location choice probabilities computed from (18) evolve with the tax rate, τ, for a high- (full lines) and low-skilled (dashed lines) agent and for 3 locations, with darker shades for more productive locations, for the numerical example $\left(N, Y, \bar{H}, \epsilon_l, \psi, \mu, s_1, s_2, a_1, a_2, a_3, S_1, S_2, S_3, N_1, N_2, N_3,\right) = (3000, 4000, 1, 1, 2, .76, .8, .6, .4, 3000, 2000, 1000, 1000, 1000, 1000)$. For simplicity, S_l and N_l are exogenously fixed over the entire support of τ.

B.1.4 Proposition 3

Redistributive income taxation not only reduces total output by the tax distortion capturing adverse labor supply reactions, as parametrized in ψ, but also by discouraging labor mobility to productive locations, as determined by $\pi_l(\tau^*, s)$. This second 'spatial cost of taxation' follows from the fact that a purely redistributive income tax reduces the extent to which total incomes depend on labor income. To see this more formally, note that the total cost of public funding for a tax increase from τ_1 to τ_2, $C(\tau_1, \tau_2)$, can be written as

$$C(\tau_1, \tau_2) = \underbrace{\frac{\tau_2^{\psi}}{\psi} Y(\tau_2) - \frac{\tau_1^{\psi}}{\psi} Y(\tau_1)}_{\text{increase in tax distortion}} + \underbrace{Y(\tau_1) - Y(\tau_2)}_{\text{reduction in tax base}} \tag{33A}$$

where $Y(\tau_1)$ denotes (endogenous) equilibrium economy-wide income under tax τ_1, the first term captures the increase in the tax distortion and the second term captures the spatial cost of taxation, or the reduction in the tax base through the fiscal effects on location decisions described in equation (30A). This can be further decomposed as

$$C(\tau_1, \tau_2) = \frac{\tau_2^{\psi}}{\psi} Y(\tau_2) - \frac{\tau_1^{\psi}}{\psi} Y(\tau_1) + Y(\tau_2) - Y(\tau_1) + \frac{\tau_2^{\psi}}{\psi} Y(\tau_1) - \frac{\tau_2^{\psi}}{\psi} Y(\tau_2) \tag{34A}$$

Slightly rewriting this expression yields equation (26), which implies that the indirect spatial cost of taxation exceeds the direct distortion cost if

$$\begin{aligned}
\frac{\tau_2^{\psi}}{\psi}\left(\frac{Y(\tau_2)}{Y(\tau_1)} - 1\right) + 1 - \frac{Y(\tau_2)}{Y(\tau_1)} &> \frac{\tau_2^{\psi}}{\psi} - \frac{\tau_1^{\psi}}{\psi} \\
\left(1 - \frac{Y(\tau_2)}{Y(\tau_1)}\right)\left(1 - \frac{\tau_2^{\psi}}{\psi}\right) &> \frac{\tau_2^{\psi} - \tau_1^{\psi}}{\psi} \\
\left(\psi - \tau_2^{\psi}\right)\left(1 - \frac{Y(\tau_2)}{Y(\tau_1)}\right) &> \tau_2^{\psi} - \tau_1^{\psi} \\
1 - \frac{Y(\tau_2)}{Y(\tau_1)} &> \frac{\tau_2^{\psi} - \tau_1^{\psi}}{\psi - \tau_2^{\psi}} \\
\frac{Y(\tau_2)}{Y(\tau_1)} &< \frac{\psi - 2\tau_2^{\psi} - \tau_1^{\psi}}{1 - \tau_2^{\psi}}
\end{aligned} \tag{35A}$$

Figure A22 illustrates a particular numerical example an finds that the spatial costs of taxation dominate the non-spatial distortion costs for low and intermediary tax rates. This suggests that the spatial costs of taxation may not be trivial in real-world applications.

B.1.5 Proposition 4

To see how divergent development affects the overall and spatial distribution of fiscal preferences, denote the first two moments of the overall distribution of the most preferred tax rates of each agent within time period t, $\bar{\tau}_t^{*N}(\alpha, \tau_t^*)$ and $\sigma_t^{\bar{\tau}^{*N}}(\alpha, \tau_t^*)$, by

Figure A22: **The cost of taxation**

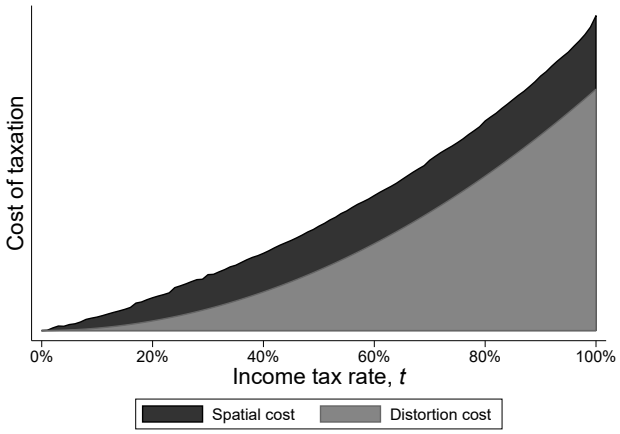

Note: This figure plots the output foregone for every tax rate on the horizontal axis and decomposes it into the spatial and distortion costs in equation (26), for the numerical example $(L, N, a_l, \alpha, \epsilon, \psi) = \left(30, 2000, \frac{l}{L}, 2, 3.3, 2\right)$.

$$\begin{aligned}\bar{\tau}_t^{*N}\left(\alpha, \tau_t^*\right) &= \int_{s=1}^{\infty}\int_{l=1}^{L} \pi_{l,t}\left(s, \tau_t^*\right) \tau_{l,t}\left(s, \tau_t^*\right) \phi\left(s\right) dlds \\ \sigma_t^{\bar{\tau}^{*N}}\left(\alpha, \tau_t^*\right) &= \int_{s=1}^{\infty}\int_{l=1}^{L} \pi_{l,t}\left(s, \tau_t^*\right) \left(\tau_{l,t}\left(s, \tau_t^*\right) - \bar{\tau}_t^{*N}\left(\alpha, \tau_t^*\right)\right)^2 \phi\left(s\right) dlds\end{aligned} \tag{36A}$$

with $\pi_{l,t}\left(s, \tau_t^*\right)$ and $\tau_{n,l,t}^*\left(s, \tau_t^*\right)$ as defined in equation (32A) and (20) at time t. Note that these distributions depend on the equilibrium tax rate, τ_t^*, as this in turn determines the equilibrium distribution of (effective) labor, N^* and S^*, across locations in the short run.

While equation (36A) captures the total amount of fiscal preference heterogeneity in the electorate, to also analyze spatial differences in fiscal preferences, respectively denote the expected tax preference of the local electorate in each location, l, and its variance by

$$\begin{aligned}\bar{\tau}_{l,t}^{*L}\left(\alpha, \tau_t^*\right) &= \int_{s=1}^{\infty} \pi_l\left(s, \tau_t^*\right) \tau_l\left(s, \tau_t^*\right) \phi\left(s\right) ds \\ \sigma_t^{\bar{\tau}^{*L}}\left(\alpha, \tau_t^*\right) &= \int_{l=1}^{L} \left(\bar{\tau}_{l,t}^{*L}\left(\alpha, \tau_t^*\right) - \bar{\tau}_t^{*L}\left(\alpha, \tau_t^*\right)\right)^2 dl\end{aligned} \tag{37A}$$

with $\bar{\tau}_t^{*L}\left(\alpha, \tau_t^*\right) = \frac{1}{L}\int_{l=1}^{L} \bar{\tau}_{l,t}^{*L}\left(\alpha, \tau_t^*\right) dl$ the average tax rate across locations.

Note that $\sigma_t^{\bar{\tau}^{*N}}\left(\alpha, \tau_t^*\right)$ and $\sigma_t^{\bar{\tau}^{*L}}\left(\alpha, \tau_t^*\right)$ capture the variance in individual and local fiscal preferences within period t. If unequal development increases spatial variation in fiscal preferences, $\sigma^{\bar{\tau}^{*L}}$, it makes it more difficult to propose a tax rate that satisfies inhabitants in every location. Such increasing spatial variation does not necessarily translate to heightened overall preference heterogeneity, $\sigma^{\bar{\tau}^{*N}}$, as the latter also depends on labor mobility.[24] Divergent development may simultaneously increase interregional fiscal disagreement ánd labor mobility to leading regions, and if the latter force is sufficiently strong, may serve to homogenize overall fiscal preferences despite growing spatial disagreements.

[24] Labor mobility is primarily determined by the Fréchet parameter of location choices, ϵ, the local housing supply, H_l, and residential amenities, ϵ_l: it is decreasing in the former and increasing in the latter two.

Proposition B.1.3 already established that divergent development stimulates labor mobility to the fastest growing locations, and especially for high-skilled agents. To additionally determine how divergent development affects fiscal preferences, $\tau^*_{l,n}(s_n, \tau^*)$, note that substituting for equilibrium consumption, $c^*_l(s_n, \tau^*)$ and $h^*_l(s_n, \tau^*)$, from equation (16) in equation (15) allows to write the conditional indirect utility of agent n with human capital endowment s_n in location l under equilibrium redistributive tax τ^* as

$$v_{l,n}(s_n, \tau^*) = \xi_{l,n}\epsilon_l\mu^\mu\bar{H}^{1-\mu}\frac{(1-\tau^*)a_l s_n + \left(\tau^* - \frac{\tau^{*\psi}}{\psi}\right)\frac{Y}{N}}{\left((1-\tau^*)a_l S_l + \left(\tau - \frac{\tau^\psi}{\psi}\right)\frac{Y}{N}N_l\right)^{1-\mu}} \tag{38A}$$

To simplify, rewrite $Y = \sum_{l=1}^{L} a_l S_l = S\sum_{l=1}^{L} a_l \frac{S_l}{S} = S\bar{a}$ with $\bar{a} = \sum_{l=1}^{L} a_l \frac{S_l}{S} = \frac{Y}{S}$ the average productivity of effective labor,

$$v_{l,n}(s_n, \tau^*) = \xi_{l,n}\epsilon_l\mu^\mu\bar{H}^{1-\mu}\frac{(1-\tau^*)a_l s_n + \left(\tau^* - \frac{\tau^{*\psi}}{\psi}\right)\bar{a}\frac{S}{N}}{\left((1-\tau^*)a_l S_l + \left(\tau - \frac{\tau^\psi}{\psi}\right)\bar{a}\frac{S}{N}N_l\right)^{1-\mu}} \tag{39A}$$

Subsequently, rewrite $\frac{S}{N} = \bar{s} = f_n s_n$, with $\bar{s}$ the average human capital endowment in the economy, $\frac{\alpha}{\alpha-1}$, and denote by f_n the agent-specific skill multiplier that captures how many times this average skill endowment exceeds the agent's endowment. Similarly, denote by f_l the location-specific productivity multiplier that expresses the productivity of a location relative to the average productivity of effective labor $\bar{a} = f_l a_l$. This yields

$$v_{l,n}(s_n, \tau^*) = \xi_{l,n}\epsilon_l\mu^\mu\bar{H}^{1-\mu}\frac{(1-\tau^*)a_l s_n + \left(\tau^* - \frac{\tau^{*\psi}}{\psi}\right)f_l a_l f_n s_n}{\left((1-\tau^*)a_l S_l + \left(\tau - \frac{\tau^\psi}{\psi}\right)f_l a_l f_n s_n N_l\right)^{1-\mu}} \tag{40A}$$

Further rewriting $S_l = N\int_{s\in1}^{\infty}\pi_l(s,\tau^*)s\phi(s)\,ds = N_l\bar{s}_l = N_l f_{l,n}s_n$, with $\bar{s}_l$ the local average human capital endowment, $\bar{s}_l = \int_{s\in1}^{\infty}\pi_l(s,\tau^*)s\phi(s)\,ds$, and $f_{l,n}$ the location- and agent-specific multiplier that reflects how many times an agent's skill endowment exceeds the average *local* endowment, $\bar{s}_l$, allows to further simplify this expression to

$$\begin{aligned} v_{l,n}(s_n, \tau^*) &= \xi_{l,n}\epsilon_l\mu^\mu\bar{H}^{1-\mu}\frac{(1-\tau^*)a_l s_n + \left(\tau^* - \frac{\tau^{*\psi}}{\psi}\right)f_l a_l f_n s_n}{\left((1-\tau^*)a_l N_l f_{l,n} s_n + \left(\tau - \frac{\tau^\psi}{\psi}\right)f_l a_l f_n s_n N_l\right)^{1-\mu}} \\ &= \xi_{l,n}\epsilon_l\mu^\mu\bar{H}^{1-\mu}\frac{a_l s_n f_n\left[(1-\tau^*)f_n^{-1} + \left(\tau^* - \frac{\tau^{*\psi}}{\psi}\right)f_l\right]}{\left(a_l s_n N_l f_n\left[(1-\tau^*)f_{l,n}f_n^{-1} + \left(\tau - \frac{\tau^\psi}{\psi}\right)f_l\right]\right)^{1-\mu}} \end{aligned} \tag{41A}$$

$$= \frac{\xi_{l,n}\epsilon_l \mu^\mu \bar{H}^{1-\mu} a_l^\mu s_n^\mu f_n^\mu}{N_l^{1-\mu}} \frac{(1-\tau^*) f_n^{-1} + \left(\tau^* - \frac{\tau^{*\psi}}{\psi}\right) f_l}{\left((1-\tau^*) f_{l,n} f_n^{-1} + \left(\tau - \frac{\tau^\psi}{\psi}\right) f_l\right)^{1-\mu}}$$

$$= \frac{\xi_{l,n}\epsilon_l \mu^\mu \bar{H}^{1-\mu} a_l^\mu \bar{s}}{N_l^{1-\mu}} \frac{(1-\tau^*) \frac{s_n}{\bar{s}} + \left(\tau^* - \frac{\tau^{*\psi}}{\psi}\right) f_l}{\left((1-\tau^*) \frac{\bar{s}_l}{\bar{s}} + \left(\tau - \frac{\tau^\psi}{\psi}\right) f_l\right)^{1-\mu}}$$

The numerator of the second fraction in equation (41A) captures the marginal utility of taxation on spendable income, which depends positively on a location's productivity deficit with the average productive amenity, $f_l = \bar{a}/a_l$. It reflects that growing productivity differentials with the rest of the economy increase the magnitude of redistributive transfers relative to local wages and, hence, the gain in purchasing power for a given increase in the redistributive tax, τ. With housing consumption, $\mu < 1$, this effect may be partially compensated by the fact that the marginal utility of taxation also depends positively on a location's relative productivity deficit in the denominator. This reflects that any tax increase's positive effect on local purchasing power in the numerator is partially offset by rising housing prices in the denominator, due to increasing purchasing power in the housing market. Intuitively, any local purchasing power increase through redistributive taxation is partially siphoned to landlords in the form of elevated rents.

The assumption that fiscal choices are made after location choices in figure 13 implies that fiscal preferences only depend on this second fraction, as the first remains constant within locations. Hence divergent development and labor mobility solely affect fiscal preferences through their effects on relative underdevelopment, f_l, and expected local human capital endowments, $\bar{s}_l$. While the complicated form of equation (41A) prevents a tractable derivation of their effects on fiscal preference heterogeneity, figure A23 highlights some implications that help understand why the direct effect of divergent development is to increase heterogeneity, which tends to be compensated by the labor mobility it triggers.

Figure A23a first illustrates the relation between relative underdevelopment and individually preferred tax rates. The assumption of fully redistributive taxation implies that agents with skill endowments above $\bar{s} f_l$ prefer zero tax rates, as they are net contributors to the tax system. This skill threshold declines in local productivity, a_l, implying that a larger fraction of inhabitants in leading locations will share a preference for zero tax rates, to avoid paying transfers to lagging locations. The assumption of convex tax distortion costs, ψ, implies that preferred tax rates increase concavely in relative underdevelopment, f_l, for agents with skill endowments below this threshold. Hence, all else equal, rising underdevelopment tends to homogenize the fiscal preferences of agents with positive tax preferences as agents with lower tax preferences experience more pronounced increases in their preferred tax rates. As the expected local human capital endowment reflects aggregate housing purchasing power in each location, the willingness to pay taxes increases in

Figure A23: **Local fiscal preferences and relative underdevelopment**

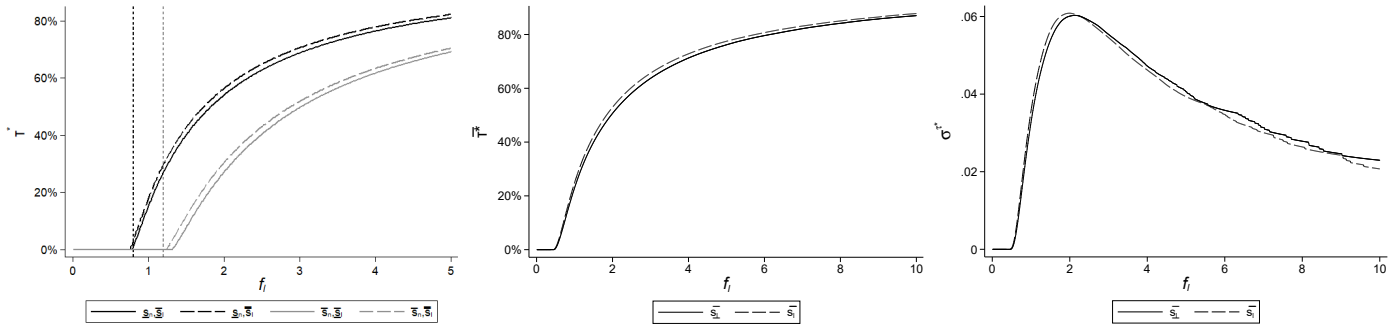

(a) Individual tax preferences, $\tau^*_{n,l}$ (b) Expected tax preferences, $\bar{\tau}^*_l$ (c) Variance in tax preferences, $\sigma^{\bar{\tau}^*_l}$

Note: This figure shows the relation between fiscal preferences and relative underdevelopment, f_l, in equation 41A as computed from the numerical example $(\mu, \psi, \underline{s_n}, \bar{s_n}, \bar{s}, \underline{\bar{s}_l}, \bar{\bar{s}}_l, \alpha) = (.8, 1.8, 1.6, 2.4, 2, 1.8, 2.2, 2)$. Figure A23a shows the most preferred tax rates for a low (black) and high (grey) skilled agent when expected local skill is low (full lines) or high (dashed lines). Figures A23b and A23c show the average preferred tax rate and its standard deviation when expected local human capital endowments are low (full lines) or high (dashed lines).

$\bar{s}_l$, as taxation serves to equalize spendable income and, hence, housing purchasing power.

Figures A23b and A23c trace the consequences for the distribution of fiscal preferences in each location. Mirroring the case of individual tax preferences, figure A23b clarifies that the mean of individually preferred tax rates rises concavely with relative underdevelopment, and does so at higher rates in locations with elevated human capital endowments. Figure A23c shows that the variance of local fiscal preferences exhibits a right tailed distribution across the support of relative underdevelopment. Starting from extreme overdevelopment, $f_l \approx 0$, inhabitants in locations that are sufficiently productive relative to the rest of the economy share homogeneous preferences for zero tax rates to avoid paying transfers to the rest of the country. Increasing relative underdevelopment then gradually increases the number of lower skilled agents who prefer positive tax rates, unambiguously increasing the variance of fiscal preferences. This goes on until relative underdevelopment reaches a threshold value beyond which further increases homogenize fiscal preferences, up to the logical endpoint of extreme underdevelopment where all agents prefer full taxation (not shown). As fiscal preferences increase concavely in relative underdevelopment, the initial rise in fiscal preference heterogeneity is steeper than its subsequent fall.

Figure A23 clarifies two things. First, productive locations exhibit *lower* fiscal preference heterogeneity as their disproportionate contribution to redistributive taxation reduces their willingness to pay taxes. Labor mobility towards leading locations thus serves to homogenize preferred tax rates by making them less right tailed. Second, an increase in the tax base, $\bar{a}$, and hence in relative underdevelopment, $f_l = \bar{a}/a_l$, leads to a more pronounced *ceteris paribus* increase in the variation of preferred tax rates in leading locations due to the concavity of preferred tax rates. Nevertheless, barring extremely underdeveloped locations that are likely sparsely populated, fiscal preference heterogeneity remains lower in leading locations even if the willingness to pay taxes increases with the tax base.

These results allow an assessment of how divergent development affects fiscal preference

heterogeneity and how this effect depends on labor mobility. First, its direct effect is to magnify the productivity differentials between locations, as the agglomerated technological innovation process described in equation (24) favors more productive locations. This unambiguously increases spatial fiscal preference heterogeneity, $\sigma_t^{\bar{\tau}^{*L}}(\alpha, \tau_t^*)$. Second, whether it also increases overall fiscal preference heterogeneity, $\sigma_t^{\bar{\tau}^{*N}}(\alpha, \tau_t^*)$, crucially depends on labor mobility. As labor mobility is exclusively oriented towards leading locations, see equation (32A), it serves to increase the average wage income in the economy and, hence, both the tax base, $\bar{a}$, and the willingness to pay taxes. This serves to increase fiscal preference heterogeneity within all locations in all but the most underdeveloped locations, see also figure A23c, raising overall fiscal preference heterogeneity by rendering the distribution of preferred tax rates more right tailed. On the other hand, mobility serves to reduce the preferred tax rates of agents relocating from lagging to leading locations. For agents preferring non-zero tax rates before relocation, this serves to homogenize tax preferences by rendering the distribution of preferred tax rates less right tailed. This homogenizing force depends on relative underdevelopment, f_l, since larger productivity differentials between locations lead to more homogeneous fiscal preferences for low tax rates in leading locations and trigger larger inflows into these leading locations for a given amount of labor mobility. As the former effect increases in human capital while the latter effect declines in it, and higher-skilled agents are more responsive to increasing labor mobility, this suggests an implicit mobility threshold within each time period below which divergent development increases overall fiscal preference heterogeneity.[25] This implies that, conditional on the increase in the variance of preferred taxes resulting from divergent development in the early period, there is an implicit threshold of labor mobility that compensates this increase and stabilizes it in the early period. If actual labor mobility is below this threshold, divergent development increases the variance of individually preferred tax rates.

Figure A24 contextualizes these findings by comparing the simulated results of section 6 for $t = 1$, when productive amenities are identical across locations, and $t = 200$, when technological innovations magnified local productivity differentials over 199 time periods, see also figure A33. The light grey line shows the initial distribution of preferred tax rates, τ_n^*, at $t = 1$. The dark grey line shows what the corresponding distribution would look like after 199 periods of divergent development if labor would have been immobile illustrating that divergent development increased the variance of preferred tax rates by increasing them in lagging regions and decreasing them in leading regions. The effects of labor mobility are decomposed in a tax base effect (dashed black line) and a relocation effect (full black line). The dashed line shows how preferred tax rates would change if agents remain located in their original locations of $t = 1$ but output would raise to the

[25] To see that increasing mobility can increase the variance of preferred tax rates, consider the case where an increase in labor mobility leads agent n to relocate from l_1 to l_2, with $a_{l_1} < a_{l_2}$ and $s_n > f_{l_1}\bar{s}$, such that the agent preferred a zero tax rate before relocating. While the resulting increase of the average wage with $\frac{s_n}{S}(a_{l_2} - a_{l_1})$, increases the willingness to pay taxes and, hence, the variation in fiscal preferences, the preferred tax rate of the agent remains at zero and there is no ofsetting homogenizing effect.

simulated level of $t = 200$, when location choices are made as described in equation (32A). Clearly, labor mobility further increases the willingness to pay taxes by increasing the tax base and render preferred tax rates more right tailed. Finally, the full black line shows the equilibrium distribution of preferred tax rates in $t = 200$, when agents make location choices as described in (32A). It confirms that relocation served to lower preferred tax rates and render the distribution of preferred tax rates less right-skewed.

Figure A24: **Decomposition of the fiscal effects of divergent development**

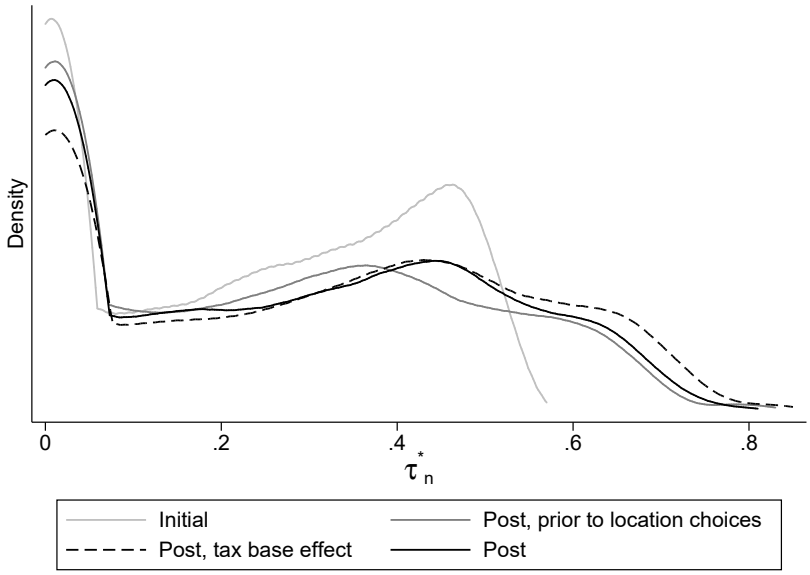

Note: This figure shows the distribution of preferred tax rates, computed from equation (41A) based on the baseline simulated results in periods $t = 1$ and $t = 200$ of section 6. The light grey line shows the equilibrium distribution of τ_n^* at $t = 1$. The dark grey line shows the distribution at $t = 200$ if labor would have been completely immobile and location choices are as made in $t = 1$. The dashed black line shows the distribution at $t = 200$ if labor would have been completely immobile but total output would equal the simulated output level when location choices are made based on equation (32A). The full black line shows the equilibrium distribution of τ_n^* at $t = 200$.

To further illustrate this, figure A25 exploits the fact that location choices of equation (30A), but not within-period utility of equation (20), depend on local housing supplies to analyze how increasing labor mobility affects the overall variation of fiscal preferences for a particular numerical example, largely calibrated as in table 7. To do so, it considers three possible economies with low, intermediate and high regional inequality, respectively corresponding to the following calibrations of local productivity: $a_l = \sqrt[20]{l/L}$; $a_l = \sqrt[2.5]{l/L}$; $a_l = \sqrt[1.25]{l/L}$. For each economy, the left panels of the figure show the mean individual tax rate along with a 95% confidence interval when labor mobility is low (light grey), intermediate (dark grey) or high (black), corresponding to the following calibrations of local housing supplies: $H_l = \left(a_l^1 / \sum_k^L a_l^1\right) L$; $H_l = \left(a_l^4 / \sum_k^L a_l^4\right) L$; $H_l = \left(a_l^5 / \sum_k^L a_l^5\right) L$. Note that while the housing supply is normalized to sum to $L\bar{H} = L$ in each scenario, it is increasingly allocated to productive locations to simulate the effects of increasing mobility.

Figure A25: **Local tax preferences when mobility increases**

Low regional inequality

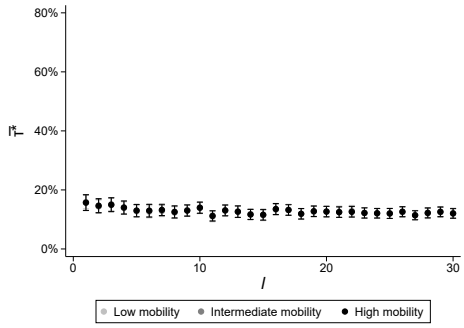

(a) Unweighted

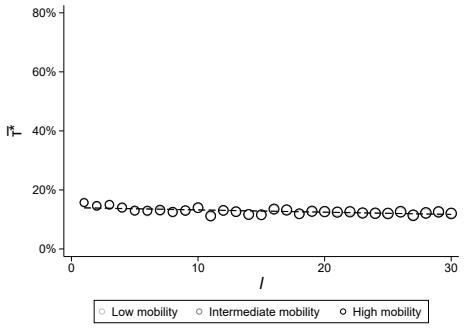

(b) Population-weighted

Intermediate regional inequality

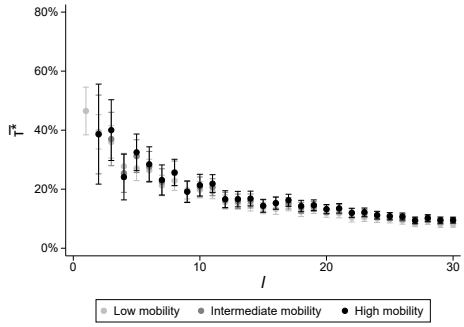

(c) Unweighted

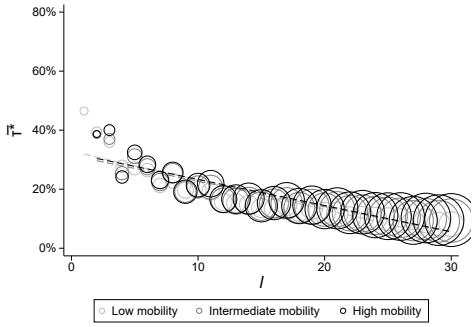

(d) Population-weighted

High regional inequality

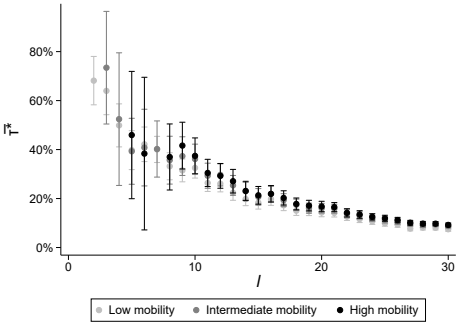

(e) Unweighted

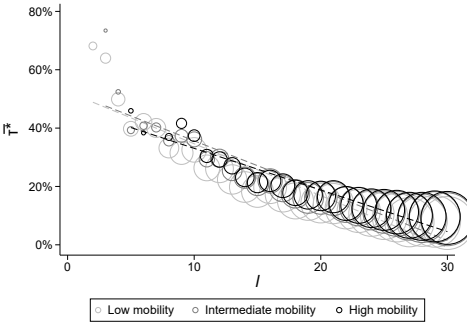

(f) Population-weighted

Note: This figure shows the relation between fiscal preferences and labor mobility for the numerical example $(L, N, T, \alpha, \epsilon, \mu, \bar{\mu}_a, \dot{\mu}_a, \sigma_a, \eta, \psi) = (30, 10000, 1.4, 3.3, .76, 1.002, .0001177, .03, 2, 1.4)$ for an economy with low regional inequality, $a_l = \sqrt[20]{l/L}$, intermediate inequality, $a_l = \sqrt[2.5]{l/L}$, and high inequality, $a_l = \sqrt[1.25]{l/L}$ when labor mobility is low (light grey), $H_l = \left(a_l^1 / \sum_k^L a_l^1\right) L$, intermediate (dark grey), $H_l = \left(a_l^4 / \sum_k^L a_l^4\right) L$ or high (black), $H_l = \left(a_l^5 / \sum_k^L a_l^5\right) L$. The left panels show the mean preferred tax along with a 95% confidence interval for each location; the right panels shows them scaled by population size, N_l, more populated locations having larger dots.

The figure confirms that when regional inequality is low and productivity differentials

between regions are small, both location choices and tax preferences remain similar when labor mobility increases as the minimal wage differentials between locations render workers unresponsive to increasing labor mobility and the minimal relocation that does occur does not noticeably affect the willingness to pay taxes. With intermediate productivity differentials, figure A25c shows that fiscal preferences become less variable and lower in productive locations while figure A25d confirms that increasing mobility now leads to stronger agglomeration in leading locations. Both forces homogenize fiscal preferences by concentrating the labor force in locations with relatively stable fiscal preferences for lower tax rates. With large productivity differentials, these results become even more pronounced. This suggests that labor mobility reduces the variation in fiscal preferences when productivity differentials rise, which is confirmed in figure A26.

Figure A26: **Divergent development and fiscal preference heterogeneity**

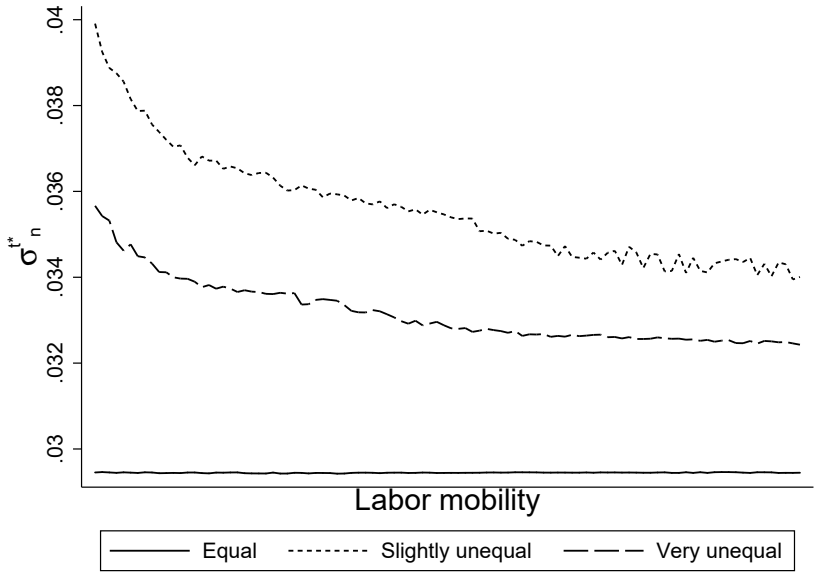

Note: This figure shows the variance of preferred tax rates of the three economies described in figure A25, when labor mobility is gradually increased from $H_l = \left(a_l^1 / \sum_k^L a_l^1\right) L$ to $H_l = \left(a_l^5 / \sum_k^L a_l^5\right) L$ on the horizontal axis.

Finally, note that in the case of equal development, with $\phi = 0$ in equation (24), labor becomes immobile as there are no longer any spatial wage differences that may trigger relocation decisions, implying that $\pi_l(s, \tau^*)$ remains constant over time. In addition, productivity growth equalizes across space and f_l also becomes time- and location-independent. As a result, under equal development, individual tax preferences remain stable over time. Moreover, if there are no productivity differences between locations in the initial period, overall and spatial variation in fiscal preferences are minimized as any slight productivity differential must increase the preference distance to the average tax rate for at least some agents of identical type, s_n, by introducing a wedge in their most preferred tax rates.

B.1.6 Proposition 5

Political choices are made after location choices, see section 4.8, so the spatial distribution of (effective) labor, N_l^* and S_l^*, and places of residence are fixed in the short run. As a result, the utility differential in equation (21) only depends on the discrepancy between the individually preferred tax rate in equation (20) and the one proposed by the mainstream party as defined in equation (19). Proposition 4 establishes that fiscal preferences remain stable over time with equal development, implying that political discontent also remains stable under constant tax decision rules. The same proposition also establishes that average tax preferences diverge between leading and lagging locations when economic development is unequally distributed across space, such that the expected preference distance to the tax rate proposed by the mainstream party must increase in at least one subset of locations. If labor mobility is perfectly inelastic to wages, e.g. $\epsilon = 0$, this is the only effect and divergent development necessarily increases aggregate political discontent, $\int_{s=1}^{S} \int_{l=1}^{L} \pi_{l,t}(s, \tau^*) D_{n,t}(s, \tau_t^*) \phi(s) ds$. In the opposite case of perfectly elastic mobility, full agglomeration in the most productive location implies productivity differentials no longer affect fiscal preferences and the model becomes isomorphic to one of equal development, with stable and minimal fiscal preference heterogeneity hence stable and minimal aggregate political discontent. This implies an implicit threshold for labor mobility below which divergent development increases aggregate political discontent.

B.1.7 Proposition 6

Slightly reformulating equation (19), recall that the mainstream party proposes the tax rate that is most preferred by the median tax voter:

$$\tau^*\left(L, N, \alpha, \epsilon, \mathbf{a}, \psi, \eta\right) = \arg\max_{\tau} \int_{l=1}^{L} \underbrace{\pi_l\left(s = \sqrt[\alpha]{2}, \tau\right)}_{\text{Electoral weight}} \tau_l^*\left(s = \sqrt[\alpha]{2}, \tau\right) dl \tag{42A}$$

The location choice probabilities described in equation (32A), $\pi_l(s, \tau)$, thus serve as importance weights for the expected indirect utility, $v_l(s, \tau)$, of the decisive agent with the median human capital endowment of $s = \sqrt[\alpha]{2}$. As divergent development stimulates labor mobility towards leading locations, see proposition 2, it follows that, with divergent development, the fiscal preferences of inhabitants of the most productive locations gain increasing political weight. Proposition 4 established that leading regions favor lower redistributive tax rates. Hence, under divergent development, the mainstream party proposes a redistributive income tax rate that increasingly falls short of the preferred tax rate in lagging regions. Proposition 5 clarifies that political discontent is entirely driven by the discrepancy between individually preferred and mainstream proposed tax rates. It follows that political discontent in this model predominantly arises in lagging regions.

B.1.8 Proposition 7

Proposition 5 explains that the direct effect of divergent development is to pull the preferred tax rates of locations apart by increasing wage differentials and that labor mobility mediates this process in two ways. First, as it is exclusively directed towards leading locations, it increases the willingness to pay taxes by increasing the average wage in the economy, especially in lagging locations. Second, it relocates the labor force from lagging to leading locations, lowering the preferred tax rates by increasing the wage income of relocated agents. The skill-biased nature of labor mobility, see proposition 3, implies that the former effect tends to be more pronounced than the latter, as those most likely to respond to labor mobility are also most likely to have low to zero preferred tax rates before relocation. Finally, proposition 6 clarifies that labor mobility lowers the extent to which the equilibrium tax rate is tailored to lagging locations due to their loss of electoral power.

As a result, labor mobility operates as an engine that on the one hand lowers the number of agents with very distinct tax preferences by relocation, yet increases the distinctiveness of fiscal preferences for those that remain in lagging locations by increasing their willingness to pay taxes. Its effect on radical vote shares crucially depends on whether it eliminates more alienated voters through relocation than it creates new alienated voters favoring higher taxes due to the increased tax base. Skill bias implies that increasing labor mobility may increase radical vote shares during an initial stage, by primarily relocating high-skilled laborers from lagging to leading locations and thereby contributing to a polarization of wages as well as fiscal preferences. As it gradually also serves to relocate lower-skilled agents from lagging to leading locations, which are most susceptible to political discontent as per proposition 6, it eventually contributes to lowering radical vote shares by reducing the number of agents with distinct fiscal preferences.

B.1.9 Proposition 8

One way to formalize the idea of increasing redistributive transfers in the model is to assume that the mainstream party does not target the median tax voter, but proposes the tax rate most preferred by a higher percentile $p > 50$. In that case, as long as radical parties remain a minority, equilibrium tax rates will be higher than those in the baseline scenario, which has two effects. First, the location choice probabilities in equation (32A) become less sensitive to wages and productive amenities, implying that lagging regions with low productive amenities will be better able to retain their population with divergent development, increasing fiscal preference heterogeneity by leading to nominal wage decompression. Second, by giving more electoral power to the poor, this shifts political discontent from lagging to leading regions. As leading regions are more densely populated, redistributive policies risk increasing the number of discontented voters.

B.1.10 Proposition 9

An adverse productivity of size Δ_s shocking hitting lagging regions, with $f_l < 1$, further increases their relative underdevelopment from $f_l = \frac{Y/S}{a_l}$ to $f_l = \frac{Y/S}{a_l+\Delta_s}$, leaving the productive amenities in leading regions intact. Equation (41A) implies that in the short run, when labor is immobile and hence the average local human capital endowment $\bar{s}_l$ remains fixed, this increases the preferred income tax. As lagging regions, and especially the least productive locations, typically favor tax rates that are well beyond those preferred by the median tax voter, see appendix B.1.6, adverse productivity shocks further magnify their preference distance to the implemented redistributive tax rate, τ^*. This unambiguously increases political discontent of the local electorates in lagging regions as defined in (21), which may shift some mainstream voters to abstain or vote for the radical party and similarly may shift some non-voters to radicalism. However, if the adverse shock is small relative to existing productivity differentials, the effect on radical vote shares will be small: those that already voted radical maintain their votes and the small increase in discontent will only lead a fraction of the other voters to shift to abstention and/or radicalism. In the longer run, the overall electoral effects of adverse productivity shocks are further reduced by labor mobility from affected to unaffected leading regions, reducing the pool of potential discontented voters, though local vote shares for radical parties remain elevated.

B.2 Model primitives

The model of section 2 essentially describes how agents that differ in human capital sort across locations, taking into account local productive amenities and housing costs as well as the redistributive decisions made by the government; and how this government, in turn, determines the optimal income tax rate, lump-sum redistribution and productive investments to maximize a social welfare function that captures the tax distortion and the spatial effects of fiscal policy. This section relies on particular numerical examples to further clarify the role played by the model's primitives, or the set of parameter values that determine the spatial equilibria, roughly in their order of appearance in section 2.

The particular numerical application used here calibrates an economy comprising $L = 30$ locations and $N = 2000$ agents. To generate the distribution of local productive amenities, a_l, I simply let $a_l = \frac{l}{L}$. This implies that local productivity linearly increases when moving from location $l = 1$ to location $l = 30$, as shown in figure A18 below.

Agents' human capital endowments are drawn from a Pareto distribution with shape parameter α. Figure A28 below demonstrates that the skill distribution becomes increasingly concentrated around the lower bound of 1 for higher choices of α, though the fat tails imply a small number of 'genius' agents endowed with extremely elevated skill levels.

Figure A27: **Economic geography**

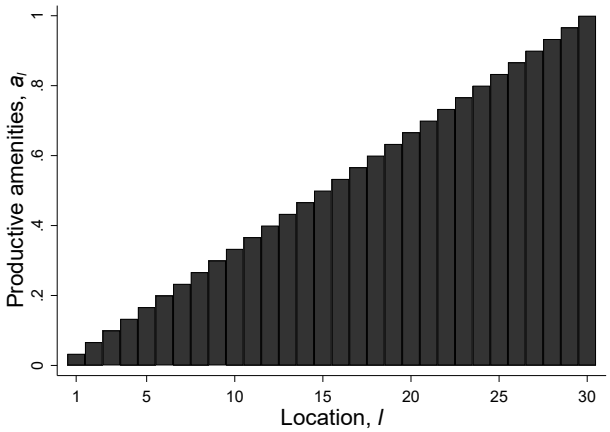

Note: This figure plots the calibrated productive amenities for each location, l.

Figure A28: **Skill distributions for different choices of α**

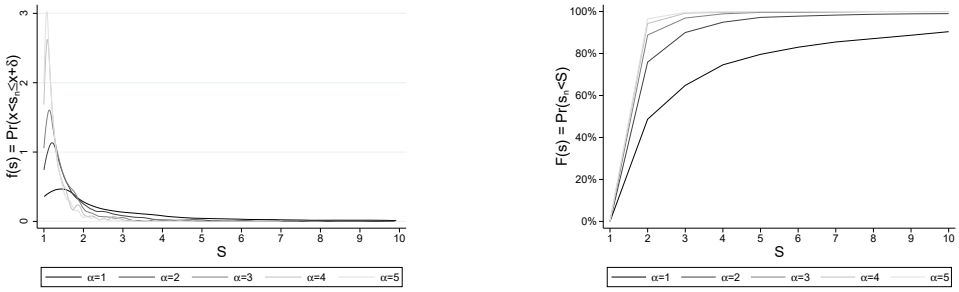

(a) Probability density function

(b) Cumulative distribution function

Note: This figure plots the probability density functions and cumulative distribution functions for s for different choices of the scale parameter for the Pareto distribution, α, based on 1000 draws and right-truncated at s=10.

Following Rosen (1979) and Roback (1982), agents' location preferences are drawn from a Fréchet distribution with shape parameter ϵ. Figure A29 shows that, similar to the Pareto distribution, draws for the Fréchet utility shifters cluster more tightly around their expected value of 1 the higher the value of the shape parameter, ϵ, though the fat right tail implies that some agents will have very strong idiosyncratic preferences for one particular location, see also figure A30a. As mentioned by Monte et al. (2018, p. 3886): *"Smaller (larger) values for the Fréchet shape parameter (ϵ) imply more (less) heterogeneity in preferences for residence-workplace pairs, which magnifies (diminishes) the effects of changes in commuting costs on welfare".*

Figure A29: **Location preference distributions for different choices of ϵ**

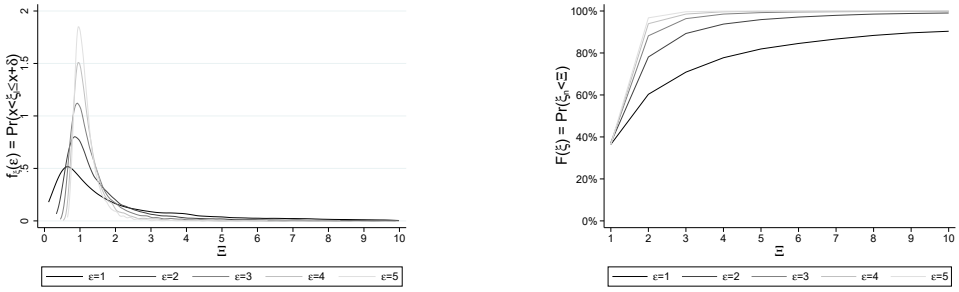

(a) Probability density function (b) Cumulative distribution function

Note: This figure plots the probability density and cumulative distribution functions for ξ for different choices of the scale parameter for the Fréchet distribution, ϵ, based on 1000 draws and right-truncated at ξ=10.

The latter implication is also clear in figures A30a, which shows the full distribution of $(N \times L)$ location preference parameters, $\xi_{l,n}$, for each location, $l \in L$ and agent $n \in N$, when ϵ is calibrated to equal 3.3 and α equals 2. Figure A30b then shows the set of location preference parameters for one particular agent, $n = 1$, which has a clear preference for location 10. Additionally, figure A30c shows that the vast majority of agents have maximum values for their location preferences below 2, such that living in their most preferred location maximally doubles their utility. However, a small number of agents experience very strong preferences for one particular location, with location preference parameter values implying that living in their most-preferred location increases their utility up to thirtyfold. This also becomes apparent in figure A30d, which shows that the ratio of the first-to-second highest location preference parameters usually hovers around 1 increases to as much as 30 for a small number extremely location-attached agents.

Figure A30: **Calibrated location preference distribution** ($\epsilon = 3.3$)

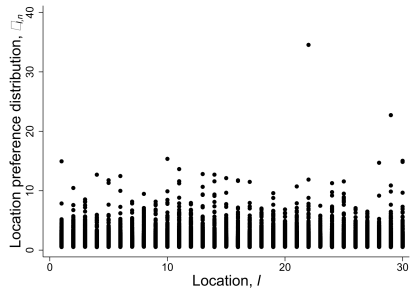

(a) For all agents & locations

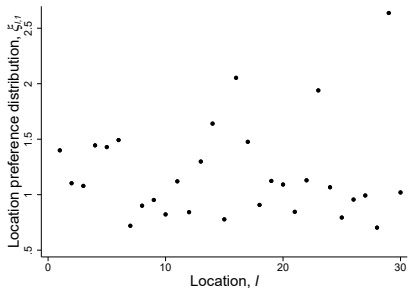

(b) For agent 1

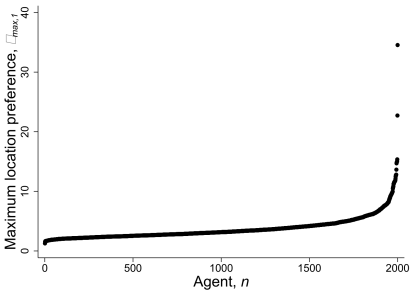

(c) For all agents

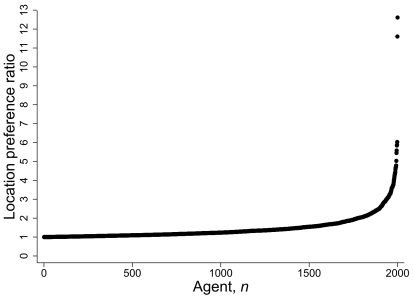

(d) Preference ratio for all agents

Note: Figure A30a plots the full distribution of location preference parameters for each agent n over each location l, $\epsilon_{l,n}$; figure A30b plots it for agent $n = 1$. Figure A30c plots the maximum parameter values for each agent n, $max\,(\epsilon_n)$. Figure A30d plots the ratio of the first-to-second highest location preference parameter for each agent n.

In introducing a redistributive government, I follow Bolton and Roland (1997) in assuming that income taxation results in deadweight losses such that if a government decides on a particular income tax, $0 \leq t \leq 1$, the total amount of revenues it receives equal $\left(\tau - \frac{\tau^{\psi}}{\psi}\right) Y$, with Y total wage income. Figure A31 clarifies that the higher the value of the tax distortion parameter, ψ, the less distorting taxation becomes as more tax revenues (grey lines) can be generated for a given tax rate, t, while the aggregate income loss due to tax distortions (red line) also decrease in ψ.

Figure A31: **Tax distortion for different choices of ψ**

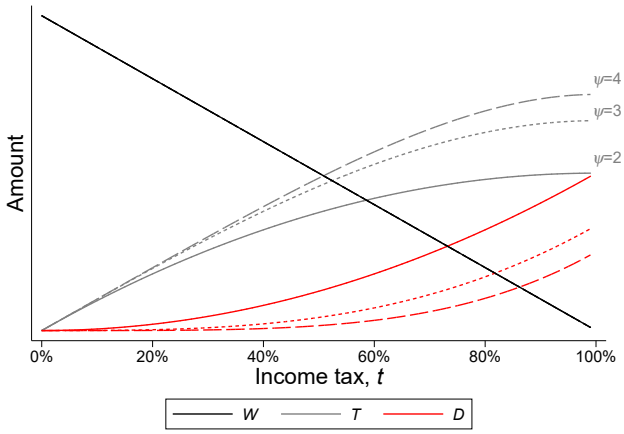

Note: This figure plots total net wage income, W, total tax revenues, T, and the amount of income lost to the tax distortion, D, for each possible tax rate, t, and for different possible choices of the tax distortion parameter, ψ.

B.3 Detailed model implications: baseline calibration

Figure A32 first summarizes the main features of the *ex post* spatial equilibrium for the numerical example discussed in section 6 and the baseline parameter values listed in table 8.[26] More specifically, the left panel shows the spatial equilibrium in the initial period, $t = 1$, while the right panel shows how this equilibrium evolves over time between $t = 1 \rightarrow 200$. As discussed in section 4, figure A32b reproduces the standard finding that divergent development allows more productive locations to attract more (effective) labor supplies and pay higher wages, but that the agglomeration costs of increasing rents, R_l, prevent them to attract all (effective) labor. Also note the increasing upward trend in average skill endowment productive locations, illustrating proposition 3 that redistributive taxation primarily discourages agents with lower human capital endowments to locate in productive locations. It also shows that expected utilities, u, equalize across space following the free mobility assumption and the lump-sum transfers from high to low earners. Crucially, this implies that location preference parameters, ξ, are higher on average in less productive locations to sufficiently compensate for the lower nominal wages and render agents of identical type indifferent between staying and relocating.

Additionally, figure A33 shows the evolution in local productive amenities as determined by the exogenous process of technological innovation described in equation (24), which confirms that it leads to growing productivity differentials between locations.

Turning to some more detailed implications, figure A34 shows the evolution in the nominal wage distribution. Figure A34a shows its typical right-tailed distribution where a small proportion of agents earn progressively higher wages, which is mainly a product of the assumption that human capital endowments are Pareto-distributed. Figure A34b

[26] In what follows, locations are always sorted from least (l=1) to most (l=30) productive. This implies that location index numbers may sometimes refer to different locations, when technological innovations reverses their order in the local productivity hierarchy.

Figure A32: ***Ex post* spatial equilibrium**

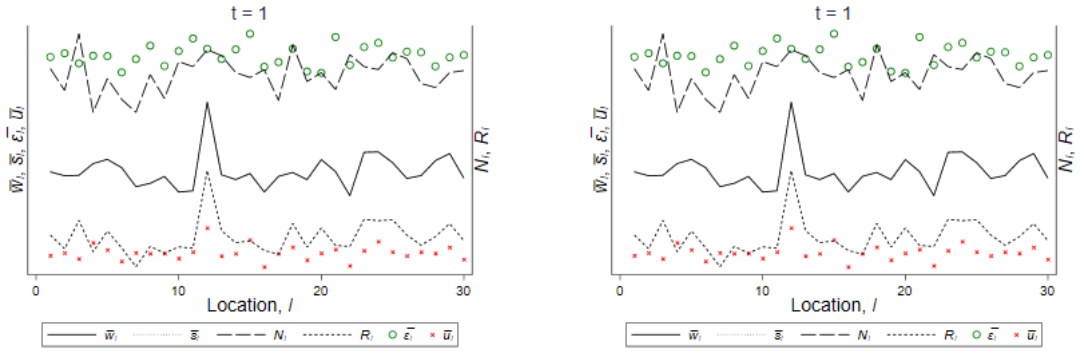

(a) At $t = 1$ (b) Between $t = 1$ and $t = 200$

Note: Figure A32a plots the *ex post* equilibrium average labor supply, N_l, local average human capital, $\bar{s}_l$, wages, $\bar{w}_l$, rents, r_l, location preference parameters, $\bar{\epsilon}_l$, and utility, $\bar{u}_l$, at each location l in $t = 1$ while dynamic figure A32b plots how this equilibrium evolves over time for every ten-year interval between $t = 1$ and $t = 200$.

Figure A33: **Technological innovations**

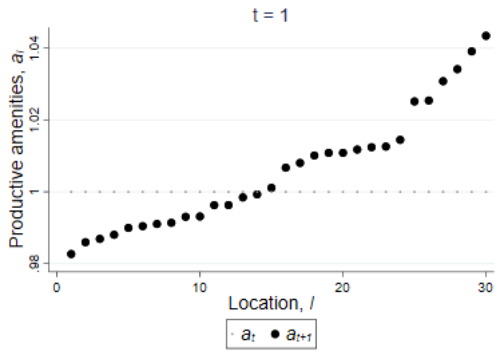

Note: This dynamic figure shows the impact of technological innovations on local productive amenities, as defined in equation (24). Locations are always sorted from least (l=1) to most (l=30) productive.

visualizes that the expected wages in each location diverge as a result of divergent development, which allows agents to earn progressively higher wages in leading locations (here depicted in light grey), and the finding that redistributive income taxation primarily stimulates labor mobility of higher skilled agents, see proposition 2.

Subsequently, figure A35 shows how the within-period individual fiscal preferences defined in equation (20) evolve over time. Figure A35a shows that the distribution of most preferred tax rates gradually becomes more right-tailed with divergent development, as agents in lagging regions are increasingly dependent on redistributive transfers to benefit from the economic growth gains primarily realized elsewhere. Figure A35b clarifies that preferred tax rates tend to decrease in human capital endowments, as high-skilled agents tend to be net contributors to the tax system irrespective of their location; and in local productive amenities, as increasing productivity differentials reduce the relative magnitude of redistributive transfers with respect to the local wages in productive locations. Hence, as suggested by proposition 4, there is a distinct spatial pattern in fiscal preferences, as inhabitants of low-productive locations increasingly prefer welfare state expansion while

Figure A34: **(Local) Equilibrium wages,** w

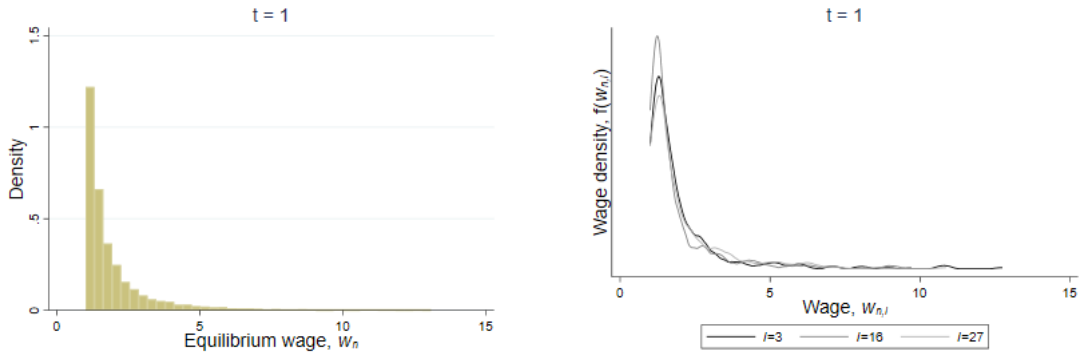

(a) Overall (b) In locations $l = 5, 1, 29$

Note: These dynamic figures show how the overall and spatial wage distributions evolve over every ten-year interval between $t = 1$ and $t = 200$. Local wage distributions are shown for the 5^{th}, 19^{th} and 29^{th} least productive locations.

inhabitants of productive locations tend to prefer the opposite of welfare state contraction.

Figure A35: **Fiscal preference distributions,** $\tau^*_{n,l^*_n}(s_n)$

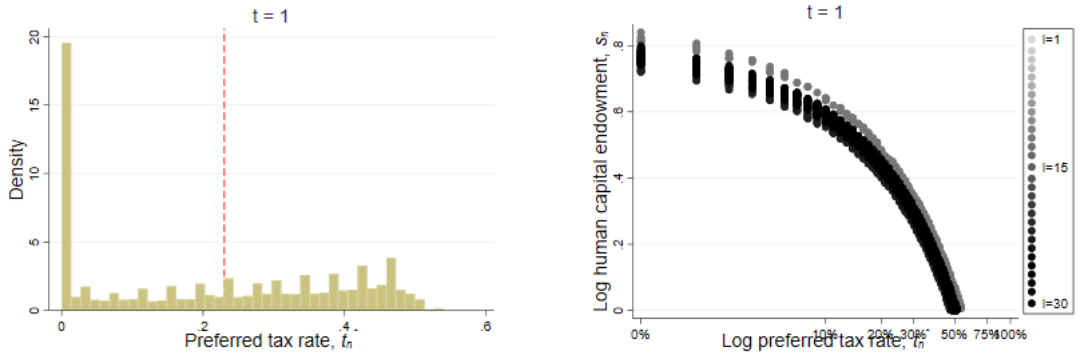

(a) Preferred income taxes (b) Tax preferences by skill type (log scale)

Note: These dynamic figures show the evolution of within-period distribution of the most-preferred tax rates of each agent, as defined in equation (20), for every ten-year interval between $t = 1$ and $t = 200$. Dynamic figure A35a shows the overall distribution of most preferred tax rates, with the most preferred tax rate of the median tax voter highlighted by the dashed red line, while figure A35b provides a breakdown by skill type and location, depicting the fiscal preferences of agents residing in more productive locations in darker shades of grey.

Finally, figure A36 traces the political consequences of these growing fiscal disagreements, showing growing spatial political frictions over optimal redistributive policy. Figure A36a first illustrates that high-skilled agents favoring zero tax rates tend to experience the largest relative utility losses from taxation (black dots), as they are net contributors of the social welfare state, while the more numerous low-skilled agents favoring tax increases also suffer growing relative utility losses of the redistributive tax being too low. Moreover, there is a separating equilibrium with far left susceptibility in low-productive locations versus far-right susceptibility in productive locations. This is partially a consequence of the fact high-skill agents share a preference of zero tax rates and labor mobility driving them to more productive locations with divergent development, and partially a consequence of the increasing wage gaps favoring productive locations. Figures A36b and A36c

nevertheless confirms that agents that are most alienated from government policy tend to live in unproductive locations, see proposition 6. Although the practical significance of these findings depends on the magnitude of λ, or the region of tolerance in equation (22), it is clear that political alienation increases with divergent development. This suggests that agglomeration economies may trigger negative political spillovers, as the excessive concentration of economic activity could fuel interregional redistributive conflicts that are easily exploited by separatist and populist movements. As political extremism may come with its own costs, for instance stemming from government instability and more difficult policy formulation, the political cost of agglomeration may well outweigh its benefits.

Figure A36: **Political discontent,** $D_{l,n}\left(s_n, l_n^*, \tau^*, \tau_n^*\right)$

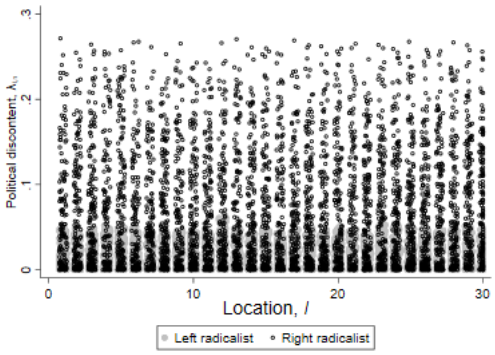

(a) Political discontent, $D_{l,n}\left(s_n, l_n^*, \tau^*, \tau_n^*\right)$

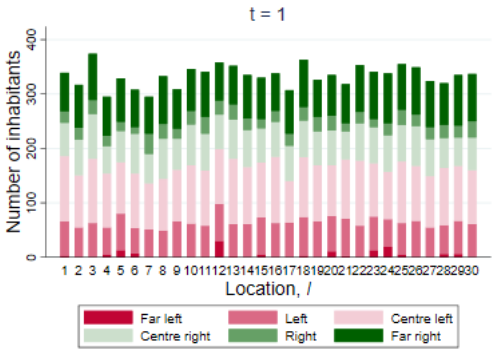

(b) Number of alienated voters.

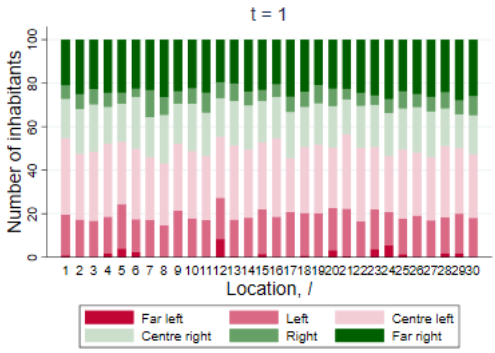

(c) Share of alienated voters.

Note: Figure A36b shows the evolution of the average political discontent defined in equation (21 experienced by agents in the baseline calibration summarized in table 7. Figure A36b)

Figure A37: 5-Arcminute grid overlay of Europe

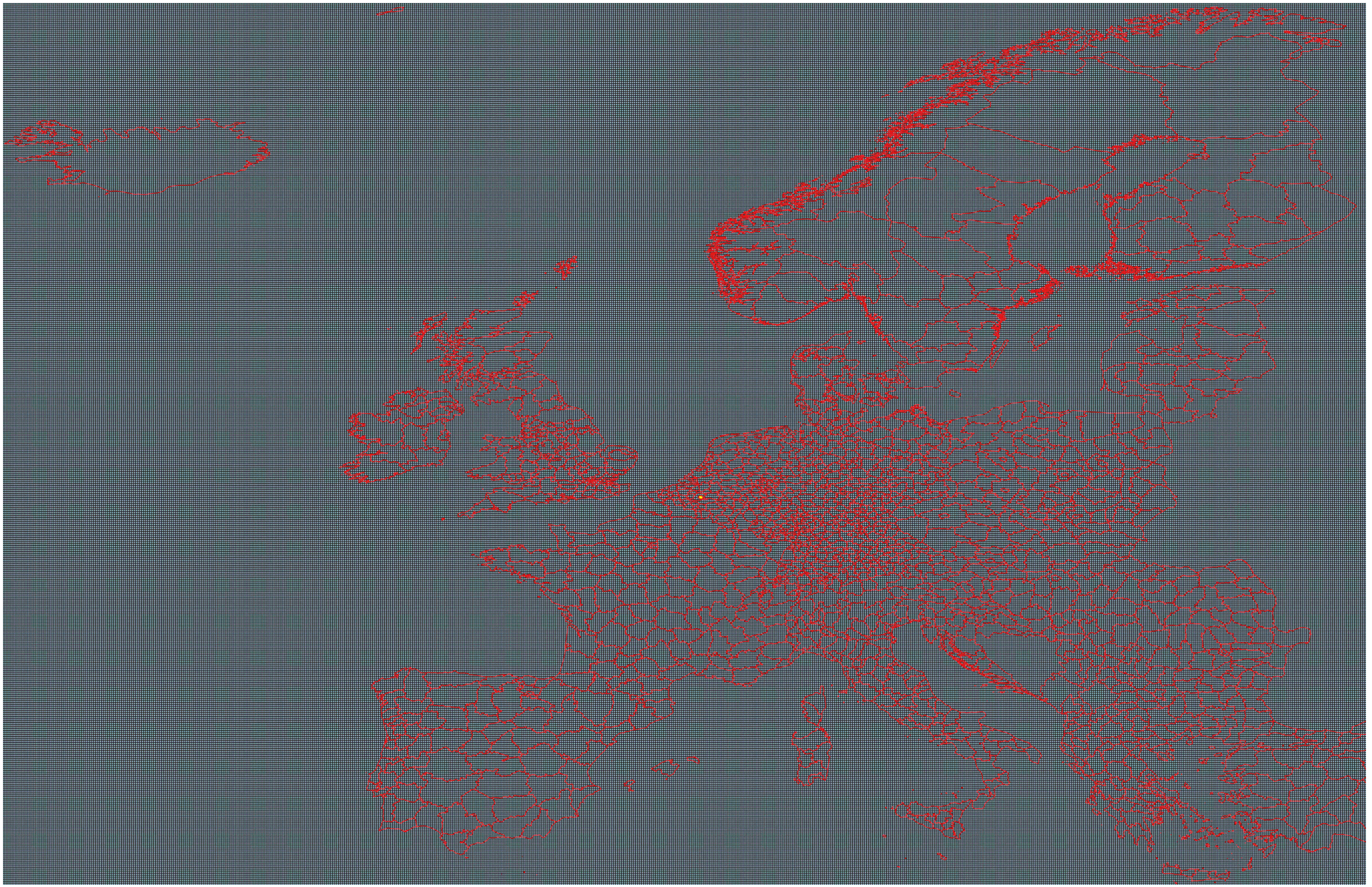

Note: This figure shows the spatial grid, as described in section A.1.1, overlaid with the current borders of European regions at the NUTS3 level (version 2021) in red.

Figure A38: **Spatial population distribution over time**

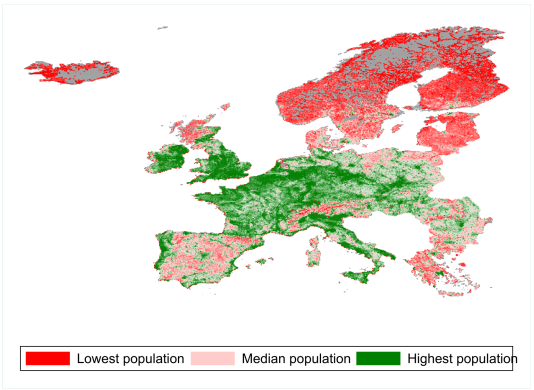

(a) 1800

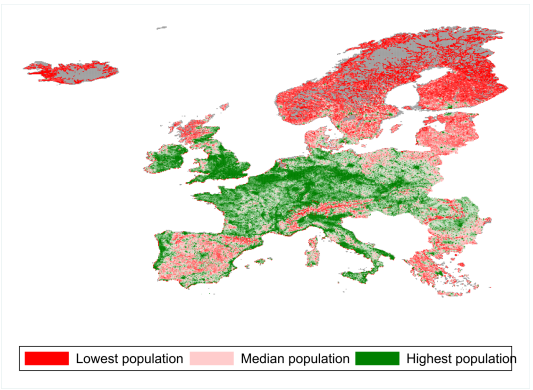

(b) 1850

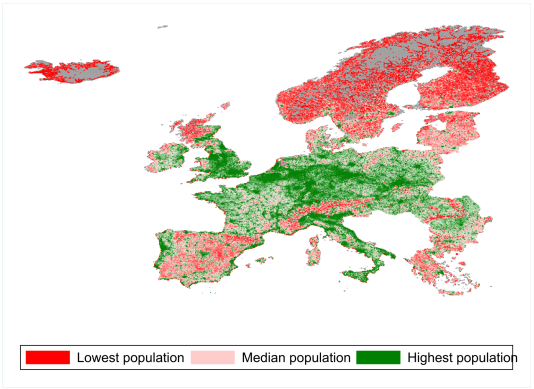

(c) 1900

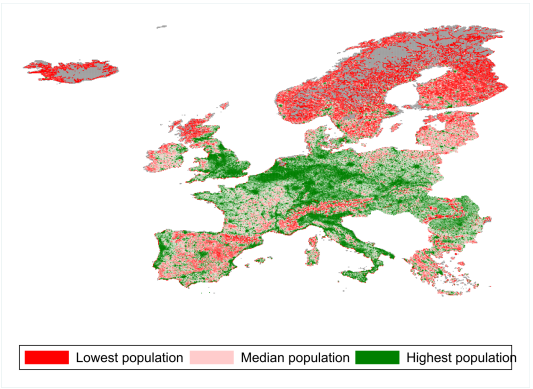

(d) 1950

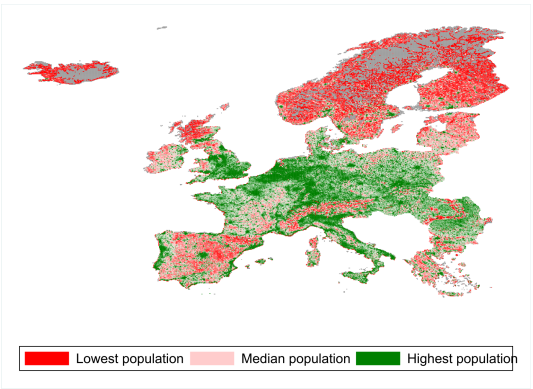

(e) 2000

Note: This figure shows the evolution of estimated spatial population distribution over the past quarter millennium. Depopulated grid cells are shown in grey.

Figure A39: **Spatial GDP distribution over time**

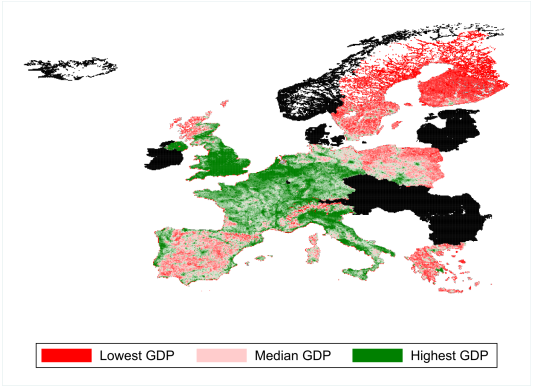

(a) 1800

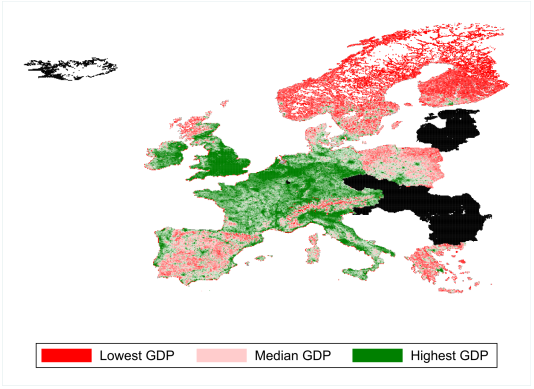

(b) 1850

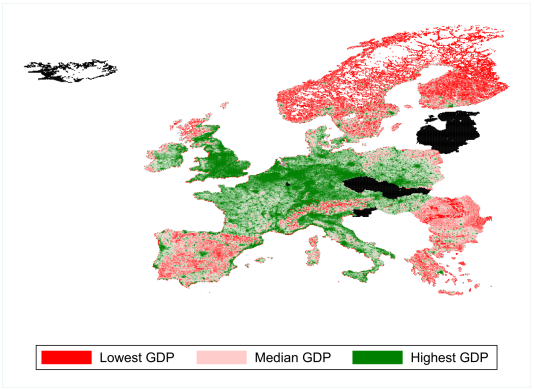

(c) 1900

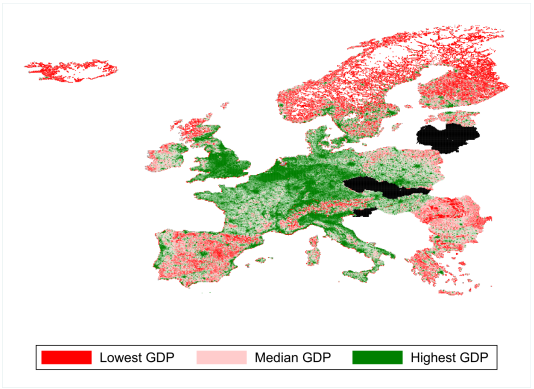

(d) 1950

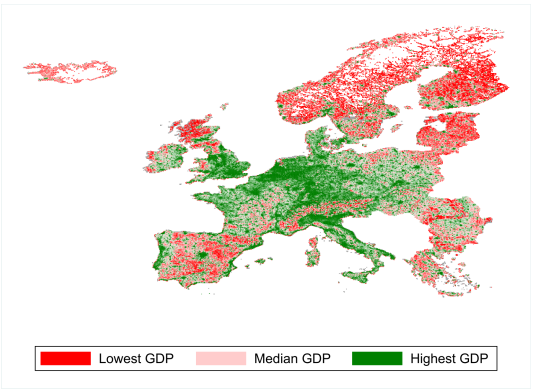

(e) 2000

Note: This figure shows the evolution of estimated spatial GDP distribution over the past quarter millennium. Countries lacking GDP information in Bolt and Van Zanden (2020) are shown in black.

Figure A40: **Spatial per capita GDP distribution over time**

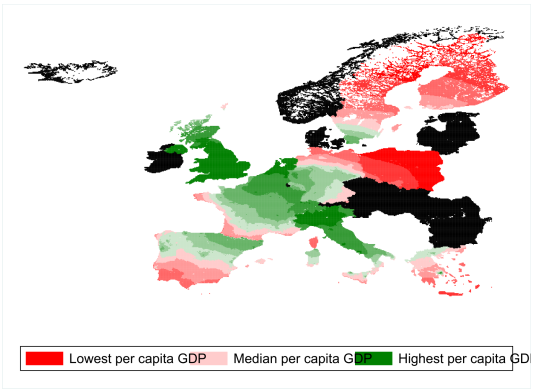

(a) 1800

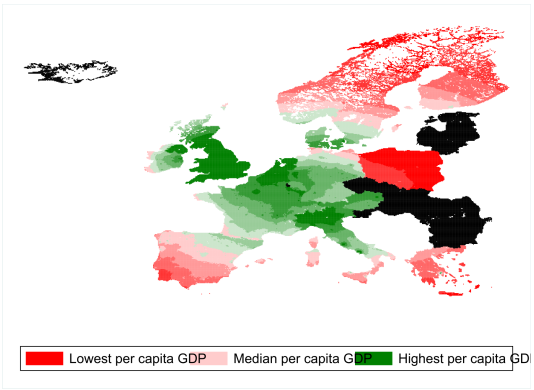

(b) 1850

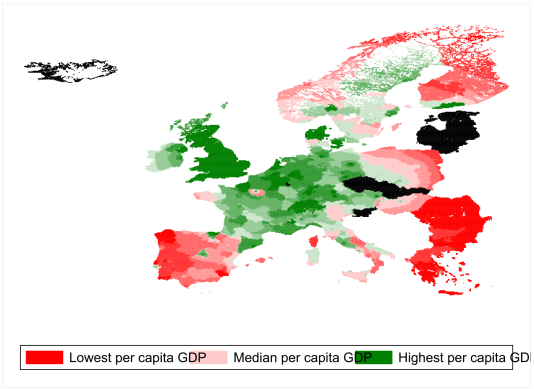

(c) 1900

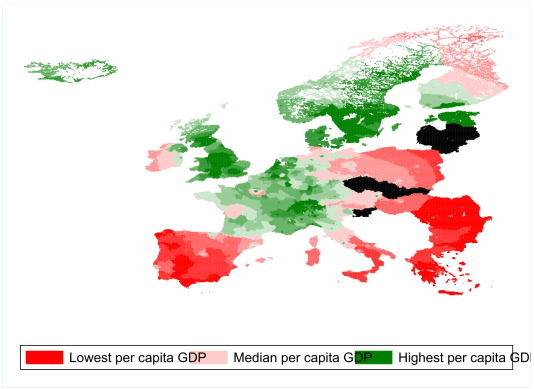

(d) 1950

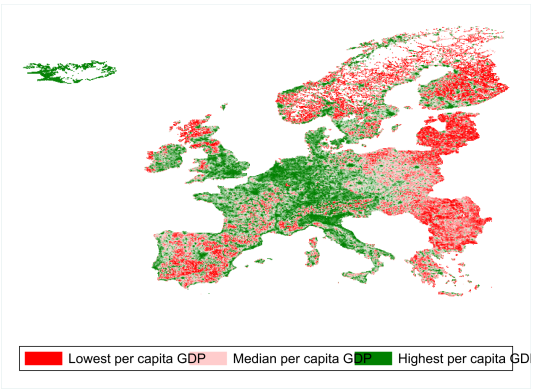

(e) 2000

Note: This figure shows the evolution of estimated spatial GDP distribution over the past quarter millennium. Countries lacking GDP information in Bolt and Van Zanden (2020) are shown in black.

Figure A41: **Spatial population-based market access distribution over time**

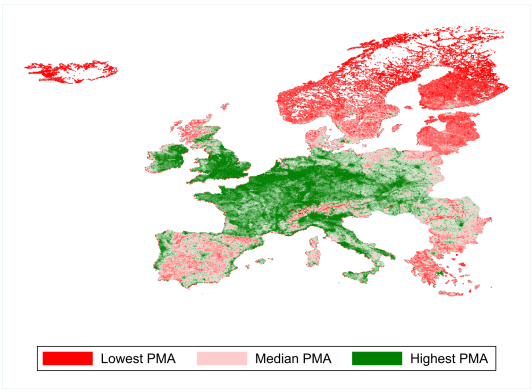

(a) 1800

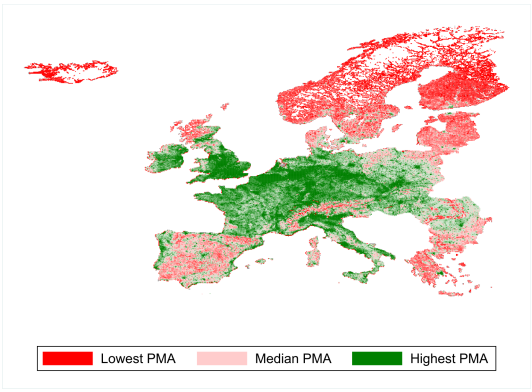

(b) 1850

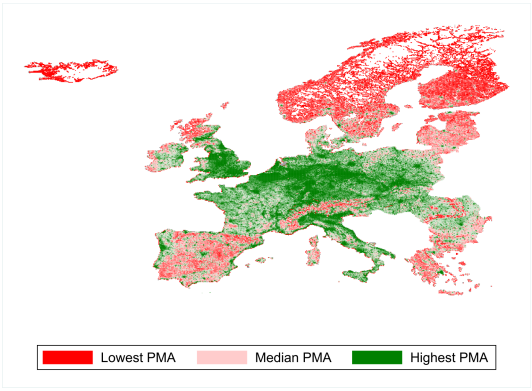

(c) 1900

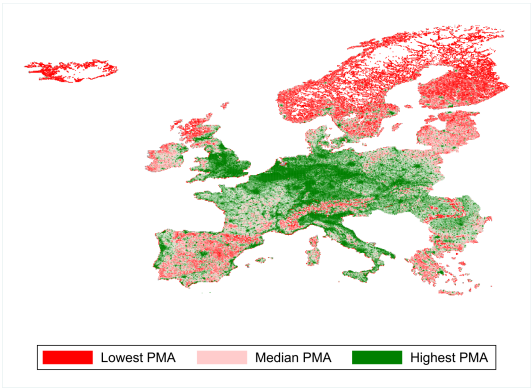

(d) 1950

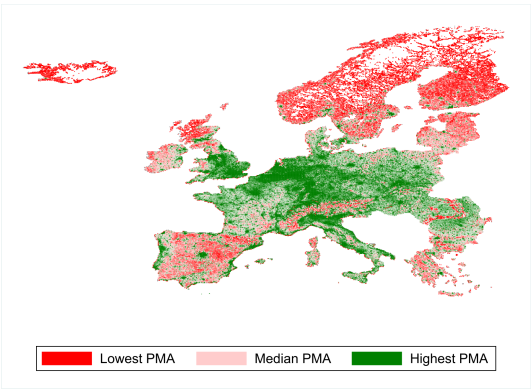

(e) 2000

Note: This figure shows the evolution of estimated population-based market access over the past quarter millennium. Depopulated grid cells are shown in grey.

Figure A42: **Gridded evolution: details**

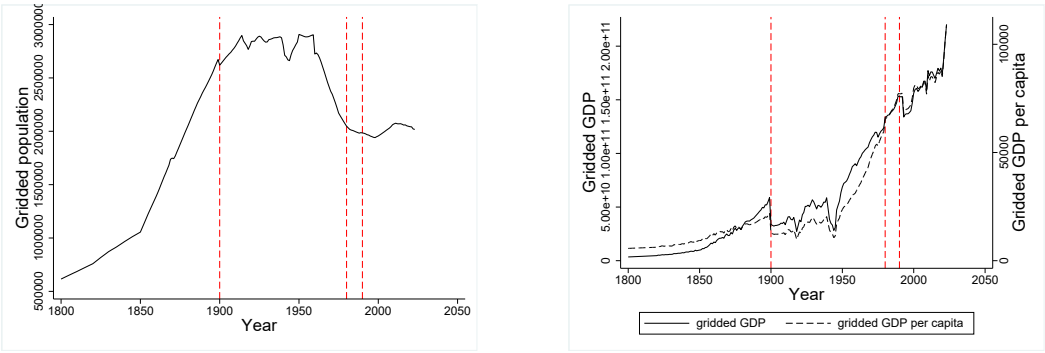

(a) Population (b) (per capita) GDP

Note: This figure shows the estimated trajectory of population and (per capita) GDP for the grid cell with the highest initial population in 1800. The vertical red lines highlight years in which the subnational target and/or the proxy variable used to estimate the gridded trajectory change.

Figure A43: **Full versus unilluminated population distribution**

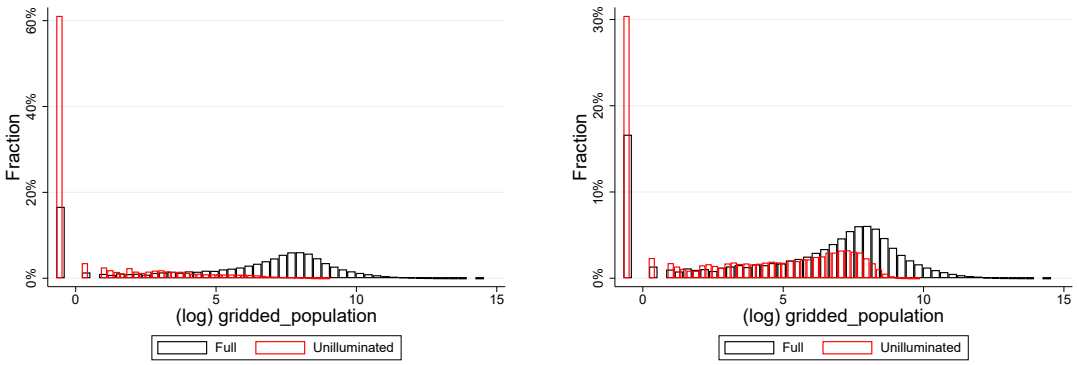

(a) DMSP (b) VIIRS

Note: This figure shows the 2010 log population distribution across all (black) and unilluminated (red) grid cells for DMSP and VIIRS separately. 0.5 was added to gridded population to visualize depopulated grid cells.

Figure A44: **Correlation of proxy variables with Maddison country GDP**

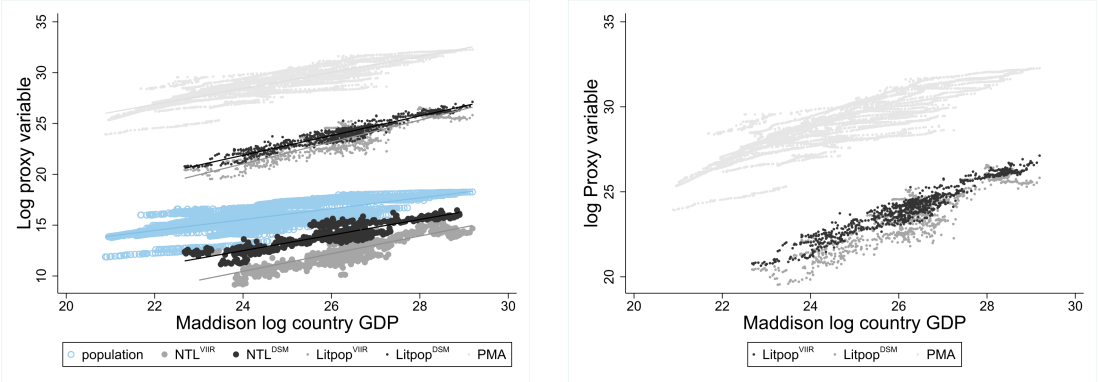

(a) All proxies (b) Final proxies

Note: Figure A44a shows the correlation between all (intermediary) proxy variables of country population, gross NTL and litpop product and population-based market acces (pma) with reported country GDP in Bolt and Van Zanden (2020). Figure A44b zooms in on the three final proxy variables of Litpop and pma that are used used in the final calibrations.

Figure A45: **Correlation of proxy variables with RW regional GDP**

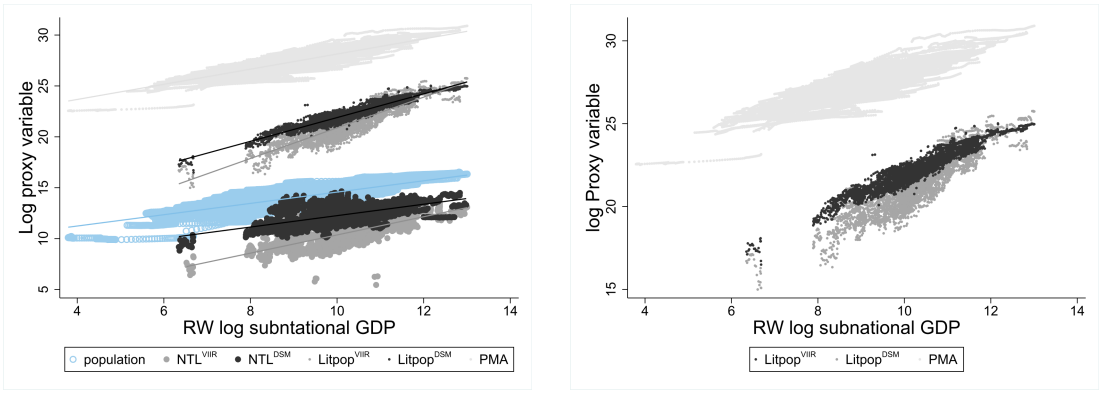

(a) All proxies (b) Final proxies

Note: Figure A45a shows the correlation between all (intermediary) proxy variables of country population, gross NTL and litpop product and population-based market acces (pma) with reported regional GDP in Rosés and Wolf (2021b). Figure A45b zooms in on the three final proxy variables of Litpop and pma that are used used in the final calibrations.

Figure A46: **Correlation of proxy variables with ARDECO NUTS3 GDP**

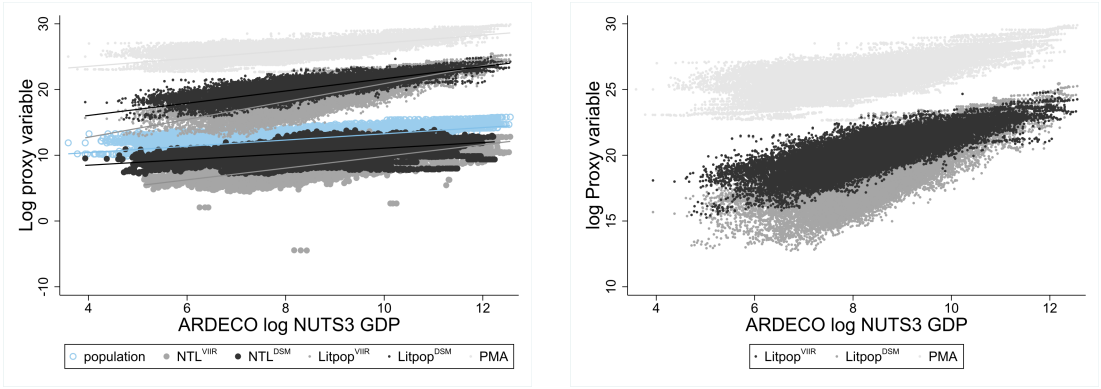

(a) All proxies (b) Final proxies

Note: Figure A46a shows the correlation between all (intermediary) proxy variables of country population, gross NTL and litpop product and population-based market acces (pma) with reported NUTS3 GDP in ARDECO (2023). Figure A46b zooms in on the three final proxy variables of Litpop and pma that are used used in the final calibrations.

Figure A47: **Correlation of proxy variables with Eurostat NUTS3 GDP**

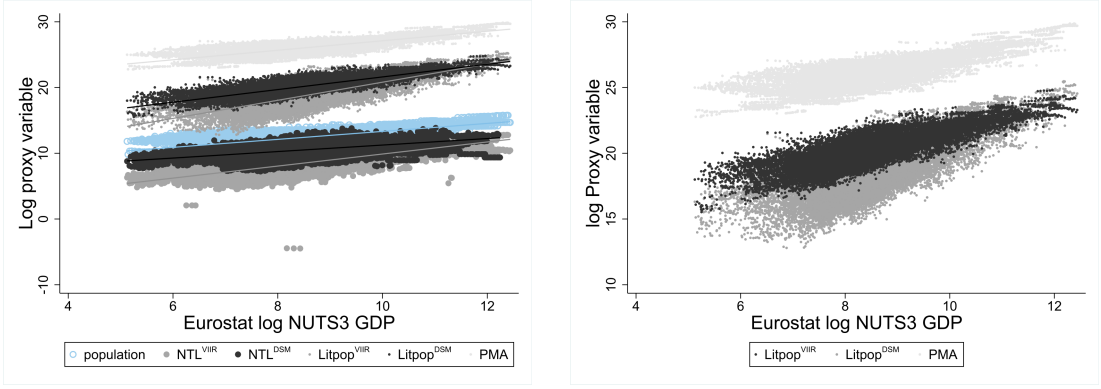

(a) All proxies (b) Final proxies

Note: Figure A47a shows the correlation between all (intermediary) proxy variables of country population, gross NTL and litpop product and population-based market acces (pma) with reported NUTS3 GDP in Eurostat (2023a). Figure A47b zooms in on the three final proxy variables of Litpop and pma that are used used in the final calibrations.

Figure A48: **Correlations between GDP proxies**

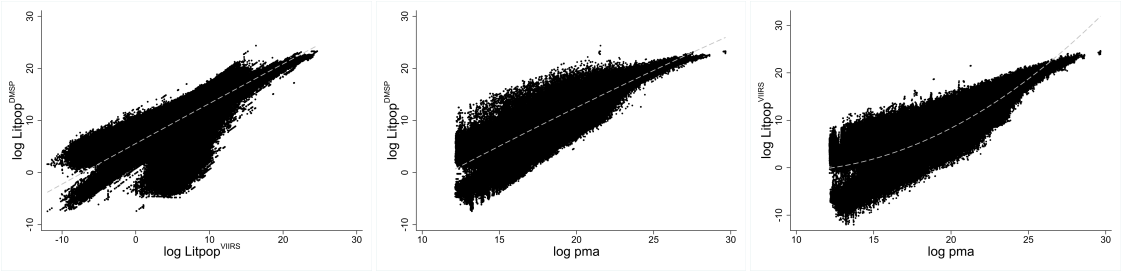

(a) $Litpop^{DMSP}$ & $Litpop^{VIIRS}$ (b) $Litpop^{DMSP}$ & PMA (c) $Litpop^{VIIRS}$ & PMA

Note: This figure shows scatter plots for the overlapping observations for the three GDP proxies.

Figure A49: **Electoral trends in the CLEA by country**

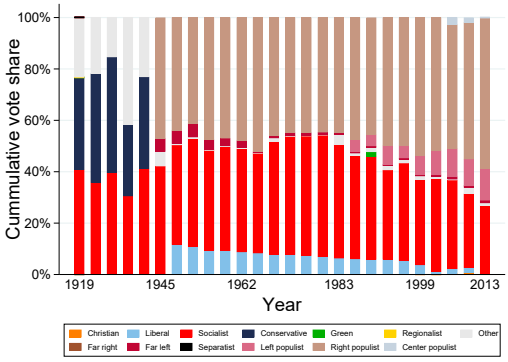

Austria

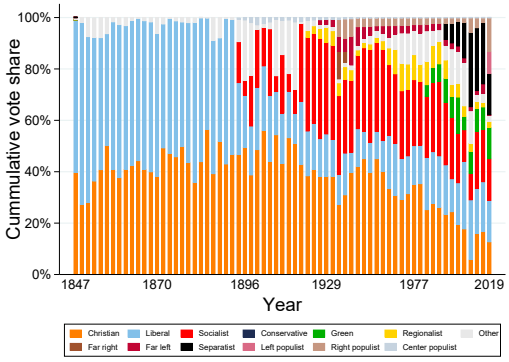

Belgium

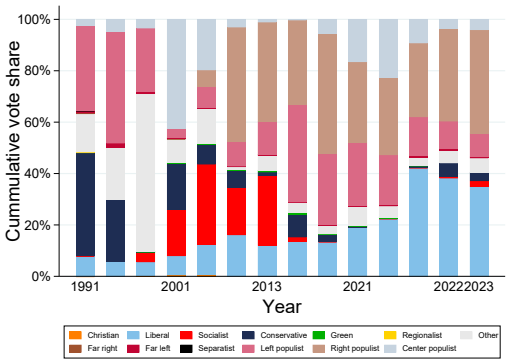

Bulgaria

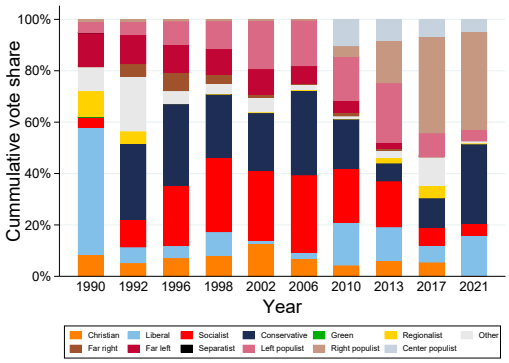

Czech Republic

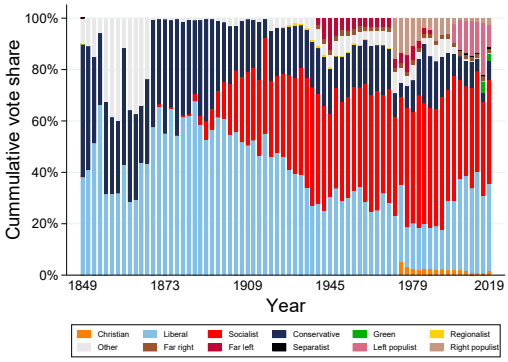

Denmark

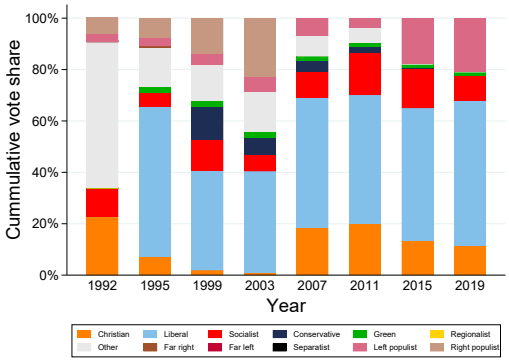

Estonia

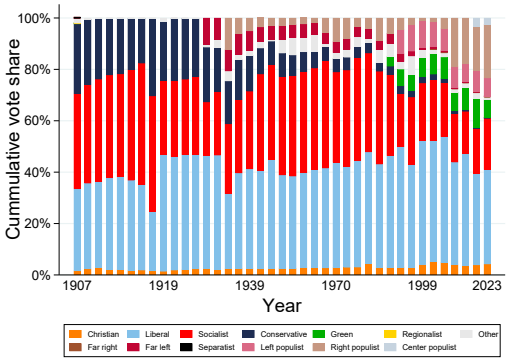

Finland

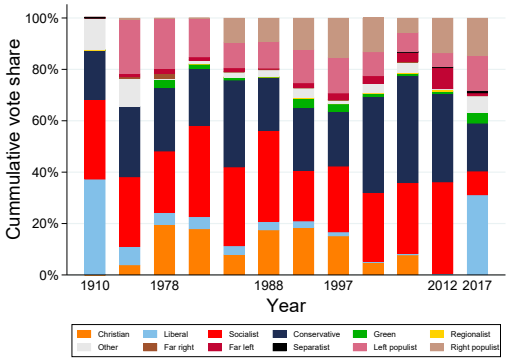

France

Note: This figure plots country-specific historical trends in the vote shares received by political parties in the the available elections of the CLEA by party taxonomy.

Figure A49: **Electoral trends in the CLEA by country**

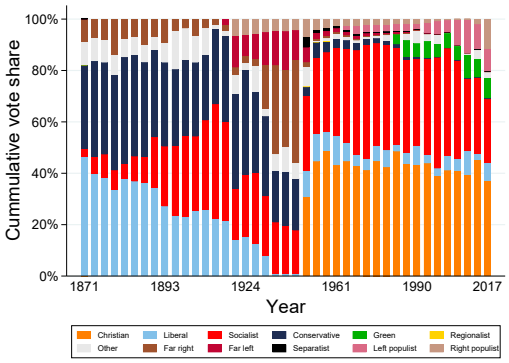

Germany (Bundesrepublik)

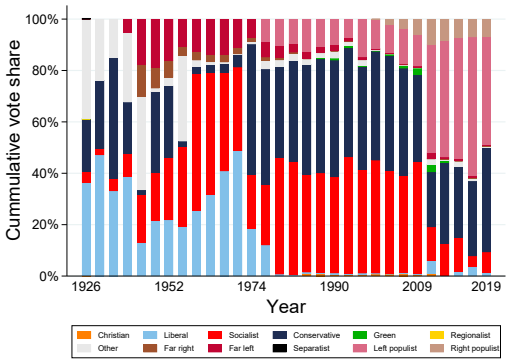

Greece

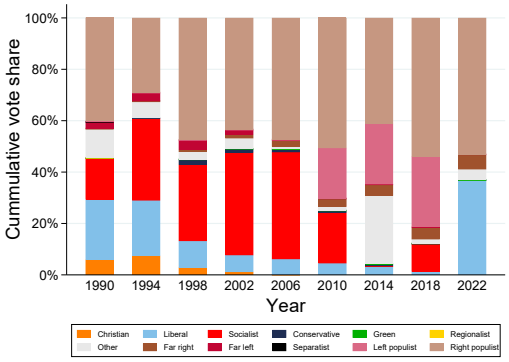

Hungary

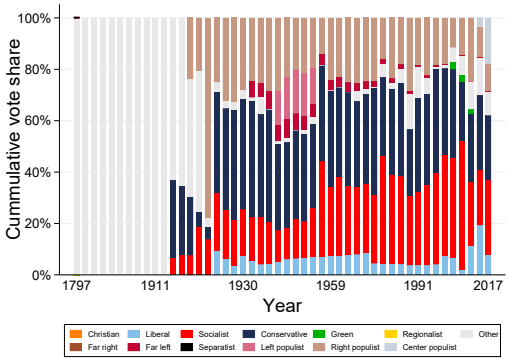

Iceland

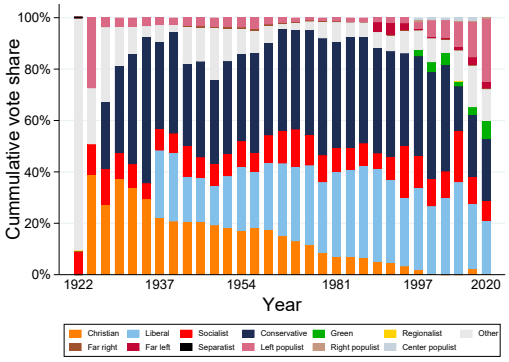

Ireland

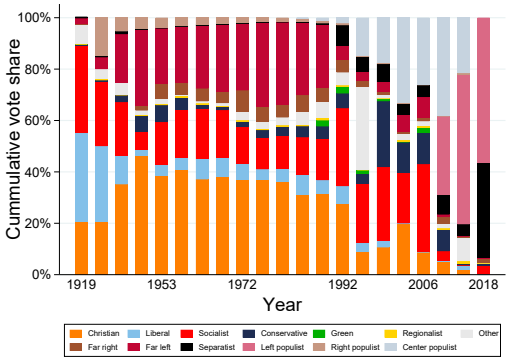

Italy

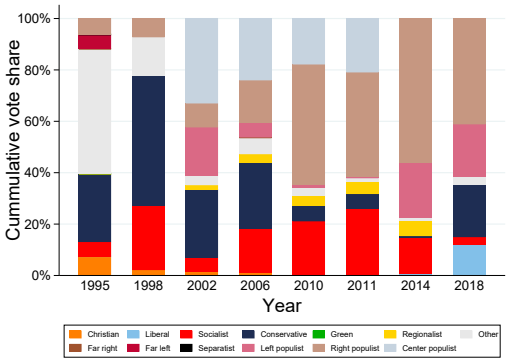

Latvia

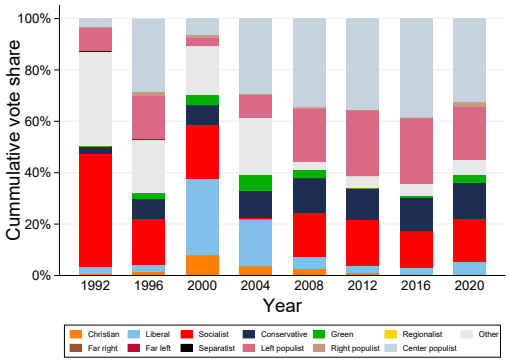

Lithuania

Note: This figure plots country-specific historical trends in the vote shares received by political parties in the the available elections of the CLEA by party taxonomy.

Figure A49: **Electoral trends in the CLEA by country**

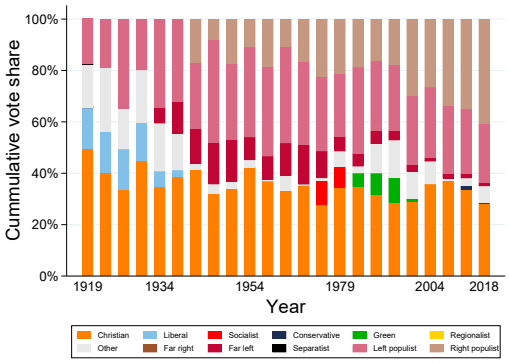

Luxembourg

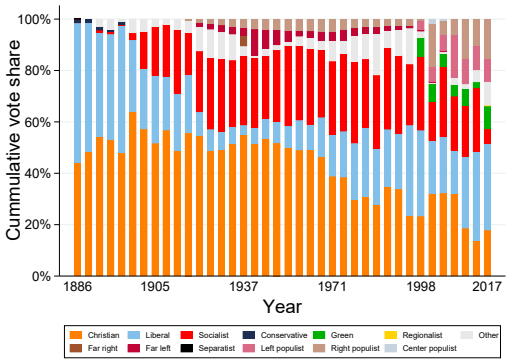

Netherlands

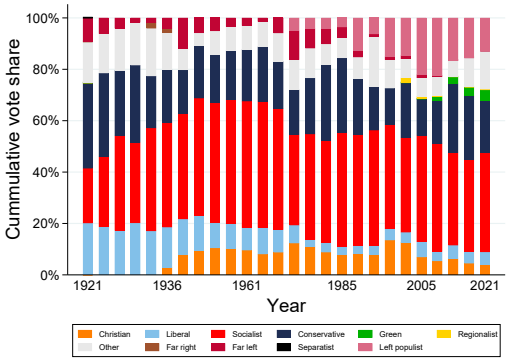

Norway

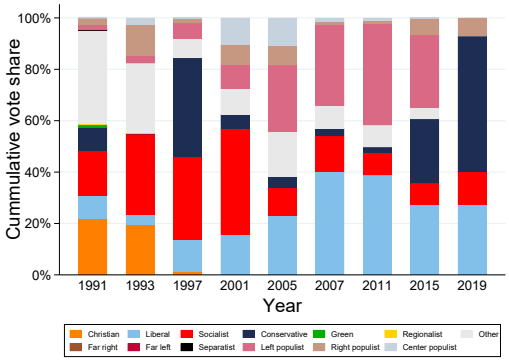

Poland

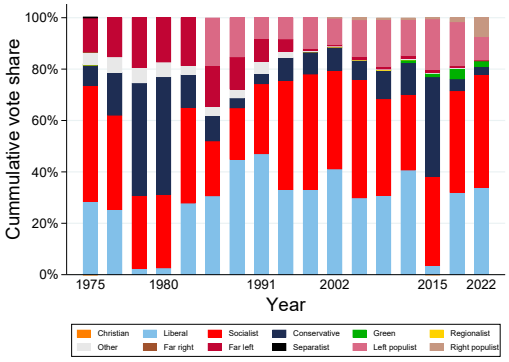

Portugal

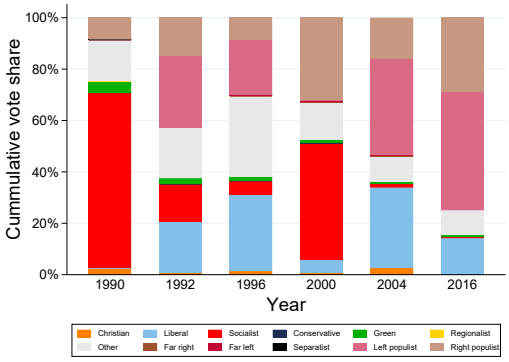

Romania

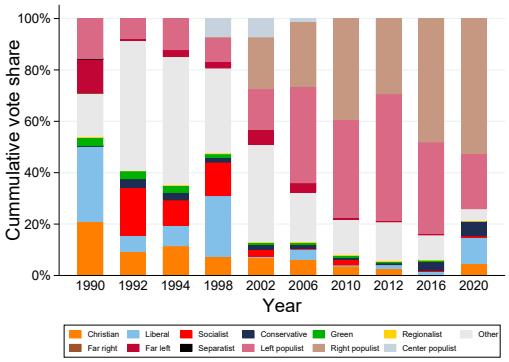

Slovakia

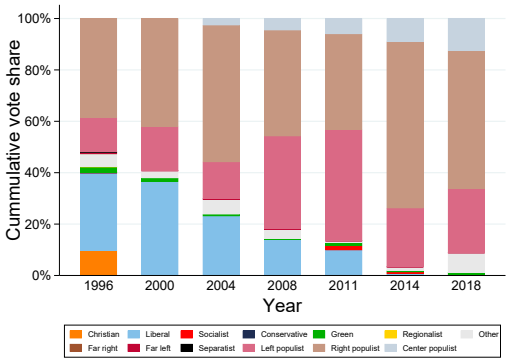

Slovenia

Note: This figure plots country-specific historical trends in the vote shares received by political parties in the the available elections of the CLEA by party taxonomy.

Figure A49: **Electoral trends in the CLEA by country**

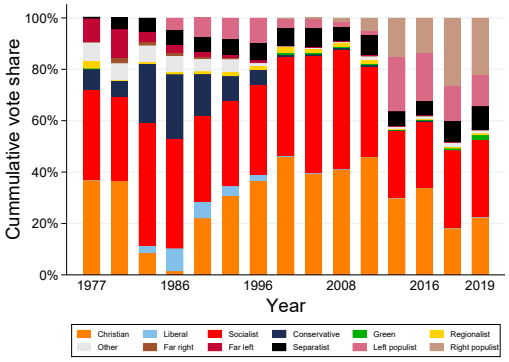

Spain

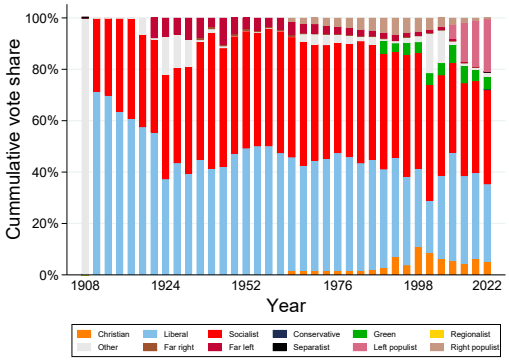

Sweden

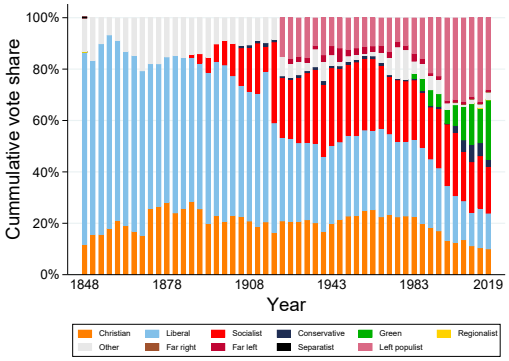

Switzerland

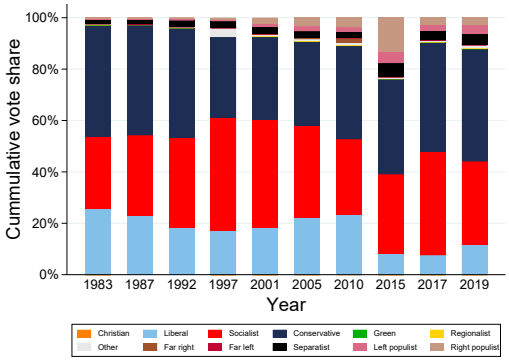

United Kingdom

Note: This figure plots country-specific historical trends in the vote shares received by political parties in the the available elections of the CLEA by party taxonomy.

Figure A50: **Targeted moments: observed versus simulated values**

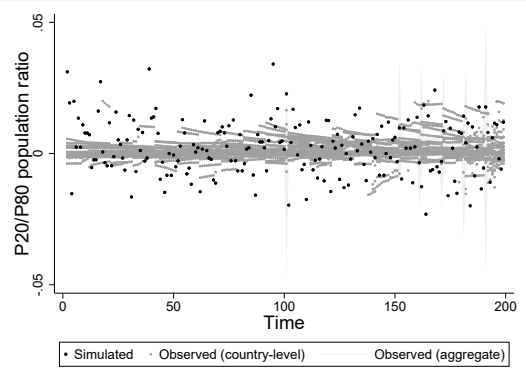

(a) Top quintile population ratio growth

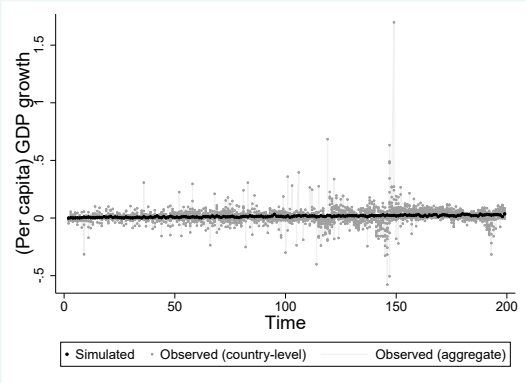

(b) Per capita GDP growth

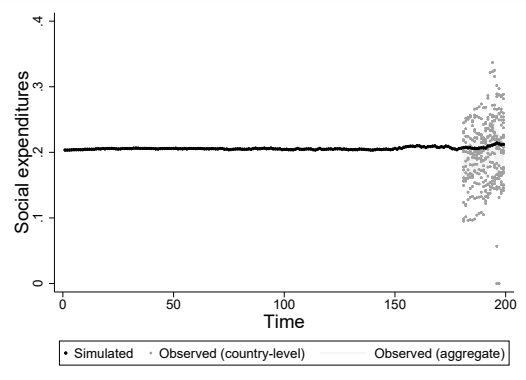

(c) Social expenditures (τ^*)

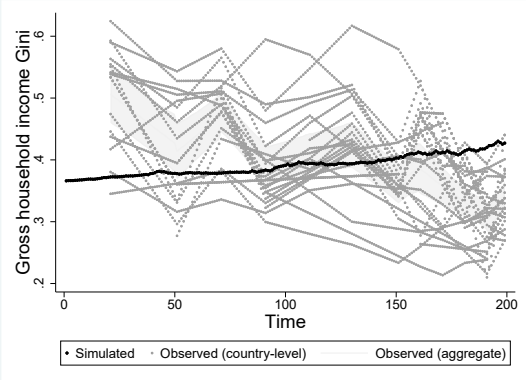

(d) Gross household income Gini

Note: This figure shows simulated (black) and observed (grey) moments of the baseline calibration discussed in section 6 for the calibrated parameter values in table 7. The simulated population quintile ratio expresses the population share of the 20% most productive locations, $\sum_{l=24}^{30} / \sum_{l=1}^{30}$; the observed population quintile ratio expresses the population share of the 20% most populated NUTS3 regions in each European country in the sample and is computed from the gridded population data in the SPEED. Simulated per capita GDP growth expresses nominal wage growth; observed per capita GDP growth captures the country-level growth in real per capita GDP as computed from the SPEED. Simulated redistributive transfers express the equilibrium tax rate, τ^*, of equation 19; observed redistributive transfers are proxied by the available information on social expenditure shares in OECD.Stat (2024). Finally, simulated income inequality is measured by the Gini coefficient of nominal wages; observed income inequality is measured by the gross household Gini coefficients reported in CLIO Infra (2014).

Figure A51: **Simulations: outcome evolutions across scenarios**

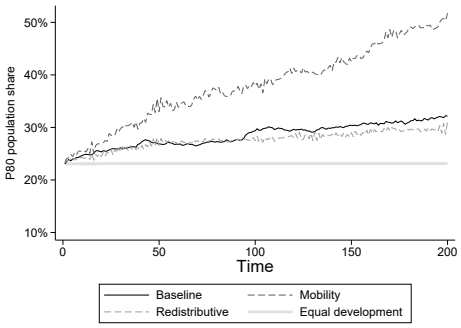

(a) P80/P20 population, N^{P20}

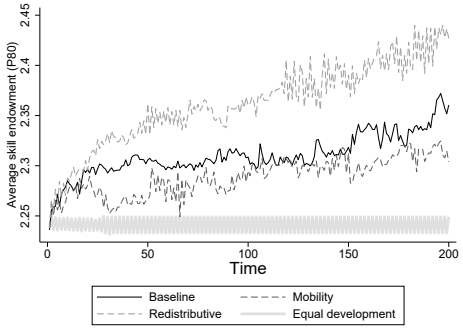

(b) Expected skill in leading locations, $\bar{s}^{P20}$

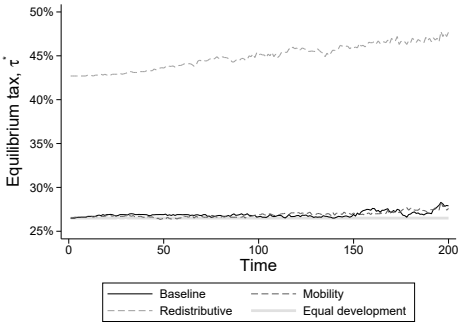

(c) Equilibrium tax, τ^*

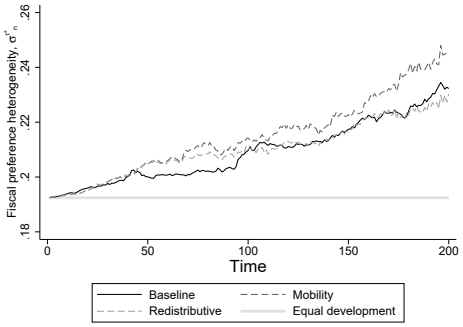

(d) Fiscal preference heterogeneity, $\sigma^{\bar{\tau}^{*N}}$

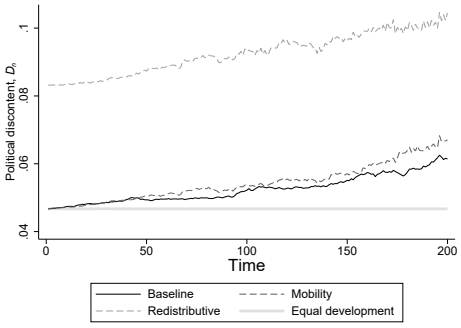

(e) Political discontent, $\bar{D}$

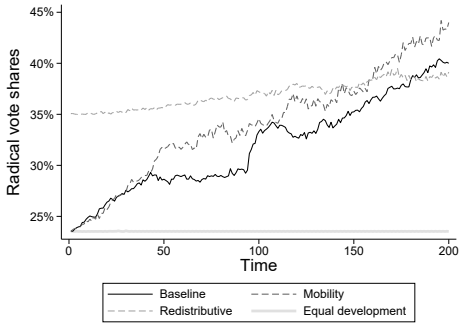

(f) Radical vote share, RVS

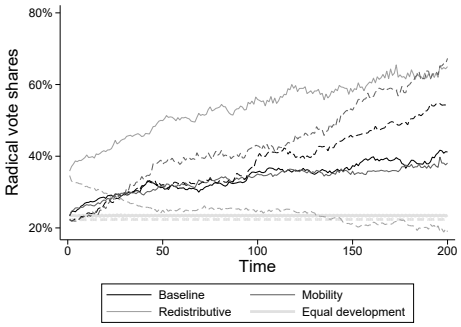

(g) Radical vote share, leading vs lagging

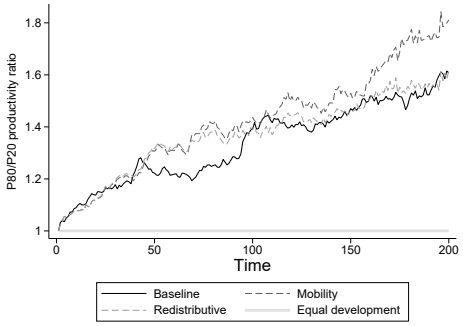

(h) P80/P20 productivity ratio, $a^{P80/P20}$

Note: This figure shows the evolution of several focal politico-economic variables discussed in section 6 for the different calibrations listed in table 7. Figure A51g plots radical vote shares in the 80% least productive ('lagging') regions in dashed lines and those of the 20% most productive ('leading') regions in the full lines.

Table A6: Corrections and additions to CLEA

Denmark	1903	due to their unusual discrepancy, valid votes are replaced with votes cast in the constituency of *frederiksvaerk*.
	1910	due to their unusual discrepancy, valid votes are replaced with votes cast in the constituencies of *koebenhavns 4 valgkreds* and *thisted*.
France	1981	added missing electoral results for the constituency of *val-doise 5* from Wikipedia.
	2007	dropped the constituencies *Savoy 1-Savoy 3*, as they were not used and appear to duplicate *Savoie 1-Savoie 3*.
Germany	1957-1961	corrected the constituency name of *stadt hannover sud* to *stade-bremervörde* for constituency number 217.
	1965-1972	corrected the constituency name of *düsseldorf-mettamnn ii* to *düsseldorf-mettamnn i* for constituency number 63.
	1961	corrected the constituency name of *düren* to *donauwörth* for constituency number 58.
	1976	corrected the constituency name of *friesland-* to *friesland-wilhelmshaven*.
	1990-1994	corrected the constituency name of *saarbrücken i* to *saarbrücken ii* for constituency number 272.
	1998	corrected the constituency name of *saarbrücken i* to *saarbrücken ii* for constituency number 58.
Hungary	2002	swapped party votes with total candidate votes.
Italy	2001-2013	as several valid votes figures don't match official reports, e.g. here for *Calabria* in 2001 (944962 in CLEA versus 1065850 in report), they are recomputed by dividing party votes by their share.
	2007	results for the missing Aosta Valley constituency are added from the official results.
Lithuania	2012	party votes replaced with candidate votes in the constituency of *Naujamiescio*.
Netherlands	1886-1917	many uncontested elections lacking (winning) party information in the CLEA: added available party information for the 1886-1887 elections; winning parties from uncontested elections with a 100% vote share in 1897-1913 and full election results for 1917 from the Huygens Instituut.
Portugal	2015	divided the party votes for the *UDC* party in the constituency of *Leida* by 10.
Switzerland	1939-2007	winning parties of uncontested elections added with 100% vote share from Wikipedia pages, e.g. this page for 2007.
	1999-2015	party votes computed from aggregate candidate votes for parties with different names but identical party number, to avoid overcounting.
UK	1983-1987	corrected the constituency names of *Inverness-shire and Ross and Cromarty, Western Isles* and *Stirlingshire and Clackmannanshire, West Stirlingshire* to *Witney* and *Woking*.
	1992	corrected the constituency names of *Inverness-shire and Ross and Cromarty, Western Isles* and *Stirlingshire and Clackmannanshire, West Stirlingshire* to *Witney* and *Wirral West*.
	1997	corrected the constituency names of *Inverness-shire and Ross and Cromarty, Western Isles* and *Stirlingshire and Clackmannanshire, West Stirlingshire* to *Western Isles* and *Westmorland & Lonsdale*.
	2001	corrected the constituency names of *Inverness-shire and Ross and Cromarty, Western Isles* and *Stirlingshire and Clackmannanshire, West Stirlingshire* to *Weston-Super-Mare* and *Wigan*.
	2005	corrected the constituency names of *Inverness-shire and Ross and Cromarty, Western Isles* and *Stirlingshire and Clackmannanshire, West Stirlingshire* to *Woodspring* and *Wolverhampton South West*.
	2010-2015	corrected the constituency names of *Inverness-shire and Ross and Cromarty, Western Isles* and *Stirlingshire and Clackmannanshire, West Stirlingshire* to *Wokingham* and *wolverhampton North East*.
	2017	corrected the constituency names of *Inverness-shire and Ross and Cromarty, Western Isles* and *Stirlingshire and Clackmannanshire, West Stirlingshire* to *Wirral South* and *Wirral West*.
		corrected valid votes in the constituencies of *Rother Valley* and *Brentford and Isleworth* to 49488 and 61629 respectively from Wikipedia.

Table A7: Wikipedia party classifiers

Type	#	*Type*	#	*Type*	#	*Type*	#
euroscepticism	310	antisemitism	16	national syndicalism	4	alter globalism	1
liberalism	251	souveranism	16	political protestantism	4	anti LGBTQ rights	1
nationalism	226	anti fascism	15	right libertarianism	4	anti elitism	1
regionalism	211	joke party	15	selfdetermination	4	anti elitist	1
conservatism	209	national liberalism	15	spiritual left	4	anti germanism	1
christian democracy	205	secularism	15	stalinism	4	anti leninism	1
social democracy	202	political catholicism	14	technocracy	4	anti militarism	1
pro europeanism	188	radicalism	14	third way	4	anti nationalism	1
national conservatism	170	revolutionary socialism	14	centralism	3	anti nuclear power	1
conservative liberalism	166	anti establishment	13	christian nationalism	3	anti socialist	1
social conservatism	157	european federalism	13	christian socialism	3	anticommunism	1
socialism	144	fascism	13	civil libertarianism	3	antiliberalism	1
right wing populism	134	christian	12	conservative christian	3	atheism	1
democratic socialism	111	social Liberalism	12	consumer protection	3	atlanticism	1
social liberalism	109	decentralization	11	identity politics	3	austrian economics	1
green politics	108	reformism	11	irredentism	3	autarky	1
communism	106	animal welfare	10	justice	3	basicincome	1
agrarianism	96	far right	10	laicism	3	catchall party	1
populism	89	illiberalism	10	libertarian socialism	3	civic engagement	1
economic liberalism	81	anti abortion	9	parliamentarism	3	climate change denial	1
marxism leninism trotskyism	79	anti austerity	9	populist	3	collaborationism	1
republicanism	77	anti globalism	9	revolutionary nationalism	3	collectivism	1
ecologism	74	humanism	9	traditionalism	3	communitarianism	1
direct democracy	66	laissez faire	9	welfare chauvinism	3	cultural conservatism	1
progressivism	62	patriotism	9	anti abortionism	2	disability rights	1
separatism	60	internationalism	8	authoritarianism	2	economic democracy	1
minority rights	57	localism	8	big tent	2	economic socialism	1
anti capitalism	56	nazism	8	christian fundamentalism	2	elderly rights	1
anti immigration	54	anti globalization	7	christian humanism	2	fiscal deregulation	1
federalism	53	anti racism	7	confederalism	2	fiscal federalism	1
feminism	53	corporatism	7	constitutional monarchism	2	human rights	1
anti communism	51	eurocommunism	7	cultural liberalism	2	liberal nationalism	1
environmentalism	51	fiscal conservatism	7	degrowth	2	meritocracy	1
centrism	49	reactionism	7	democracy	2	militarism	1
liberteraniarism	40	anarchism	6	egalitarianism	2	neutralism	1
neo nazism fascism	32	civic nationalism	6	equality	2	nonsectarianism	1
trotskyism	32	devolution	6	identitarianism	2	pluralism	1
classical liberalism	31	multiculturalism	6	interculturalism	2	popular socialism	1
anti corruption	30	protectionism	6	islamism	2	pro immigration	1
autonomy	28	syndicalism	6	isolationism	2	pro life	1
pacifism	28	unionism	6	joke party satire	2	pro transparency	1
anti islam	27	animal rights	5	market socialism	2	rural development	1
christian right	25	liberal democracy	5	nordic model	2	russophilia	1
left wing populism	25	neoliberalism	5	open government	2	social market economy	1
monarchism	24	participatory democracy	5	ordeoliberalism	2	subsidiarity	1
pensioners interests	20	progressive liberalism	5	paternalistic	2	transparency	1
unitarism	19	royalism	5	privacy	2	ultranationalism	1
economic nationalism	18	social justice	5	radical populism	2	veterans interests	1
christian left	17	social progressivism	5	right wing socialism	2	womens rights	1
left wing nationalism	17	anti liberalism	4	stewardship theology	2		
pirate politics	17	christian conservatism	4	syncretic politics	2		
anti clericalism	16	marxism	4	theocracy	2		

Note: This table lists ideological positions and their frequency from Wikipedia pages describing the European parties in the CLEA.

Table A8: Synthesized party classification of the CLEA

Country	*Party*	*last year*	*Populist, P*			*Extremist, E*			*P*	*E*	*R*
			LP	*CP*	*RP*	*FL*	*FR*	*S*			
Austria	BDS	1959				W				W	W
Austria	BZO	2013			WNP		P		WNP	P	WNP
Austria	CSP	1930					W			W	W
Austria	DFP	1966			W				W		W
Austria	DL	2008				W				W	W
Austria	FPO	2013			WNP		WP		WNP	WP	WNP
Austria	FRANK	2013		P	WN				WNP		WNP
Austria	GRUNE	1990	N						N		N
Austria	KPO	1949				W				W	W
Austria	LDM	2013		P					P		P
Austria	NEOS	2013			W				W		W
Austria	OVP	2013			W				W		W
Austria	SLP	2013				W				W	W
Austria	heimatblock	1930					W			W	W
Belgium	CD&V+NVA	2007						W		W	W
Belgium	Flemish Block	2014			WNP		WP	W	WNP	WP	WNP
Belgium	Frontpartij	1932					W			W	W
Belgium	Kommunistische Partij van België	2019				W				W	W
Belgium	LDD	2014		P	W				WP		WP
Belgium	LES BELGES D'ABORD	2019			W		W		W	W	W
Belgium	Lutte Ouvrière	2019				W				W	W
Belgium	NVA	2014			N			W	N	W	WN
Belgium	National Front	2010			P		WP		P	WP	WP
Belgium	PP	2019			WNP		WP		WNP	WP	WNP
Belgium	PVDA	2019	N			WP			N	WP	WNP
Belgium	Rex	1939					W			W	W
Belgium	VNV	1939			W		W		W	W	W
Belgium	Wallonie insoumise	2019	W			W			W	W	W
Bulgaria	ABC	2021	N						N		N
Bulgaria	ATAKA	2021	N		WP		WP		WNP	WP	WNP
Bulgaria	BBB	1991		P					P		P
Bulgaria	BCP	2023				W				W	W
Bulgaria	BKP	1997				W				W	W
Bulgaria	BMPO	2022			WP		WP		WP	WP	WP
Bulgaria	BNF	2001					W			W	W
Bulgaria	BNUND	2021					W			W	W
Bulgaria	BP	2021			W		W		W	W	W
Bulgaria	BRPk	2001				W				W	W
Bulgaria	BSP	2023	W						W		W
Bulgaria	CNB	2023				W				W	W
Bulgaria	DBG	2013			N				N		N
Bulgaria	DSB	2005			N				N		N
Bulgaria	GERB	2023		P	N				NP		NP
Bulgaria	IMRO	2001	N		WP		WP		WNP	WP	WNP
Bulgaria	IMRONFSB	2021	N		WP		WP		WNP	WP	WNP
Bulgaria	KOD	2022			W				W		W
Bulgaria	NDSV	2005		P					P		P
Bulgaria	NFSB	2013	N		P		WP		NP	WP	WNP
Bulgaria	NMSB	2022			P		P		P	P	P
Bulgaria	OP	2017			W		W		W	W	W
Bulgaria	RB	2014	N	P	W				WNP		WNP
Bulgaria	REVIVAL	2023			WP		P		WP	P	WP
Bulgaria	RZS	2013			P		P		P	P	P
Bulgaria	SEBG	2021	W	P					WP		WP
Bulgaria	SKB	2013				W				W	W
Bulgaria	TISN	2021		P					P		P
Bulgaria	V+NFSB	2021			W		W		W	W	W
Bulgaria	Volya-NFSB	2021			WP		WP		WP	WP	WP
Czech Republic	ANO2011	2021		P	N				NP		NP
Czech Republic	ANS	2021					W			W	W
Czech Republic	CS	2013			P		P		P	P	P
Czech Republic	CSNS2005	2010	W						W		W
Czech Republic	DSSS	2013					W			W	W
Czech Republic	KONS	2010			N				N		N
Czech Republic	KSC	1990				WP				WP	WP
Czech Republic	KSCM	2017	N			WP			N	WP	WNP
Czech Republic	ND	2006					W			W	W
Czech Republic	NF	2017				W				W	W
Czech Republic	PB	2017			W				W		W
Czech Republic	PBCZ	2021			W				W		W

continued on next page

continued

Country	*Party*	*last year*	*Populist, P*			*Extremist, E*			*P*	*E*	*R*
			LP	*CP*	*RP*	*FL*	*FR*	*S*			
Czech Republic	PRISAHA	2021		P					P		P
Czech Republic	SPD	2017			WP		WP		WP	WP	WP
Czech Republic	SPOZ	2013	W						W		W
Czech Republic	SPR-RSC	2010					WP			WP	WP
Czech Republic	SZ	2021	N						N		N
Czech Republic	TRIK	2021					W			W	W
Czech Republic	UPD	2013	N		WP		WP		WNP	WP	WNP
Czech Republic	VV	2010		P					P		P
Denmark	DNSAP	1943					W			W	W
Denmark	DPP	2019	N		WP		WP		WNP	WP	WNP
Denmark	ERG	2019				WP				WP	WP
Denmark	F	2015						W		W	W
Denmark	FrP	2019		P	W		W		WP	W	WP
Denmark	IA	2019						W		W	W
Denmark	N	2019						W		W	W
Denmark	NB	2019			W		WP		W	WP	WP
Denmark	NQ	2019						W		W	W
Denmark	S	2019						W		W	W
Denmark	SK	2019					W			W	W
Denmark	Tj	2019				P		W		WP	WP
Denmark	VS	1987				W				W	W
Estonia	EER	2019			N				N		N
Estonia	EIP	2015					W			W	W
Estonia	EKRE	2019			WP		WP		WP	WP	WP
Estonia	ERSP	1992					P			P	P
Estonia	EVR	2019			N				N		N
Estonia	IERP	1992		P					P		P
Estonia	PEEK	1995			P		P		P	P	P
Finland	AD	2019			W				W		W
Finland	IKL	1939			W		W		W	W	W
Finland	KOK+IKL	1933			W		W		W	W	W
Finland	KTP	2019				W				W	W
Finland	LIIK	2023		P					P		P
Finland	PMP	1945				W				W	W
Finland	PS	2023			WNP		P		WNP	P	WNP
Finland	SI	2003					W			W	W
Finland	SKDL	1987				W				W	W
Finland	SKE	2023					W			W	W
Finland	SKP	2023				W				W	W
Finland	SKS	2007					W			W	W
Finland	SML	2023					W			W	W
Finland	SMP	1962			P		P		P	P	P
Finland	ST	2019		P					P		P
Finland	STPV	1929				W				W	W
Finland	VAS	2019	N						N		N
Finland	VKK	2023					W			W	W
France	AF	1978					W			W	W
France	DED	2017					W			W	W
France	DEG	2017				W				W	W
France	DLF	2017		P	W		W		WP	W	WP
France	FDG	2012				W				W	W
France	LFI	2017	WP			WP			WP	WP	WP
France	LO	2002				WP				WP	WP
France	MNR	2002			W		W		W	W	W
France	MPF	2007			N				N		N
France	OCI	1973				W				W	W
France	PCF	2017	N			WP			N	WP	WNP
France	RS	2017						W		W	W
Germany	AJDDV	2017					W			W	W
Germany	AfD	2013			WNP		WP		WNP	WP	WNP
Germany	BGD	2013					W			W	W
Germany	CM	2005					W			W	W
Germany	DKP	2013				W				W	W
Germany	DNVP	1932					W			W	W
Germany	DR	2017					W			W	W
Germany	DRP	1912					W			W	W
Germany	DRP+AS	1893					W			W	W
Germany	DRP+AS+CS	1907					W			W	W
Germany	DRP2	1912					W			W	W
Germany	DRP3	1949					W			W	W
Germany	DSU	2005			W				W		W

continued on next page

continued

Country	*Party*	*last year*	*Populist, P*			*Extremist, E*			*P*	*E*	*R*
			LP	*CP*	*RP*	*FL*	*FR*	*S*			
Germany	FDVP	1924			W				W		W
Germany	KPD	2009				W				W	W
Germany	MLDP	2017				W				W	W
Germany	NPD	2017	N				W		N	W	WN
Germany	NSDAP	1933					W			W	W
Germany	NSFB	1924					W			W	W
Germany	PDS	2009	WNP			P			WNP	P	WNP
Germany	PRO	2005			W				W		W
Germany	PRO2	2002			W				W		W
Germany	ProDM	2013			W		W		W	W	W
Germany	REP	2013			P		P		P	P	P
Germany	SGP	2017				W				W	W
Germany	USPD	1920				W				W	W
Germany	WAV	1949			W				W		W
Greece	ANEL	2012	N		WP		P		WNP	P	WNP
Greece	ANTA	2019				W				W	W
Greece	DIKKI	2004	P			P			P	P	P
Greece	DIMAR	2012	N						N		N
Greece	DIMAR+PASOK	2015	N						N		N
Greece	DX	2019					W			W	W
Greece	EA	1974				W				W	W
Greece	EDA	1958				W				W	W
Greece	EE	2012					W			W	W
Greece	EEK	2019				W				W	W
Greece	EL	2019			WP		WP		WP	WP	WP
Greece	EM	1932				W				W	W
Greece	EPEN	1989					W			W	W
Greece	ES2	2019					W			W	W
Greece	FP	1936					W			W	W
Greece	HF	2004					W			W	W
Greece	KKE	2000	N			WP			N	WP	WNP
Greece	KdP	2012				W				W	W
Greece	LAE	2019	W			W			W	W	W
Greece	LAOS	2015			WNP		WP		WNP	WP	WNP
Greece	MERA	2004				W				W	W
Greece	MERA25	2019	P			P			P	P	P
Greece	OKDE	2019				W				W	W
Greece	PAME	1964				W				W	W
Greece	PE2	2019	W						W		W
Greece	PG	2000					W			W	W
Greece	PM	1936				W				W	W
Greece	SYN	2004	P			WP			P	WP	WP
Greece	SYRIZA	2019	WNP			P			WNP	P	WNP
Greece	XA	2019			W		WP		W	WP	WP
Hungary	AMÉP	1994					W			W	W
Hungary	DMP	2018				W				W	W
Hungary	EGY	2018			N				N		N
Hungary	FIDESZ	1990			WP		WP		WP	WP	WP
Hungary	FIDESZ+KDNP	2022			WP		WP		WP	WP	WP
Hungary	FIDESZ+KDNP+SZDSZ	1990			WP		WP		WP	WP	WP
Hungary	FIDESZ+SZDSZ	1990			WP		WP		WP	WP	WP
Hungary	FIDESZ+VP	1994			WP		WP		WP	WP	WP
Hungary	FKGP	2018			WP		P		WP	P	WP
Hungary	Fidesz+KDNP+MDF+MPP	2006			WP		WP		WP	WP	WP
Hungary	JOBBIK	2018	N		WP		P		WNP	P	WNP
Hungary	KDNP	2006					P			P	P
Hungary	KNP–KD	1990					W			W	W
Hungary	LMP	2018	N						N		N
Hungary	MDF	2010			W				W		W
Hungary	MDF+FIDESZ	2002			WP		WP		WP	WP	WP
Hungary	MDF+NYUP	2006			W				W		W
Hungary	MHM	2022					WP			WP	WP
Hungary	MIÉP	2018			P		WP		P	WP	WP
Hungary	MIÉP+FKGP	2014			WP		P		WP	P	WP
Hungary	MPP+Fidesz	2006			WP		WP		WP	WP	WP
Hungary	MPP+Fidesz+KDNP	2010			W		W		W	W	W
Hungary	MPP+Fidesz+KDNP+VP	2010			W		W		W	W	W
Hungary	MSZP+MSzMP	2002				W				W	W
Hungary	MSzMP	2002				W				W	W
Iceland	AB	1995				P				P	P
Iceland	BFl	1923		P	W				WP		WP

continued on next page

continued

Country	*Party*	*last year*	*Populist, P*			*Extremist, E*			*P*	*E*	*R*
			LP	*CP*	*RP*	*FL*	*FR*	*S*			
Iceland	IB	2016			W		W		W	W	W
Iceland	KI	1937				W				W	W
Iceland	PFI	2017				W				W	W
Ireland	CPI	2016				W				W	W
Ireland	ICP	2007					W			W	W
Ireland	IFP	2020					W			W	W
Ireland	ISN	2007				W				W	W
Ireland	PBP	2020				W				W	W
Ireland	SW	2002				W				W	W
Ireland	WP	2020				WP				WP	WP
Italy	AN	2006					P			P	P
Italy	DN+MSI	1992					WP			WP	WP
Italy	FI	2006		P					P		P
Italy	FI+LN	2001		P	N			W	NP	W	WNP
Italy	FIAN	2006		P					P		P
Italy	FN2	2001					W			W	W
Italy	FdI	2013	N		P		WP		NP	WP	WNP
Italy	FdI+FI	2018	N		WP		P		WNP	P	WNP
Italy	FdI+FI+LN+NcI+UdC	2018	N		WP		WP	W	WNP	WP	WNP
Italy	GN	2018						W		W	W
Italy	IRS	2006						W		W	W
Italy	IV	2013						W		W	W
Italy	IaI	2018					W			W	W
Italy	IdV	2008		P					P		P
Italy	LAM	2001					WP			WP	WP
Italy	LD+MSFT	2008					WP			WP	WP
Italy	LVR	2006						W		W	W
Italy	LdP	2018	W						W		W
Italy	M5S	2018	N	P					NP		NP
Italy	MIS	1946						W		W	W
Italy	MSFT	2013					WP			WP	WP
Italy	MSI	1968					WP			WP	WP
Italy	PCI	2018				WP				WP	WP
Italy	PCI+DC+PSI-PSDI	1987				W				W	W
Italy	PCL	2013				W				W	W
Italy	PD++EU+IEI+CPI	2018	N						N		N
Italy	PD++EU+IEI+CPI+SVPPATT	2018	N						N		N
Italy	PD+UV+EPAV	2018	N						N		N
Italy	PDAC	2013				W				W	W
Italy	PSI	1948				W				W	W
Italy	PSIUP	1968				W				W	W
Italy	PSdA	2013						W		W	W
Italy	PaP	2018	W			W			W	W	W
Italy	PdCdI	1948				P				P	P
Italy	PdL	2008		P					P		P
Italy	RC	2013	NP			WP			NP	WP	WNP
Italy	SA	2008				WP				WP	WP
Italy	SC2	2008				W				W	W
Italy	SCR	2018				W				W	W
Italy	SEL	2013	N			P			N	P	NP
Italy	SN	2008						W		W	W
Italy	UfS	2008			W				W		W
Italy	dF	2013						W		W	W
Latvia	ATM	2018			WN				WN		WN
Latvia	JL	2006		P					P		P
Latvia	JS	2018	WP			P			WP	P	WP
Latvia	KPV-LV	2018		P	W				WP		WP
Latvia	LKS	2014	N						N		N
Latvia	LNNK	1995			WNP		WP		WNP	WP	WNP
Latvia	LPP/LC	2011		P					P		P
Latvia	LRA	2018			N				N		N
Latvia	NSS	2006					W			W	W
Latvia	SDPS	2018	N						N		N
Latvia	TB/LNNK	1995					P			P	P
Latvia	ZRP	2011		P					P		P
Latvia	ZZS	2018			N				N		N
Lithuania	EAPL-CFA	1996	N						N		N
Lithuania	FRONTAS	2008				WP				WP	WP
Lithuania	LCP	2016		P					P		P
Lithuania	LCP+LSDS	2012		P					P		P
Lithuania	LCP+LTS	2020			P		P		P	P	P

continued on next page

continued

Country	*Party*	*last year*	*Populist, P*			*Extremist, E*			*P*	*E*	*R*
			LP	*CP*	*RP*	*FL*	*FR*	*S*			
Lithuania	LNDP	2000					W			W	W
Lithuania	LSP	1996				W				W	W
Lithuania	LTS	1996					P			P	P
Lithuania	LTS+PJL	2016			W		WP		W	WP	WP
Lithuania	LTS2	1992					P			P	P
Lithuania	LVSZ	2020	N						N		N
Lithuania	PJL	1996			W		WP		W	WP	WP
Lithuania	SLF	2012				W				W	W
Lithuania	Socialist	2016		W					W		W
Lithuania	TPP	1996		P					P		P
Lithuania	TPrP	2008		P					P		P
Lithuania	TS-LKD	2016		P					P		P
Luxembourg	ADR	2018			NP		WP		NP	WP	WNP
Luxembourg	KPL	2018				WP				WP	WP
Luxembourg	LSAP	2018	N						N		N
Netherlands	BIJ1	2017				W				W	W
Netherlands	CPN	1922				W				W	W
Netherlands	FvD	2017			WP		WP		WP	WP	WP
Netherlands	LPF	2003		P	W				WP		WP
Netherlands	NCPN	2003				W				W	W
Netherlands	NSBiN	1937					W			W	W
Netherlands	VNL	2017			W				W		W
Norway	DEM	2021			W				W		W
Norway	KSP	2013					W			W	W
Norway	NKP	2021				W				W	W
Poland	K15	2015		P	W				WP		WP
Poland	KORWIN	2015					P			P	P
Poland	KWiN	2019			W		WP		W	WP	WP
Poland	LPR	2007			P		P		P	P	P
Poland	PPN	1991					W			W	W
Poland	PPP	2011				W				W	W
Poland	PRAWICA	2019					W			W	W
Poland	PWN	1991					W			W	W
Poland	PX	1993			P		P		P	P	P
Poland	PZZ	1991				P				P	P
Poland	PiS	2015	N		WP		P		WNP	P	WNP
Poland	ROP	1997					P			P	P
Poland	RZM	2015				P				P	P
Poland	SRP	1991		P			W		P	W	WP
Poland	UPR	1997			W		P		W	P	WP
Poland	ZChN	1993			P		P		P	P	P
Poland	sp	2007	N						N		N
Portugal	AND	2022					W			W	W
Portugal	APU	1985				W				W	W
Portugal	BE	2022	N			WP			N	WP	WNP
Portugal	BE+UPD	2002	N			WP			N	WP	WNP
Portugal	CHEGA	2022			WP		WP		WP	WP	WP
Portugal	E	2022			W		W		W	W	W
Portugal	MPT	2022	N						N		N
Portugal	PCP-PEV	2022	N			WP			N	WP	WNP
Portugal	PCTPMRPP	2022				W				W	W
Portugal	PND	2011			W				W		W
Portugal	PNR	2019			W		W		W	W	W
Portugal	POUS	2011				W				W	W
Portugal	PPV-CDC	2015			W				W		W
Romania	AUR	2004			WP		WP		WP	WP	WP
Romania	FDSN	1992	W						W		W
Romania	FDdR	2004	W						W		W
Romania	PNGCD	2004			W		W		W	W	W
Romania	PNL	1992			N				N		N
Romania	PPT	2004					W			W	W
Romania	PRM	2004			WP		WP		WP	WP	WP
Romania	PRU	2016			P		WP		P	WP	WP
Romania	PSD+PC	2004	W						W		W
Romania	PSMR	2004				W				W	W
Romania	PSR	2004				W				W	W
Romania	PUNR	2004			P		P		P	P	P
Slovakia	.99	2020	W						W		W
Slovakia	ANO	2006		P					P		P
Slovakia	HNR	2006		P	W		W		WP	W	WP
Slovakia	HZDS+LSNS	2012			W		W		W	W	W

continued on next page

continued

Country	*Party*	*last year*	*Populist, P*			*Extremist, E*			*P*	*E*	*R*
			LP	*CP*	*RP*	*FL*	*FR*	*S*			
Slovakia	KSS	2016				WP				WP	WP
Slovakia	LSNS	2020			W		WP		W	WP	WP
Slovakia	MH	2020			N				N		N
Slovakia	OLaNO	2012		P	N				NP		NP
Slovakia	PSNS	2002			P		WP		P	WP	WP
Slovakia	SDKU	2002			N				N		N
Slovakia	SMER	2020	W	P					WP		WP
Slovakia	SOP	1998		P					P		P
Slovakia	SOS	2020			P		WP		P	WP	WP
Slovakia	SaS	2020			N				N		N
Slovakia	VLAST	2020			WP		WP		WP	WP	WP
Slovakia	VZDOR	2002				W				W	W
Slovakia	ZRS	2010	P			WP			P	WP	WP
Slovenia	DeSuS	2014	N						N		N
Slovenia	LMS	2018		P					P		P
Slovenia	NPS	2014					W			W	W
Slovenia	Nsi	2018			NP		P		NP	P	NP
Slovenia	SAB	2018			N				N		N
Slovenia	SJN	2004		P					P		P
Slovenia	SLS	2018			N				N		N
Slovenia	SLS+SKD	2000			N				N		N
Slovenia	SLS+SMS	2008			N				N		N
Slovenia	SMC	2014			N				N		N
Slovenia	SNS	2018			WP		WP		WP	WP	WP
Slovenia	SPS	2018				W				W	W
Spain	AES	2008					W			W	W
Spain	AHC	2019				W		W		W	W
Spain	AMAIUR	2011	N					W	N	W	WN
Spain	AN18	2008					W			W	W
Spain	ARALAR	2008						W		W	W
Spain	AUN	2004					W			W	W
Spain	BNG	2019	N			P		W	N	WP	WNP
Spain	CDC	2016						W		W	W
Spain	CHA	2019				P				P	P
Spain	COMPROMIS	2019				P				P	P
Spain	CUP	2019				WP		W		WP	WP
Spain	CV	2008					W			W	W
Spain	CdG	2016				W				W	W
Spain	CiU	2011						W		W	W
Spain	Cs	2019			N				N		N
Spain	DIL	2015						W		W	W
Spain	DN	2015			W		W		W	W	W
Spain	DNE	2011					W			W	W
Spain	E-2000	2011			W		W		W	W	W
Spain	EA+EE	1993				W		W		W	W
Spain	EC	2000						W		W	W
Spain	ECP	2019	P			P			P	P	P
Spain	EHB	2019				P		W		WP	WP
Spain	ENV	2000						W		W	W
Spain	ERC	2011						W		W	W
Spain	ERC-CatSí	2016						W		W	W
Spain	ERCS	2019						W		W	W
Spain	ERPV	2019						W		W	W
Spain	EU	2004				W				W	W
Spain	EUIB	2008				W				W	W
Spain	EUiA	2000				W				W	W
Spain	EV-AV	2008						W		W	W
Spain	FEI	2000					W			W	W
Spain	FET	2019					W			W	W
Spain	FN	2000					W			W	W
Spain	FPG	2004				W		W		W	W
Spain	FR	2019						W		W	W
Spain	FrE	2008					W			W	W
Spain	GBAI	2019						W		W	W
Spain	GIL	2000					W			W	W
Spain	HB	1996				WP		W		WP	WP
Spain	I-E	2015				W				W	W
Spain	ICEV	2000	N						N		N
Spain	ICV	2004	N						N		N
Spain	ICV–EUiA	2008	N			W			N	W	WN
Spain	IU	2015	N			WP			N	WP	WNP

continued on next page

continued

Country	*Party*	*last year*	*Populist, P*			*Extremist, E*			*P*	*E*	*R*
			LP	*CP*	*RP*	*FL*	*FR*	*S*			
Spain	IU CLM	2004	N			P			N	P	NP
Spain	IU-CM	2008	N			P			N	P	NP
Spain	IU-UP	2015	N			P			N	P	NP
Spain	IUA	2000	N			WP			N	WP	WNP
Spain	IUC	2015	N			WP			N	WP	WNP
Spain	IUE	2004	N			WP			N	WP	WNP
Spain	IULV-CA	2015	N			WP			N	WP	WNP
Spain	IUN-NEB	2004	N			WP			N	WP	WNP
Spain	IUdA	2011	N			WP			N	WP	WNP
Spain	JxCat	2019						W		W	W
Spain	LI	2008				W				W	W
Spain	MFE	2008					W			W	W
Spain	MSR	2004					W			W	W
Spain	NABAI	2019						W		W	W
Spain	PAL	2008			W				W		W
Spain	PCE	2019				W				W	W
Spain	PCE-EPK	2019				W				W	W
Spain	PCOE	2019				W				W	W
Spain	PCPC	2015				W				W	W
Spain	PCPC2	2019				W				W	W
Spain	PCPE	2019				W				W	W
Spain	PCPG	2008				W		W		W	W
Spain	PCTE	2019				W				W	W
Spain	PIRATA.CAT	2011						W		W	W
Spain	PNT	2004					W			W	W
Spain	PODEMOS	2015	WNP			P			WNP	P	WNP
Spain	POSI	2008				W				W	W
Spain	PSM-EN	1996						W		W	W
Spain	PSP	1977				W				W	W
Spain	PYLN	2019						W		W	W
Spain	PxC	2016					W			W	W
Spain	PxCAT	2008			W		W		W	W	W
Spain	UCdE	2011				W				W	W
Spain	UDELP	2016						W		W	W
Spain	UN	2004					W			W	W
Spain	UP	2019	P			WP			P	WP	WP
Spain	UPC	1979				W				W	W
Spain	UPMMÉS	2016	W			W			W	W	W
Spain	UPyD	2016			N				N		N
Spain	VOX	2019			WP		WP		WP	WP	WP
Sweden	AFS	2022			W		W		W	W	W
Sweden	MED	2022			W				W		W
Sweden	NMR	2022					W			W	W
Sweden	PFr	2022			W		W		W	W	W
Sweden	SKA	2022			W		W	W	W	W	W
Sweden	SNF	1936					W			W	W
Switzerland	AGT	2007				W				W	W
Switzerland	AL+PSTPOP	2007				W				W	W
Switzerland	EAG	2019				W				W	W
Switzerland	EDU	2019			W				W		W
Switzerland	FA	2019				W				W	W
Switzerland	FPS	1999			WP		P		WP	P	WP
Switzerland	JSVP	2019			W				W		W
Switzerland	KPS	1939				W				W	W
Switzerland	LDT	2015			WP		P		WP	P	WP
Switzerland	MCG	2019			WP		P		WP	P	WP
Switzerland	PC	2015				W				W	W
Switzerland	PNOS	2019					W			W	W
Switzerland	PSTPOP	2019				WP				WP	WP
Switzerland	SD	2015			P		WP		P	WP	WP
Switzerland	SOL	2007				WP				WP	WP
Switzerland	SVP	2019			WP		WP		WP	WP	WP
Switzerland	VA	2011			W		W		W	W	W
UK	AWL	2010				W				W	W
UK	BNP	2019					W			W	W
UK	CLGB	2010				W				W	W
UK	CPB	2010				W				W	W
UK	CPGB	2015				W				W	W
UK	DUP	2019			W				W		W
UK	ED	2019					W	W		W	W
UK	GPEW	2019	N						N		N

continued on next page

continued

Country	*Party*	*last year*	*Populist, P*			*Extremist, E*			*P*	*E*	*R*
			LP	*CP*	*RP*	*FL*	*FR*	*S*			
UK	GWL	2019						W		W	W
UK	ISP	2005						W		W	W
UK	LTUG	1992				W				W	W
UK	LiGB	2015			W		W		W	W	W
UK	Lun+TUSC	2015				W				W	W
UK	NFDDSS	2015					W			W	W
UK	PBB	2005				W				W	W
UK	PBP+LiP	2010				W				W	W
UK	PLAID	2019	N					W	N	W	WN
UK	PSC	2010				W				W	W
UK	RCP	1983				W				W	W
UK	RESPECT	2015	P			WP			P	WP	WP
UK	RFr	1992				W				W	W
UK	RU	2019			P		P		P	P	P
UK	SAL	2001				W				W	W
UK	SNP	2019	N					W	N	W	WN
UK	SPGB	1983				W				W	W
UK	ScJP	2010						W		W	W
UK	TUSC	2015				W				W	W
UK	UKIP	2019			WNP		WP		WNP	WP	WNP
UK	VERITAS	2001			W				W		W
UK	VPP	2019			W				W		W
UK	WRPa	2019				W				W	W

Note: This table lists all the political parties in the CLEA that are classified as radical (R) following the procedure in appendix A.2.2 and reports the source(s) for each classification: 'N' for Inglehart and Norris (2019), 'P' for the PopuList and 'W' for Wikipedia. Political party acronyms are harmonized using keyword search on Wikipedia. The third column reports the last recorded election year for each party in the CLEA. Populist parties, P, are further subdivided as left, LP, centre, CP or right, RP; Extremist parties, E, are subdivided as far left, FL, far right, FR, or separatist, S. Party coalitions are identified by the + sign. Time, country and party coverage differs by source, as further explained in appendix A.2.2.

Table A9: Party taxonomy by country in CLEA

Country	*Conservative*	*Liberal*	*Socialist*	*Christian*	*Green*	*Regionalist*	*Populist*	*Far left*	*Far right*	*Separatist*	*Other*
Austria	1	3	3	2	1	0	0	4	0	0	19
Belgium	0	6	6	5	3	6	0	2	1	3	22
Bulgaria	7	12	8	1	3	0	0	5	1	0	177
Czech Republic	13	15	9	3	0	5	0	2	3	0	49
Denmark	4	9	6	1	1	0	0	1	2	6	10
Estonia	2	3	2	2	2	0	0	0	1	0	27
Finland	1	6	3	2	3	0	0	3	4	0	26
France	10	7	4	1	2	0	0	4	2	1	4
Germany	19	9	1	4	3	1	0	4	9	0	49
Greece	9	11	12	1	1	0	0	7	4	0	48
Hungary	12	6	13	3	3	0	0	2	3	0	115
Iceland	1	4	5	0	1	0	0	2	0	0	14
Ireland	1	2	3	1	1	1	0	4	2	0	8
Italy	9	10	16	9	1	9	0	5	6	10	51
Latvia	4	1	5	3	0	2	0	0	1	0	33
Lithuania	7	4	6	4	3	1	0	1	0	0	31
Luxembourg	1	4	0	1	1	0	0	1	0	0	10
Netherlands	1	5	2	11	1	1	0	2	1	0	44
Norway	4	3	2	5	1	1	0	1	0	0	14
Poland	12	9	9	7	2	1	0	0	1	0	98
Portugal	3	4	3	0	3	1	0	3	0	0	2
Romania	0	3	6	3	2	0	0	1	1	0	159
Slovakia	2	13	4	3	1	2	0	2	0	0	61
Slovenia	0	4	2	1	1	0	0	1	0	0	34
Spain	4	11	40	6	8	41	0	12	14	28	101
Sweden	1	4	1	0	0	0	0	0	2	1	50
Switzerland	3	5	5	3	3	1	0	8	1	0	195
UK	7	8	13	3	2	8	0	7	2	6	379

Note: This table provides a country-specific breakdown of the political parties in the CLEA by the party taxonomy developed in appendix A.2.2. The residual category contains the following ideological positions: *Agrarian*, *Anarchist*, *Animal rights*, *Anti establishment*, *Anti-communist*, *Cartel*, *Center*, *Centrist*, *Direct democracy*, *Elderly*, *Europeanist*, *Euroscepticism*, *Fascist*, *Federalist*, *Feminist*, *Humanist*, *Independent*, *Islam*, *Joke*, *Libertarian*, *Micro*, *Minority rights*, *Multiculturalism*, *Nationalism*, *Nationalist*, *Pensioner's rights*, *Pirate*, *Populist*, *Progressivism*, *Republican*, *Right*, *Spiritual*, *Spiritual Left*, *Unionist*, *Unitarism* and *Youth*.

Table A10: **Divergent development and discontent, 1847-2023: OLS estimates**

Full historical sample

	$\bar{\bar{y}}$	$\underline{y}$	$\dot{y}$	$\bar{\bar{y}}$	$\underline{y}$	$\dot{y}$
y	0	0	.01	.06**	-.01	.04*
	(.01)	*(.02)*	*(.02)*	*(.02)*	*(.01)*	*(.02)*
$Q^2_{P80/P20}$				.09***	.03	.04**
				(.03)	*(.02)*	*(.02)*
$Q^3_{P80/P20}$				.16***	.07	.09**
				(.03)	*(.05)*	*(.04)*
$Q^4_{P80/P20}$				.34***	.29***	.29***
				(.06)	*(.06)*	*(.06)*
$y \times Q^2_{P80/P20}$				-.06*	.03**	-.03
				(.03)	*(.02)*	*(.03)*
$y \times Q^3_{P80/P20}$				-.08***	.03	-.04
				(.03)	*(.03)*	*(.03)*
$y \times Q^4_{P80/P20}$				-.07**	-.04	-.06**
				(.03)	*(.04)*	*(.03)*
N	44258	44258	44258	44258	44258	44258
Adjusted R ^{2}	0	0	0	.218	.219	.218

Note: This table reports OLS results from equation (11). Dependent variables: the combined constituency-level party vote shares of radical, extremist or populist parties in the CLEA. Political parties are classified as radical, extremist or populist if they are categorized as such by at least one of the three classifications in table A8. Independent variables: relative per capita GDP, $y = \bar{\bar{y}}$, or the ratio of constituency to country per capita GDP; the population share in the bottom or top quintile of gridded per capita GDP, $y = \underline{y}$ and $y = \dot{y}$; and dummy variable indicating countries that are in the second, third and fourth quartiles of the P80/P20 per capita GDP ratio, $Q^2_{P80/P20}$ through $Q^4_{P80/P20}$. Constituency-level GDP is approximated by spatializing reported country GDP using satellite data on nighttime lights, see section 2.2. Total observations, N, and adjusted R^2 are reported in the bottom. Standard errors are robust to heteroskedasticity and clustered at the country-level.

Table A11: **Divergent development and discontent, 1992-2023: 2SLS-estimates**

Extended party definition

	Radicalism			Extremism			Populism		
	$\bar{\bar{y}}$	$\underline{y}$	$\dot{y}$	$\bar{\bar{y}}$	$\underline{y}$	$\dot{y}$	$\bar{\bar{y}}$	$\underline{y}$	$\dot{y}$
y	-.73**	1.17***	-1.48*	-.39*	.65***	-.77	-.69**	1.12**	-1.4*
	(.34)	*(.44)*	*(.78)*	*(.21)*	*(.25)*	*(.49)*	*(.34)*	*(.43)*	*(.75)*
Method	2SLS	2SLS	2SLS	2SLS	2SLS	2SLS	2SLS	2SLS	2SLS
N	18442	18442	18442	18442	18442	18442	18442	18442	18442
Hansen J p-value	.19	.13	.29	.6	.36	.92	.23	.15	.35
First stage results:									
Roman road distance	-.54**	.37**	-.23**	-.54**	.37**	-.23**	-.54**	.37**	-.23**
	(.22)	*(.13)*	*(.1)*	*(.22)*	*(.13)*	*(.1)*	*(.22)*	*(.13)*	*(.1)*
Ruggedness	-.02***	.01**	-.01***	-.02***	.01**	-.01***	-.02***	.01**	-.01***
	(0)	*(0)*	*(0)*	*(0)*	*(0)*	*(0)*	*(0)*	*(0)*	*(0)*
F-statistic	14.4	5.2	35.6	14.4	5.2	35.6	14.4	5.2	35.6

Note: This table reports 2SLS from equation (27). Dependent variables: the combined constituency-level party vote shares of radical, extremist or populist parties in the CLEA. Political parties are classified as radical, extremist or populist if they are categorized as such by any of the three classifications in table A8. The mean (and standard deviation) of radical, extremist and populist vote shares in the panel are .257 (.247), .172 (.171) and .237 (.242). Independent variables, y: relative per capita GDP, $\bar{\bar{y}}$, or the ratio of constituency to country per capita GDP; and the population share in the bottom or top quintile of gridded per capita GDP, $\underline{y}$ and $\dot{y}$. Constituency-level GDP is approximated by spatializing reported country GDP using satellite data on nighttime lights or, if that is unavailable, an indicator of market access, see section 2.2. Independent variables are instrumented by centered distances to Roman roads and ruggedness; the first stage results are reported in the bottom panel. The mean (and standard deviation) of $\bar{\bar{y}}$, $\underline{y}$ and $\dot{y}$ are .982 (.51), .212 (.228) and .194 (.304). Total observations, N, and the Hansen J test of overidentifying restrictions are reported in the middle panel. Standard errors are robust to heteroskedasticity and clustered at the country-level.

Table A12: **Divergent development and discontent, 1847-2023: 2SLS-estimates**

Full historical sample

	Radicalism			Extremism			Populism		
	$\bar{\bar{y}}$	y	$\dot{y}$	$\bar{\bar{y}}$	y	$\dot{y}$	$\bar{\bar{y}}$	y	$\dot{y}$
y	-.4**	.21***	-.77*	-.27***	.16***	-.5**	-.25	.11*	-.53
	(.17)	*(.07)*	*(.4)*	*(.09)*	*(.04)*	*(.23)*	*(.15)*	*(.07)*	*(.33)*
Method	2SLS	2SLS	2SLS	2SLS	2SLS	2SLS	2SLS	2SLS	2SLS
N	44258	44258	44258	44258	44258	44258	44258	44258	44258
Hansen J p-value	.19	.13	.33	.28	.18	.55	.15	.11	.21
First stage results:									
Roman road distance	-.53***	.83***	-.27***	-.53***	.83***	-.27***	-.53***	.83***	-.27***
	(.17)	*(.23)*	*(.08)*	*(.17)*	*(.23)*	*(.08)*	*(.17)*	*(.23)*	*(.08)*
Ruggedness	-.01***	.01**	-.01***	-.01***	.01**	-.01***	-.01***	.01**	-.01***
	(0)	*(0)*	*(0)*	*(0)*	*(0)*	*(0)*	*(0)*	*(0)*	*(0)*
F-statistic	7.6	10.1	9.3	7.6	10.1	9.3	7.6	10.1	9.3

Note: This table reports 2SLS from equation (27). Dependent variables: the combined constituency-level party vote shares of radical, extremist or populist parties in the CLEA. Political parties are classified as radical, extremist or populist if they are categorized as such by any of the three classifications in table A8. The mean (and standard deviation) of radical, extremist and populist vote shares in the panel are .155 (.215), .113 (.16) and .119 (.199). Independent variables, y: relative per capita GDP, $\bar{\bar{y}}$, or the ratio of constituency to country per capita GDP; and the population share in the bottom or top quintile of gridded per capita GDP, y and $\dot{y}$. Constituency-level GDP is approximated by spatializing reported country GDP using satellite data on nighttime lights or, if that is unavailable, an indicator of market access, see section 2.2. Independent variables are instrumented by centered distances to Roman roads and ruggedness; the first stage results are reported in the bottom panel. The mean (and standard deviation) of $\bar{\bar{y}}$, y and $\dot{y}$ are .967 (.387), .229 (.327) and .172 (312). Total observations, N, and the Hansen J test of overidentifying restrictions are reported in the middle panel. Standard errors are robust to heteroskedasticity and clustered at the country-level.

Table A13: **Divergent development and discontent, 1992-2023: 2SLS-estimates**

Adding country and year fixed effects

	Radicalism			Extremism			Populism		
	$\bar{\bar{y}}$	y	$\dot{y}$	$\bar{\bar{y}}$	y	$\dot{y}$	$\bar{\bar{y}}$	y	$\dot{y}$
y	-.19**	.39***	-.3*	-.09	.16**	-.17	-.11**	.26**	-.16*
	(.09)	*(.12)*	*(.17)*	*(.06)*	*(.07)*	*(.12)*	*(.06)*	*(.13)*	*(.08)*
Method	2SLS	2SLS	2SLS	2SLS	2SLS	2SLS	2SLS	2SLS	2SLS
N	18442	18442	18442	18442	18442	18442	18442	18442	18442
Year fixed effects	yes	yes	yes	yes	yes	yes	yes	yes	yes
Country fixed effects	yes	yes	yes	yes	yes	yes	yes	yes	yes
First stage results:									
Roman road distance	-.55**	.38**	-.24**	-.55**	.38**	-.24**	-.55**	.38**	-.24**
	(.23)	*(.14)*	*(.11)*	*(.23)*	*(.14)*	*(.11)*	*(.23)*	*(.14)*	*(.11)*
Ruggedness	-.02***	.01*	-.01***	-.02***	.01*	-.01***	-.02***	.01*	-.01***
	(0)	*(0)*	*(0)*	*(0)*	*(0)*	*(0)*	*(0)*	*(0)*	*(0)*
F-statistic	10.4	4.1	18.1	10.4	4.1	18.1	10.4	4.1	18.1

Note: This table reports 2SLS from equation (27). Dependent variables: the combined constituency-level party vote shares of radical, extremist or populist parties in the CLEA. Political parties are classified as radical, extremist or populist if they are categorized as such by any of the three classifications in table A8. The mean (and standard deviation) of radical, extremist and populist vote shares in the panel are .159 (.172), .111 (.139) and .124 (.16). Independent variables, y: relative per capita GDP, $\bar{\bar{y}}$, or the ratio of constituency to country per capita GDP; and the population share in the bottom or top quintile of gridded per capita GDP, y and $\dot{y}$. Constituency-level GDP is approximated by spatializing reported country GDP using satellite data on nighttime lights or, if that is unavailable, an indicator of market access, see section 2.2. Independent variables are instrumented by centered distances to Roman roads and ruggedness; the first stage results are reported in the bottom panel. The mean (and standard deviation) of $\bar{\bar{y}}$, y and $\dot{y}$ are .982 (.51), .212 (.228) and .194 (.304). Total observations, N, and the Hansen J test of overidentifying restrictions are reported in the middle panel. All regressions include country and year fixed effects. Standard errors are robust to heteroskedasticity and clustered at the country-level.

Table A14: **Divergent development and discontent, 1992-2023: 2SLS-estimates**

Decomposition

	Populism						**Extremism**								
	Left			Right			Far left			Far right			Separatist		
	$\bar{\bar{y}}$	$\underset{\cdot}{y}$	$\dot{y}$	$\bar{\bar{y}}$	$\underset{\cdot}{y}$	$\dot{y}$	$\bar{\bar{y}}$	$\underset{\cdot}{y}$	$\dot{y}$	$\bar{\bar{y}}$	$\underset{\cdot}{y}$	$\dot{y}$	$\bar{\bar{y}}$	$\underset{\cdot}{y}$	$\dot{y}$
y	-.14*	.28***	-.24	-.21	.3	-.46	-.04	.07	-.08	-.04	.07	-.08	-.11	.17*	-.22
	(.07)	*(.1)*	*(.16)*	*(.16)*	*(.22)*	*(.35)*	*(.04)*	*(.05)*	*(.09)*	*(.04)*	*(.05)*	*(.09)*	*(.07)*	*(.1)*	*(.15)*
Method	2SLS	2SLS	2SLS	2SLS	2SLS	2SLS	2SLS	2SLS	2SLS	2SLS	2SLS	2SLS	2SLS	2SLS	2SLS
N	18442	18442	18442	18442	18442	18442	18442	18442	18442	18442	18442	18442	18442	18442	18442
Hansen J p-value	.31	.39	.28	.2	.21	.2	.97	.82	.92	.97	.82	.92	.52	.37	.65
First stage results:															
Roman road distance	-.54**	.37**	-.23**	-.54**	.37**	-.23**	-.54**	.37**	-.23**	-.54**	.37**	-.23**	-.54**	.37**	-.23**
	(.22)	*(.13)*	*(.1)*	*(.22)*	*(.13)*	*(.1)*	*(.22)*	*(.13)*	*(.1)*	*(.22)*	*(.13)*	*(.1)*	*(.22)*	*(.13)*	*(.1)*
Ruggedness	-.02***	.01**	-.01***	-.02***	.01**	-.01***	-.02***	.01**	-.01***	-.02***	.01**	-.01***	-.02***	.01**	-.01***
	(0)	*(0)*	*(0)*	*(0)*	*(0)*	*(0)*	*(0)*	*(0)*	*(0)*	*(0)*	*(0)*	*(0)*	*(0)*	*(0)*	*(0)*
F-statistic	14.4	5.2	35.6	14.4	5.2	35.6	14.4	5.2	35.6	14.4	5.2	35.6	14.4	5.2	35.6

Note: This table reports 2SLS from equation (27). Dependent variables: the combined constituency-level party vote shares of left and populist parties as well as far left, far right or separatist parties in the CLEA. Except for separatist parties, which are only identified by Wikipedia, political parties are majority classified if they are categorized to these respective caegories in at least two of the three classifications in table A8. The mean (and standard deviation) of left populist, right populist, far left, far right and separatist vote shares in the panel are .021 (.063), .103 (.154), .025 (.053), .073 (.114), .02 (.08). Independent variables, y: relative per capita GDP, $\bar{\bar{y}}$, or the ratio of constituency to country per capita GDP; and the population share in the bottom or top quintile of gridded per capita GDP, $\underset{\cdot}{y}$ and $\dot{y}$. Constituency-level GDP is approximated by spatializing reported country GDP using satellite data on nighttime lights or, if that is unavailable, an indicator of market access, see section 2.2. Independent variables are instrumented by centered distances to Roman roads and ruggedness; the first stage results are reported in the bottom panel. The mean (and standard deviation) of $\bar{\bar{y}}$, $\underset{\cdot}{y}$ and $\dot{y}$ are .982 (.51), .212 (.23) and .194 (.304). Total observations, N, and the Hansen J test of overidentifying restrictions are reported in the middle panel. All regressions include country and year fixed effects. Standard errors are robust to heteroskedasticity and clustered at the country-level.